

FPGA Design and Implementation of a Framework for Optogenetic Retinal  
Prosthesis

by

Musa Salah Musa Al-Yaman

A thesis submitted to the Department of Electrical and Electronic Engineering

In conformity with the requirements for

The degree of Doctor of Philosophy of Newcastle University

Department of Electrical and Electronic Engineering

Newcastle University

(April, 2015)

Copyright ©Musa Al-Yaman, 2015

## **Abstract**

There are 285 million people worldwide with a visual impairment, 39 million of whom are completely blind and 246 million partially blind, known as low vision patients. In the UK and other developed countries of the west, retinal dystrophy diseases represent the primary cause of blindness, especially Age Related Macular Degeneration (AMD), diabetic retinopathy and Retinitis Pigmentosa (RP).

There are various treatments and aids that can help these visual disorders, such as low vision aids, gene therapy and retinal prosthesis. Retinal prostheses consist of four main stages: the input stage (Image Acquisition), the high level processing stage (Image preparation and retinal encoding), low level processing stage (Stimulation controller) and the output stage (Image displaying on the opto-electronic micro-LEDs array). Up to now, a limited number of full hardware implementations have been available for retinal prosthesis.

In this work, a photonic stimulation controller was designed and implemented. The main rule of this controller is to enhance framework results in terms of power and time. It involves, first, an even power distributor, which was used to evenly distribute the power through image sub-frames, to avoid a large surge of power, especially with large arrays. Therefore, the overall framework power results are improved. Second, a pulse encoder was used to select different modes of operation for the opto-electronic micro-LEDs array, and as a result of this the overall time for the framework was improved. The implementation is completed using reconfigurable hardware devices, i.e. Field Programmable Gate Arrays (FPGAs), to achieve high performance at an economical price. Moreover, this FPGA-based framework for an optogenetic retinal prosthesis aims to control the opto-electronic micro-LED array in an efficient way, and to interface and link between the opto-electronic micro-LED array hardware architecture and the previously developed high level retinal prosthesis image processing algorithms.

## **Acknowledgements**

First praise is to Allah, the Almighty God, for always inspiring me and guiding me to the right path.

I would like to express my sincere gratitude to my supervisor Dr. Patrick Degenaar; he has been a wonderful supervisor and has guided me in all situations and hard times during this project. His timely and efficient contributions helped me to shape this work into its final form. Many thanks for being there every day to discuss and talk with me about both scientific and non-scientific topics.

I would like also to express my sincere respect and gratitude to Dr. Alex Bystrov, my second supervisor, for his valuable comments and insightful advice.

I would like to thank the University of Jordan for the generous scholarship which was awarded to me.

My special thanks to my colleagues and friends: Dr. Walid Al Atabany, Dr. Arfan Ghani, Dr. Rolando Berlinguer Palmimi, Dr. Kamyar Mehran, Graeme Coapes, Hubin Zhao, Jun Luo, John Barret, Micheal Evan, Nabeel Fattah and Ahmad Soltan.

My gratitude extends to my family, from whom I received both encouragement and compassion. In particular, I am blessed with a loving mother and father, who continued to provide valuable support throughout my PhD. This thesis is dedicated to them.

My wife, thank you for bearing the trouble of the long years of my PhD. You are always the source of happiness in my life. I promise a wonderful life ahead.

## **Statement of Originality**

I hereby certify that all of the work described within this thesis is the original work of the author. Any published (or unpublished) ideas and/or techniques from the work of others are fully acknowledged in accordance with the standard referencing practices.

(Musa Salah Al-Yaman)

(April, 2015)



## List of Achievements

### *International conference papers*

Al Yaman M, Ghani A, Bystrov A, Degenaar P, Maaskant P: ***FPGA design of a pulse encoder for optoelectronic neural stimulation and recording arrays.*** Biomedical Circuits and Systems Conference (BioCAS), 2013 IEEE, pp.190, 193, Oct. 31 2013-Nov. 2 2013, **(Personal presentation).**

Al Yaman M, Degenaar P: ***FPGA design of an even power distributor for optoelectronic neural stimulation.*** Applied Electrical Engineering and Computing Technologies (AEECT), 2013 IEEE Jordan Conference, pp.1, 4, 3-5 Dec. 2013, **(Personal presentation).**

Al Yaman M, Bystrov A, Degenaar P: ***An FPGA design for dual-spectrum Visual Scene Preparation in Retinal Prosthesis.*** IEEE Engineering in Medicine and Biology Society (EMBC'14) 2014 IEEE, Aug. 26 2014-Aug. 30 2014, **(Personal poster).**

### *Local conferences and meetings contributions*

Al Yaman M, Degenaar P: ***Anisotropic diffusion filter for real time image Simplification for visual prosthesis.*** Annual Research Conference (ARC 2015) that was held on the 21<sup>st</sup> - 22<sup>nd</sup> January 2015, at School of EECE Newcastle University, **(Personal presentation).**

Al Yaman M, Degenaar P: ***Scene Simplification for Retinal Prosthesis Stimulation.*** Annual Research Conference (ARC 2014) that was held on the 23<sup>rd</sup> - 24<sup>th</sup> January 2014, at School of EECE Newcastle University, **(Personal presentation).**

Al Yaman M, and Degenaar P: ***Design and FPGA implementation for individually addressable optoelectronic arrays controller for optogenetic neural stimulation.*** Annual Research Conference (ARC 2013) that was held on the 23<sup>rd</sup> - 24<sup>th</sup> January 2013, at School of EECE Newcastle University, **(Personal poster).**

### **Group presentations**

12 presentations to the neuro-prosthesis lab group.

### **Awards**

Won the best third poster award in ARC 2013 for uSystems group.

Won second paper presentation award in ARC 2014 for uSystems group.

## Table of Contents

Abstract.....	2
Acknowledgements.....	3
Statement of Originality.....	4
List of Achievements.....	5
Table of Contents.....	6
List of Figures.....	9
List of Tables.....	12
Chapter 1 Medical Background and Literature Review.....	13
1.1 Chapter Overview.....	13
1.2 Medical Background.....	14
1.2.1 Human Visual System.....	15
1.2.2 The Eye.....	15
1.2.3 The Retina.....	17
1.2.4 Retina Diseases.....	20
1.2.5 Retina Diseases Treatment.....	23
1.3 Visual Prosthesis Review.....	26
1.3.1 Retinal Prostheses.....	28
1.3.2 Optic Nerve Prostheses.....	31
1.3.3 Visual Cortex Prostheses.....	32
1.4 Visual Enhancement Review.....	35
1.4.1 General Review for Image Segmentation.....	36
1.4.2 Vision Enhancement for Visual Impairments.....	39
1.5 Conclusion.....	42
Chapter 2 System Level Architecture Design.....	44
2.1 Chapter Overview.....	44
2.2 Image Acquisition.....	45
2.2.1 Imaging Sensor.....	46
2.2.2 Dual Spectrum Imaging.....	51
2.3 High Level Processing.....	52

2.3.1	Image Preparation.....	52
2.3.2	Retinal Encoding .....	56
2.4	Low Level Processing.....	60
2.4.1	Frame Encoding and Even Power Distributor .....	61
2.4.2	Pulse Encoder .....	67
2.5	Optoelectronic Micro-LED Array .....	70
2.6	Conclusion .....	75
Chapter 3	Implementation.....	77
3.1	Chapter Overview .....	77
3.2	Implementation Platform.....	78
3.3	The Development Kit .....	80
3.4	Image Simplification Design.....	83
3.4.1	Visible Preparation .....	85
3.4.2	IR Preparation .....	90
3.4.3	Mixing IR-Visible.....	92
3.5	Frame Encoding and Even Power Distributor .....	94
3.5.1	Sorting.....	97
3.5.2	Pulse Width Modulation (PWM).....	100
3.5.3	Control Signal Generation .....	102
3.6	Pulse Encoder .....	104
3.6.1	The 16x16 Array Pulse Encoder.....	105
3.6.2	The 90x90 Array Pulse Encoder.....	108
3.7	Conclusion .....	112
Chapter 4	Analysis and Results .....	114
4.1	Chapter Overview .....	114
4.2	Computer-FPGA Communication Results .....	115
4.3	Image Preparation and Retinal Encoding Results .....	118
4.3.1	Image Simplification Results .....	119

4.3.2	Retinal Encoding Results .....	124
4.4	Optoelectronic Stimulation Controller Results.....	127
4.4.1	Even Power Distributor Results.....	127
4.4.2	Pulse Encoder Results .....	135
4.5	Optoelectronic Micro-LED Results.....	141
4.6	Conclusion .....	145
Chapter 5 Conclusions and Future Work .....		147
References.....		153

## List of Figures

Figure 1-1 Chapter one starts by describing the eye and retina .....	14
Figure 1-2 Cross section of human visual system.....	15
Figure 1-3 Schematic cross section of the human eye .....	16
Figure 1-4 Cross-section of the retina.....	17
Figure 1-5 The difference between central and peripheral vision.....	19
Figure 1-6 Rods and Cones.....	20
Figure 1-7 The effect of macular degeneration. ....	21
Figure 1-8 The tunnel vision effect.....	22
Figure 1-9 The effect of diabetic retinopathy disease. ....	22
Figure 1-10 The idea of a visual prosthesis. ....	27
Figure 1-11 A summary of different approaches to the visual prosthesis.....	28
Figure 1-12 Timeline for the progress of the retina prosthesis programme.....	30
Figure 1-13 The Image Processing Operations. ....	35
Figure 1-14 Cameraman Thresholding Segmentation. ....	37
Figure 1-15 Baboon Thresholding Segmentation.....	38
Figure 1-16 Edge-based Segmentation. ....	39
Figure 1-17 Television image enhancements. ....	40
Figure 1-18 The output of Peli's vision enhancement system (AMD).....	41
Figure 1-19 The output of Peli's vision enhancement system (RP).....	41
Figure 1-20 Applying Al-Atabany's different algorithms. ....	42
Figure 2-1 Optogenetic retinal prosthesis approach. ....	44
Figure 2-2 CCD vs. CMOS image sensor. ....	46
Figure 2-3 CMOS Image sensor. ....	48
Figure 2-4 The Far IR camera and the block diagram .....	50
Figure 2-5 The difference between using Gaussian (right column).....	54
Figure 2-6 Anisotropic diffusion is affected by the number of iterations (n).....	55
Figure 2-7 Main stages of retinal stimulation. ....	57
Figure 2-8 The main spike coding steps. ....	58
Figure 2-9 The second step in spike coding. ....	59
Figure 2-10 General system architecture of the micro-LEDs. ....	60
Figure 2-11 The function of frame encoding. ....	61
Figure 2-12 An image frame for N pixels before and after power equalization. ....	62
Figure 2-13 Even power distributor time step definition. ....	64

Figure 2-14 The four possible combinations .....	66
Figure 2-15 Two possible ways to update the micro-LEDs.....	68
Figure 2-16 The information I/O with optoelectronic stimulators .....	69
Figure 2-17 Optoelectronic LEDs.....	70
Figure 3-1 Chapter three overview.....	77
Figure 3-2 The main stages in the approach for a retinal prosthesis. ....	83
Figure 3-3 A full architecture of scene simplification .....	84
Figure 3-4 Universal Sobel Module (USM) Architecture. ....	86
Figure 3-5 A full anisotropic diffusion filter architecture.....	89
Figure 3-6 Exponentially stretching and compressing the greyscale range .....	91
Figure 3-7 The Gaussian filter with the buffer .....	92
Figure 3-8 The main flow chart for the even power distributor. ....	97
Figure 3-9 The sorting stage.....	99
Figure 3-10 The PWM stage.....	101
Figure 3-11 The control signal generator. ....	103
Figure 3-12 The 16x16 array pulse encoder internal architecture.....	106
Figure 3-13 The 16x16 pulse encoder ASM diagram.....	107
Figure 3-14 Internal structure for the 90x90 micro-LED controller .....	110
Figure 3-15 The 90x90 pulse encoder ASM diagram,.....	111
Figure 4-1 Chapter Four overview. ....	114
Figure 4-2 Experimental setup for Optoelectronic Neural Stimulation.....	115
Figure 4-3 The experimental setup with USB to SPI interface. ....	116
Figure 4-4 The MCP2210 SPI timing. ....	117
Figure 4-5 Dual spectrum image simplification .....	119
Figure 4-6 The IR preparation pathway. ....	120
Figure 4-7 The detailed IR scene exponentially adjusted. ....	121
Figure 4-8 The visible preparation pathway. ....	122
Figure 4-9 The difference of stimulator output. ....	123
Figure 4-10 The outputs of the bipolar cells and the reconstructed image.....	124
Figure 4-11 The analogue and digital spike coding.....	126
Figure 4-12 Direct and even power distributions for the 64x64 Lena image. ...	128
Figure 4-13 The power versus different array sizes .....	129
Figure 4-14 The power distribution for the 64 x64 Lena image.....	130
Figure 4-15 The power distribution for the 64 x64 Lena image.....	132

Figure 4-16 The current drawn by the optoelectronic micro-LEDs .....	133
Figure 4-17 The current drawn by the optoelectronic micro-LEDs .....	133
Figure 4-18 The current drawn by the optoelectronic micro-LEDs .....	134
Figure 4-19 Four possible even PWM states. ....	135
Figure 4-20 The number of clock cycles versus array utilization.....	136
Figure 4-21 The percentage of filling array versus the percentage .....	137
Figure 4-22 The energy utilization of the neural stimulator .....	138
Figure 4-23 The number of clock cycles versus the array utilization.....	139
Figure 4-24 The power meter with different mismatch measurements. ....	142
Figure 4-25 The measured illumination for different operating voltages .....	143
Figure 4-26 Optoelectronic LEDs mismatch. ....	143
Figure 4-27 Optoelectronic LEDs intensities.....	144
Figure 4-28 Two patterns: (A) Smiling face (B) Star .....	144
Figure 5-1 The visual prosthesis processing stack. ....	148
Figure 5-2 The completed parts of the optogenetic retinal prosthesis framework. .....	149

## List of Tables

Table 1-1 Summary of the major retinal diseases.....	23
Table 1-2 Groups working on visual prostheses .....	34
Table 2-1 Light spectrum comparison.....	46
Table 2-2 The differences between visible and infra-red images.....	52
Table 2-3 Modes of operation for the 16x16 $\mu$ LEDs Array.....	73
Table 2-4 The four different mode operations.....	74
Table 3-1 Comparison between different implementation platforms. ....	81
Table 3-2 The FPGA used resources with maximum frequency and power .....	93
Table 3-3 Comparison between the CPU/FPGA processing time.....	93
Table 3-4 The FPGA used resources .....	104
Table 3-5 The FPGA used resources .....	108
Table 4-1 The Min_F_Trans calculated and actual measurements. ....	117
Table 4-2 The four possible states.....	131
Table 4-3 The FPGA used resources .....	140



# **Chapter 1 Medical Background and Literature Review**

## **1.1 Chapter Overview**

The old adage “A picture is worth a thousand words” reflects the importance of vision in our life. Large amounts of the information that we receive comes through our eyes, so great care must be taken in the treatment of our eyes. The human eye takes the light reflected from objects and converts this light to electrical signals, and then these signals are sent to the brain for visual perception.

Extreme visual impairment is considered to be one of the most feared disabilities around the world. Several conditions may cause it; certain illnesses such as cataracts can be treated surgically, and in some cases pharmaceutical interventions are possible. Most untreatable visual impairment conditions come from retinal disorders. These retinal disorders can be divided into two categories; firstly, disorders where patients suffer from a loss of visual acuity such as Age-related Macular Degenerations (AMD), and secondly disorders where patients suffer from a reduction in the overall visual field such as Retinitis Pigmentosa (RP).

Nowadays, there is strong interest from researchers seeking solutions to these untreatable retinal disorders. Such solutions involve gene therapy, retinal transplantation and visual prosthesis. Some of these solutions can be useful for patients who still have some residual vision. Others, like the stem cell transplantation and prosthetic vision, can be useful for those who have no residual vision. Most of these techniques are still under research and they face considerable challenges and it could take many years before these new developments lead to available treatments. Despite this, there are some promising outcomes from the prosthetic vision approach. Patients with such systems can now detect large moving objects and patterns.

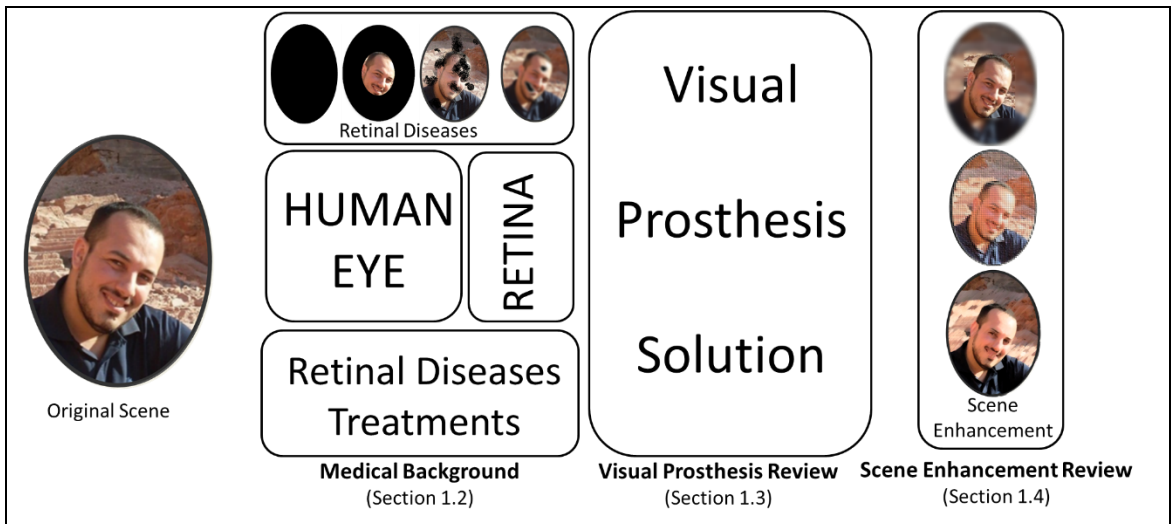


**Figure 1-1** Chapter one starts by describing the eye and retina, the diseases and possible treatments, and then moves to a review of visual prostheses as a solution to some retinal diseases, and concludes with a review of scene enhancement algorithms

A summary of this chapter is shown in Figure 1-1, where in Section 1.2 the human visual system is described, with detailed information about the eye. The most important eye part, from a visual prosthesis view, is the retina and this is discussed completely, including its layers, disorders and possible aids and treatments. Section 1.3 reviews the current available visual prosthesis approaches and their respective advantages and limitations. In Section 1.4, the vision enhancement technique is presented as an alternative solution for coping with the low vision problem. Section 1.5 concludes the chapter and introduces the next chapter.

## 1.2 Medical Background

In this section the medical background and the anatomy of the human visual system is described from an engineering point view. This important background is useful to fully understand the specifications and requirements of the project, so an overview of the human visual system is introduced, focusing on the eye as a sensing organ. The eye consists of different parts, perhaps the most complicated of which is the retina. The most detailed description is given of this, including its diseases, as it is the main interest of this thesis. Following this, there is a consideration of a number of possible treatments for these diseases, such as visual prosthesis treatment, as it could be a solution for some severe eye diseases.

### 1.2.1 Human Visual System

The human visual system is one of the most complicated sensory systems in nature. In humans, vision is the main way of gathering information from the surrounding world. The human visual system consists of the eye, optic nerve, lateral geniculate nucleus and visual cortex, as shown in Figure 1-2. The chief function of the eye is to translate patterns of light into neural signals, and these are then sent to the visual cortical areas of the brain, which extract the intended visual information from them.

In the human visual system, the eye receives the pattern of light and converts it into neural signals, which are initially processed by the retina, and then travel via optic nerves to the lateral geniculate nucleus (LGN). This is considered a place for the relay of visual information from the retina. From the LGN, the signals continue to the visual cortex, where further visual processing takes place for visual perception.

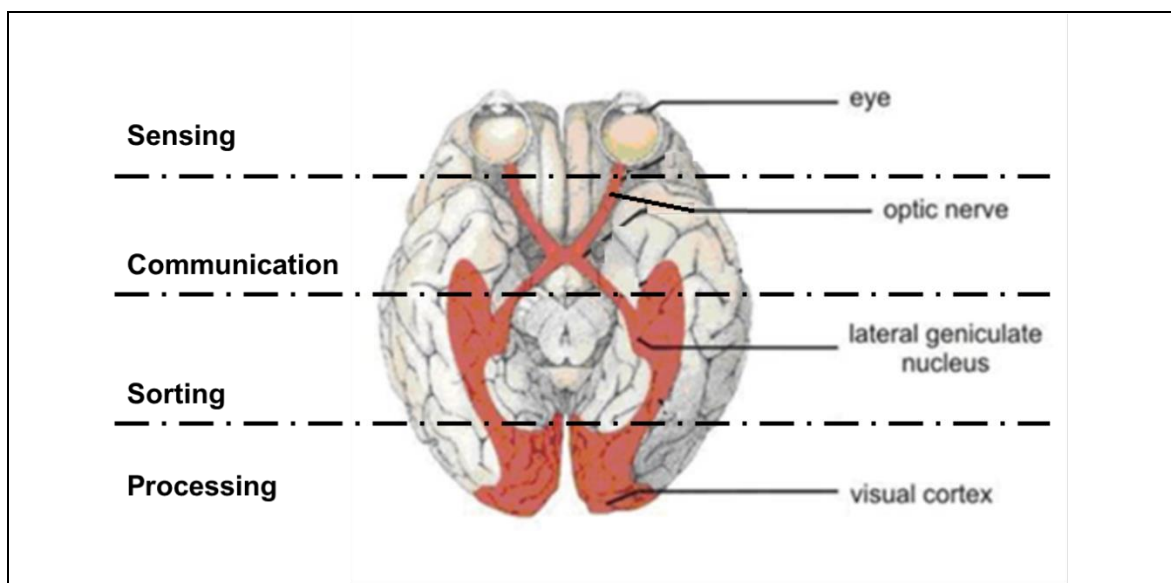


*Figure 1-2 Cross section of human visual system, showing the main components of human visual system with functionality [1]*

### 1.2.2 The Eye

The human eye from an engineering point of view is considered the visual system transducer. It has an optical system which collects light and focuses it through the cornea and lens onto photoreceptors. These photoreceptors are light-sensitive neurons that convert the light into electrical signals, and are part of a thin layer of neural tissue called the retina. Other functions of the retina are to process these signals and communicate with the next part of the human visual

system. Figure 1-3 displays a cross section of the human eye [2], with the main parts of the human eye listed below:

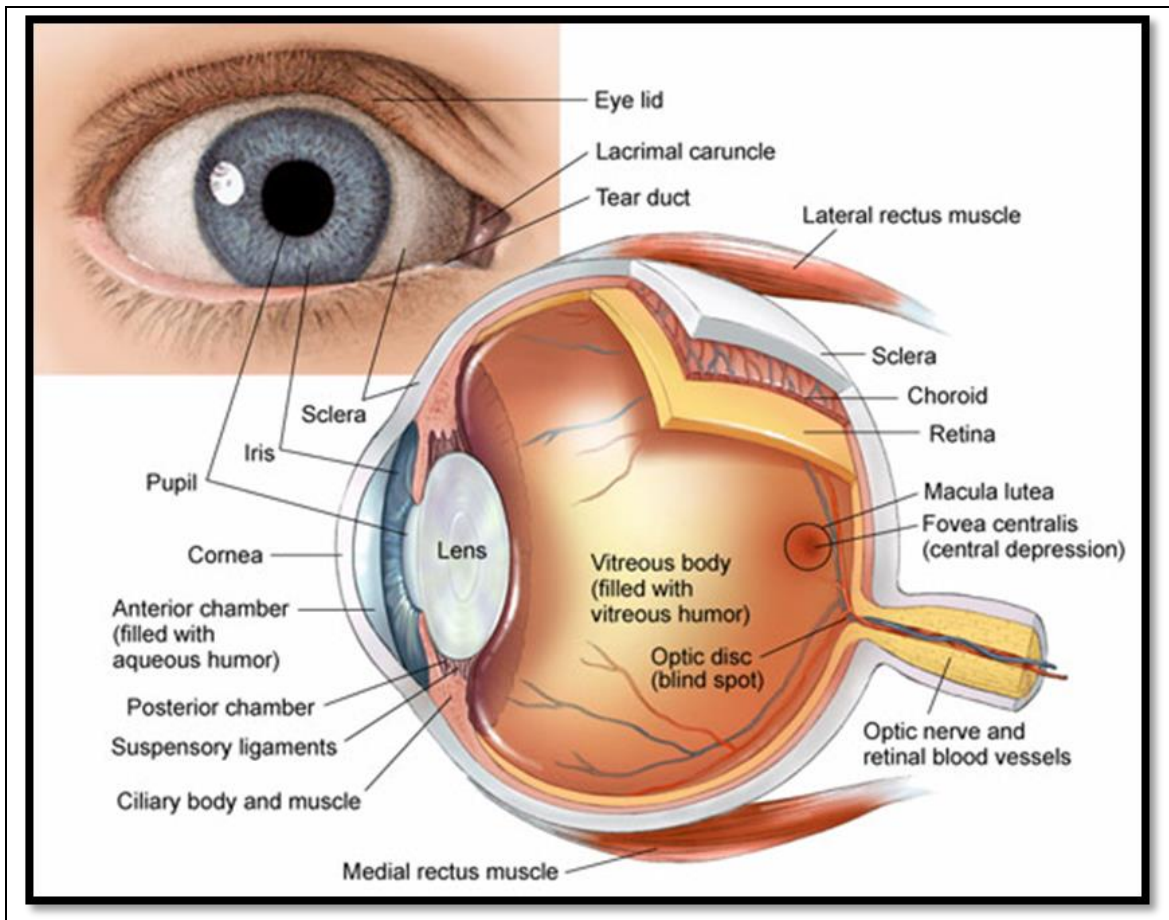


*Figure 1-3 Schematic cross section of the human eye, showing its main components and their corresponding positions inside the eye [3]*

**The pupil:** a black-looking hole, which allows light to enter the eye.

**The iris:** surrounds the pupil. It is a circular, coloured muscle that changes the size of the pupil so more or less light is permitted to enter the eye.

**The cornea:** shields both the iris and pupil. It is a strong transparent membrane, and allows a sharp image to be formed on the rear of the eye (retina).

**The lens:** transparent tissue, consisting of many fibres behind the iris. It is suspended by muscles that contract and relax to change the shape of the lens by a method named accommodation. This method allows humans to form a sharp image on the retina.

**The retina:** a photosensitive tissue resides in the back of the eyeball. The retina is considered the photo-sensing element and the first processing layer in the

visual process. This makes it one of the most essential elements in the human visual process, as will be discussed further below.

**Fovea:** part of the retina, which is responsible for sharp vision.

### 1.2.3 The Retina

The first processing layer in the visual system is the retina, which is placed at the back of human eye; it is a very important light sensitive layer. The retina has three main functions: sensing the light and converting it into an electrical signal, doing simple processing, and communicating with the next visual system part. Physically, the retina is composed of many layers. A simplified cross section of the retina layers with their main functionality is shown in Figure 1-4. After the eye receives light and focuses it onto the retina, it must travel through all the layers of the retina before reaching the photoreceptors. The receptors are linked to bipolar cells, where simple filter processing happens, and the latter cells synapse with retinal ganglion cells. These ganglion cells are essential because the axons transmit information from the eye to the optic nerve.

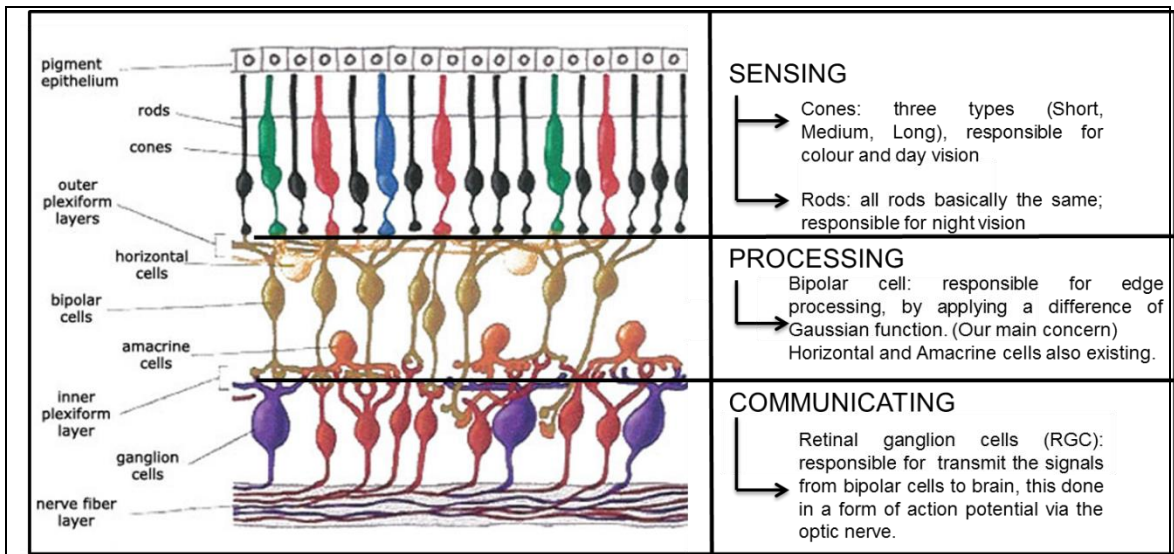


**Figure 1-4 Cross-section of the retina.** The light arises from the bottommost section of the figure and travels through the retina before reaching the eye photoreceptors [4]

Firstly, the sensing layer contains two forms of photoreceptors, rods and cones. Rods are all basically the same, as they all contain the same photo pigment, which has to react appropriately to dim light, and so they are very useful for night vision. The cones, which are concentrated in the fovea, are responsible for colour and day vision. There are three types of cones, based on the photo pigments that they are sensitive to. Blue cones are mostly sensitive to short wavelengths, green

cones are mostly sensitive to middle wavelengths, and red cones are mostly sensitive to long wavelengths.

Secondly, the processing layer, which has three different types of cells, horizontal, amacrine and bipolar. My work focuses on the bipolar cells, because of their strategic position in the retina, since all the signals originating in the receptors and arriving at the ganglion cells must pass through them. Moreover, bipolar cells are responsible of enhancing the signals received from the photoreceptors [5]. They receive their inputs predominantly from the cones, with some inhibitory feedback from the horizontal cells. Bipolar cells have two main types; ON bipolar cells, which depolarize with decreasing glutamate (increasing photo response) from the connecting photoreceptors, in contrast, OFF bipolar cells hyperpolarize. The synapses surrounding ON and OFF bipolar cells to the retinal ganglion cells generate the *centre-surround* processing phenomena, Which it is characteristics can be modelled in mathematical form as a difference of two Gaussian low pass filters (DoG) [6].

Thirdly, the communication layer, which contains retinal ganglion cells (RGC), they receive the processed information from bipolar cells, and then transmit them into a form of action potentials to the brain via the optic nerve.

The visual information from each eye is transferred from the RGC through two visual pathways; Parvocellular and Magnocellular. The Parvocellular pathway receives signals coming from the cones/bipolar cells, and it is mainly responsible of the colour vision, acuity and feature detection. While the Magnocellular pathway receives signals coming from both rods and cones/bipolar cells. It is mainly responsible of movement, flicker detection, shapes and forms detection and vision at night. In this work, the main concern is the effect of spatial feature enhancement. Thus I modelled the Parvocellular pathway and the non-temporal processing aspects of the Magnocellular pathway.

An additional aspect regarding the retina in human vision is the peripheral and central vision. Peripheral vision is also known as side vision, and is the ability to see things outside the straight line of vision. To accomplish this, it utilizes the rods found outside the fovea, and these are good for detecting motion and night vision but not colour vision. On the other hand, central vision is used for fine, sharp



detailed vision. It utilizes the cones found inside the fovea to accomplish central vision; they are good for colour and fine vision but relatively weak at night vision. The differences between central and peripheral vision are shown in Figure 1-5, where the original scene for a driver is displayed. The central vision is shown in the red circle, which is where the driver focuses, while the outer scene is recognized as peripheral vision.



**Figure 1-5** The difference between central and peripheral vision. Left: the original scene. Right: the driver's central vision that focuses on the road, and peripheral vision, used on the outer scene

A further aspect for the retina photoreceptor layer (rods and cones) in vision is shown in Figure 1-6, where the left part shows the density of rods and cones in the retina, with the vision angle. If a person looks straight at something, it is imaged on the fovea (central vision). Rods are completely absent from the central fovea, due to the fact that the fovea is used for sharp vision, and they are mainly distributed on the outside (peripheral vision). The place that lacks photoreceptors is called a blind spot or the optic disc; this is because the ganglion cell axons and blood vessels leave the eye there. The right part of Figure 1-6 shows three types of vision. Firstly, photopic vision is shown, where the cones are only active if lighting is too bright. Secondly, there is scotopic vision, where the rods are only active if lighting is too dark. Third is mesopic vision, where both rods and cones are active.

Human eye can adjust the vision starting from very dark (the scotopic threshold) up to very bright levels of light (the glare limit), this feature is called the full adaption range. However, in any given time only a smaller adaption level of the full range can be active, due to the change in the values of the threshold (minimum level) as well as the limit (maximum level). Experimental results show that the subjective brightness (intensity as perceived by the human visual system

[7] is a logarithmic function of the light intensity incident on the eye. In Figure 1-6 (Right), a plot of light intensity versus subjective brightness, is shown. The idea behind the large operating dynamic range for the visual system that in certain given conditions, the current sensitivity level, which called the **adaptation level**, may change its starting and ending points. For example in Figure 1-6 (Right), the short intersecting curve characterises the **adaptation level** range of subjective brightness the eye can perceive.

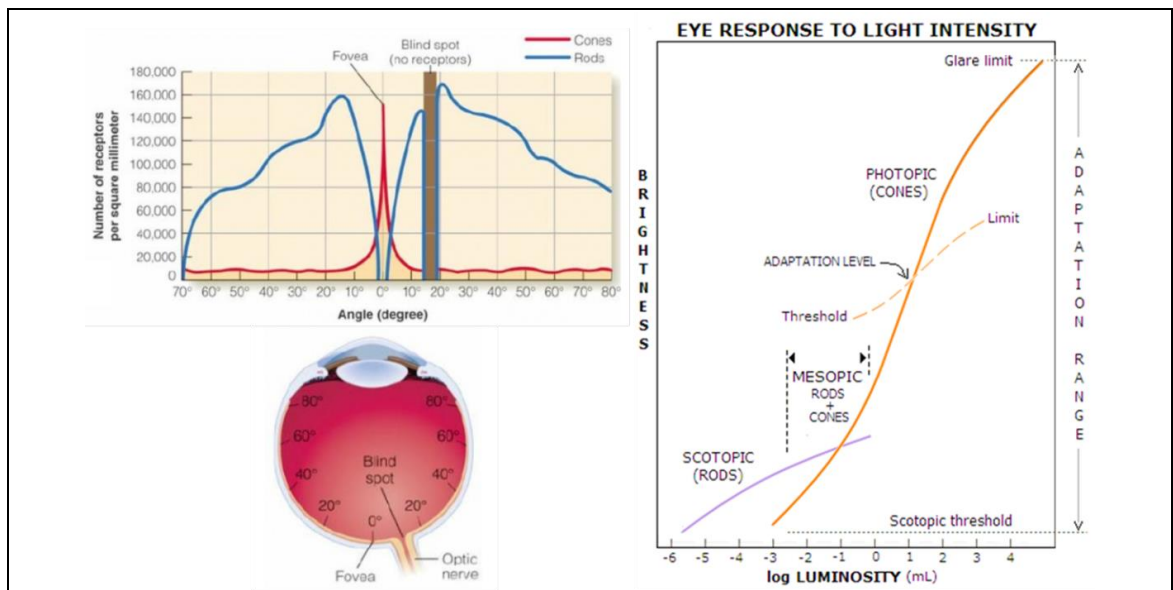


**Figure 1-6 Rods and Cones.** Left: The distribution of rods and cones across the retina. Right: The range of subjective brightness sensations, showing the adaptation level [7]

### 1.2.4 Retina Diseases

There are many eye diseases that may affect the human eye. In this work, the target is visual prostheses, especially the retinal prosthesis. Thus, the focus here is in the conditions that affect the photoreceptor layer (retinal prosthesis), or leave the visual cortex intact (cortex prosthesis).

#### A) Age-related macular degeneration (AMD)

There are two types of AMD, wet and dry, as shown in Figure 1-7. This disease affects the macula, which is the part of retina used in central vision. It causes an initial loss of central vision which may then advance to a total loss of vision and blindness, usually with people 60 years and above [8, 9].

- Dry AMD: in this case the retinal pigment epithelial layer will atrophy which in turn will affect the photoreceptors, causing a loss of central vision. About



85% of AMD is classified as dry. Young people under twenty years old are affected by a disease called Stargardt [10], which is the name of an inherited form of dry macular degeneration that affects the photoreceptor layer.

- Wet AMD represents 15% of patients with AMD. In wet AMD, new irregular blood vessels start to rise and leak underneath the macula. This causes the retinal layer to bubble under the macula, so the photo receptor cells degenerate.



**Figure 1-7 The effect of macular degeneration.** Left: normal. Middle and right: the image as a subject with dry and wet AMD, respectively, will see it. The blurring effect on the periphery of the image simulates peripheral vision

## B) Retinitis Pigmentosa (RP)

RP is the name of an inherited retinal disease that degenerates the photoreceptors [11, 12]. The degeneration starts in the sensitive cells of the outer layer (rods), causing night vision difficulty. This progresses to tunnel vision, where a person can only see a small central area, as shown in Figure 1-8. In advanced cases, the cones also degenerate, eventually leading to total blindness.

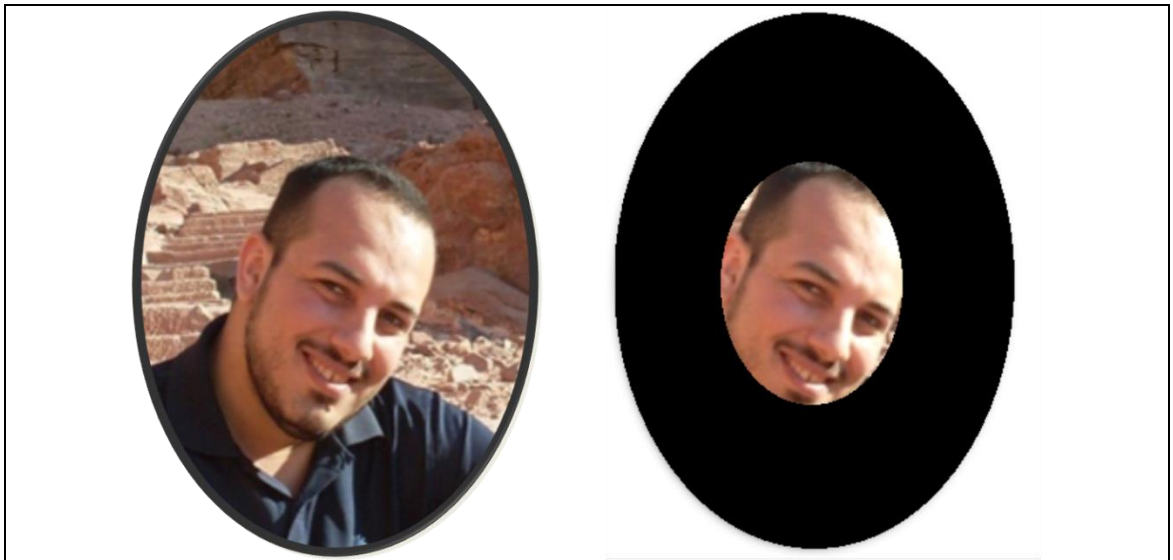


**Figure 1-8 The tunnel vision effect.** Left: normal. Right: the image as a person with a restricted field of view (tunnel vision) will see it

C) Diabetic retinopathy:

Diabetic retinopathy is one of a group of disorders arising from diabetic disease. It causes damage to the blood vessels in the retina, which causes blood to leak into the centre of the retina. These blood spots float in the patient's retina, which results in gaps in some areas of vision (black spots). Other symptoms include flashing light, double vision, restricted peripheral vision and poor night vision. Figure 1-9 gives an example of the effect of diabetic retinopathy on a normal image.



**Figure 1-9 The effect of diabetic retinopathy disease.** Left: normal. Right: the image as a person with retinopathy will see it

#### D) Glaucoma

Glaucoma is one of a group of disorders caused by high internal eye pressure [10]. The increased pressure can affect vision by optic nerve damage, which includes a loss of retinal ganglion cells. If left untreated, this leads to total blindness, due to loss of the retina communication layer. Symptoms include intense pain, redness of the eye, and finally total loss of vision.

#### E) Trauma

Eye trauma is the shock caused by an injury to the eye, which can result from physical shock from a stone or glass, or a direct chemical blow . The effects of eye trauma vary from minor injury to total blindness. In the latter, the whole retina layers are affected as far as the optical nerve.

Table 1-1 summarizes the different retinal diseases, with the most suitable visual prosthesis, and a detailed discussion of different visual prostheses is introduced below.

*Table 1-1 Summary of the major retinal diseases*

<b>Disease</b>	<b>Possible Treatment</b>	<b>Affected retinal layer</b>	<b>Visual prosthesis</b>
AMD	Drugs for wet AMD but no treatment for dry AMD	Photoreceptor layer	Retinal prosthesis
RP	No treatment currently	Photoreceptor layer	Retinal prosthesis
Diabetic Retinopathy	Drugs, laser surgery	Photoreceptor layer	Retinal prosthesis
Glaucoma	Drugs, surgery	All retina layers	Cortical prosthesis
Trauma	No treatment currently	All retina layers	Cortical prosthesis

#### **1.2.5 Retina Diseases Treatment**

Having focused on retinal diseases, this section now moves on to the treatments for these diseases. There are a large number of treatments and aids that may be helpful for visual disorders, ranging from patients with a partial loss of vision (low vision) to total loss (blindness). The treatment starts for low vision patients by using a stick and guide dog, and then patients can take the benefit of low vision aids. This progresses to taking drugs to slow down or prevent some cases from

developing into worse conditions, and gene therapy. Finally, there is prosthetic vision, where it treats totally blind people; a more detailed description of these treatments is given below.

#### A) Low Vision Aids

Reading is a popular pastime, so finding a comfortable way to read is one challenge for visually impaired people. One possible solution is using the low vision aids, which are devices that assist patients with partial sight. These can be optical, such as magnifiers, or non-optical like large print books or using a software program to magnify or increase the contrast in images.

The best reasonably priced devices are hand-held magnifiers, some of which include reading lamps in order to improve illumination. Reading glasses may be used as an alternative, with improved nose pads, so the nose can carry the weight more comfortably. An additional movable system is a device that is fixed on the reading material and enlarges it, and then it projects the image onto a pair of eyeglasses that the person wears. Another approach for low vision is scene enhancement, which means maximizing the most useful information in the scene, such as object boundaries, over the irrelevant information such as fine detail, textures and noise. This can be done through extracting important information, and then simplifying and enhancing it through different image processing techniques, which then empathizes them in the final output image. Al-Atabany has provided an application of scene enhancement algorithms [13], by applying a nonlinear compression of background texture information, while keeping the edges. The results showed improvements in visibility for subjects in patients with peripheral vision loss. One more example of enhancements for the scenes is Peli et al., who used image filters to enhance the perception of face images [14] by adaptive thresholding, which converts the image into a binary format. Their results showed improvements in visibility for subjects to the patients with central visual loss.

## B) Sensory Substitution

Visual material can be understood and handled in different domains, and then the result can be presented to the patient through other sensory substitution systems. Traditionally, these have been led by tactile systems (e.g. Braille, a long white cane). Recently, Segond et al. [15] developed a tactile vision substitution system that changes images into a 'tactile matrix' in touching base with the skin. A different means of visual interpretation can be achieved using the tongue as a substitution sensor for vision. Bachy-Rita [16] and Kupers [17] developed a camera-tongue display device to convert captured images into vibrations through an elastic cable with an array of electrodes to be sensed by the tongue. Results illustrate that patients still need to rely on a guide dog or a cane while navigating or walking. Additional substitution systems have relayed visual information to the auditory system, like Peter Meijer's vOICe system [18], this system depends on converting the visual sense into voice information that can be heard by the blind person. Another application for helping eye disorders is presented in [19], where a low-cost system is used to help visually impaired patients, by implementing a prototype of complete real time vision enhancement system for viewing the television.

## C) Gene Therapy

Gene therapy is a technique that makes uses of defective genes replacement to treat disease. Today, researchers have identified most genes that contribute to retinal degeneration, specifically for inherited eye disorders such as RP. The idea now is to replace the defective gene with one that is not defective. The first human medical experiments of gene therapy for RPE65, which is an important gene to convert dietary vitamin A into useful form for vision, have shown promising initial results [20]. However, gene therapy can prevent sight loss in young patients but cannot bring back lost vision.

## D) Retinal Cell Transplantation

Previously, solving severe corneal disease had been accomplished through cornea transplantation using an embryonic stem [21]. However, using stem cells for retinal disease is still under trial. In general, the transplanted stem cells need healthy cells in order to grow and join with

the existing healthy cells to improve overall vision. The procedure in the retina is quite complex, as new retina cells need to begin complex networks within each other [22]. Recently, the late Dr. Sasai's team at the RIKEN research institute in Japan succeeded in growing a mouse retina cell in three dimensions from embryonic stem cells [23]. However, although transplantation of retinal cells has presented some optimistic outcomes in animals, it may be some years before it becomes a clinical therapy [24]. Indeed, the process is still in the initial stages of investigation in research laboratories.

#### E) Prosthetic Vision

In visual prostheses, the visual information is processed by the retina and transmitted through visual pathways to the visual cortex through the optic nerve, so visual prostheses can be classified into three main classes:

- Retinal: this is suitable when some parts of the processing (bipolar) or communication (retinal ganglion cell) retinal layers are still functioning properly.
- Optic nerve: this is suitable when a significant number of ganglion cells are still active and their axons form the optic nerve.
- Cortical: this is required when all the retinal layers and the optic nerve axons are no longer functioning.

### **1.3 Visual Prosthesis Review**

Worldwide there are many research teams developing an artificial vision system called a "bionic eye," with the aim of returning some visual attributes to the blind [25]. The approaches of different teams vary but all have a common point, which is that they all need a system that converts real world scenes into electrical pulses. These stimulate nerve cells in the visual pathway, resulting in real world scenes formed in the visual regions of the brain. How this image can be utilized in order to understand the scene depends on the amount of information that the electronic pulses carry.

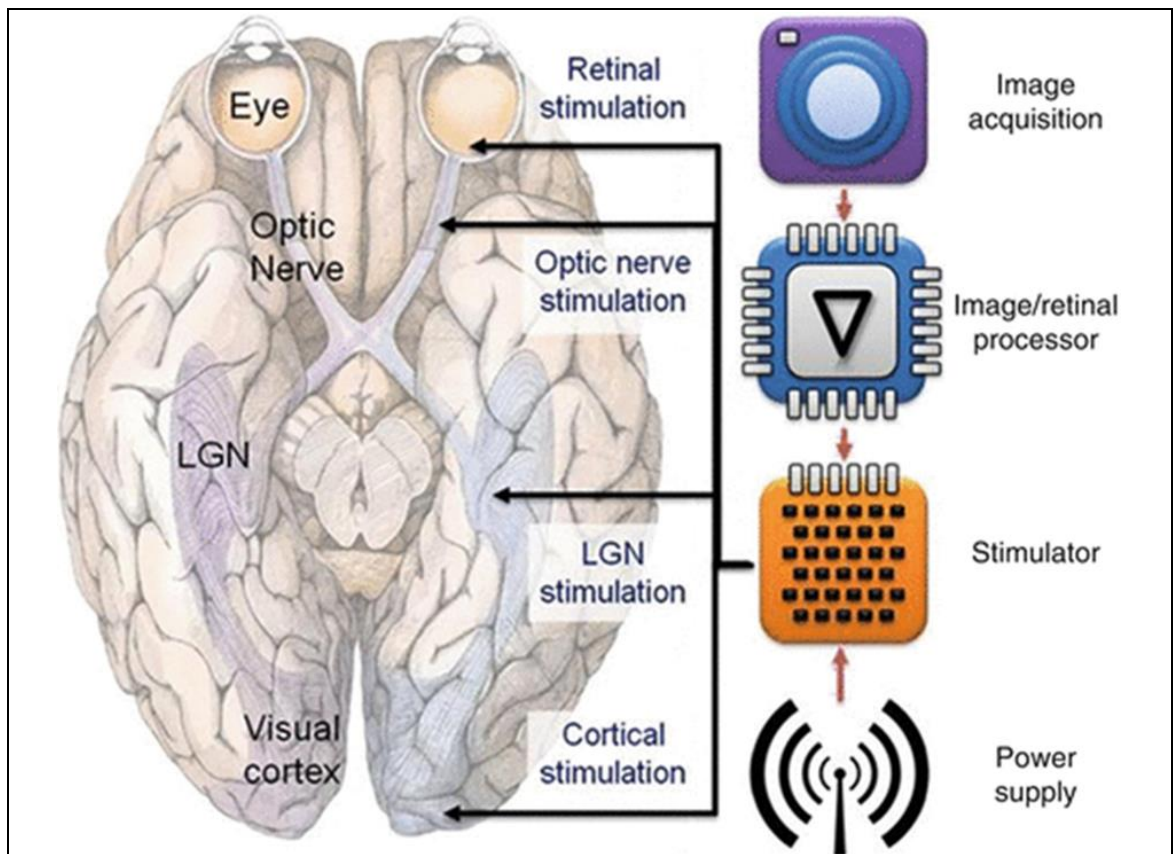


**Figure 1-10 The idea of a visual prosthesis.** It consists of four main parts: a) image acquisition, b) processing, c) stimulator and d) the power supply. The main difference with the teams is where to place the stimulator [26]

Figure 1-10 shows that the main components of the visual prosthesis system are: first, an input which is typically a camera that records the real world scenes. Second, a signal processor is used to process the scenes captured by the camera, to a suitable output form. Third, the output stimulator, which usually comes in the form of electrodes or an LED array, depends on the prosthesis type. A power supply is needed for prosthesis system operation.

In Chapter 2, a complete description of each of these components is presented. Teams working in this area are mainly different in the place where they implant the stimulator in the visual pathway, and Figure 1-11 shows the possible places for the prosthesis.



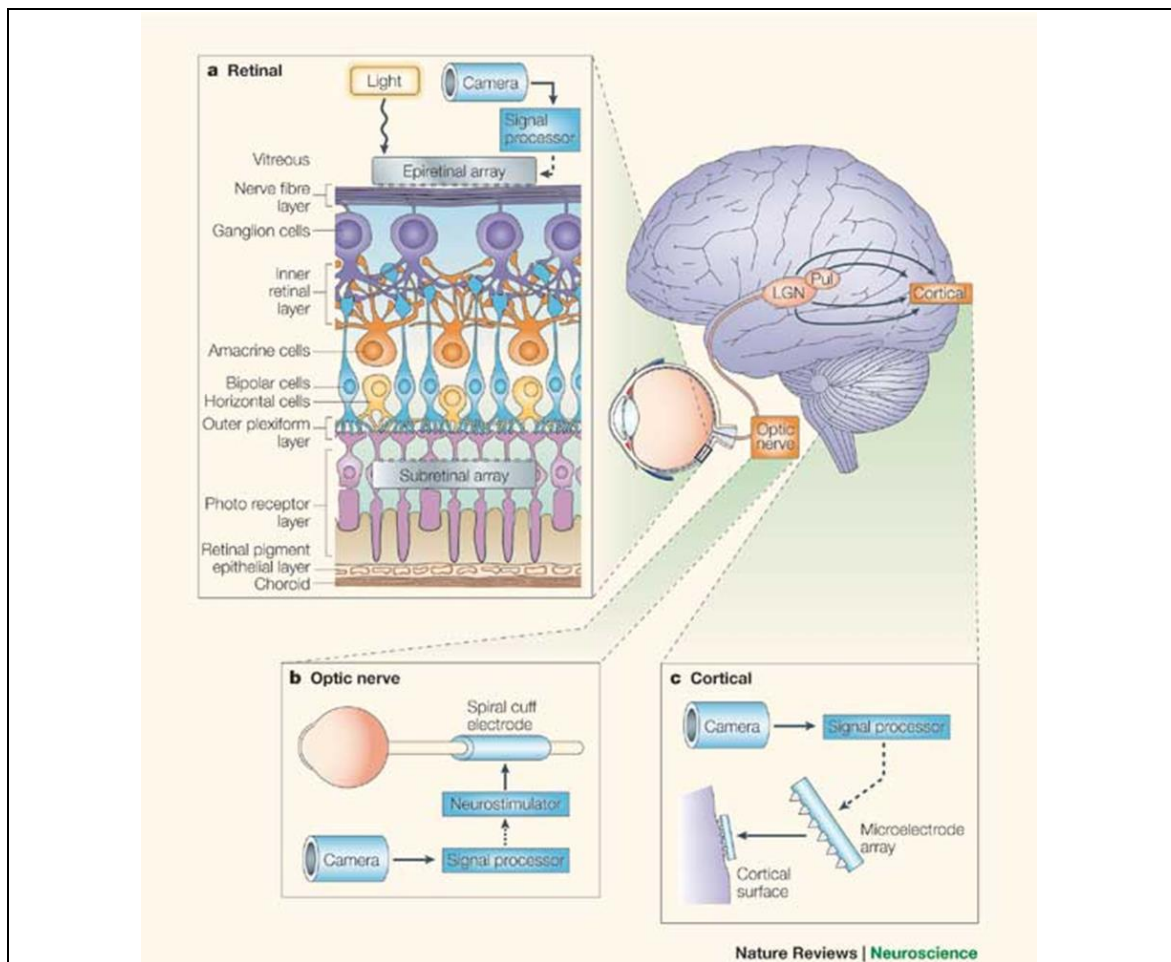


**Figure 1-11** A summary of different approaches to the visual prosthesis [27], where the visual prosthesis can be in one of the following places in the visual system: a) Retinal prostheses have a micro-LED array implanted in the retina, b) Optic nerve prostheses have electrodes implanted in the optic nerve and c) Visual cortex prostheses have electrodes implanted in the visual cortex

Visual prostheses can be classified into three main types: retinal, optical nerve, and visual cortex. This classification is based on the location of the implant. Retinal prostheses can be used for cases where the photoreceptor layer in the retina is degenerated but other layers are still functional. Optic nerve prostheses are an intermediate solution between the retinal and cortical prostheses; it can be used when a significant number of ganglion cells are still active and their axons come together to form the optic nerve. Cortex prostheses can be used when all retinal layers are degenerated. A detailed discussion of visual prosthesis types now follows.

### 1.3.1 Retinal Prostheses

A retinal prosthesis is a biomedical implant technology for the retina, used to return some useful vision to patients who have lost their vision. Retinal prostheses can be categorized further into two forms:



- **Electronic Retinal Prosthesis**

An array of electrodes is inserted into the retina by either subretinal or epiretinal approaches. Figure 1-11 shows the positions of both the subretinal and epiretinal implants inside the eye.

The subretinal implant uses light-sensitive micro-photodiodes which are inserted between the pigment epithelium layer and the outer layer of the retina, which contain the photoreceptors. The function of the light-sensitive micro-photodiodes is to replace the cones and rods with photodiodes. One benefit of subretinal implants is that we replace only the damaged photoreceptors, and other retinal pathways and the natural neural network of the eye is unaffected, thus keeping suitable spatial encoding [28-31]. Examples of subretinal implants include the 1,500 electrodes developed by Zrenner et al. [32-34], which were implanted in the foveal rim of two RP patients. Results showed that patients were able to detect some dots and simple patterns and read large European characters. In another example, the Daniel Palanker group at Stanford University developed a subretinal photodiode array system for visual prostheses that includes an infrared image projection system fixed on goggles. Data coming from a video camera is processed in a small PC and then displayed [35, 36].

Epiretinal electrode array is inserted into the top layer of the retina, where the retinal ganglion cells are found. It bypasses the whole retinal processing so the processing unit must perform suitable image encoding [37-39]. Because it does not need any remaining active layers of the retina, the epiretinal approach needs to encode the visual information into a series of electrical pulses before sending them to the ganglion cells. This requires pre-processing the acquired scene, to simulate and encode the functions of the degenerated retinal data processing layers [40]. An example of an epiretinal implant is that of the Second Sight team [41, 42], in the Doheny Eye Institute (University of Southern California), where 16 electrode arrays were implanted in six patients. Patients were able to distinguish the direction of motion; furthermore, they had the ability to distinguish between simple shapes created with different electrodes. The next phase of the Second Sight team involves devices with 60 electrodes [43]. Research continues in the retinal prosthesis approach to enhance the

overall system by reducing the power consumption and heat generated [44]. This also includes the amount of information transmitted to the electrode grid, after applying some image processing techniques to mimic the processing of the retina [45].

Many technical problems such as power consumption, surgical damage, heat dissipation, and the biocompatibility involved in physically touching the neurons [46] can be tackled. A further problem is the spatial limitation of the subretinal and epiretinal implants, and although electrode grid implants have been developed, there is still a limitation of the electrode grid size due to the spherical shape of the eye. Problems will increase with higher grid sizes as the electrodes get smaller.

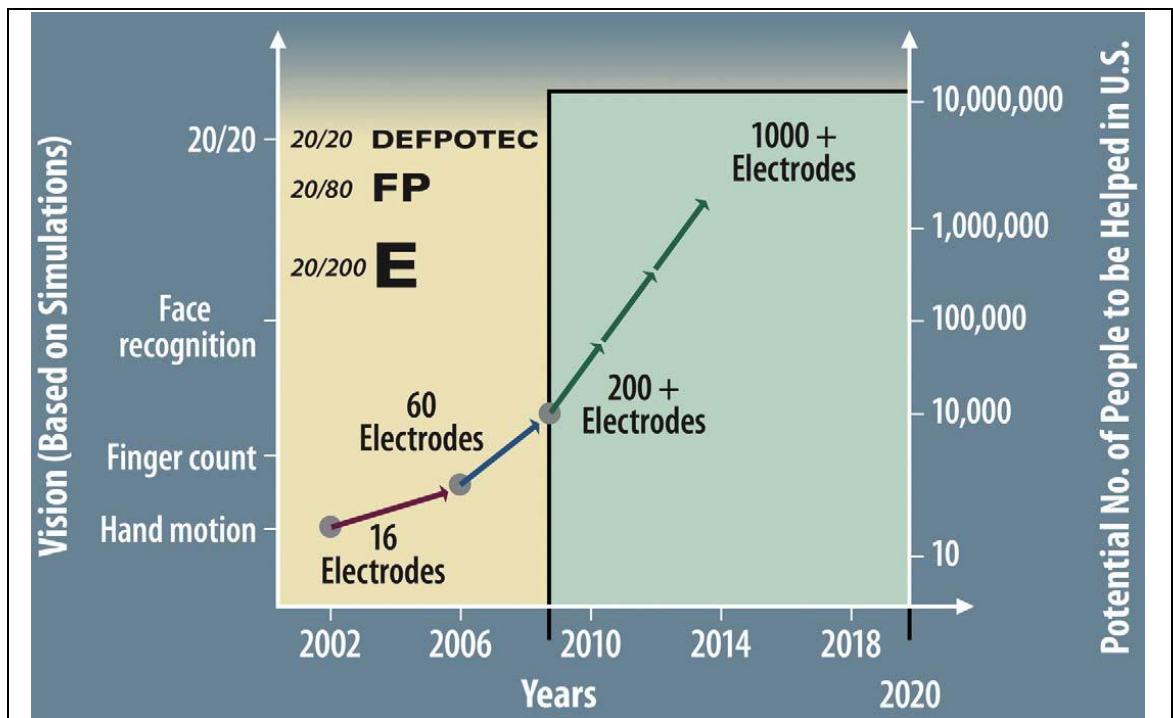


Figure 1-12 Timeline for the progress of the retina prosthesis programme [47]

A survey of the current and future prospects of different kinds of retinal prosthesis was carried out by Chader et al. [47] in 2009. According to the survey, the outlines of the progress of the retina prosthesis programme are as shown in Figure 1-12.

- Optogenetic Retinal Prostheses

This new approach, arising from the field of neuroscience, is called optogenetic and started in 2003 with the discovery of a protein called

channelrhodopsin [48]. It is injected into nerve cells, and then used as an optical switch that allows the cell to be controlled via light pulses.

To overcome the problems faced by the electrical retinal prosthesis approach, such as limited resolution, the Neurobionics group, previously at Imperial College, and now at the Electronics and Electrical Engineering department, Newcastle University, has developed a novel photo-stimulation technique. In this approach, channelrhodopsin is used to allow the stimulation of an intact layer in the retina with light rather than electricity [49]. To achieve this, a virus that contains the protein is injected into the retina, and then a fitted headset with sufficient brightness control is used to stimulate the target cell layers. Returned vision may be significantly improved over electronic approaches. By doing this, the main retinal prosthesis problem can be overcome, as there is no limitation on the stimulator array size because it is now outside the eye. The group designed two versions of the optical stimulator, the first with 256 LEDs and the second with 8,100 LEDs [50].

### **1.3.2 Optic Nerve Prostheses**

An optic nerve prosthesis is a technology used for stimulating the optic nerve directly. It is a midway solution between the retinal and cortex prostheses. This approach is useful when significant numbers of ganglion cells are still active and their axons come together to form the optic nerve. In this case, the visual information can be induced in this great cluster of ganglion cells at the optic nerve, so the conductive axons can be excited by the stimulus [51, 52]. In 2003, Veraart et al. published the findings of a case study that involved a volunteer who suffered from retinitis pigmentosa with no residual vision. An electrode was attached to an implanted neuro-stimulator and an antenna was implanted around his optic nerve. The electrical activation for the optic nerve was done via an external controller with telemetry, resulting in phosphenes perception. The volunteer wore a head-video camera, then pre-designed simple 45 patterns are displayed on a projection screen. Promising results were found as the volunteer was capable of interacting with the surroundings while doing pattern recognition and orientation perception [53]. The European MIVIP project (1996 to 1999) tested the opportunity to construct a prosthetic device for the transmission of visual information to the optic nerve of a blind patient. In their VISION project, they aimed to help develop an

active nerve electrode as an important element of an optic nerve prosthesis. Quisihi Ren's group made a mathematical model to simulate the main ways underlying the nerve impulse in a rat's optic nerve, and the developed model successfully produced long-lasting stimulation of the optic nerve [54].

The limitation with this is that to achieve high spatial resolution, more electrodes have to be inserted inside the eye. The problem is that to drive these huge numbers of microelectrodes, more power will be consumed, which in turn causes more heat dissipation to the retina, which can burn it.

### **1.3.3 Visual Cortex Prostheses**

A cortical prosthesis is used to stimulate the visual cortex directly; it is used as the last hope for patients who cannot use any retinal prosthesis forms. This is when the communication neurons (RGCs) in the retina are no longer functional, e.g. blindness due to glaucoma or physical injury. The first trials of cortical prostheses started in 1929, when Foerster tested the effects of the electrical stimulation of the occipital lobe of the human cortex [55]. The first human experiment was done on a 52 year old woman in 1968 by Brindley and Lewin [56]. Currently, a number of groups are working on the cortical stimulation approach, where stimulation of the visual cortex is done by powerful microelectrodes. These include a group at the John Moran Laboratories at the University of Utah, where their research focus is on the interface between implanted devices, which could selectively stimulate neurons, and the functioning neurons in the visual pathways. Their interface bypasses the faulty parts in the visual pathway and directly stimulates neural pathways [57]. Another group is CORTIVIS, which is a European research project conducted over the last few years to perform intracortical micro-stimulation [58-60]. The CORTIVIS project objective was to develop models in the field of visual restoration and to prove the feasibility of a cortex prosthesis, as a way through which a limited visual sense may be restored to blind people.

The cortical visual prosthesis is beneficial over other prostheses because it comes over all the visual pathway neurons heading to the primary visual cortex. Therefore, this approach can potentially be used to return vision to the largest number of blind patients.

As a summary of the usefulness of these prosthetic vision approaches according to blindness conditions, the retinal prosthesis approaches seem to be useful for severe visual impairment, or those who have at least some functional retinal ganglion cells (RGCs). On the other hand, for conditions such as diabetic retinopathy and glaucoma, visual cortex and optic nerve prostheses may provide solutions. Table 1-2 summarises the different groups working on visual prostheses.

**Table 1-2 Groups working on visual prostheses**

<b>Visual Prostheses</b>	<b>Country</b>	<b>University</b>	<b>Team leader</b>	<b>List of Ref.</b>
Retinal Prostheses	USA	Harvard Medical School	Prof. Rizzo	[61, 62]
	USA	University of Southern California (Second Sight)	Prof. de Juan, Prof. Humayun, Prof. Weiland	[43, 63]
	USA France	Stanford University (Pixium Vision)	Prof. Palanker	[36, 64]
	Germany	University Eye Hospital Tübingen (Retina AG)	Prof. Zrenner	[65, 66]
	Germany	University of Bonn	Prof. Eckmiller	[67, 68]
	UK	Newcastle University	Dr Patrick Degenaar	[69, 70]
	Japan	Tokyo Institute of Technology	Dr Yagi	[71, 72]
	Australia	University of New South Wales	Prof. Lovell	[73, 74]
Optic Nerve Prostheses	Belgium	University of Catholique de Louvain, Microelectronics Lab	Prof. Jean Delbecke, Dr Trullemans	[75, 76]
Visual Cortex Prostheses	USA	University of Utah	Prof. Normann	[60, 77]
	Spain	University Miguel Hernandez	Prof. Fernandez	[78, 79]
	USA	Illinois Institute of Technology	Prof. Philip Troyk	[80, 81]

## 1.4 Visual Enhancement Review

In this section, some essential visual prosthesis image processing operations are reviewed, and a general description of these operations is introduced. Then, there is a focus on image segmentation operation, which can be done using different methods, so it is important to use the most suitable method for visual prosthesis. Finally, the section reviews the vision enhancement algorithms for visually impaired patients with low vision conditions, and the main aim of these enhancements is to make the best use of the remaining visual sighting for low vision patients.

Image processing operations can be categorised by the kind of information they process; this categorization is referred to as an image processing pyramid [82], as represented in Figure 1-13. Starting from the lowest level where the pre-processing operation includes basic image transformations. There are many examples of pre-processing such as edge detection, contrast enhancement and filtering. Segmentation operations happen at the borderline between the low and intermediate levels. The segmentation is used to identify the objects or regions in an image which have some common properties. There are many examples of segmentation such as colour detection, thresholding and region growing. After segmentation, operations move toward classification, ending with the highest level, where recognition of the description and scene interpretation occurs.

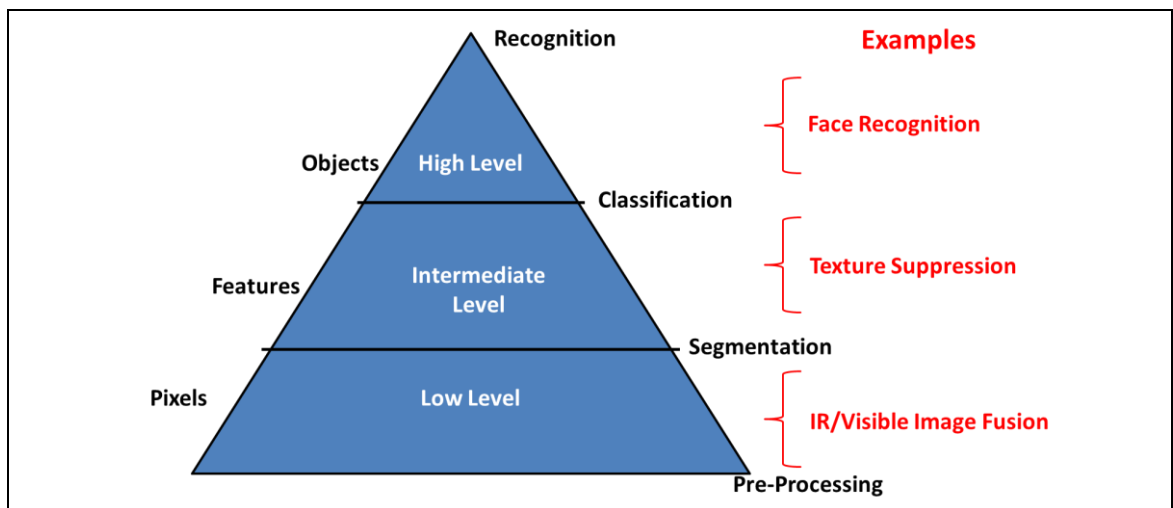


**Figure 1-13 The Image Processing Operations.** The operation is divided into three main levels according to the data with which they are dealing

In this project, the level at which the work lies is the segmentation level, with all necessary pre-processing needed for the image data.

### **1.4.1 General Review for Image Segmentation**

Image segmentation is an essential step in image analysis where the objective is to divide an image into a number of regions. Image segmentation algorithms are based on two properties of intensity values, mainly discontinuities and similarities. Methods based on discontinuities in intensity values identify the images using sudden changes in intensity values. In the second method, groups of pixels of similar values are combined together as one class.

Image segmentation's main goal is to divide an image into multiple similar segments based on colour, texture, boundary, etc., and extract objects that are of interest. There are many different schemes for the classification of various image segmentation techniques [83] [84]. In order to give an overview of image segmentation algorithms as they relate to visual prosthesis, the two main groups are presented next.

- **Thresholding Segmentation**

Thresholding is an easy and simple to implement segmentation technique. A suitable threshold is selected so that the pixels above the threshold are classified into one class and the pixels below the threshold are classified into another. This type of output image is known as a binary image, which is defined as an image where the pixel has a value of 0 or 1. Selecting an optimal threshold is a key challenge faced in the threshold based segmentation technique.

There are many different methods used to select a suitable threshold [85]. For example, the mode method is a type of histogram-based thresholding method. It uses the concept of a valley to calculate the threshold. In this method, the minimum intensity value is selected as the threshold in the valley between the two peaks (background and object). A good example for applying the valley concept is shown in Figure 1-14.



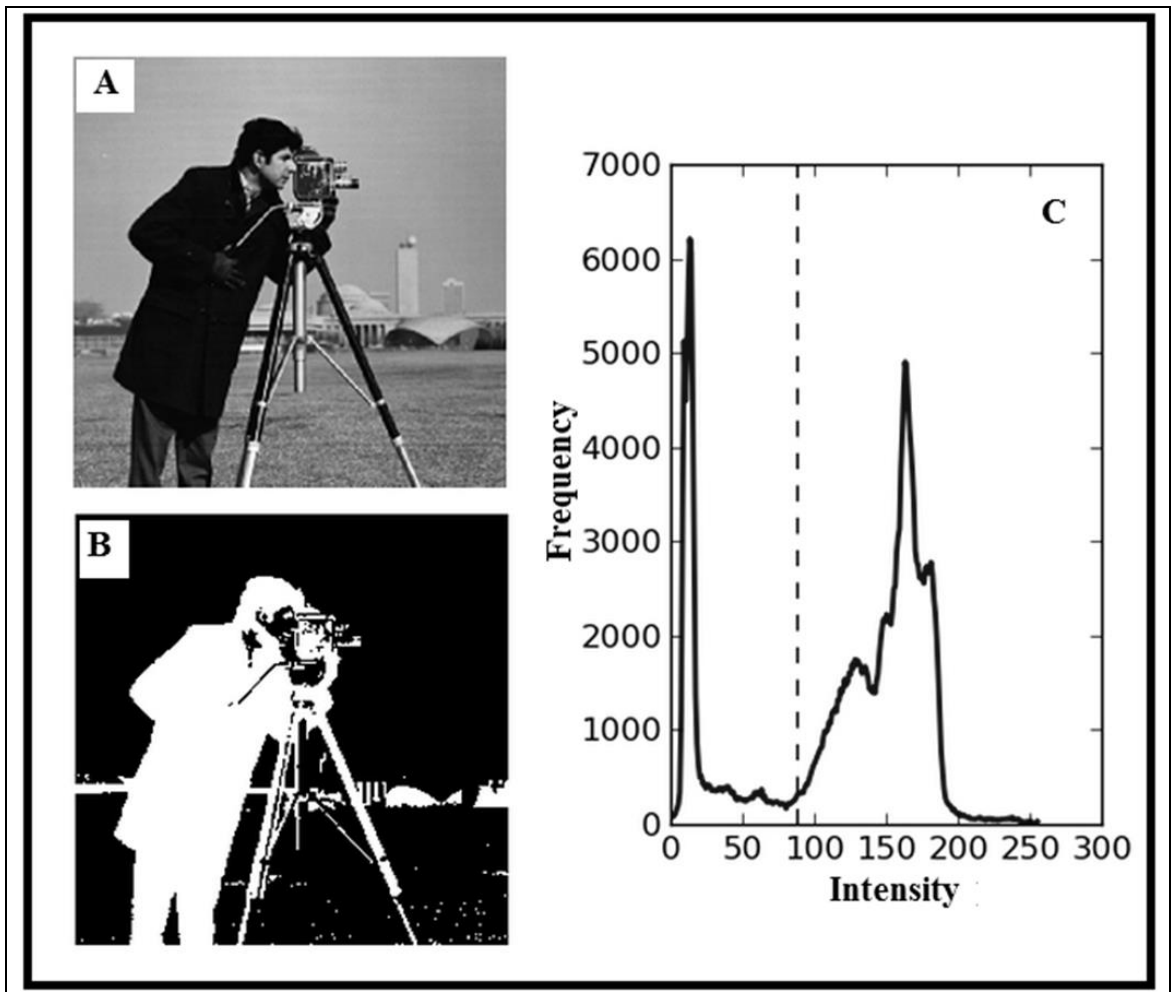


**Figure 1-14 Cameraman Thresholding Segmentation.** (A) Original cameraman image, (B) Binary output image and (C) the histogram for image pixels [86]

Baboon image thresholding is shown in Figure 1-15, where the thresholding was done using the Otsu method and the minimum error method, which are clustering-based methods. The Otsu method uses the variance of the background and object pixels [87]. The optimal threshold is obtained by maximizing either the variance between the two classes or minimizing the variance within the same class. Although an advanced method for selecting the thresholding value is used, in the resulting image many of the original details are removed, since there are no clear borders between the object and background in this image.

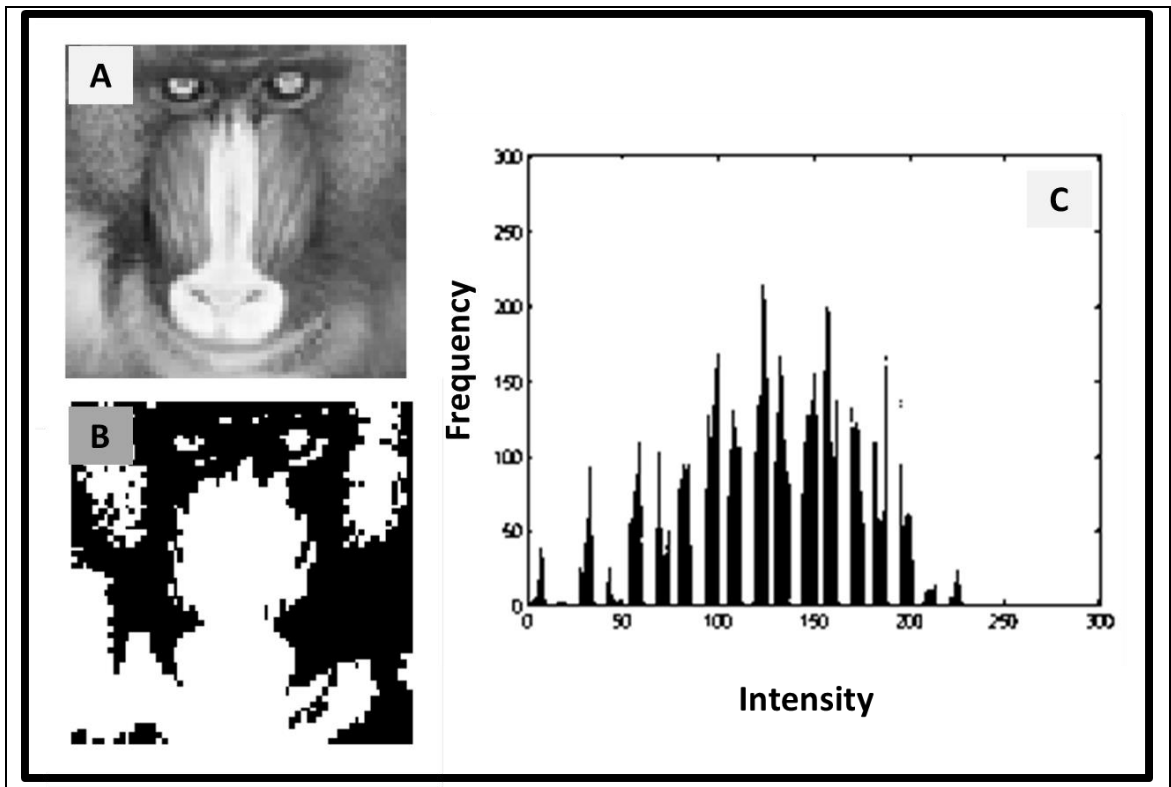


**Figure 1-15 Baboon Thresholding Segmentation.** (A) Original Baboon image, (B) Binary output image after applying the Otsu thresholding method and (C) the histogram for image pixels [88]

The major problem with thresholding is that only the intensities of individual pixels are considered. The relationships between pixels, e.g. gradient, are not taken into consideration. There is no guarantee that pixels identified to be in one object of the image by thresholding are contiguous. The other problem is that thresholding is very sensitive to noise, as it is more likely that a pixel will be misclassified when the noise level increases.

- Edge-based Segmentation

Edge-based segmentation contains a set of methods that depend on information about detected edges in the image. Many methods have been developed for edge detection, but the common aspect with these methods is the use of first order derivatives. The Canny edge detector is an example of first order derivatives [89]. An optimum smoothing filter can be estimated by first-order derivatives of Gaussians. Other popular first-order edge detection methods are: the Prewitt detector, the Sobel detector, and the Roberts's detector, and each of these can be used with different filter sizes. There are also zero crossing-based edge detection approaches, which search for zero crossing points in the second order derivative, as shown in Figure 1-16. Edge-based segmentation algorithms are usually of low

computational complexity, but they tend to find edges which are irrelevant to the object.

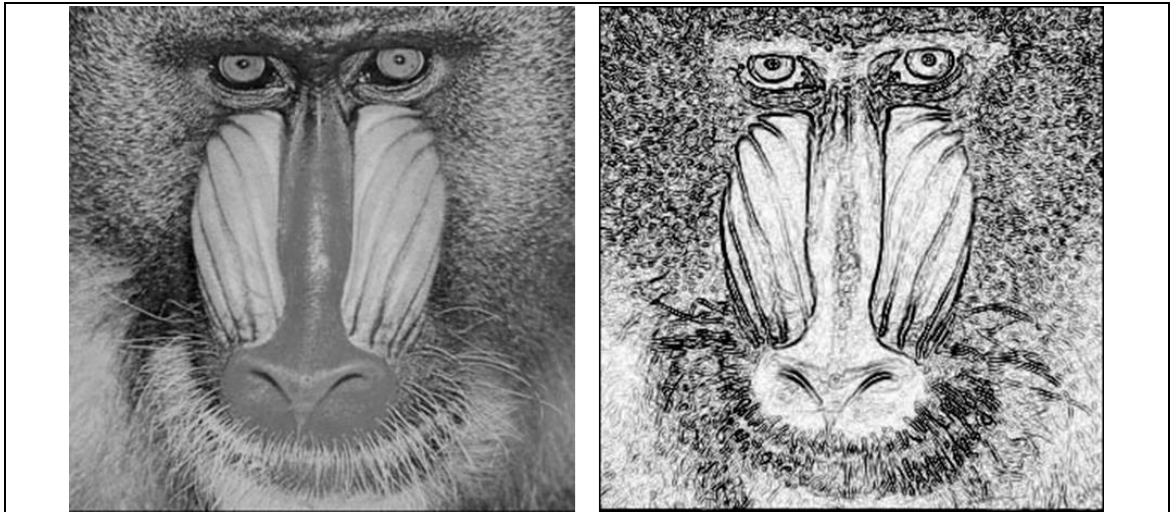


**Figure 1-16 Edge-based Segmentation.** Original Baboon image (Left) Laplacian second order edges (Right) [90]

All of the above methods of image segmentation can be used for specific applications, and for visual prostheses edge-based segmentation is used. It uses the first (Sobel) and second (Laplacian) order derivatives to segment the image, and further the extracted edges are overlaid on the original image. Thus, the main image can be simplified and unnecessary details are removed within these edges. Further details about the vision enhancement process are given below.

#### **1.4.2 Vision Enhancement for Visual Impairments**

Because the research on gene therapy and retinal prostheses is still in its early stages, maximizing the remaining information flows to the visual cortex could benefit patients with low vision conditions. Electronic vision enhancement systems may be able to provide support for low vision devices, if some vision still exists, by imaging the visual scene, processing it, and returning it to the user.

The basic concept is to use head mounted cameras to image the scene and process it, then feedback visual information to allow the user to achieve maximum recognition of the scene.

The first attempt at enhancing the visual information for patients with retinal dystrophy was in 1988 by Lawton, who used image processing filters to enhance words presented digitally to three AMD patients [91]. Results showed that the reading rates were increased two to four times. From enhancing words to real

images, Peli et al. used image enhancement filters to enhance the perception of face images [92]. His filter divided the image into low and high spatial frequency components, separately enhancing both of them and finally recombining them.

In 2007, Wolffsohn et al. carried out an experiment to test the benefit of applying image enhancement algorithms on watching television, as shown in Figure 1-17 [93]. His experiment involved visually impaired participants. The algorithms he used involved overlaying edges on the original scenes using different kinds of edge detection filters.



**Figure 1-17 Television image enhancements.** Left: Original image, Middle: the detected edges and Right: the edges coloured and overlaid on the original television image [93]

Head Mounted Displays (HMDs) play a significant role in developing image processing algorithms for low vision patients. Peli et al. developed a head mounted see-through system for visually impaired AMD and tunnel vision patients [94]. His system is constructed from three parts: an input camera fixed on goggles, a controller to process the captured video, and a display, which shows the see-through scene.

For AMD patients, Figure 1-18 shows on the left the original scene, where people with AMD will have difficulty discerning details at the end of the corridor. In the middle, conventional magnification is used to solve this problem. Although this solution enables the patients to see more details of the distant object, it restricts their field of vision, and as a result the chair (obstacle) cannot be seen. On the right is the Peli solution for this problem, where the edges are extracted and superimposed in the centre of the scene. The advantage of this solution is that the patients still have their wide field of vision.

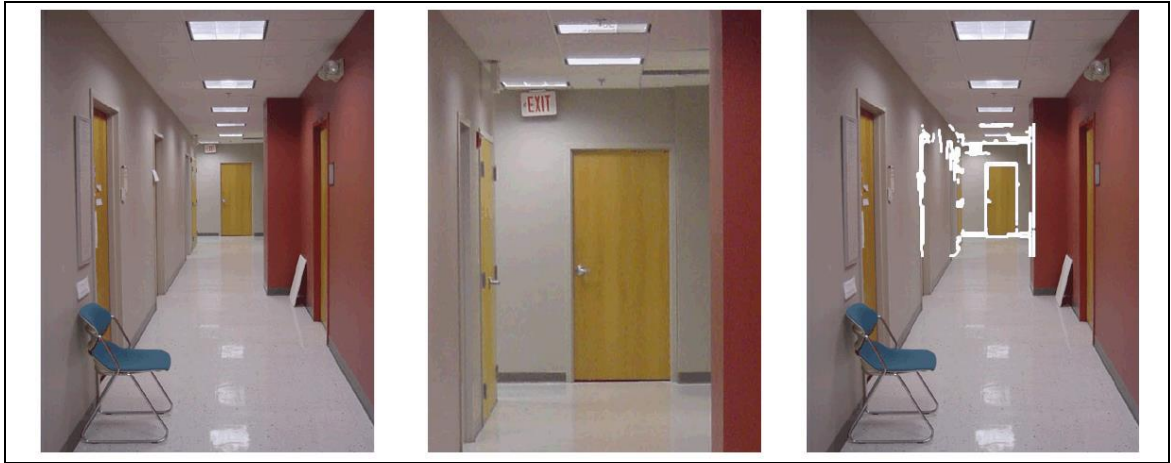


**Figure 1-18** The output of Peli's vision enhancement system (AMD). Left: the original scene. Middle: magnification assists in seeing details of the distant object, but restricts the field of vision. Right: Superimposed edge of resized image enhances visibility in the central area, while the full field of view is maintained [94]

For RP patients, Figure 1-19 shows the original scene on the left. In the middle, a traditional low vision aid solution is shown for tunnel vision patients, where demagnification of the scene is used to solve this problem. Although this solution enables the patients to see more objects, the expense is seeing them smaller. On the right, the Peli solution for this problem can be seen, where the system compresses the scene, and then the latter scene edges are extracted and superimposed onto the original scene. The advantage of this solution is that the patients still have their high resolution and the wide field view edges.



**Figure 1-19** The output of Peli's vision enhancement system (RP). Left: Original scene. Middle: Demagnification assists in seeing the whole field of vision, but losing the high resolution central vision. Right: Superimposed edge images enhance visibility in the central area, while the full field of view is maintained [94]

Bowers et al. carried out an evaluation of a night vision system [95]. The vision system used the vision multiplexing concept, in which a grey scale image was minified and overlaid on the natural view of the scene.

Vargas-Martín et al. [96] used FPGA to develop a portable head mounted aiding system that performs digital image zooming, edge enhancement of the visual scene, and the vision-multiplexing method described in Peli's paper. Toledo et al.

developed an FPGA implementation for Peli's vision-multiplexing method [97]. In his implementation, the final system was able to achieve 60 frames per second for 384x288 frame size.

Al-Atabany [98] [99] presented three image enhancement algorithms to enhance central vision loss: image cartoonization, edge overlaying and tinted reduced outlined nature (TRON) algorithms. These algorithms have been tested on both patients in trials and Al-Atabany retina model. Image cartoonization has been previously defined in the image processing community but Al-Atabany was the leading user of cartoonization on patients with retinal degenerations. In edge overlay, Al-Atabany provided a technique, aimed first, to enhance the segmentation of the important features, such as the edges, and second, to improve the removal of the background textures. As a final point, the TRON algorithm has benefits over edge overlaying only images, which keeps chromatic information. The result of applying these filters is shown in Figure 1-20.

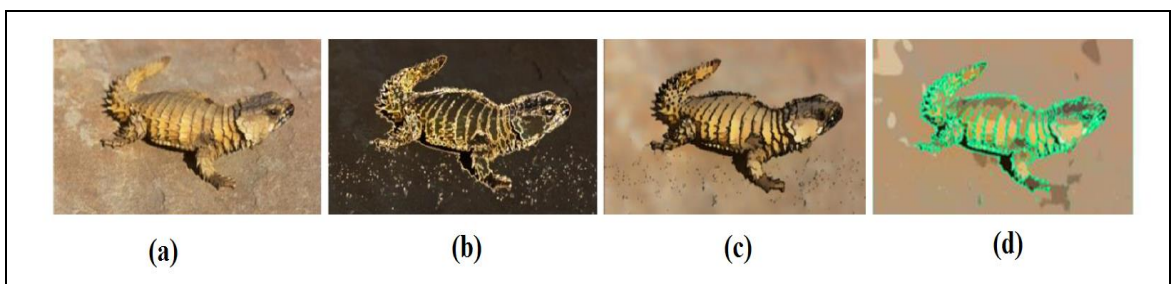


**Figure 1-20 Applying Al-Atabany's different algorithms.** (a) the original image (b) the TRON image (c) the cartoonization image and (d) the Edge Overlaying image [100]

Some of these image enhancement algorithms need to be applied in visual prostheses, because they aim to maximize the useful information in the scene before sending these images to the final output display. Additional details of the operation used in the current project are introduced in Chapter 2.

## 1.5 Conclusion

Some retinal diseases, such as AMD and RP, are still untreatable. Much work has been done to restore vision or stop the progression of impairment, and rehabilitation via visual aids is a near term solution for patients suffering from retinal diseases. This can be via sensory substitution, prosthesis, or enhancement. However, significant challenges face these technologies, such as

spatial resolution limitations, the stability and degradation of electrodes, and surgery complications.

In this chapter, the medical background of the visual system was introduced, starting with the components of the visual system, and then moving on to the eye, especially the retina, retinal diseases and possible treatments. Then there was a review of the field of different types of visual prosthesis. Finally, the field of visual scene enhancement was reviewed.

After this review of the visual system, it can be seen that the visual prosthesis system can compensate for the dysfunctional parts of visual systems that result from some diseases, with the following requirements:

- The input: In the human visual system, the photoreceptors layer senses light, which is then focused by the optical lens, and converted into an electrical signal. In a visual prosthesis, an image sensor with suitable optical lenses is needed to convert the light to an electrical signal.
- The processing: In the human visual system, the scene is processed mainly by the bipolar layer, which then prepares the electrical pulses to interface with the next communication layer. In a visual prosthesis, different levels of processing are needed, like scene simplification. Preparing the electrical signal to interface with the next layer can be done by an image processor unit.
- The output: In the human visual system, the communication layer sends the processed signals to the brain to perform visual perception. In a visual prosthesis, the processed signal needs to be connected again to the visual pathway, and this connection can be done in different places to continue to the brain to perform visual perception. The connection can be electrical through electrodes or optical through LEDs.

In the next chapter, an overview of the full system of optogenetic retinal prostheses is discussed in detail, and each system requirement is introduced in depth.



## Chapter 2 System Level Architecture Design

### 2.1 Chapter Overview

Optogenetic retinal prosthesis is a new approach in the field of retinal prosthesis. In this approach, the retina communication circuitry is re-engineered by injecting a virus into an intact retina layer, and the injection process genetically modifies this layer to become light sensitive. Then an intensive blue light [101] is required to stimulate the photosensitized layer, and this layer can compensate for the photoreceptor layer, which enables patients with retinal problems to have part of their vision returned.

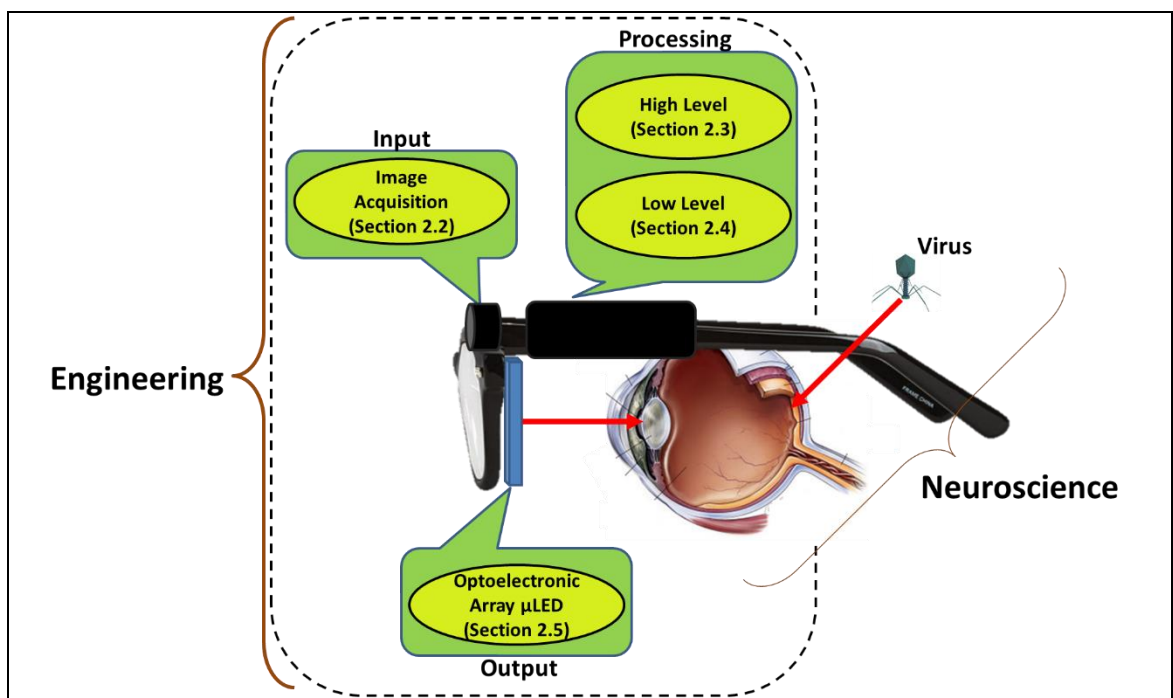


**Figure 2-1 Optogenetic retinal prosthesis approach.** Consisting of collaboration between neuroscience and engineering, the neuroscience side deals with altering an unbroken retinal layer to become light sensitive, while the engineering system makes up the image acquisition as an input stage, high level processing stage, low level processing stage and finally output stage

The optogenetic retinal prosthesis approach is based on collaboration between the neuro and engineering sciences, where optogenetics is a field of neuroscience in which the neurons are controlled using light. These neurons have been genetically modified to be light sensitive. The engineering part deals with this approach as a system consisting of four main stages: input, high level processing, low level processing and output. Figure 2-1 shows the stages of the



optogenetic retinal prosthesis approach, from the engineering system level overview.

**Input stage:** this is the same for all other visual prosthesis approaches, and concerns image acquisition. In Section 2.2, the different possible technologies for obtaining an image are compared, and this comparison is used to select the most suitable technology, with the optimal setting that will give the desired functions for our optogenetic retinal prosthesis approach.

**High level processing:** this is the same for all other visual prosthesis approaches, and concerns image preparation and retinal processing. In Section 2.3, the image preparation is discussed, which consists of image simplification and retargeting. The main use of image simplification is to remove unnecessary details, such as the background textures, and to keep the important information, such as edges. While image retargeting resizes the image to fit the micro-LED array size. Then retinal image processing is introduced, which is an important process aimed at compensating for the functionality of the affected retinal layer(s).

**Low level processing:** this is specific for each visual prosthesis approach, and for the optogenetic retinal approach it is concerned with how to control the photonic stimulator. Section 2.4 will present the main contribution of this study, which is the photonic controller that aims, firstly, to avoid the power surges that may happen when a large number of LEDs light for a short period of time. This is accomplished by an even power distributor. Second aim is to achieve the best timing by using a pulse encoder that sends control data to the micro-LEDs.

**Output stage:** this is about the stimulator, the main difference between the visual prosthesis approaches noted here, in terms of its type and where to place it. The optogenetic retinal prosthesis approach focuses on the micro-LED array as output, and Section 2.5 presents the different versions of the micro-LED, and explains the addressing modes and working schemas for them. Section 2.6 concludes the chapter and introduces the next.

## 2.2 Image Acquisition

The input stage of any visual prosthesis system starts with image acquisition, which is done using an imaging array. The interaction between the light and objects depends on the energy carried by the light, as shown in Table 2-1. The

energy in visible light is capable of causing an electronic excitation in eye molecules, and this energy can change the bonding or chemistry of eye molecules.

**Table 2-1 Light spectrum comparison [102]**

Name	Wavelength	Frequency (Hz)	Photon Energy (eV)
<b>Gamma ray</b>	less than 0.01 nm	more than 30 EHz	124 keV – 300+ GeV
<b>X-ray</b>	0.01 nm – 10 nm	30 EHz – 30 PHz	124 eV – 124 keV
<b>Ultraviolet</b>	10 nm – 380 nm	30 PHz – 790 THz	3.3 eV – 124 eV
<b>Visible</b>	380 nm–700 nm	790 THz – 430 THz	1.7 eV – 3.3 eV
<b>Infrared</b>	700 nm – 1 mm	430 THz – 300 GHz	1.24 meV – 1.7 eV
<b>Microwave</b>	1 mm – 1 meter	300 GHz – 300 MHz	1.24 $\mu$ eV – 1.24 meV
<b>Radio</b>	1 mm – 100,000 km	300 GHz – 3 Hz	12.4 feV – 1.24 meV

### 2.2.1 Imaging Sensor

Visible image sensors are used to convert the visible light with a wavelength of 390-700nm into electrical signals. There are various types of visible image sensors, but the most famous types are the CCD (charge coupled device), and the CMOS (complementary metal oxide semiconductor). Each of these types uses different technologies for taking images.

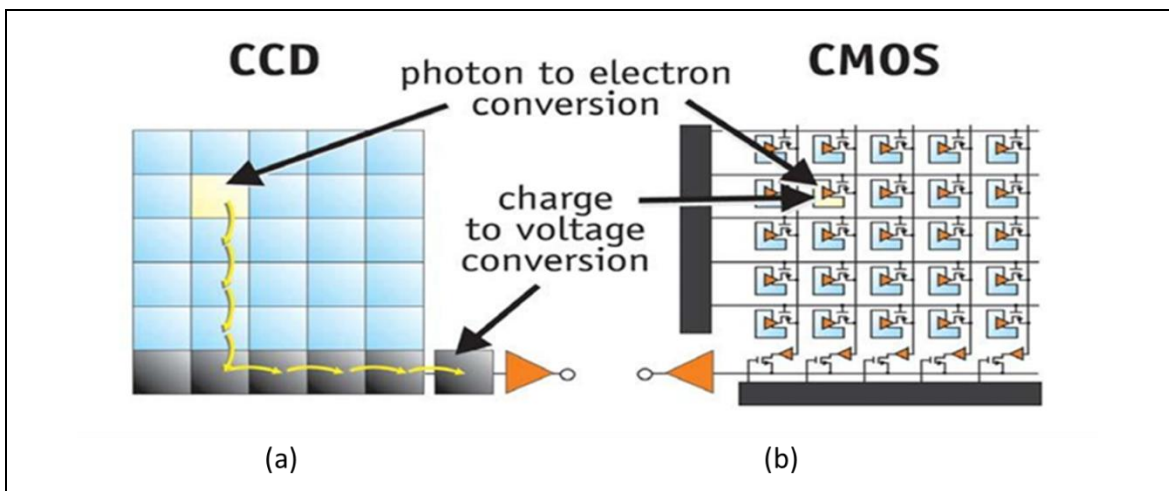


**Figure 2-2 CCD vs. CMOS image sensor.** In CCD (a), the photons are transferred to the row as analogue and are then converted to digital, while in the photon conversion in CMOS (b) every pixel has its specific charge-to-voltage conversion, and the sensor includes amplifiers, and ADC, so that the chip generates digital output bits [103]

Starting with CCD sensor technology, in order to read the number that indicates the accumulated charges of every cell in the image, the CCD photo-gate converts

the light into electrical charges over the exposure time [104]. In the read out, the pixel's accumulated charge is sequentially shifted into a common amplifier then the analogue to digital conversion (ADC) is done out of the sensor, as shown in Figure 2-2 (a). The drawbacks of CCD image sensors are that the process of shifting slows the readout speed, and multiple chips have to be used with the CCD chip due to the difficulties of integrating other components with it in a single chip. This makes the size of the camera large and complex in design, and these chips also consume a large amount of power [105].

Moving to the CMOS sensor technology, which is shown in Figure 2-2 (b), it shows that each pixel can be read individually. It uses transistors, typically three, to convert a charge to voltage. This makes the readout process very fast. The drawbacks of CMOS image sensors are that the light sensitivity of a CMOS chip is lower than CCD, because every pixel on a CMOS sensor has many transistors located beside it. Moreover, a large number of the photons received by the chip hits the transistors rather than hitting the photodiode [103], and the images created by CMOS are low-quality and high-noise images compared to the CCD images due to the large number of transistors in each pixel.

The CMOS image sensor was chosen over the CCD as the input device in this optogenetic retinal prosthesis system; this selection was based on the advantages discussed above for the CMOS sensor, including its small size, lower power consumption, and faster reading of the output. The drawback of the low image quality is solved using a micro lens that focuses the light into the photodiode area. Further explanation of the technologies used in the CMOS image sensor is given below.

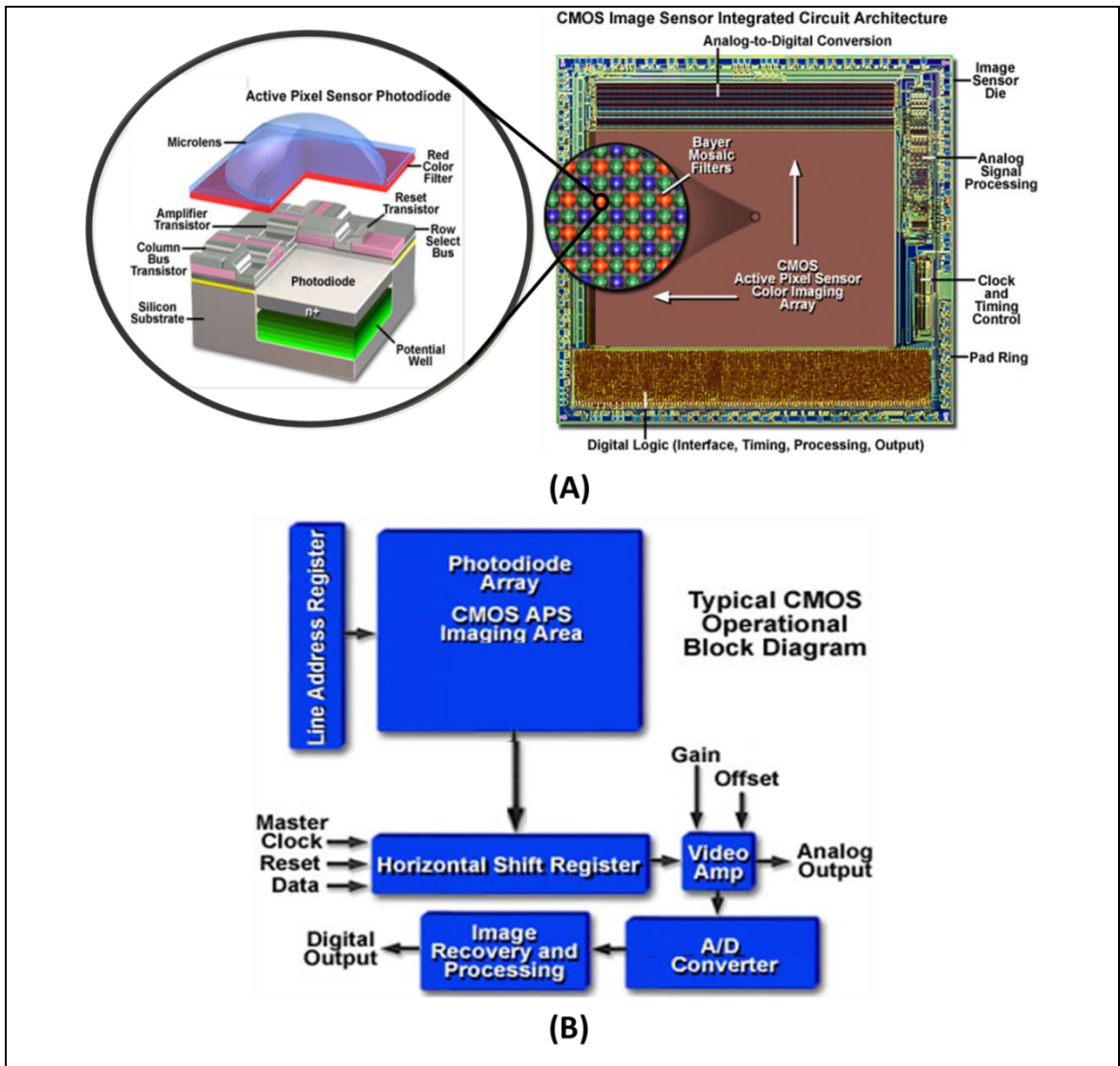


**Figure 2-3 CMOS Image sensor.** (A) the integrated circuit of the CMOS sensor with zoom into the Bayer filter, then zoom in for the red filtered pixels. (B) a block diagram of the CMOS sensor showing the main operation blocks [5]

The structure of the CMOS image sensor is explained in Figure 2-3, where in part A the internal architecture of the sensor is shown. The active pixel sensor (APS) array is surrounded by the other functional blocks, and all of the CMOS sensor's blocks are in the same image chip.

As illustrated in Figure 2-3(A) the Active Pixel Sensor (APS) is only sensitive to light intensity, but colours can be distinguished using filters typically arranged in a Bayer pattern. The APS zooms out to see a pattern of red, blue and green filters that are organized in a mosaic shape, named after engineer Bryce E. Bayer [106], who was working at Kodak Labs. The Bayer pattern is a square array with red, green and blue (RGB) colour filters such that individual pixels only transmit one of the three colours. However, there are two green squares for each red and blue

square to emulate the eye's extra sensitivity to green light. Then each individual pixel value is combined to make up the final colour pixel information, using other image processing techniques, as nearest neighbour or linear interpolation, the correct colour for each pixel in the array can be concluded.

A higher magnification view of the red filter and micro-lens is displayed; it presents a 3-D picture of the usual CMOS sensor pixel, including the photosensitive area (photodiode), busses, the micro-lens, the Bayer red filter, and three transistors. The first transistor is the amplifier transistor, which is used to convert the charge to voltage; this voltage is sent as output to the column bus, while the second transistor is the reset transistor, used to control the time of photon accumulation. The last transistor is the row-select transistor, which controls the readout process by connecting the column bus with the pixel output. The figure also shows a silicon potential well lying underneath the surface, used to accumulate the electrons produced from the interaction between the photodiode region of the pixel and the light.

Figure 2-3B displays a block diagram for the CMOS image sensor basic operation; the first step of its operation is to reset all pixels in the same row. This is done when the integration period begins by the time and control circuit. The second step is the selection of one row at a time, arranged by the line address register, to go over the whole array from the first to the last row. The next steps depend on CMOS output type; there are two possible types of output for the CMOS sensor device, either analogue or digital, but the digital output type has more steps than the analogue. Detailed steps for the operation are listed below.

Starting with analogue output, after the integration step has been done, the third step is to send the integrated value of each pixel to the horizontal shift register by the control circuitry. The fourth step, after the shift register has been filled, is shifting the pixel values serially (one pixel at a time) to the analogue video amplifier. The final step for the analogue output type is selecting the gain of this amplifier, which can be done either by software or hardware.

Moving on to the digital output CMOS sensor, this does the same three steps of analogue outputs, and then it continues to use the ADC converter, where pixels are converted into a digital array of binary digits. Furthermore, the digital pixel

data is processed, and this process varies from one sensor to another. Some examples of processing remove defects that occur in "bad" pixels and generate RGB colours using a Bayer Correction equation. Finally, the frame is presented on the digital output port.

An alternative imaging technology is based on Indium Gallium Arsenide (InGaAs) and Indium Phosphide (InP) rather than silicon [107, 108]. Imagers based on these substrates are capable of detecting  $1000\text{nm} < \text{wavelengths} < 4000\text{nm}$  ( $200\text{meV} < \text{photon energies} < 1\text{eV}$ ) which are suitable for the short wave, and mid wave infrared imaging systems. At such energies, thermal emission rather than reflection begins to dominate. Thus, such wavelengths are suitable for many applications such as vehicle detection and heat loss from buildings.

For Far IR light, all bodies emit an infrared radiation spectrum according to the blackbody radiation law proposed by Max Planck in 1900. Photons at such energies (less than 200 meV) cannot be detected via semiconductor diodes, since this energy is not sufficient to change the bonding or chemistry for these semiconductors. Therefore, it can be detected using micro-bolometer devices. These cannot separate wavelengths, but simply integrate all the photons received in the ( $4\mu\text{m}-14\mu\text{m}$ ) IR range, as shown in Figure 2-4.

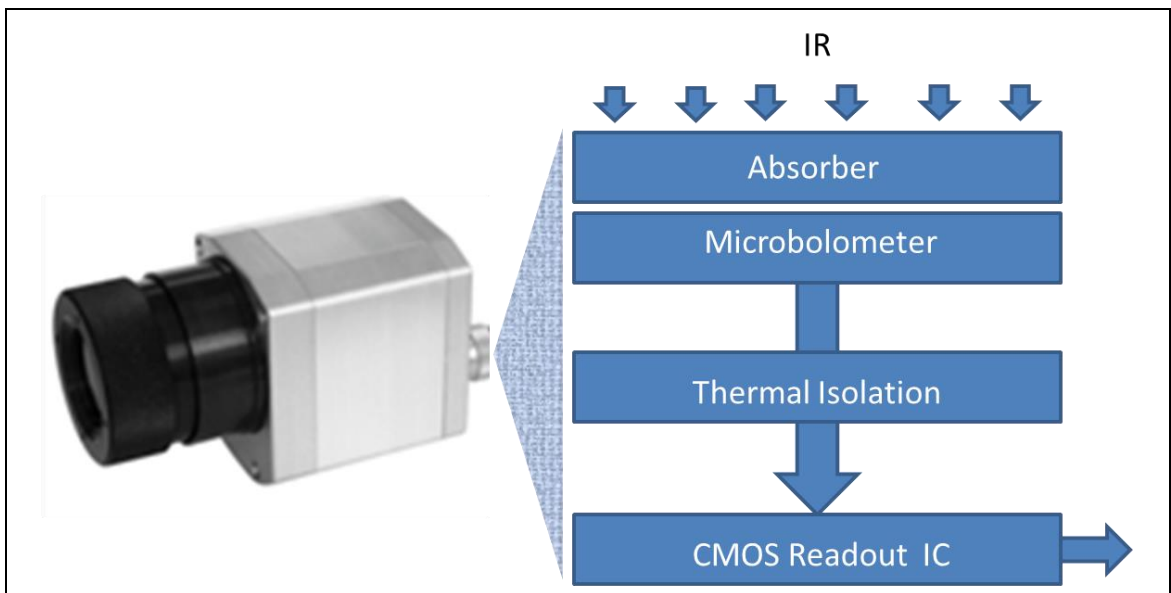


**Figure 2-4** The Far IR camera and the block diagram display the principles of operation. The absorber is usually made of micro-bolometer, and then absorbs heat, which affects the micro-bolometer temperature. Finally, the CMOS read out does some signal processing, such as gain control, before having the final output

### 2.2.2 Dual Spectrum Imaging

For a visual prosthesis system, it is suggested to use dual (Visible-IR) spectrum imaging to distinguish between live and non-live objects. The live objects are subsequently emphasized in the output image, this helps a patient to see them in the scene, also it can be used to speed-up the simplification algorithm. The concept of infrared-assisted scene segmentation was presented by Al-Atabany [109] to fuse to visible and IR images. This image fusion means joining relevant information from two or more images into a single image so the final image is more useful than any of the source images. Image fusion has been applied in several application areas such as astronomy and remote sensing [110-112], security and investigation [113-116], and medical diagnosis [117-119].

From the literature, image fusion applications can be divided into:

- 1) Multi-view fusion: the required images are taken from the same device with different views, i.e. constructing 3D view of the objects [120], or the same device with images taken at different times to notice changes between them, such as detecting tumours from medical images. It is also done in order to mix important information from low quality night-time images with the contexts extracted from a high quality image of the daytime at the same viewpoint, such as in surveillance cameras [115]. Other types involve multi-focus, where images are taken repetitively with different focal lengths to construct a multi-focus image [121]. Finally, there is the multi-resolution case, where a high-resolution image is produced using noisy images with low resolution [122-124].
- 2) Multi-modal fusion: images are taken from different sensors (e.g. visible and infrared). The advantage of using different sensors is to provide a more informative image which cannot be achieved using a single sensor.

A new dual spectrum visual processing algorithm for visual prostheses utilising infra-red imaging to assist the segmentation and pre-processing of the visual image is presented in this work. Where infra-red imaging is used since it is sensitive to different wavelength ranges rather than visible imaging, as Table 2-2 illustrates. Previously, Al-Atabany demonstrated a non-linear shrinking approach [125], to increase the effective field of view for patients with tunnel vision, by spatially compressing the background texture more than main object in the visual

scene. Here, the thermal information extracted from an infrared camera is used, in order to assist in segmenting key visual features based on the object temperature. The processor heavy feature recognition systems can then be replaced with this new thermal based segmentation algorithm; in addition, it can be used to provide the user with useful thermal information (e.g. tea temperature) in its own right.

**Table 2-2 The differences between visible and infra-red images**

Feature	Visible image	IR image
<b>Wavelength</b>	390-700 nanometre	700 nanometre - 1 millimetre
<b>Human eye can detect</b>	Yes	No
<b>Frequency (Hz)</b>	790 THz - 430 THz	430 THz - 300 GHz
<b>Photon Energy (eV)</b>	1.7 eV - 3.3 eV	1.24 meV - 1.7 eV

## 2.3 High Level Processing

Retinal prosthesis development is presently moving towards providing a return to some functional vision for those with the Retinitis Pigmentosa disease. Although exciting progress is being made in the field, most of the retinal prosthesis devices are unlikely to return perfect vision in the first instance. Therefore, the best presentation of the visual scene needs to be explored. The key task is to return mobility and live object recognition to the patients. Therefore, some form of reduction of the visual information should be applied before transfer to the retina, to make the best use of the useful visual information being sent. In particular, scene segmentation can reduce unimportant textures, and thus enhance the perception of the important features.

### 2.3.1 Image Preparation

Natural scenes contain large amount of information content, so image preparation is required step before any retinal processing; the background textures and noise must be extracted and live objects should be emphasized. After that the prepared image should be retargeted to fit the size of the retinal final output stage.

Different filters are used for texture and noise removal, Gaussian filtering is a commonly used kernel for this purpose [126]. While it is effective at noise



removal, it removes high frequency information, thus blurring the edges of the significant object boundaries.

Median filtering can be used to remove speckle noise. It is applied uniformly across an image, smoothing all pixels which appear to be considerably different to their neighbours. Thus, while it is very effective in the elimination of speckle noise, it is often at the expense of a slight blurring of the scene [126].

Al-Atabany uses a non-linear anisotropic smoothing technique to eliminate noise and background textures, while avoiding smoothing across object boundaries [13]. It is an iterative process which progressively smooths the image while maintaining the edges by reducing the diffusivity at those locations having a larger likelihood to be edges.

To compare the linear and non-linear filters according to blur effects on the edges, the linear/non-linear filters were applied to the same image for a different number of iterations, as shown in Figure 2-5. It can be noticed that even when a small number of iterations are used, the linear Gaussian filter blurs the edges, but using non-linear filters does not affect the edges of the image, giving better results for the visual prosthesis.

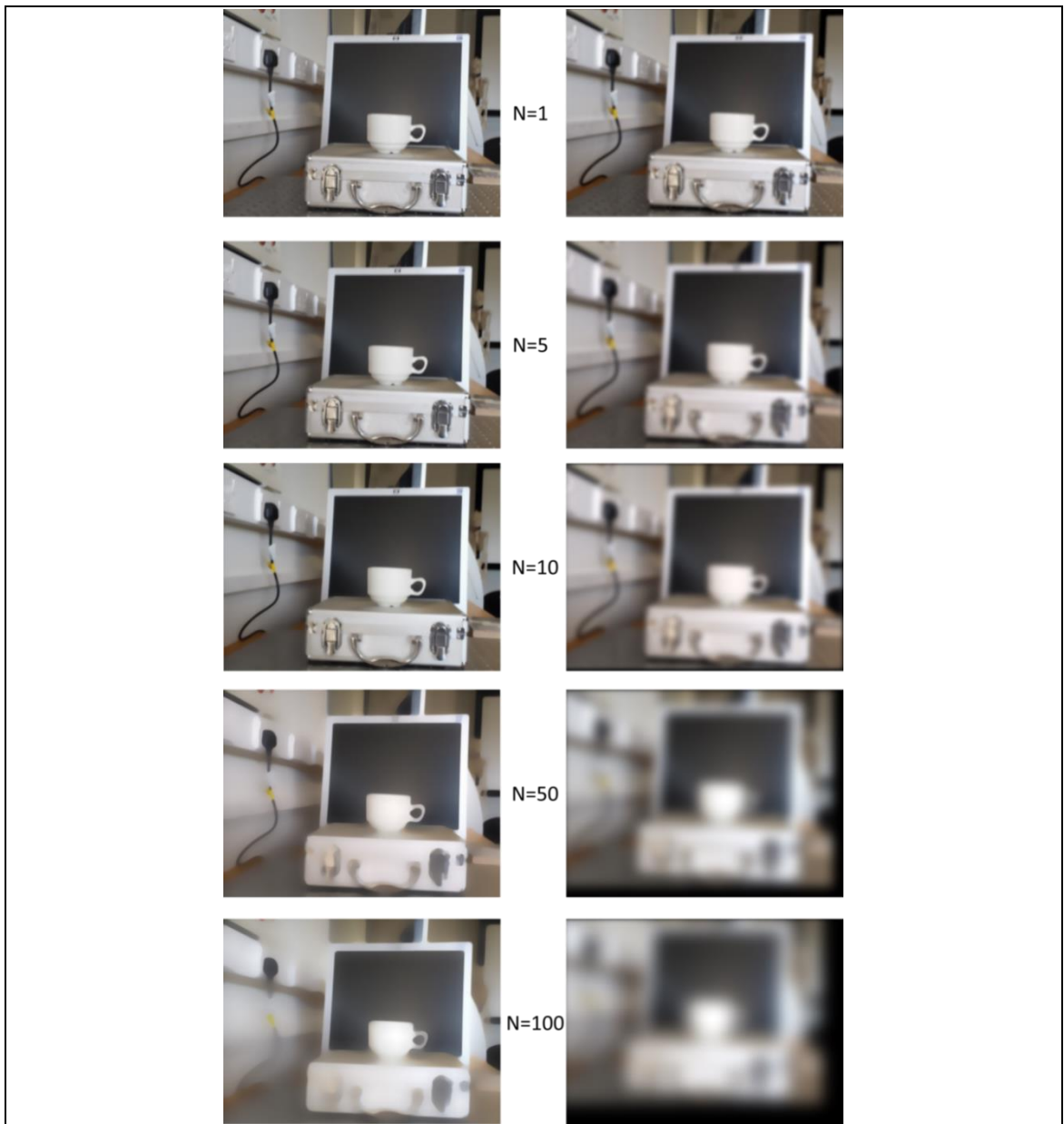


**Figure 2-5** The difference between using Gaussian (right column) with the following number of iterations from top to bottom,  $t=1, 5, 10, 50, 100$ , and the same image using a non-linear anisotropic diffusion filter (left column) with the same number of iterations

The non-linear filter used by Al-Atabany [13] for retinal prosthesis pre-processing, was adopted from the original algorithm suggested by Perona and Malik in 1990. This filter iteratively increases the image smoothness while preserving the edges, by decreasing the diffusivity at the locations that have a larger possibility of being edges [127]. The equation of the anisotropic diffusion in the discrete domain is:

$$I^{n+1} = I^n + \Delta K [\nabla(C \cdot \nabla I_H) + \nabla(C \cdot \nabla I_V)]$$

$$C = \frac{1}{1 + \sqrt{(\nabla_H I)^2 + (\nabla_V I)^2}} \quad (2-1)$$

Where  $n$  denotes the iteration number between 1 and  $n$ ;  $\nabla$  is the gradient operator;  $C$  is the diffusion coefficient;  $\Delta K$  is the smoothing step (it controls the accuracy and the speed of the smoothing) and  $I_H, I_V$  represents the diffusion in horizontal and vertical directions.

The anisotropic diffusion simplification depends on two factors: the number of iterations ( $n$ ) and the smoothing step ( $\Delta K$ ). These control the accuracy and speed of the smoothing. The effect of varying these two factors is explained in Figure 2-6, where the level of detail to be removed is increased by raising the number of iterations; the speed of the removal process is increased by raising the value of the time step.

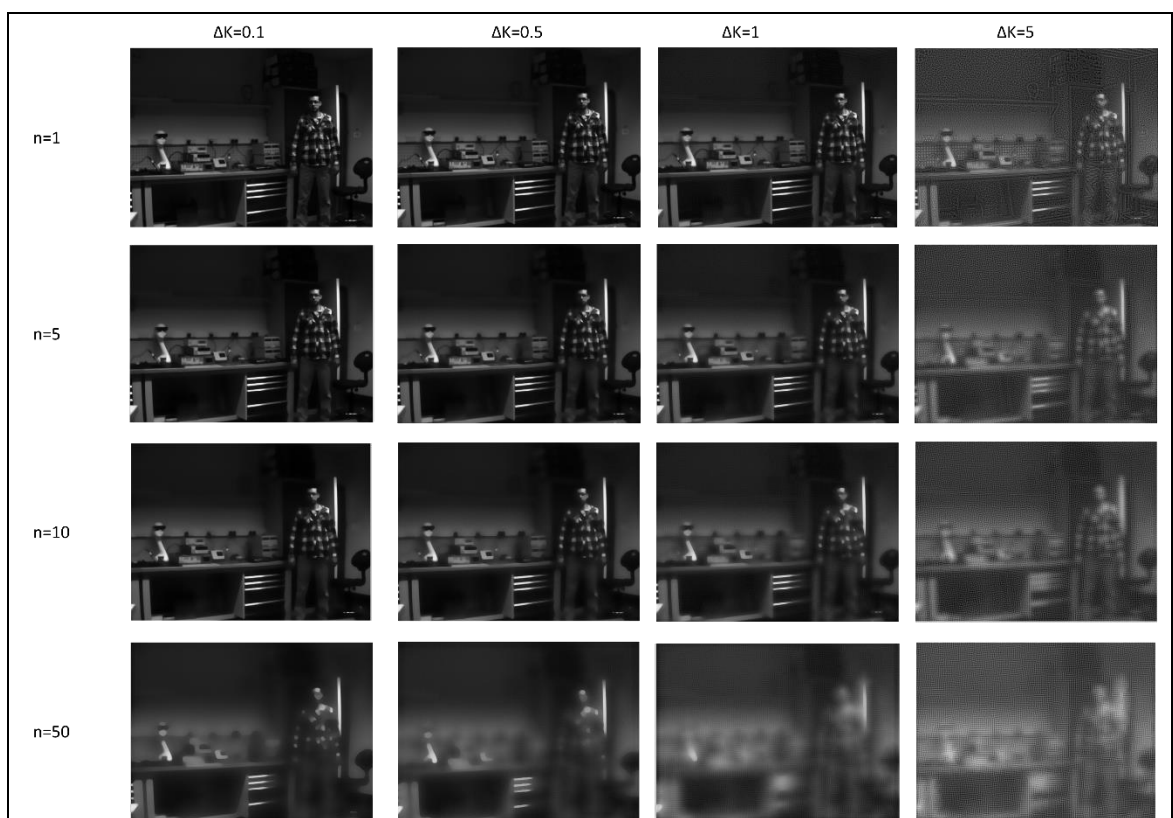


**Figure 2-6** Anisotropic diffusion is affected by the number of iterations ( $n$ ) that control the level of simplification by removing the finer details when  $n$  increases, and the smoothing step ( $\Delta K$ ) used to control accuracy by increasing the speed of smoothing when  $n$  increases

After simplify the image it needs to be retargeted to fit the size of the visual stimulators. Avidan and Shamir [128] is proposed a retargeting algorithm titled seam carving. In this algorithm, the dimensions of an image are changed by removing a connected path of pixels, named a seam. This step is repeated for the input image until it achieves the target size. Another image retargeting algorithm was proposed by Zhang et al. [129], who suggested using a

shrinkability matrix, where the compression of each pixel of the image is done according to its shrinkage value. The main advantage of this algorithm over seam carving is that it illustrates a lower number of artefacts than the seam carving method. Due to the way it works, it shrinks the image rather than removing pixels to reduce the size. Later, Al-Atabany [125] combined both approaches by using seam carving to generate the importance matrix for shrinking. This method is called SAS (Seam Assisted Shrinkability).

### **2.3.2 Retinal Encoding**

After the image has been captured, it is then simplified and resized. The next step is the retinal image processing, which is different from one visual prosthesis approach to another. There are three possible routes for retinal prosthesis stimulation [99], as described in Figure 2-7.

- I. Cone Cell Stimulation: could provide central vision, requiring only enhanced versions of the visual scene. As discussed in section 1.2, the main function of these cells is sensing.
- II. Bipolar Cell Stimulation could restore peripheral vision, but would need additional retinal processing. As discussed in Section 1.2, the main function of these cells is processing.
- III. Ganglion Cell Stimulation is similar to that for bipolar cells but potentially requires the additional step of spike encoding. As discussed in Section 1.2, the main function of these cells is communication.

In the second and third routes, additional retinal processing is needed so further details of these retinal processes are explained below.

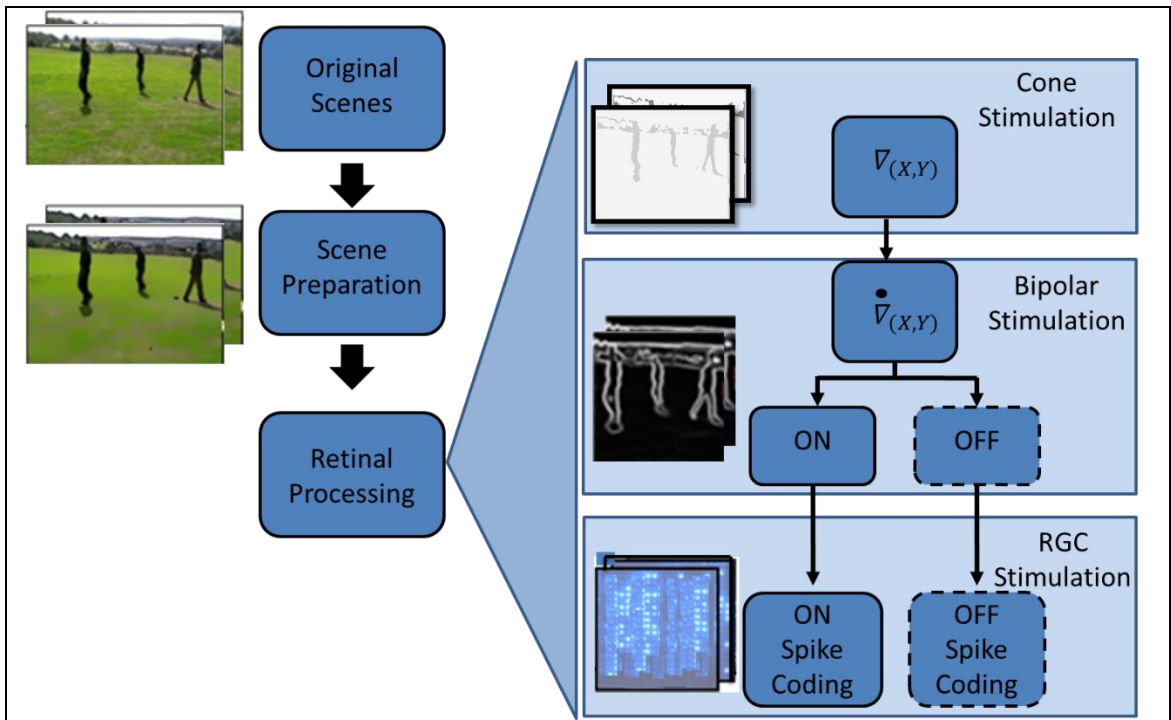


**Figure 2-7 Main stages of retinal stimulation.** The processed image (stimulation profile) is converted into multiple sub-binary images (stimulation frames) that need to be lit

As described earlier, the second layer (bipolar cells) is an edge enhancement layer; this can be mathematically modelled through applying a difference of Gaussian function, so if the second route is taken (Bipolar Cell Stimulation) the difference of Gaussian function needs to be implemented, to compensate the functionality of this layer.

With the third route, both previous retinal processing and spike encoding are required. Spike encoding is a type of neural encoding, where the relation between stimulus (detectable change in the environment) and the neuron response is studied. Many neuron models are available, ranging from a simple integrate-and-fire neuron model [130], to a more advanced Hodgkin-Huxley neuron model [131]. In this work, Izhikevich's neuron model [132] was used to determine action potential events. This is because of its power and simplicity, and can be described as in the following equation:

$$v' = 0.04V^2 + 5V + 140 - U + I_{stim} \quad (A)$$

$$u' = a(bV - U) \quad (B) \quad (2-2)$$

$$if (V > threshold) \text{ then } V \leftarrow c, U \leftarrow U + d \quad (C)$$

Where:

- $V$  is the membrane potential
- $U$  is the recovery potential
- $\tau = \frac{d}{dt}$  where  $\tau$  is the time step for ganglion spike determined to (1ms).
- $a, b, c,$  and  $d$  are the parameters to determine the type of neuron. These parameters are determined as (0.02, 0.2, -65, 6), respectively. This selection is used since it gives characteristics similar to that of retinal ganglion cell firing patterns. Since most retinal ganglion cells neurons are excitable, that is, they are quiescent but can fire spikes when stimulated.
- $I_{stim}$  is the stimulus due to the spatio-temporal derivative of the segmented scene.

In this iterative model, equation 2-5 (b) describes the reset state, which happens if an action potential has occurred in the previous frame (i.e. when  $V_{new}$  exceeds a threshold, typically determined as 30mV), and then the cell needs to be reset to its resting membrane potential ( $c$ ), and  $u$  is incremented by parameter ( $d$ ).

When an action potential is determined (i.e. when  $V_{new}$  exceeds a threshold, typically determined as 30mV), an output pulse needs to be generated.

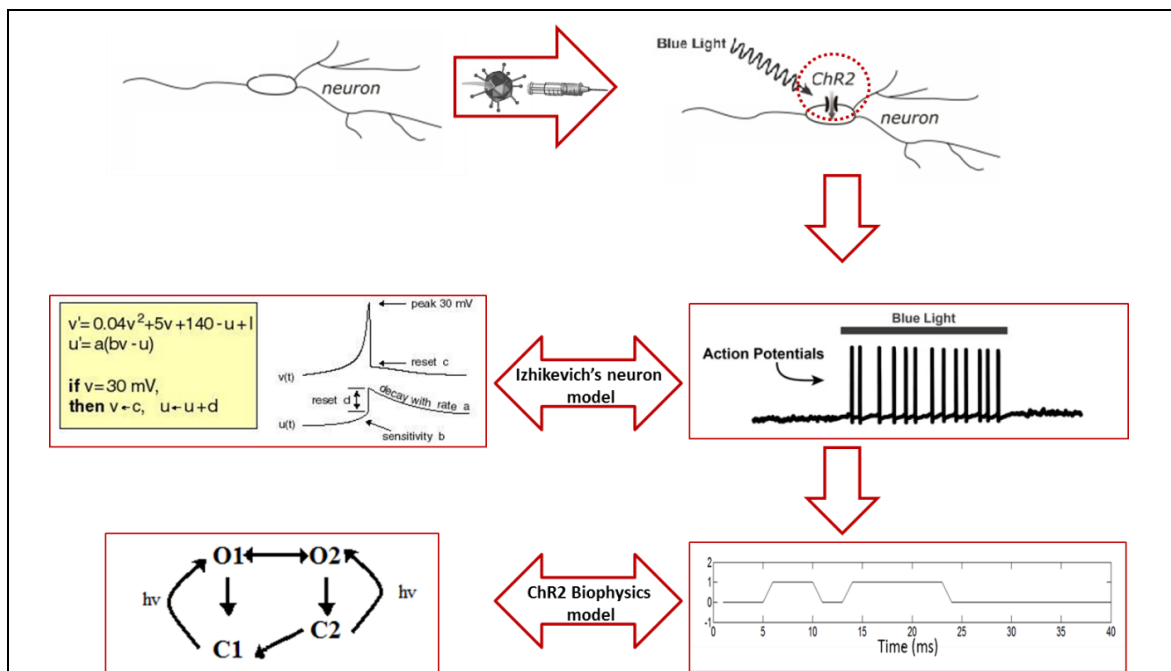


**Figure 2-8 The main spike coding steps.** It consists of using the Izhikevich neuron model to represent soma dynamics, then the effect of ChR2 biophysics is considered when converting analogue pulses into digital pulses

The spike coding involves two steps, as shown in Figure 2-8. The first step is to model the neuron soma dynamics, this is achieved by using the Izhikevich's neuron model, as described in equation 2-2. The second step is to convert the analogue neuron pulses into digital pulses. This conversion considers the nonlinear biophysics of channelrhodopsin. Where in the case of input action potential (i.e. when  $V$  exceeds a threshold, typically determined as 30mV), a digital output pulse needs to be generated. The required output pulse width depends on the stimulus intensity and the sensitivity of the channelrhodopsin encoded cells. The output of these pulses can be either simple fixed width, or more advanced different width. In this work the latter is used, since it is more realistic; the channelrhodopsin actually has light and dark adapted states [133], for which the dark (short) is more efficient, thus requires less lighting, once stimulated, channelrhodopsin moves to the less efficient light (long) adapted form; this form requires around 50ms to recover. Therefore two output pulse widths are determined as shown in Figure 2-9, in the dark state a shorter (5ms) output pulse is generated, lower lighting is needed. While in the light state a longer (10ms) output pulse is generated, higher lighting is needed.

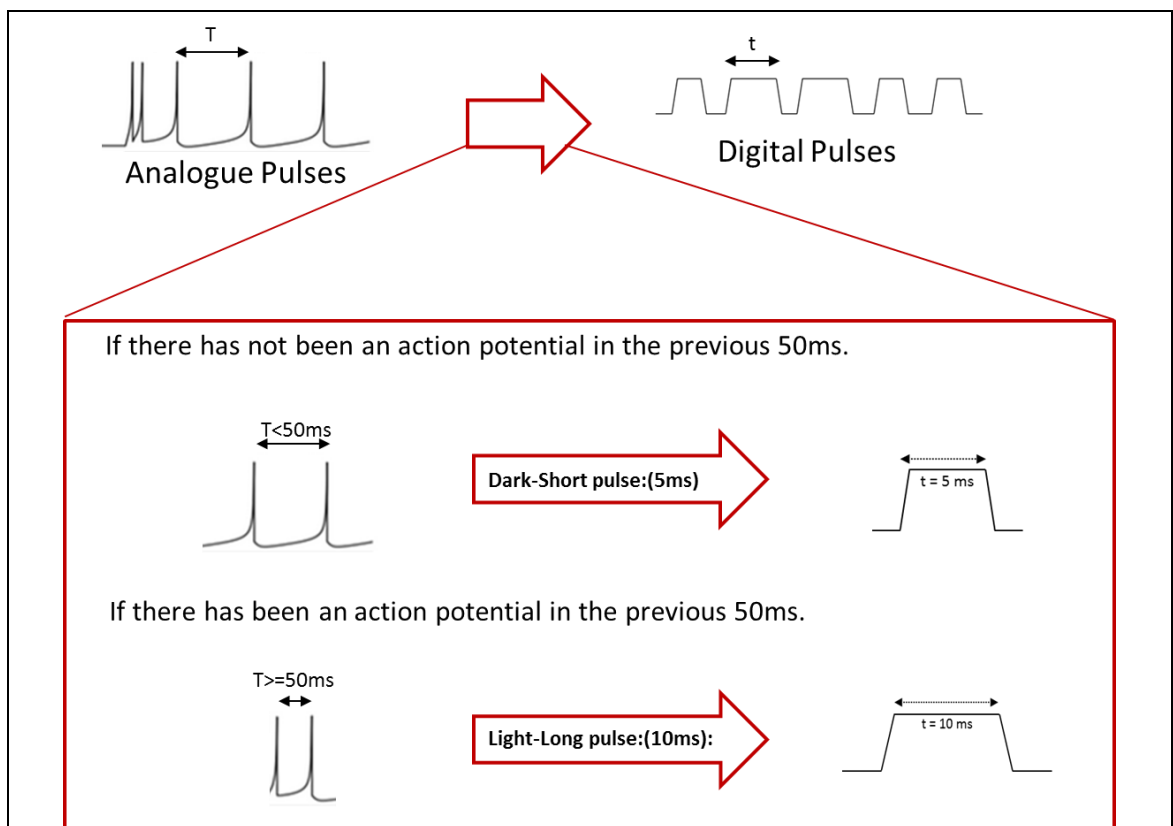


**Figure 2-9 The second step in spike coding.** It converts the analogue into digital pulses, considering the biophysics of ChR2

## 2.4 Low Level Processing

Now, at this stage more specific processing is needed to display the image in the right way in the final output stage. This processing depends on the type of stimulator. In this work, the main interest is the optogenetic retinal prosthesis. This prosthesis uses an optical stimulation rather than electrical, thus a photonic stimulation controller is presented to perform the needed low level processing. It consists of three blocks: a frame encoder, an even power distributor and a pulse encoder.

The first block, the frame encoding, is used to convert the frame into pulses, which varies with time, the variation is related to the pixels intensities. The second block is the even power distributor, is used to have an equal number of ON state LEDs through each time step, and this is done to avoid power surges, which happen when a large number of ON state LEDs light for short period, especially when larger optoelectronic micro-LEDs are used. In order to understand the third block properly, a general overview of the output optoelectronic micro-LEDs is presented next.

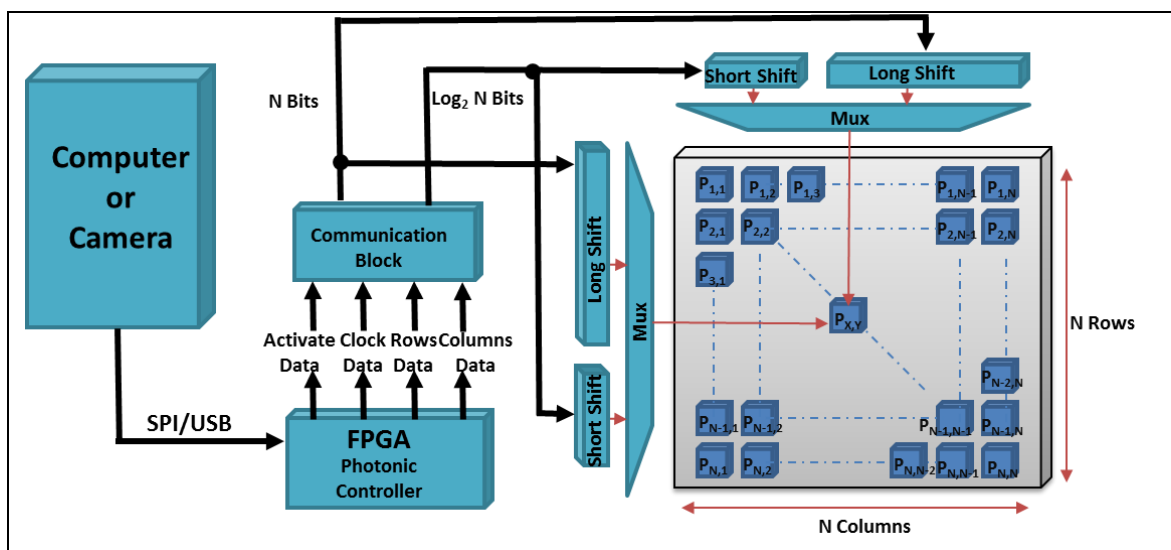


**Figure 2-10 General system architecture of the micro-LEDs.** It consists of  $N \times N$  micro-LEDs and there are two ways to operate them, either by long or short shift. Also, the I/O for the photonic stimulator controller is presented, where it has input through a computer or camera

The general architecture of the optoelectronic micro-LEDs is shown in Figure 2-10. The LEDs are placed into an array structure which has the same number of columns and rows (for ease of control). Two addressing modes are available for optoelectronic micro-LEDs. The first addressing mode is called short shift, in



which an individual LED can be changed/selected, depending on the optoelectronic micro-LEDs version, by sending both row and column addresses for the LED position in the array. The second addressing mode is called long shift, in which a row/column of LEDs can be changed by shifting its new values. Previously, the addressing mode of the optoelectronic micro-LEDs was set manually (via switches). In the photonic stimulation controller used in this study, a pulse encoder block is introduced to control the optoelectronic micro-LEDs automatically by mix addressing mode. This selects the short or long shift according to the image pixel values, leading to better timing results.

### 2.4.1 Frame Encoding and Even Power Distributor

In the optogenetic retinal prosthesis approach, the neurons are photosensitized. It is therefore possible to use a micro-LED array to stimulate neural activity, via short high intensity pulses of light. These pulses are used to display the frames (images) processed in the previous stages. To relate the image pixel values to these intensity pulses, the frame encoding is done.

In the input device (a computer/camera) the processed image is converted into a one dimensional array before sending to the photonic controller, this array is converted into a two dimensional array again in the frame encoding, as shown in Figure 2-11, then the new array dimensions are the frame pixels and time. To relate each pixel intensity to time, pulse width modulation was employed, where each pixel intensity is directly related to the width of the ON pulse.

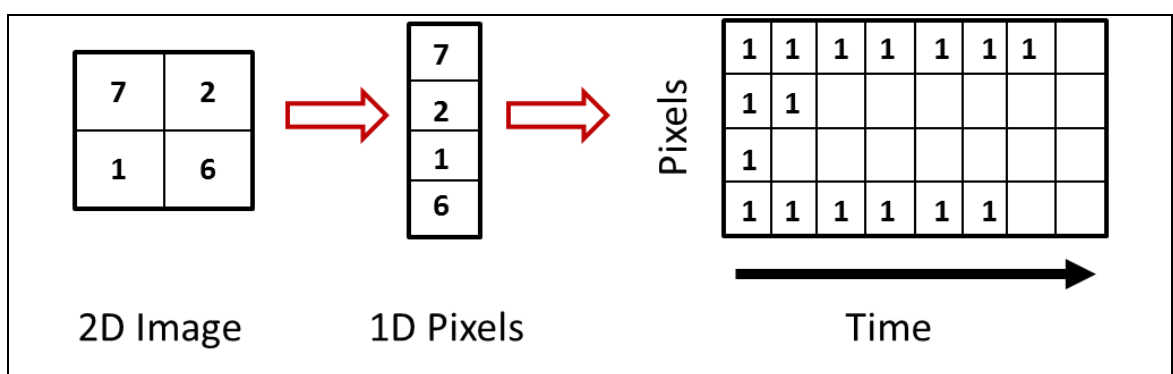


**Figure 2-11 The function of frame encoding.** It receives a one dimensional array of pixels, then each pixel intensity is related to the ON pulse width

The main idea of the even power distributor is to equally spread the ON-states LEDs during each time step. The main problem is the scaling issue with power supply spikes, i.e. if large numbers of LEDs are turned on simultaneously, this can lead to power supply inefficiency and intensity droop. To combat this, a smoothing methodology was developed to redistribute pulses through the full frame time, to smooth out power fluctuations. Before the even power distributor, all ON-state LEDs start at the same time ( $T\text{-frame}_{\text{start}}$ ), but after the even power distributor, the total number of ON-state LEDs will be equal along the frame time. This smooths the power drawn from the power source, as illustrated in Figure 2-12, where the ON-state LEDs are redistributed during the whole frame time, rather than the same beginning time.

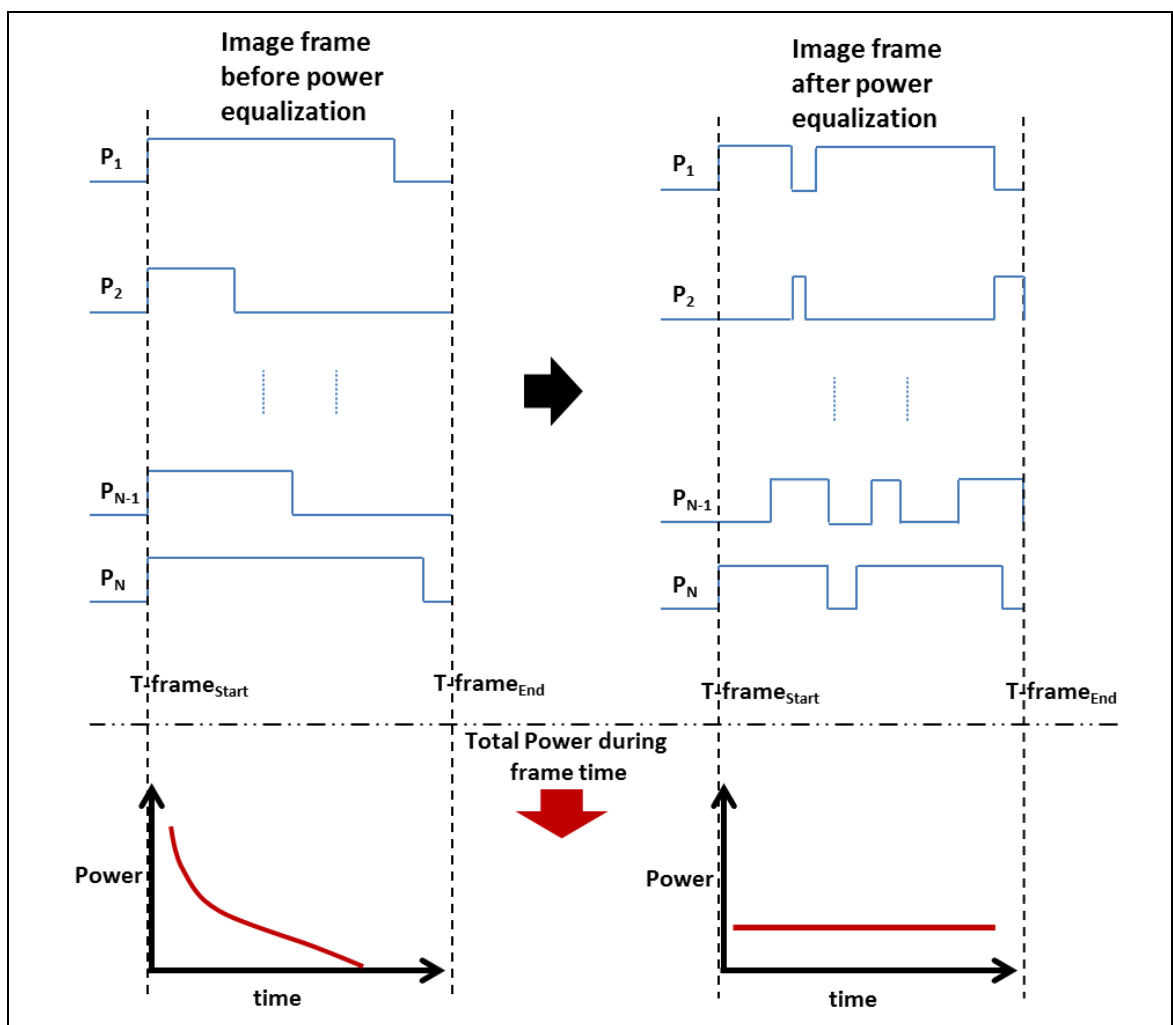


**Figure 2-12 An image frame for  $N$  pixels before and after power equalization.** Before power equalization, all the pixels start the on period at the same time ( $T\text{-frame}_{\text{start}}$ ), and then it becomes off proportional to pixel intensity. The idea of the even power distributor is to redistribute the on time during the whole frame time so that not all the frames start at the same time

To clearly illustrate the concept of even power distributor the following example is introduced:

An image consists of **4** pixels with the following intensities (**5, 1, 2, and 4**), maximum intensity level is **6**, minimum intensity level is **0**, and the number of sub-frames is **6** then:

A: Using direct conversion Controller the sub-frames will be distributed as following:

Pixel Intensity	SF1	SF2	SF3	SF4	SF5	SF6
<b>Pixel1 Intensity = 5</b>	1	1	1	1	1	0
<b>Pixel2 Intensity = 1</b>	1	0	0	0	0	0
<b>Pixel3 Intensity = 2</b>	1	1	0	0	0	0
<b>Pixel4 Intensity = 4</b>	1	1	1	1	0	0
<b>Total On Pixels</b>	<b>4</b>	<b>3</b>	<b>2</b>	<b>2</b>	<b>1</b>	<b>0</b>

B: Using New Even power PWM Controller the sub-frames will be distributed as following:

Pixel Intensity	SF1	SF2	SF3	SF4	SF5	SF6
<b>Pixel1 Intensity = 5</b>	1	1	1	1	1	0
<b>Pixel2 Intensity = 1</b>	1	0	0	0	0	1
<b>Pixel3 Intensity = 2</b>	0	0	0	0	1	1
<b>Pixel4 Intensity = 4</b>	1	1	1	1	0	0
<b>Total On Pixels</b>	<b>2</b>	<b>2</b>	<b>2</b>	<b>2</b>	<b>2</b>	<b>2</b>

The definition of time step can vary according to each defined level, as illustrated in Figure 2-13, where:

- I. Frame: is a time sequence within a video.
- II. Sub-Frame: an intensity levels within a frame.
- III. Micro-Frame: a mismatch of levels within a sub-frame due to manufacturing issues. This level is used to compensate the different levels of illuminations for different LEDs within a sub-frame, this is used also to reduce the effect of low frequency response of the ChR2.

The even power distributor can be applied to two different levels: the sub-frame and micro-frame levels. Further discussions for these two levels are introduced below.

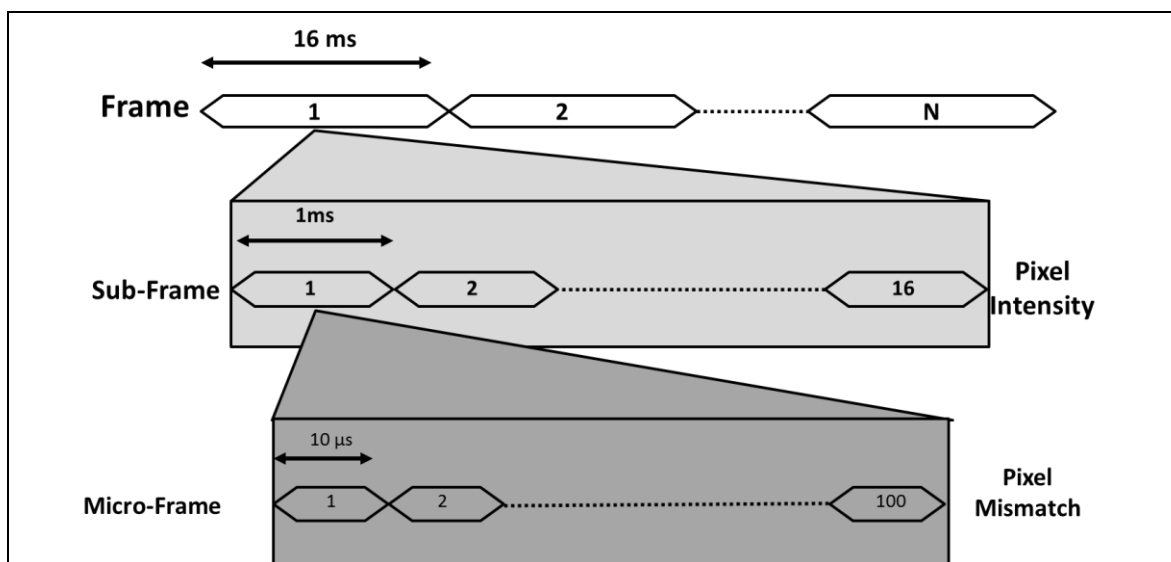


**Figure 2-13 Even power distributor time step definition.** This definition is used for images in optogenetic retinal prostheses

- Firstly, the sub-frame is used to provide intensity control by the Pulse Width Modulation (PWM) map, according to the dynamic range of the pixels intensities. For example, if each pixel in the processed frame (image) has an intensity value in the range (0-15), then to display the frames (images) in a proper way, each frame is divided into 16 sub-frames. The grey intensities of different pixels can be related to the ON-state LEDs using PWM, where each pulse width equals the pixel intensity value.
- Secondly, a micro-frame is used to provide intensity mismatch control. The mismatch here means that the illumination of LEDs operating at the same

voltage is different, due to the LED manufacturing process. At a certain operating voltage, the optoelectronic micro-LED array has a fixed mismatch map, which can be calculated and then directly related to the number of micro-frames needed to have the LEDs at ON-state. After that, the PWM map is again applied within each micro-frame, and at this level the PWM is used according to the range of the pixel intensities mismatch. The previous example can be extended, where each pixel in the processed frame (image) has an intensity value in the range 0-15, and each frame is divided into 16 sub-frames. If the array has a mismatch range between 0-99, each sub-frame is divided into 100 micro-frames, and different pixel intensity mismatches can be compensated for using PWM. Each pulse width equals the pixel intensity mismatch value (after being modified so that they are directly related).

The four possible combinations for applying/removing the even power distributor block on the sub-frame/micro-frame level are:

1. Remove the even power distributor from the sub-frame level, and remove the even power distributor from the micro-frame level.
2. Apply even power distributor to the sub-frame level, and remove the even power distributor from the micro-frame level.
3. Remove the even power distributor from the sub-frame level, and apply the even power distributor to the micro-frame level.
4. Apply the even power distributor to the sub-frame level, and apply the even power distributor to the micro-frame level.

In Figure 2-14, an example of an 8x8 image is introduced, with 64 pixels and an intensity range of 0-3. Their intensities distribution, done through four sub-frames, is shown in the second row, where it can be either directly distributed or completed using even power. Each sub-frame is further divided into 100 micro-frames, with the first sub-frame for both direct and even distribution being shown in the third row. The micro-frame is used to compensate for the different levels of illumination (mismatch) for array LEDs, and again the micro-frames can be distributed either directly or evenly. These are the four possible combinations for applying, or not, the even power block.

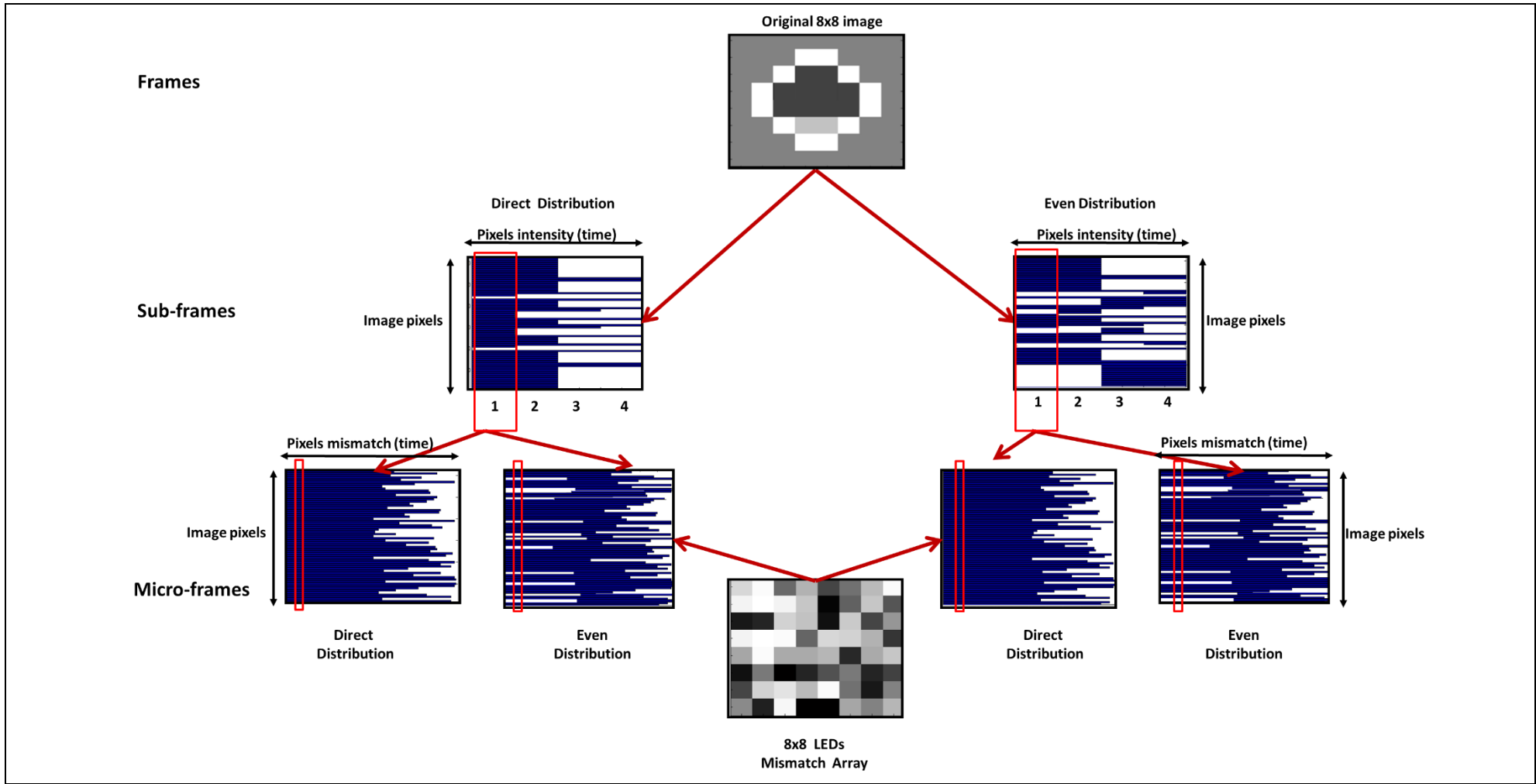


Figure 2-14 The four possible combinations for applying/removing the even power distributor block on sub-frame/micro-frame level

### 2.4.2 Pulse Encoder

The third block in the photonic stimulation controller is the pulse encoder; this block utilizes the sparse nature of retinal code, so it is possible to adapt the system using this block to minimize information transfer to the optoelectronic micro-LED array.

Previously, in Figure 2-10, the general architecture of optoelectronic micro-LEDs is shown, alongside the square array structure used to control it easily. It is controlled by an active CMOS chip which can maintain a micro-LED in either the ON or OFF state. There are two addressing modes of operation: pixel update, or row update, whereby information is sent to either change the ON/OFF state of an individual pixel, or all the pixels in a given row. Updating the displayed frame on the micro-LEDs can be achieved by either rastering through all the rows, or by simply changing the states of those pixels that require a state change, as shown in Figure 2-15.

The number of clock cycles required to update the whole array (**Total\_Clk\_Cycles**) considering **N** rows/column array, using either **Row** or **Pixel** mode is given in the following equation:

$$\mathbf{Total\_Clk\_Cycles} = \begin{cases} (N + 1)N_{R>0} & (a) \text{ (Row Mode)} \\ (1 + (\log_2 N)) \sum_{P=1} & (b) \text{ (Pixel Mode)} \end{cases} \quad (2-3)$$

Where  $N_{R>0}$  is the number of rows with at least one pixel to update, and  $\sum_{P=1}$  is the summation of total number of pixels to update. Subsequent to sign off at the shift register, the extra clock cycle in the equations is taken to update an individual pixel or row.

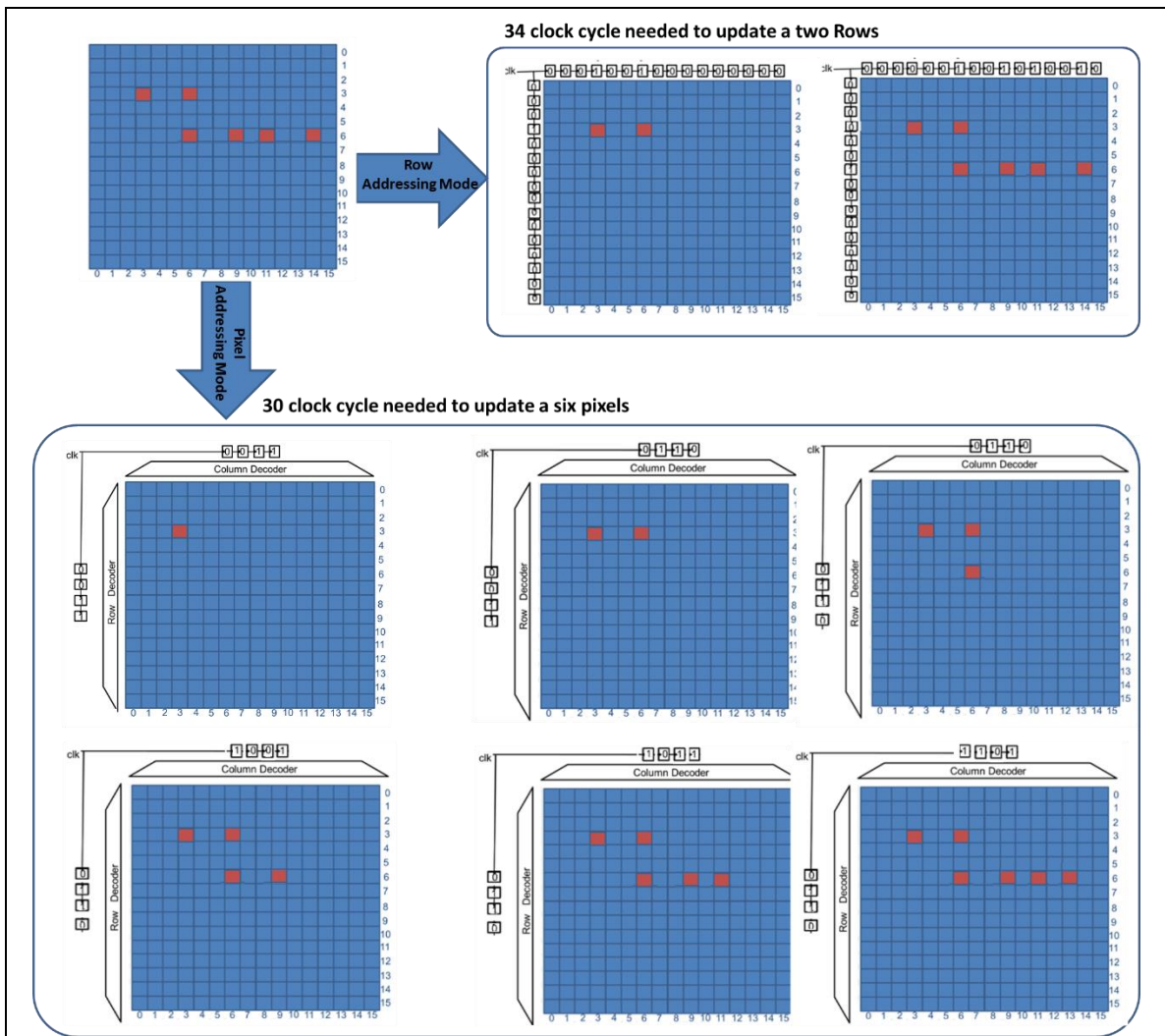


**Figure 2-15 Two possible ways to update the micro-LEDs.** In row addressing mode, 34 cycles are needed to update any two rows, while in pixel addressing mode 30 cycles are needed to update six pixels. This number is varied, depending on the total number of pixels needing to be changed

Row rastering mode is efficient if the majority of pixels require updating. Where there are empty rows, skipping these with row update can be efficient, and for sparse arrays, pixel updating is most efficient. Thus, for an individual row, the determination of when to use pixel or row update, assuming a single row, is given by:



$$\sum_{P=1}^N \leq \frac{N}{\log_2 N} \quad (2-4)$$

i.e. for a 16x16 array if there are more than four pixels requiring a change in any given row then it is more efficient to update it with a row update methodology. In Newcastle University, the optogenetic retinal prosthesis group previously updated the optoelectronic micro-LEDs using only the pixel addressing, but a mixed mode control methodology is introduced here which is optimized for both pixel addressing and row addressing. In this mode, each row is categorized to the proper addressing (pixel, row), according to the threshold value calculated by equation 2-4, leading to better timing results. Figure 2-16 shows the difference between operating the optoelectronic micro-LEDs array with and without the mixed mode introduced by pulse encoder. It can be noticed that, without mixed mode, each sub-frame time ( $F_i$ ) is equal, but with mixed mode the sub-frame time can be different from one sub-frame to another. The extra time ( $S_i$ ) can be used to read sensing information about the chip status.

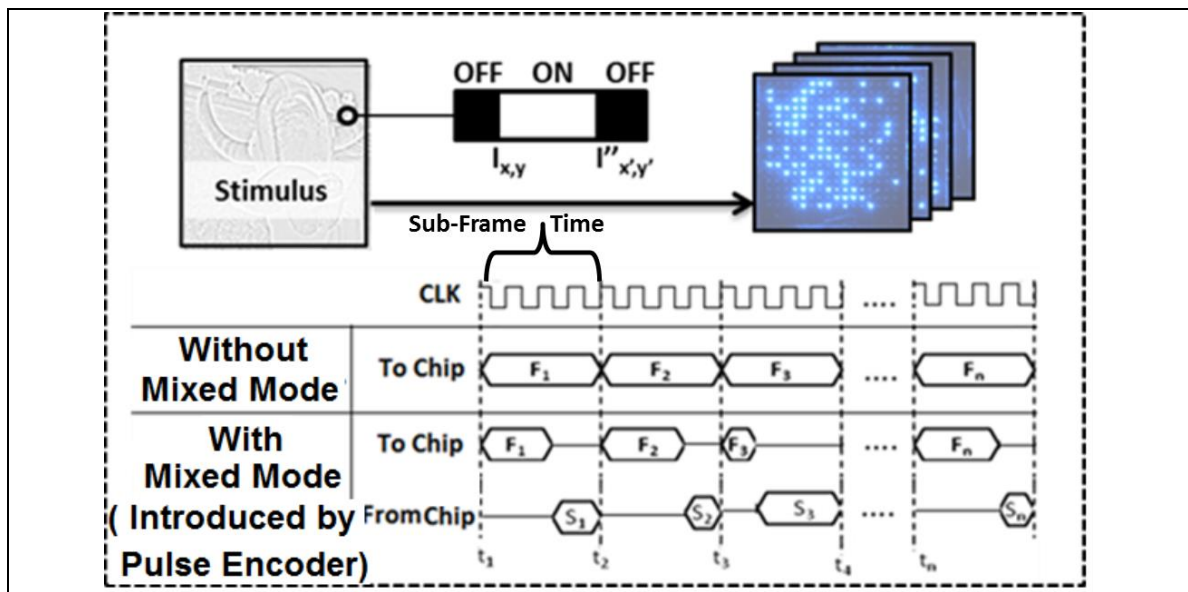


**Figure 2-16** The information I/O with optoelectronic stimulators for optogenetic neural stimulation. A control and clock signal provide activation of the chip. Incoming information is split into sub-frames ( $F_i$ ) which provide the PWM. Sensor information ( $S_i$ ) about LEDs status can be extracted in the time periods between sub-frame updates

The pulse encoder can be considered a step toward final control of optical neural stimulator arrays, in particular for visual prostheses. The mixed addressing mode update can thus be introduced to provide more flexible timing and so give extra frame time for sensing the status of the array.

## 2.5 Optoelectronic Micro-LED Array

The final stage of the optogenetic retinal prosthesis system is the optoelectronic micro-LED array. It utilises Gallium Nitride material, which has extended illumination capabilities compared to normal silicon LEDs that are suitable for optogenetic retinal prosthesis. Two versions of the micro-LED array were implemented, and the first version was on 16x16 arrays. The second version was scaled up to a 90x90 array. Both versions are shown in Figure 2-17.

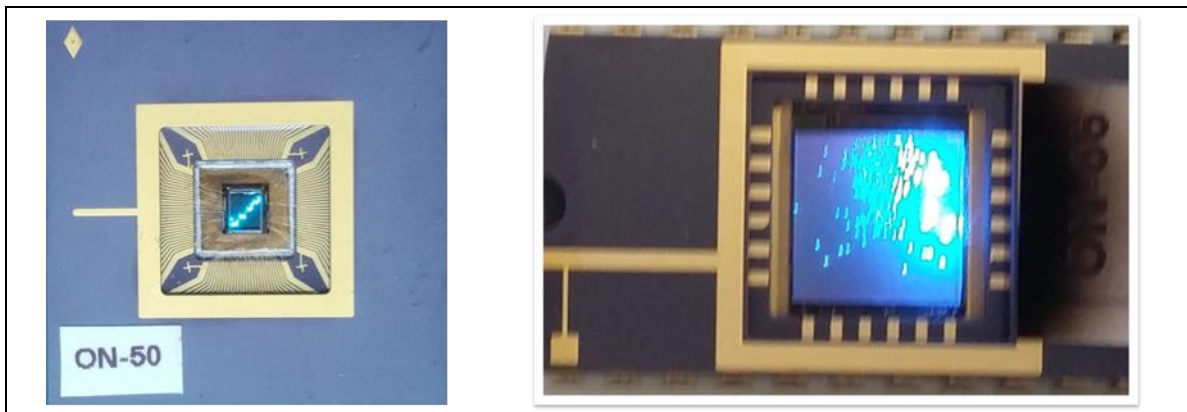


**Figure 2-17 Optoelectronic LEDs.** The 16x16 micro-LED array (left) and the 90x90 micro-LED array (right) chips

The micro-LED development involves a design of a CMOS controller/driver chip; it is used to address individual LEDs by an array of surface electrodes, which can be bump bounded to control individual micro-LEDs. The previous process contains three main parts: the LED fabrication, how it is bounded with the CMOS driver, and how the CMOS driver is used to control the LEDs. Each of these three parts is explained below.

**I. LED array fabrication:**

The first version of the fabricated micro-LEDs was done on 16x16 arrays and bonded with the equivalent CMOS control chips. The array size of 16x16 had a chip size of 2.4mm x 2.4mm, and spacing between centres of LEDs of 150µm. It was used for initial biological experiments and testing. For more advanced features, such as displaying more complicated day life images, 90x90 micro-LED arrays were developed. The array size 90x90 had a chip size of 8mm x 8mm, determined by the bonding pitch of the bonding machine. The spacing between each LED was 80µm.

**II. Micro-LEDs and CMOS bonding:**

Both the CMOS controller and the micro-LEDs need to be connected electrically, and the bonding method used is called a controlled collapse chip connection (C4), sometimes called a Flip Chip. It uses solder bumps placed onto the chip pads of a wafer during the final wafer processing step. Then, to attach the CMOS chip to micro-LED wafer, the latter is flipped over, its pads aligned to CMOS chip pads, and the solder reflowed to complete the connection.

**III. CMOS driver chip:**

The CMOS control circuit consists of three main blocks: the first block is the communication circuit, which is used to receive the image information from the pulse encoder, and shift data into array pixels. The second block is the pixel logic, which is used to determine the needed logic states to turn each pixel ON/OFF. The third block is the array controller, which is used to select different addressing modes, and provide the correct timing signal for different enables, such as shifting, reading and writing.

The main difference in the two versions of micro-LEDs, except for size, is the CMOS driver, and more details about each CMOS driver version are given below:

A) 16x16 micro-LEDs CMOS driver:

The CMOS driver chip implements a pixel logic block to maintain pixels in ON/OFF states. If the corresponding row and column are addressed (i.e. their logic value is equal to one), the selected pixel is toggled.

The controller block controls a mux that selects between four modes of operation, which are shown in Table 2-3.

- **Direct Mode**, which has 36 LEDs in the centre of the 16x16 micro-LEDs, is connected directly to external output pins, and then each LED can be controlled individually. This mode is simple and used for diagnosis purposes.
- **AER Mode** is used to address a single micro-LED; it uses four pins for the row pixel address, four pins for the column pixel address (both row and column use a 4x16 decoder to generate the address), an AddrValid pin (used to indicate address should be decoded, in order to distinguish between address 0000, and no data), one pin for the clock, and one pin for enable.
- **High Speed Raster Mode**, which is used to update a single row at a time, can be used to raster through the image row by row to test the whole array. It uses 16 parallel pin inputs, with one pin used to shift the row value serially, one pin for the clock, and one pin for enable.
- **Slow Speed Raster Mode**, which is considered a pure serial mode for both rows and columns. It is slow, but has the advantage of low pin count, and also in cases of lighting the entire array, this mode is the most efficient. It uses one pin for rows, one pin for columns, one pin for the clock and one pin for enable.

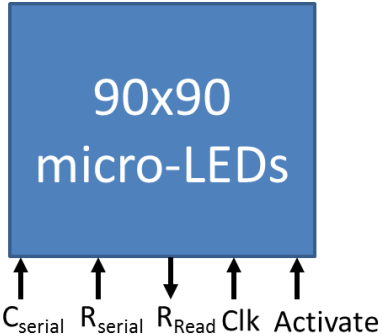
**Table 2-3 Modes of operation for the 16x16  $\mu$ LEDs Array**

Mux Select 1	Mux Select 0	Operation	# I/O
0	0	Direct Mode	
0	1	AER Mode	
1	0	High Speed Raster Mode	
1	1	Slow Speed Raster Mode	

B) 90X90 micro-LEDs CMOS driver:

The CMOS driver chip implements pixel memory block to maintain pixels in ON/OFF states. If the corresponding row and column are addressed (i.e. the logic value is equal to one) the selected pixel is either set or reset (depending on the sent command). The controller block selects from four modes of operation, as tabulated in Table 2-4.

**Table 2-4 The four different mode operations**

Row	Column	Mode	# I/O
0	0	Shift-Shift Write (Long)	
0	1	Shift-Shift Read (Long)	
1	0	Pixel-Reset (Short)	
1	1	Pixel-Set (Short)	

All data in the new version are sent using the serial mode. The first bit of the first burst is used to determine the operation mode, because the chip has two inputs, one for row and one for column, there are two control bits having four combinations. The first mode is the Shift-Shift Write, used to shift 90 bit data information for the row and the column. The second mode is the Shift-Shift Read, used to read the row data. It can be used to utilize the extra time available when using the pulse encoder. The third mode is the Pixel Reset mode, used to clear a single pixel. Finally, the Pixel Set mode is used to set a single pixel.

## 2.6 Conclusion

In this chapter, a full system overview for a visual prosthesis has been explored. The system was introduced in four stages: input, high level processing, low level processing and output. The first two are common to all visual prosthesis approaches, while the rest depend on the approach used.

**Input Stage:** this concerns image acquisition, where a comparison between different images is performed, to select the most suitable for the application. Then, the idea of using image fusion is introduced using dual spectrum visible/IR imagers, for image acquisition.

**High Level Processing Stage:** this is about preparing the image, which includes simplifying the image and removing unrelated details. Then, image retargeting is performed, where important information in the image is emphasized when the image is non-linear resized. After that, retinal processing operations are performed, as they are necessary to compensate for the missing retinal layer(s) functionality.

**Low Level Processing Stage:** with an optogenetic retinal prosthesis, the image must be prepared for the final micro-LED display. This includes the frame encoding that relates the received frame with time, which is achieved by pulse width modulation (PWM). Then, the frame is divided into sub-frames and micro-frames, where the even power distributor is used to spread the ON-state pulses through the frame time. After that, the pulse encoder is used to choose the best way to send data to the micro-LEDs, since it can receive the data in different ways.

**Output Stage:** with the optogenetic retinal prosthesis, this concerns the micro-LEDs, and different versions of micro-LEDs are described, as well as their different modes of operation.

The next chapter introduces the implementation of certain algorithms in the high and low processing stages, where in the high level processing, the dual spectrum IR/Visible scene preparation is explained. Next, at low level processing, a detailed discussion of the photonic stimulator controller implementation is provided.

## Relative contributions

Subject	Contribution
Mr Musa Al-Yaman	<ul style="list-style-type: none"><li>- Developed and implemented all different parts of the Photonic Stimulation Controller</li><li>- Implemented the Dual-spectrum Image preparation and validating the algorithm</li><li>- Implemented the Izhikevich neuron model</li></ul>
Dr. Walid Al Atabany	<ul style="list-style-type: none"><li>- Developed and implemented all the different parts of the <i>Image Retargeting</i> algorithm</li><li>- Originally suggested the Dual-spectrum Image preparation approach</li></ul>
Dr. Patrick Degenaar	<ul style="list-style-type: none"><li>- Suggested the Izhikevich neuron model to implement the Retinal Ganglion Cells (RGC)</li><li>- Designed and implemented the 90x90 optoelectronic micro-LEDs</li></ul>
Dr. Pleun Maaskant	<ul style="list-style-type: none"><li>- Designed and implemented the 16x16 optoelectronic micro-LEDs</li></ul>



# Chapter 3 Implementation

## 3.1 Chapter Overview

The main objective of this work is to find algorithms for improving the final displayed image, based on the characteristics of the human visual system, to help retinal prosthesis patients. In order to achieve the necessary real-time performance, a hardware realization of these algorithms was performed, considering the following metrics: real time processing, power consumption, flexibility and scalability.

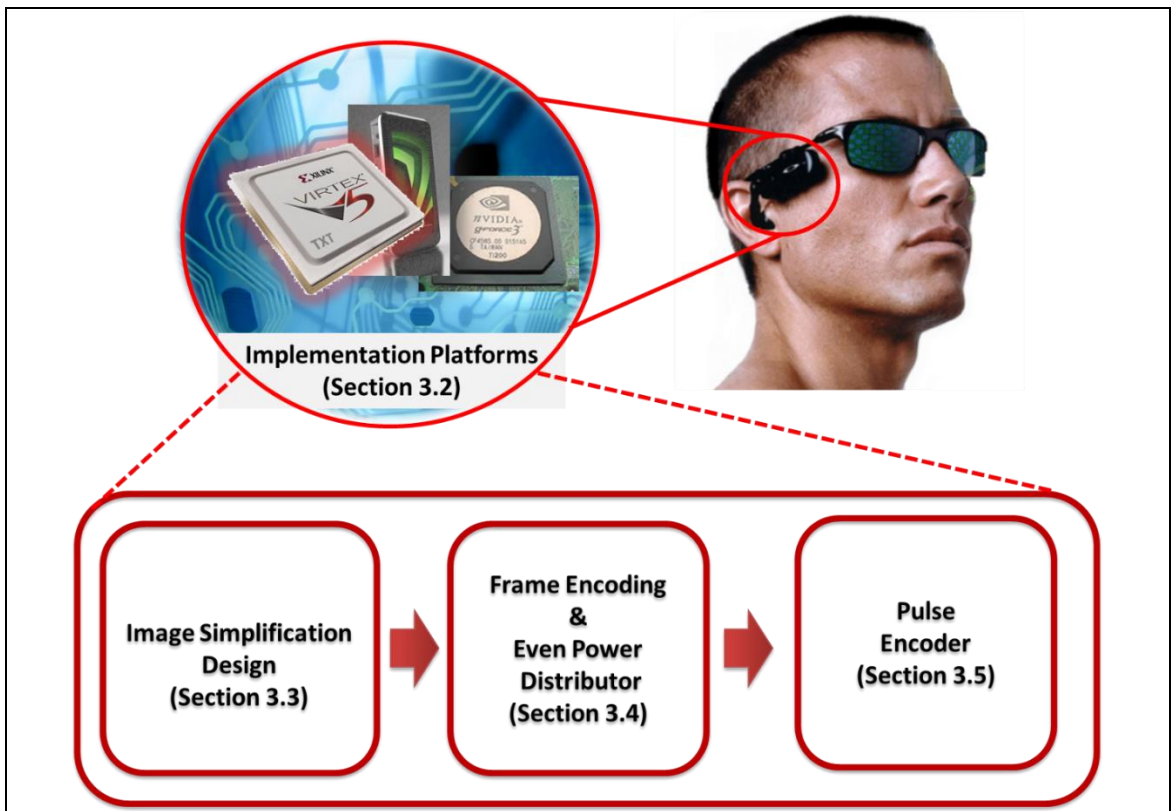


**Figure 3-1 Chapter three overview.** The chapter starts by describing the different implementation platforms, and then describes the design and implementation of three blocks used in optogenetic retinal prosthesis

In this chapter, the details of the hardware implementation for an optogenetic retinal prosthesis are presented, as shown in Figure 3-1. Section 3.2 discusses various possible hardware implementation platforms, and then a comparison of these is made, followed by the selection of the most suitable platform for retinal prosthesis system requirements. Section 3.3 discusses the image simplification algorithm implementation; this algorithm is used to emphasize the important features in the scene, using dual spectrum IR/Visible cameras. In Section 3.4, the frame encoding and even power distributor implementation is explained, which

was used to spread equally the ON state micro-LEDs to avoid power surges. Two hardware implementations of the pulse encoder are presented in Section 3.5, since two versions of the micro-LEDs, with different addressing modes, are available. The pulse encoder is used to control the micro-LEDs by selecting the most suitable addressing mode. Finally, Section 3.6 concludes the chapter and introduces the next.

### **3.2 Implementation Platform**

Recently, different options for implementing designs for algorithms have been presented, and these can be classified according to the algorithm execution of either sequential or parallel, or according to whether the architecture is fixed or reconfigurable. Next four possible implementation platforms are discussed and compared below in order to select one for the implementation of an optogenetic retinal prosthesis system.

Firstly, processors, which are hardware platforms, usually inside general purpose computers, but also embedded systems, and they are used to execute instructions within a program. The architecture of the processor is fixed after being defined, so that the user (programmer) needs to deal with this when writing programs. However, the microcontroller is a processor which is integrated with a memory and programmable peripherals to interface to embedded systems. Parallel processing has been suggested as a possible solution for high performance image processing [134]. Most solutions tend to be based upon pure SIMD (Single-Instruction-Multiple-Data). The typical SIMD approach involves distributing the image over a set of Processing Elements (PEs), with all of these PEs processing its own section of the image in parallel [135]. The idea of having a PE within each pixel of the image sensor array can lead to having thousands of processors working concurrently, and this in turn can achieve a very high processing speed. This work is called Vision chips, which have microelectronic devices that combine image sensing and processing on a single silicon die [136, 137].

Secondly, the graphics processing units (GPUs), which are primarily designed to accelerate computer graphics rendering. They have a parallel computing architecture [138] which allows a single instruction to process a set of data

simultaneously. GPUs were initially available on desktop computers and were widely used by computer games and specialized industrial design software for fast graphics processing. The hardware is well established so today's applications concentrate on the functionality rather than the small details that may affect the implementation. On the other hand, this leads to some constraints about using the existing available platform without any modification, so users must adjust their application to the most suitable form to work with the existing platform. The first versions of GPUs had a fixed rendering pipeline to take in vertex information and render pixels on a screen. Starting from 2001, GPU manufacturers introduced programmable shaders that allow developers to write their own instructions to manipulate vertices and pixels [139]. Currently, there is an increasing demand for using general purpose graphics processing units (GPGPU) rather than dedicated graphic cards, according to their ability to work as stream processors. As a result of this, an extension of APIs for C programming language is presented to program the GPGPU, the most famous of which are the two parallel computing platforms, CUDA ("Compute Unified Device Architecture") and OpenCL. The main difference between these two is that CUDA is used to program GPUs from the NVIDIA vendor, while OpenCL is used to program GPUs as well as CPUs, DSPs and FPGAs, from different vendors (using vendor specific SDKs).

Thirdly, Application Specific Integrated Circuit (ASIC), which is an integrated circuit customized for a particular use, rather than intended for general-purpose use. This type of implementation platform is an expensive choice, so to reduce this cost three main levels of ASIC customization are available. Firstly, there is the Gate Array level, which has unconnected silicon layers and users are allowed to customize the interconnections between these layers. It is considered the least ASIC cost and customizability. Secondly, there is the Standard Cell level, which has a library of components that can be used to make the designs. It is considered more flexible than the first level, under the condition that the library can meet design requirements. The third level is the Full Custom, which involves designs down to transistor level. It is considered the most flexible and costly level, but can provide any needed functionality for the design. ASIC designs offer the highest performance in speed and power consumption, ability to design analogue and

mixed signal circuits. However, the complexity, the inflexibility, and the cost associated with the design and fabrication is high.

Fourthly, Field Programmable Gate Array (FPGA), which is hardware that can be reconfigured as an application executes. With its inherent speed and adaptability, it seems an ideal candidate for image processing applications, with the main advantages being that it can be configured according to the needed application. These enable the user to hit the best performance of the specific designed platform; on the other hand, to make the design and include many details, this increases the general functionality of the whole system.

An FPGA generally consists of the following components:

- A matrix of programmable logic cells: The programmable logic cells are building blocks from which logic circuits are constructed. Their architecture ranges from very simple cells, such as cells that can implement any Boolean function of two one-bit inputs, to complex cells with several inputs and outputs using lookup tables to implement the logic function, these also contain one or more flip flops as storage elements.
- Input/output cells: these connect the logic cells to external signals, at the periphery of the array of the logic cells, and the input/output cells establish the link between the logic cells and the external package pins.
- A programmable routing network interconnecting the cells: FPGAs not only differ in their cell architecture, but also in the routing network, which interconnects the logic cells. The routing network usually provides direct connections between neighbouring cells, but is not only used to connect logic cells, as it also connects the logic cells to the input/output cells.

### **3.3 The Development Kit**

The FPGA consider a first step towards the final ASIC manufacturing, where it is considered a very low cost prototype, with nearly instant “manufacturing” [140]. This is because an FPGA can be considered a chip, whose final logic structure is directly configured by the end user. This leads to the use of an FPGA, so avoiding the integrated circuit production cycle.

Comparing processors with the FPGA, the latter is of great interest for its use in image processing applications, especially real-time video processing, due to its ability with design parallel processing architectures [141]. This parallelism in image processing algorithms can be applied mainly in spatial and temporal forms [82], which can be achieved using an FPGA. For example, the design could be constructed to divide the image and spread the resulting sections to multiple pipelines, all of which can process data concurrently [142, 143].

The performance of the FPGA and GPU in general purpose computation [144-149] has been well analysed, with a preference for either the FPGA or GPU according to the nature of the algorithm used in a specific application. Currently, GPUs have a large number of cores with large memory sizes, leading to very high performance. However, if a large amount of memory transfer is needed, a limited performance can be achieved, and additionally the fixed structure of GPUs can be another limitation for implementing retinal prosthesis algorithms. Table 3-1 summarises the differences between the different implementation platforms.

*Table 3-1 Comparison between different implementation platforms.*

	<b>Processor</b>	<b>GPU</b>	<b>ASIC (Digital)</b>	<b>FPGA</b>
<b>Hardware Architecture</b>	Fixed	Fixed	Fixed (after design sign-off)	Reconfigurable
<b>Level of parallelism</b>	Fixed number of pipelines	Fixed number of pipelines	Fixed number of pipelines (after design sign-off)	Flexible and reconfigurable pipelines and parallelism
<b>Power consumption</b>	Vary according to processor type	Consumes a great deal of power.	Lowest power consumption	Considerably consumes less power compared to other GPUs
<b>Implementation time</b>	Shortest	Short compared to the FPGA	Longest	Long compared to the GPU
<b>Good fit</b>	Applications that require sequential execution	Applications that require no interdependencies in the data flow	Applications that require a mass production with low power	Applications that require a great deal of low level hardware control

Many FPGA companies design development boards containing their FPGA with a number of peripherals that help the development of targeted applications. For image processing applications, the development board should have the following essential peripherals:

- Largest size of the specific FPGA family, which increases the number of algorithms that can be implemented in the same FPGA.
- Image sensor interfaced to the development board, and used to simplify getting images into the FPGA system.
- Standard communication interfaces, used to interface with a PC in the case of the biological experiments.
- The development board must have sufficient memory to buffer one or more frames of video data.

According to the project requirements listed above, the Spartan®-6 FPGA Industrial Video Processing Kit [150] has been selected, as well as the Virtex-5 ML501 evaluation board available in the lab. The experimental work can be done using two modes. The first mode is high level testing: it uses an Industrial Video Processing Kit, the main input stream comes from an Omnivision OV9715 720P Image Sensor, the output is displayed in a monitor. This mode can be used for full system low vision patient testing. The processing on the kit is based on a predefined pipeline using a soft processor from Xilinx called MicroBlaze. In this mode the main system configuration is done by utilizing the predefined pipeline and adding new blocks to it. Internally, the pipeline uses an interface called the Xilinx Video Streaming Interface (XVSI) to connect different system blocks, any new block connected to the pipeline must be modified to interface to (XVSI), because this bus interface is not standard for the MicroBlaze. The second mode is low level testing: this uses the ML501 kit, and in this mode full FPGA configuration needs to be written. The input is test patterns, which are generated from a MATLAB code written by neuroscientists. It is sent from a computer to an FPGA board via a standard RS232 COM port, and the output is displayed on opto-electronic micro-LEDs.

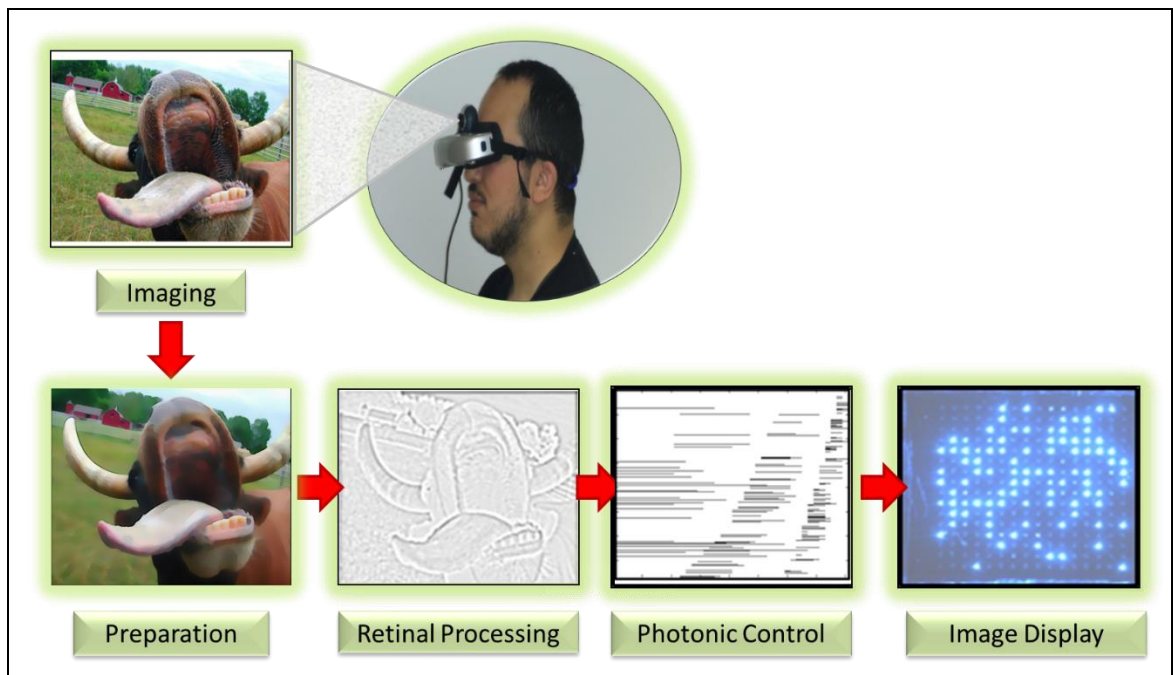


**Figure 3-2** The main stages in the approach for a retinal prosthesis start with image preparation, retinal processing, photonic control, and finally the image display.

The work completed in this thesis was performed using the second mode, low level testing, since the optogenetic retinal prosthesis is still in its initial phases, and no clinical experiments for humans have yet been approved. Figure 3-2 shows the key steps for an optogenetic retinal prosthesis [125] form of visual prosthesis. The original image flow is simplified, removing unnecessary back ground textures and enhancing edges, prior to further image processing to mimic the functions of the bypassed retinal circuitry. Finally, the processed images are redistributed to even out the power and then pulsed into the stimulator.

### 3.4 Image Simplification Design

For retinal prosthesis image simplification Al-Atabany et al. [99, 100] suggest to use an anisotropic diffusion filter, with edge enhancement to achieve a cartoonized version of the visual scene, before sending the image to display. In this work a dual spectrum IR/Visible simplification, based on Al-Atabany algorithms, is implemented for the optogenetic form of retinal prosthesis, as well it can be easily adapted for other forms of visual prosthesis, such as electronic retinal prostheses and visual cortical prostheses. The scene simplification implementation is divided into three main parts, labelled in Figure 3-3. Visible Preparation, IR Preparation and Mixing IR-Visible.

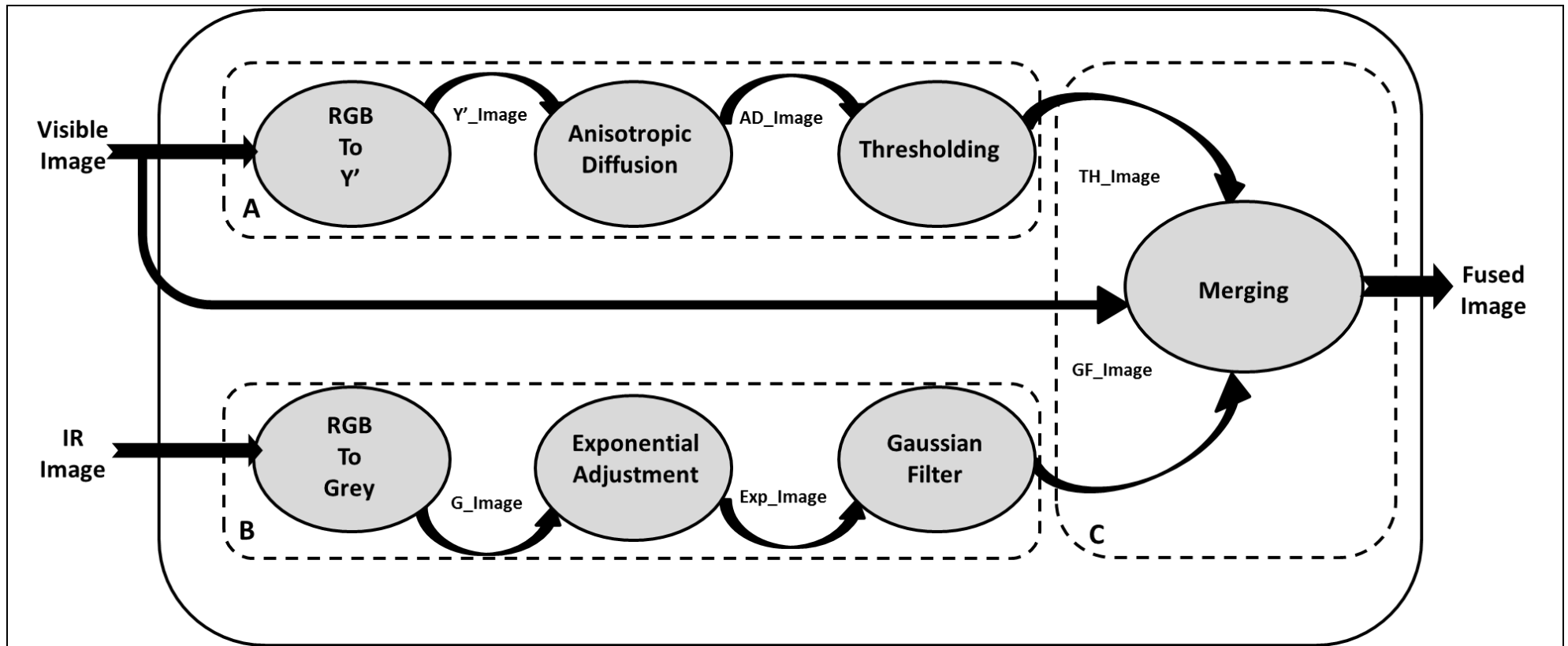


**Figure 3-3 A full architecture of scene simplification** (A) The Visible preparation and its three main steps (B) The IR preparation three main steps and (C) The merging block that produces the final Fused Image



### 3.4.1 Visible Preparation

The first part of the scene simplification is the visible preparation. This consists of three steps; the first step is the RGB to Y' conversion. Recently, retina prosthetic devices have used a grayscale image to stimulate the retina. Therefore, the visible RGB image (Visible Image) will be converted into Y'C<sub>b</sub>C<sub>r</sub> colour space, which takes human perception into account, allowing reduced bandwidth for chrominance components. The Y'\_Image is calculated using the following equation:

$$Y' = 0.25R + 0.5G + 0.09375B + 16 \quad (3-1)$$

Where Y' is the 8 bit output equivalent grayscale image. R, G and B are the 8 bit red, green and blue input colours of the image, respectively. The equation input coefficients used in this equation are powers of 2, the conversion is used the same standard equation for getting the value of Y', this includes adding fixed offset to the final result. The addition can be avoided, in order to improve the design and save FPGA resources.

The second step is the anisotropic diffusion filtering, which used to remove unnecessary background textures, without blur the edges. It was originally suggested by Perona and Malik in 1990 [127]. It is a nonlinear iterative process which increasingly smoothes an image while preserving the significant edges. The equation of the anisotropic diffusion in the discrete domain is:

$$I^{n+1} = I^n + \Delta K [\nabla(C \cdot \nabla I_x) + \nabla(C \cdot \nabla I_y)] \quad (3-2)$$

Where n denotes the iteration number between 1 and N;  $\nabla$  is the gradient operator; C is the diffusion coefficient;  $\Delta K$  is the smoothing step (it controls the accuracy and the speed of the smoothing) and  $\nabla I_x$ ,  $\nabla I_y$  represents the diffusion in horizontal and vertical directions.

In general, to convolve a 2D image with NxM mask, it requires (NxM) multiplications for each sample. However, if the mask is separable then it needs only (M+N) multiplications for each sample. The main task needed in the calculation of the anisotropic diffusion filter is the convolution with a 3x3 Sobel operator (GX, GY) shown in Figure 3-4. Applying a 3x3 Sobel operator in horizontal direction requires six multiplications, similarly in vertical direction,

which leads to **12** multiplications. Same number of multiplications is needed when using the separable property. In my design the convolution done without separation of the mask to avoid the cost of additional storage (buffer) needed to keep intermediate computations. Noticing that the Sobel operator has mask values of **1** or **2**, this case can be implemented without any multiplication using the shift operation, to save FPGA resources.

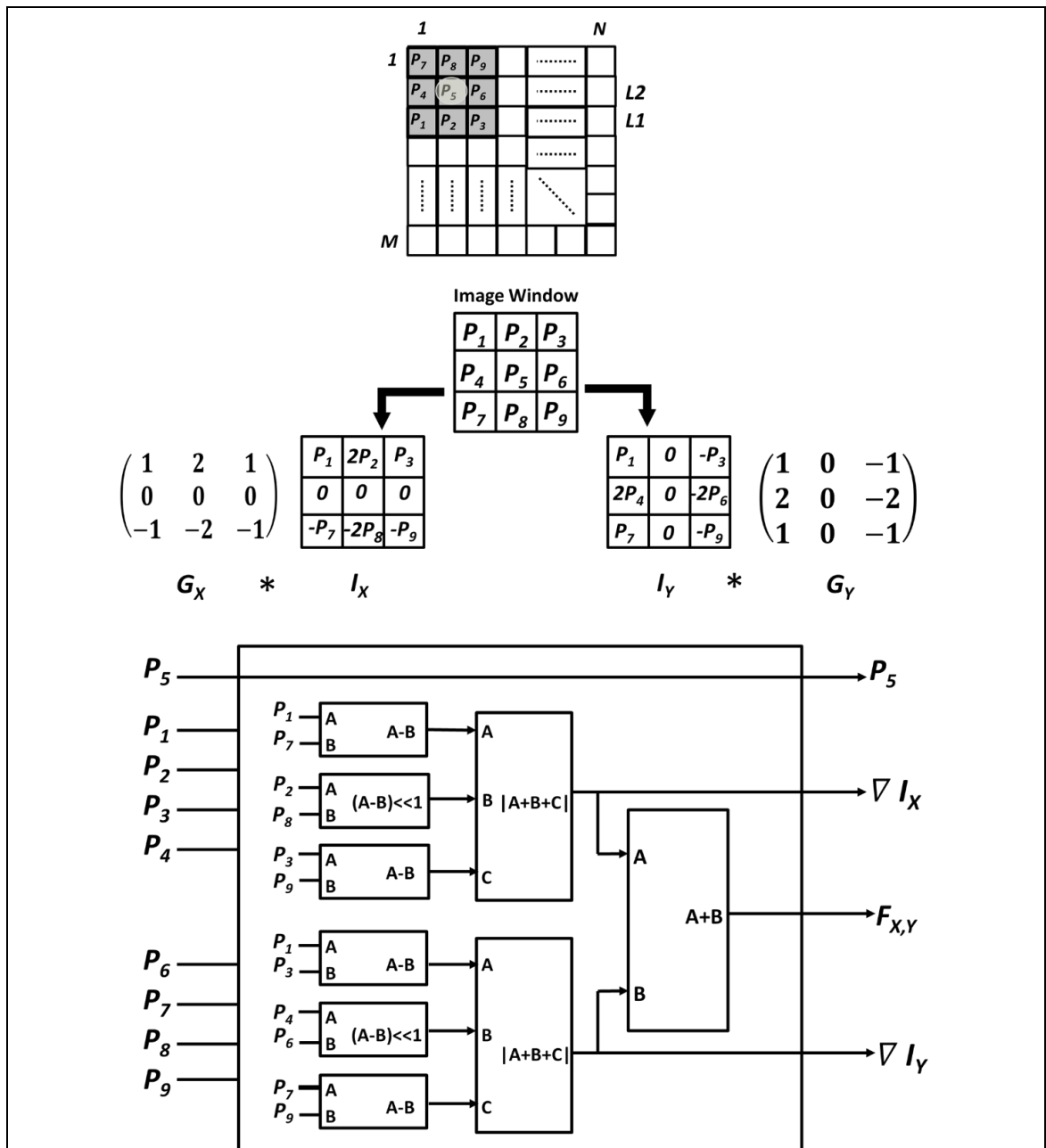


**Figure 3-4 Universal Sobel Module (USM) Architecture.** The image window and how the Sobel operator values spread over image window pixels in horizontal ( $I_x$ ) and vertical ( $I_y$ ) directions, leading to the pixel arrangement found in the main block of USM. It contains only the simple operations of addition, subtraction and shifting to achieve the final result

Figure 3-4 shows the Universal Sobel Module (USM) internal design where  $P_1, P_2, P_3, P_4, P_5, P_6, P_7, P_8$  and  $P_9$  represent the nine 8-bit pixel inputs to the Universal Sobel Module. The module consists of simple signed subtractors, shift registers and adders, and has four outputs. Initially, the first two outputs  $\nabla I_x, \nabla I_y$ , are convolution results after applying  $G_x, G_y$  respectively, with  $P_5$  neighbours in a 3x3 image window. The third output is  $F_{x,y}$  which is the summation of absolute values of the gradients using the approximation in equation 3-3. In this equation the approximation, is used to avoid the complications of finding the square of two numbers then adding them, after that finding the square root of the result. This approximation introduces an error in the magnitude of the edge, which is acceptable in the retinal prosthesis application due to two main reasons; first, the final stimulator output size limitations lead to retarget the image before displaying it. Second, the importance of having real time operation with minimum power consumption. The fourth output is the P5 output, which is used later to update the image as equation 3-2 illustrates.

$$F_{(X,Y)} = \sqrt{((\nabla I_x)^2 + (\nabla I_y)^2)} \approx |\nabla I_x| + |\nabla I_y| \quad (3-3)$$

After introducing the internal architecture of the main block (USM) in the anisotropic diffusion, I will then introduce the anisotropic diffusion filter internal architecture implementation that is shown in Figure 3-5. This starts with the entry point where the information stream arrives, labelled as the Y'\_Image, heading to Buffer 1. Buffer 1 is a Buffer used to store the pixels of the image necessary to complete the convolution operation. The minimum number of pixels needed to store for a convolution with VxV mask window and NxN image size is given in the following equation:

$$\text{Min(Buffer Size)} = V + (V - 1)N \quad (3-4)$$

This design uses a 3x3 Sobel operator for convolution, and needs a buffer size of (3+2N), where N is the number of rows or columns in the image. The buffer has nine image pixel outputs corresponding to mask coefficients, as illustrated in Figure 3-4 (P1-P9). These outputs drive the USM module.

The details of the Universal Sobel Module (USM) are explained above. To calculate the diffusion coefficient (C), one needs to be added to the (F<sub>x,y</sub>) output, from the USM, to prepare the denominator, as equation 3-5 shows.

$$C = \frac{1}{1 + \sqrt{(\nabla_x I)^2 + (\nabla_y I)^2}} \quad (3-5)$$

Then,  $\nabla I_x$ ,  $\nabla I_y$  need to be divided by  $(F_{x,y})$  plus one in order to get  $(C \cdot \nabla I_x)$  and  $(C \cdot \nabla I_y)$ , respectively. The approximated results are calculated and then rounded and stored in a lookup table which has two inputs (I, F) and one output that feeds Buffer 2. Buffer 2 has three buffers of size  $(3+2N)$ , two of which store the  $(C \cdot \nabla I_x)$  and  $(C \cdot \nabla I_y)$  that are used later to calculate  $\nabla(C \cdot \nabla I_x), \nabla(C \cdot \nabla I_y)$ , respectively. The third is used to store the pixel in the centre of the window (circled in blue), and it is used later to compute the anisotropic diffusion result, by adding to  $\nabla(C \cdot \nabla I_x), \nabla(C \cdot \nabla I_y)$  summation result, after multiplying it with  $\Delta K$ , as illustrated in equation 3-2. SUSM is the same as the USM module, except that the unused circuits are excluded to minimize the power consumption, and then  $\nabla(C \cdot \nabla I_x), \nabla(C \cdot \nabla I_y)$  is added. After this, the summation result is multiplied with  $\Delta K = 0.25$  (this value is selected based in human trails done in [100]), and then next the latter result is added to the central pixel P5. Finally, the output is returned back to input to do a next iteration (n), and this is continues until the N counter (which holds the number of iterations) equals zero; then, the final output image (AD\_Image) is ready.

The third step in the visible image preparation is the thresholding where two pre-defined threshold values,  $\tau_{min}$ ,  $\tau_{max}$  are used to set all the pixels of the (AD\_Image) below  $\tau_{min}$  to 0, and all the pixels above  $\tau_{max}$  to 255. The final image in the visible preparation stage (TH\_Image) is used in the fusing part.

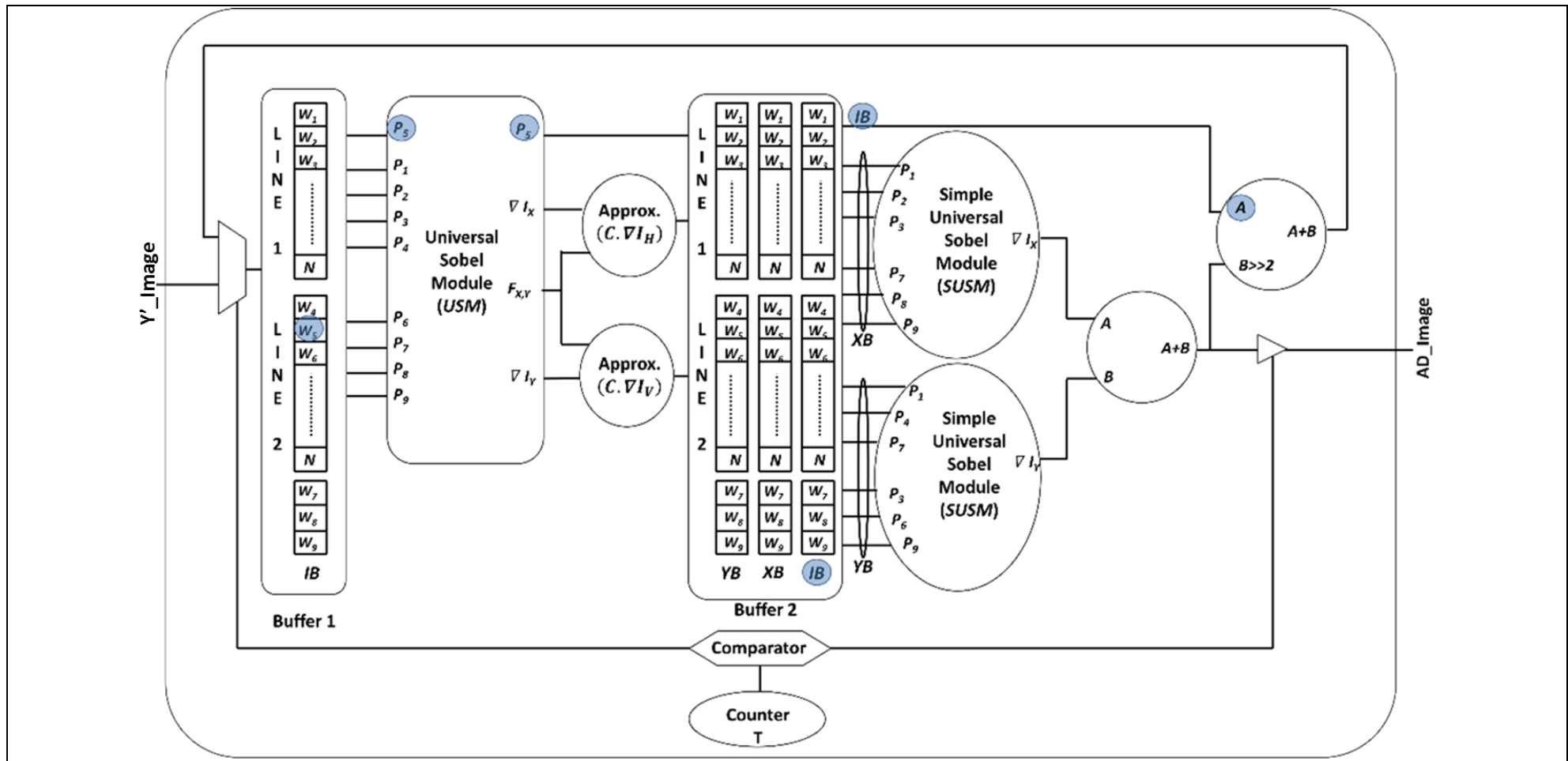


**Figure 3-5 A full anisotropic diffusion filter architecture** consisting of a Universal Sobel Module (USM), two buffers with two Simple Universal Sobel Modules (SUSM) with the same functionality of USM but eliminating unnecessary circuit elements. Finally, simple add/shift circuits with an approximation of the product terms  $(C. \nabla I_x)$  and  $(C. \nabla I_y)$

### 3.4.2 IR Preparation

The second part of the scene simplification is the IR preparation. The idea of using infrared cameras comes from the fact that all objects act as black body radiators. They thus emit thermal photons of wavelength and intensity according to their temperature. This additional spectrum is used to segment objects with temperatures different to the ambient temperature. In this work the IR camera (Optris PI 160) uses a software called **Optris PI Connect**, which does a kind of mapping to convert the thermal information into RGB colour space. Therefore, IR preparation consists of three steps; the first step starts by converting the RGB input image (IR Image) into a grey scale (G\_Image) using equation 3-6.

$$GR = 0.375R + 0.5G + 0.125B \quad (3-6)$$

The factors of the colours used in equation 3-6 are power of two, thus simplifying the multiplication process to a simple shift operation.

Then, the second step is an exponential scaling function, which utilizes equation 3-7 to segment the hot and cold objects from the surrounding background. Exponential scaling changes the dynamic range of the image in order to enhance the high intensity pixel values while decreasing the low intensity pixel values. Thus, by utilizing such scaling on both low and high ends of the image, important structures at temperature extremes can be segmented, while less important ambient temperatures at the median intensity of the image are ignored.

$$\begin{aligned} I_{\text{exp}} &= e^{0.025 \cdot I} & (a) \\ I_{\text{Nexp}} &= e^{0.025 \cdot (255 - I)} & (b) \end{aligned} \quad (3-7)$$

Where  $I$  is the original image,  $I_{\text{exp}}$  and  $I_{\text{Nexp}}$  are the exponentially scaled images for the original and its negative. Then, the two exponentially scaled images are added together and scaled exponentially in order to suppress the low intensity pixel values. The resulting image includes the segmented cold and hot objects existing in the original infrared image.

$$IR_{\text{segmented}} = e^{0.025 \cdot (I_{\text{exp}} + I_{\text{Nexp}})} \quad (3-8)$$

The input of this block is a grey scale image with 256 possible input intensities (from 0-255), so the final output for equations 3-7 and 3-8 is calculated and stored

using a lookup table in the FPGA. This allows the mapping of the input image (G\_Image) to the output image (Exp\_Image).

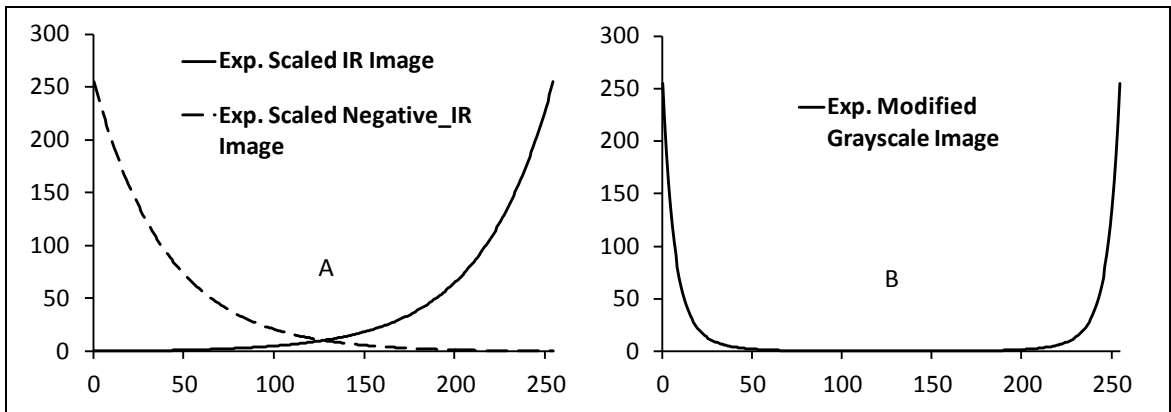


**Figure 3-6 Exponentially stretching and compressing the greyscale range for the original image and the negative of it (A). The addition of the two images is exponentially scaled in (B) [109]**

The resulting image includes the segmented cold and hot objects existed in the original infrared image. In Figure 3-6, the output greyscale range of an 8-bit intensity scale is shown.

The third step aims to remove any discontinuity, so the segmented image is smoothed by convolving it with a Gaussian filter.

$$\widehat{IR}_{\text{segmented}} = IR_{\text{segmented}} * G(x, y) \quad (a)$$

$$G(x, y) = \frac{1}{2\pi\sigma^2} e^{-(x^2+y^2)/2\sigma^2} \quad (b) \quad (3-9)$$

In FPGA implementation for the Gaussian filter, is built to utilize the same Sobel filter architecture with changing mask values, it is more efficient if the 2D mask is separated into two 1D masks. The input buffer is initialised with the size of two incoming rows from the input image (Exp\_Image), as shown in Figure 3-7 below. A simple shift left and addition are used for the calculations, as all coefficients of Gaussian filter are powers of two and the final division by 16 is done using shift right. The final image in the IR preparation stage (GF\_Image) is used as a decision map to segment and fuse the final enhanced image.

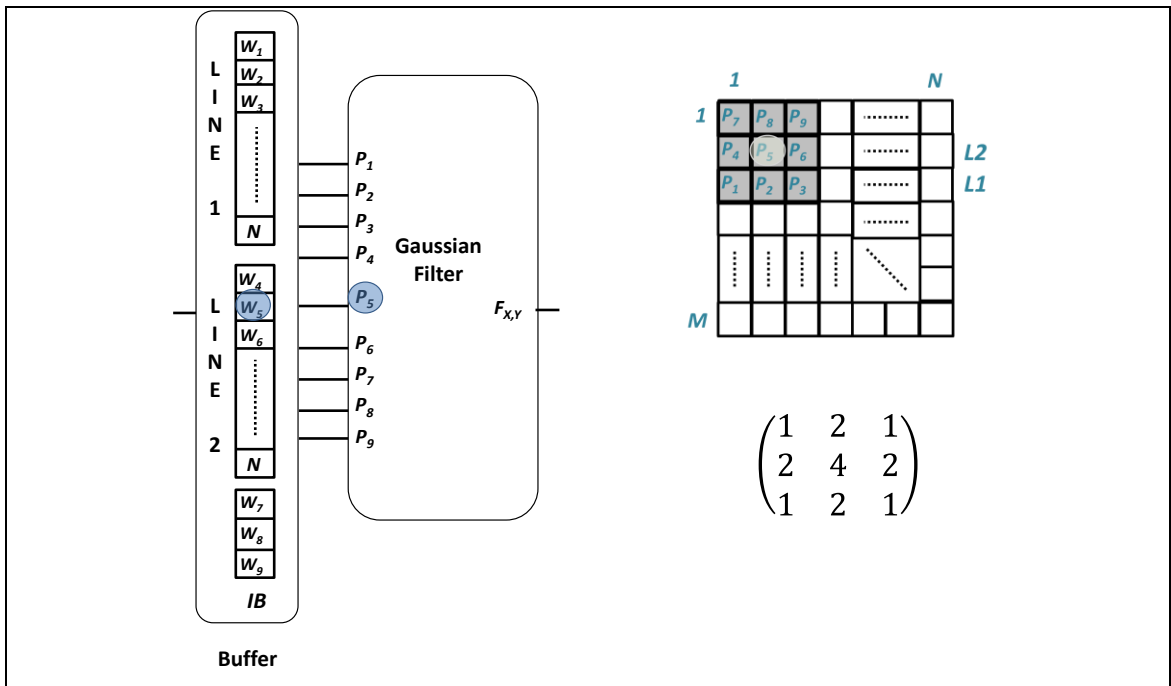


**Figure 3-7 The Gaussian filter with the buffer used to prepare the nine 8-bit data for the mask**

This infrared segmented image is used as a decision map for subsequent processing. Additionally, this map can be used to generate the retargeting map, which is based on the segmented image and can be used in the retargeting process.

### 3.4.3 Mixing IR-Visible

The third part of scene simplification is the mixing part, where the infrared segmented image (GF\_Image) is used to create weighted decision regions by which a linear combination of the pixels in the visible (Visible Image) and the cartoon visible (TH\_Image) images is used to generate corresponding pixels in the fused image. Then, the fused image is:

$$\begin{aligned}
 I_{\text{fused(Cartoon)}} &= \widehat{IR}_{\text{segmented}} * I_{\text{Visible(Cartoon)}} \\
 &+ (255 - \widehat{IR}_{\text{segmented}}) * I_{\text{Visible}}
 \end{aligned}
 \tag{3-10}$$

Currently, low resolution retina prosthesis devices do not provide chromatic information due to their low resolutions, although this may change in upcoming generations.

Finally, the design of IR/Visible preparation is synthesized using the following FPGA device: Spartan-6 XC6SLX150t-3, and in Table 3-2 the utilization of resources used in the design are presented.



**Table 3-2** The FPGA used resources with maximum frequency and power

Logic and Memory Resources	Used	Available	Utilization
Number of Slice Registers	3,115	184,304	2%
Number of Slice LUTs	1,631	92,152	2%
Number of Occupied Slices	422	23,038	2%
Maximum Internal Frequency	44.217MHz		
Est. Power Consumption	559 m W		

Most visual prostheses will be wearable technology and higher resolutions with lighter weight are desirable. In this work, the image acquisition was performed using dual spectrum IR/Visible image sensors. One counter argument to the use of dual IR/Visible images sensors is that adding an additional camera will increase the size and weight of the system. The used Optris camera is too bulky to be used in a head mounted display especially with the beam splitter arrangements. However, this was a prototype to prove the concept. Recently, a rapid improvement in the compactness and cost of these systems is available [151].

**Table 3-3** Comparison between the CPU/FPGA processing time

Image size	32x32	64x64
FPGA (40MHz)	0.09 ms	0.15 ms
CPU (2.6 GHz)	52 ms	78 ms

The IR/Visible image simplification algorithm presented in this work have been implemented on a sequential CPU processing format using the Matlab platform. Table 3-3 gives CPU's and FPGA's processing time comparison using two image sizes (32x32, 64x64). The IR/Visible algorithm was performed using these settings: convolution mask was a 3x3 Sobel, and the number of iteration used in the anisotropic diffusion was three. The CPU implementation was accomplished using a desktop computer; HP workstation XW4600 with a 2.6GHz Intel processor. The FPGA implementation was accomplished using SPARTAN-6

xc6slx150t running at 40 MHz, it can be seen that the processing speed is raised approximately by a factor of 550x using FPGA.

### 3.5 Frame Encoding and Even Power Distributor

In the optogenetic retinal prosthesis approach, the neurons are photosensitized via an opto-electronic LEDs array. The image sensor takes an image frame and then high level processing is performed on that frame, and finally the processed frame is sent to the LEDs.

Frame encoding is used to relate processed frame pixel intensities with the time needed to light the LEDs. In this work, this is accomplished by dividing each frame into a number of sub-frames equal to the different maximum frame pixels intensities. In the system used in the experiments, 16 levels of intensity were used. Thus, each pixel is represented in four bits, with the frame divided into 16 sub-frames, and then these values are used to determine the number of sub-frames that the pixel should be in the ON state.

To clearly illustrate the concept of Frame Encoding the following example is introduced: A 3x3 image consists of **9** pixels with the following intensities Image

2	4	5
12	10	8
7	15	13

Maximum intensity level is 16, Minimum intensity level is **0**, the number of sub-frames is **16**, the pixels arrive to the frame encoding as the following 1D array:

<b>P<sub>1</sub></b>	2
<b>P<sub>2</sub></b>	4
<b>P<sub>3</sub></b>	5
<b>P<sub>4</sub></b>	12
<b>P<sub>5</sub></b>	10
<b>P<sub>6</sub></b>	8
<b>P<sub>7</sub></b>	7
<b>P<sub>8</sub></b>	15
<b>P<sub>9</sub></b>	13

Then the result of frame encoding is shown below:

	SF	SF	SF	SF	SF	SF	SF	SF	SF	SF	SF	SF	SF	SF	SF	SF
	1	2	3	4	5	6	7	8	9	10	11	12	13	14	15	16
P <sub>1</sub>	1	1														
P <sub>2</sub>	1	1	1	1												
P <sub>3</sub>	1	1	1	1	1											
P <sub>4</sub>	1	1	1	1	1	1	1	1	1	1	1	1				
P <sub>5</sub>	1	1	1	1	1	1	1	1	1	1						
P <sub>6</sub>	1	1	1	1	1	1	1	1								
P <sub>7</sub>	1	1	1	1	1	1	1									
P <sub>8</sub>	1	1	1	1	1	1	1	1	1	1	1	1	1	1	1	
P <sub>9</sub>	1	1	1	1	1	1	1	1	1	1	1	1	1			

To have even number of ones in each sub-frame the following equation is used:

$$SubFrameONLEDs = \left\lfloor \sum Pi / NumberofSubFrames \right\rfloor \quad (3-11)$$

For the above example the summation of pixels values ( $\sum Pi$ ) equals **76**, the number of sub-frames equals **16**, then the number of *SubFrameONLEDs* equals  $\lfloor 76/16 \rfloor$ , which leads to have maximum **5** ON-State LEDs at each sub-frame.

The first method to have maximum **5** ON-State LEDs at each sub-frame is to use first come first serve principle. Using the same example above, we start the first five pixels ON, then every pixel finished is replaced by new one, the following distribution is obtained:

	SF	SF	SF	SF	SF	SF	SF	SF	SF	SF	SF	SF	SF	SF	SF	SF
	1	2	3	4	5	6	7	8	9	10	11	12	13	14	15	16
P <sub>1</sub>	1	1														
P <sub>2</sub>	1	1	1	1												
P <sub>3</sub>	1	1	1	1	1											
P <sub>4</sub>	1	1	1	1	1	1	1	1	1	1	1	1				
P <sub>5</sub>	1	1	1	1	1	1	1	1	1	1						
P <sub>6</sub>			1	1	1	1	1	1	1	1						
P <sub>7</sub>					1	1	1	1	1	1	1					
P <sub>8</sub>							1	1	1	1	1	1	1	1	1	1
P <sub>9</sub>											1	1	1	1	1	1
$\sum$	5	5	5	5	5	5	5	5	5	5	4	3	2	2	2	2

The problem of using this method appears in the last two rows, where the pixels did not finish during the frame time. A modified version of this method is to have a variable frame time, in which the frame time is ended when the last pixel finished, this leads to a more complicated control of frames since the input frame rate from the camera is fixed.

Another method to implement the even power distributor is to sort the pixels, then start with the largest pixels' values, this guarantees that all the pixels finish within the frame time, in the same time keeps the frame time fixed. Using the sorting solution with the example above leads to the following distribution:

	SF	SF	SF	SF	SF	SF	SF	SF	SF	SF	SF	SF	SF	SF	SF	SF
	1	2	3	4	5	6	7	8	9	10	11	12	13	14	15	16
P <sub>1</sub>														1	1	
P <sub>2</sub>													1	1	1	1
P <sub>3</sub>											1	1	1	1	1	
P <sub>4</sub>	1	1	1	1	1	1	1	1	1	1	1	1				
P <sub>5</sub>	1	1	1	1	1	1	1	1	1	1						
P <sub>6</sub>	1	1	1	1	1	1	1	1								
P <sub>7</sub>									1	1	1	1	1	1	1	
P <sub>8</sub>	1	1	1	1	1	1	1	1	1	1	1	1	1	1	1	
P <sub>9</sub>	1	1	1	1	1	1	1	1	1	1	1	1	1			
$\Sigma$	5	5	5	5	5	5	5	5	5	5	5	5	5	5	5	1

The sorting approach gives better results for the distribution, and all pixels finish within the frame time. It bear mentioning when sorting the pixels, that there is no need to accurately sort the pixels, an approximate sorting can be used. Furthermore, the locations of the pixels need to remains the same, since each pixel is corresponds to a fixed location on the micro-LEDs stimulator, so the sort operation should not change the pixels themselves, instead a sorted address table is generated, which includes the approximately sorted addresses.

The general flowchart of the final design of the even power distributor is shown in Figure 3-8. The main algorithm that takes the processed image, in a form of 1-D array, then it executes the following main three stages:

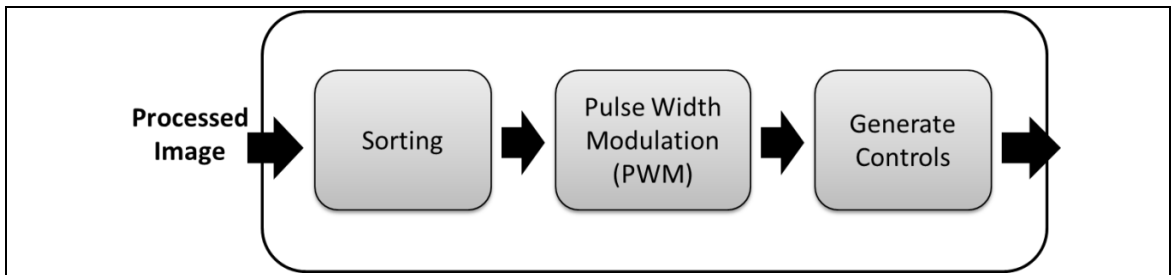


**Figure 3-8** The main flow chart for the even power distributor. It involves three main stages: sorting, Pulse Width Modulation (PWM) and generating control signals

- Sorting: the pixels in the processed image are sorted to start with the larger pixel values to ensure that they finish during frame time.
- Pulse Width Modulation (PWM): the actual PWM is done to only a certain number of pixels (Equation 3-11), to make sure there is an equal number of ON-State LEDs at each sub-frame.
- Control signal generation: the ON signals need to be sent to the stimulator are based on the used micro-LED type.

### 3.5.1 Sorting

The first stage in the even power distributor algorithm is sorting, which is an important stage since the processed image has different pixel values. The algorithm must start with the large pixels so they can finish before the frame time ends, in the same time there is a need to get the index of the largest pixels, in order to sort the indexes rather than sorting the pixels themselves. Figure 3-9 illustrates the developed sorting algorithm.

The sorting algorithm consists of the following three main steps:

**The first step** is to scan all pixels in the received 1-D array to decide to which group it belongs; where the group is a range of numbers (i.e. 0-3), the reason for using groups that the algorithm requires only approximate sorting, and this speeds up the sorting process. Determining the group of each pixel is accomplished by comparing the pixel value ( $P_i$ ) with the upper bound of each group ( $L_1, L_2, L_3, \dots, L_{n-1}$ ), if it is less than this value the number of elements in the current group ( $T_1, T_2, T_3, \dots, T_n$ ) is incremented by one. Another calculation in the first step is to accumulate the summation of pixels' values into a variable called **Total**, which used later to determine the number of ones in each sub-frame.

In the previous example the 1-D array, is divided into four groups (0-3, 4-7, 8-11, 12-16), after applying the first step of the sorting stage, the results are as following:

	Range	L	T
Group1	0-3	$L_1 = 3$	$T_1 = 1$
Group2	4-7	$L_2 = 7$	$T_2 = 3$
Group3	8-11	$L_3 = 11$	$T_3 = 2$
Group4	12-16	-	$T_4 = 3$
<b>Total=76</b>			

**The second step** is to calculate the bases; where the base is the starting address of each group, the number of pixels in each group ( $T_1, T_2, T_3... T_n$ ) is used in this calculation. The smallest values group base address ( $B_1$ ) starts at zero, then second group base address ( $B_2$ ) starts at address ( $T_1$ ), after that the third group base address ( $B_3$ ) starts at ( $T_1+T_2$ ), this continues until the last group base address ( $B_n$ ) starts at ( $T_1+T_2+...+T_{n-1}$ ). Another calculation in the second step is to find the *SubFrameONLEDs* value, using equation 3-11, which represents the number of ON-State LEDs in each sub frame.

The outcomes of the second step are shown below:

	Range	L	T	B
Group1	0-3	$L_1 = 3$	$T_1 = 1$	$B_1 = 0$
Group2	4-7	$L_2 = 7$	$T_2 = 3$	$B_2 = 1$
Group3	8-11	$L_3 = 11$	$T_3 = 2$	$B_3 = 4$
Group4	12-16	-	$T_4 = 3$	$B_4 = 6$
<b>Total=76</b>				
<i>SubFrameONLEDs</i> = 5				

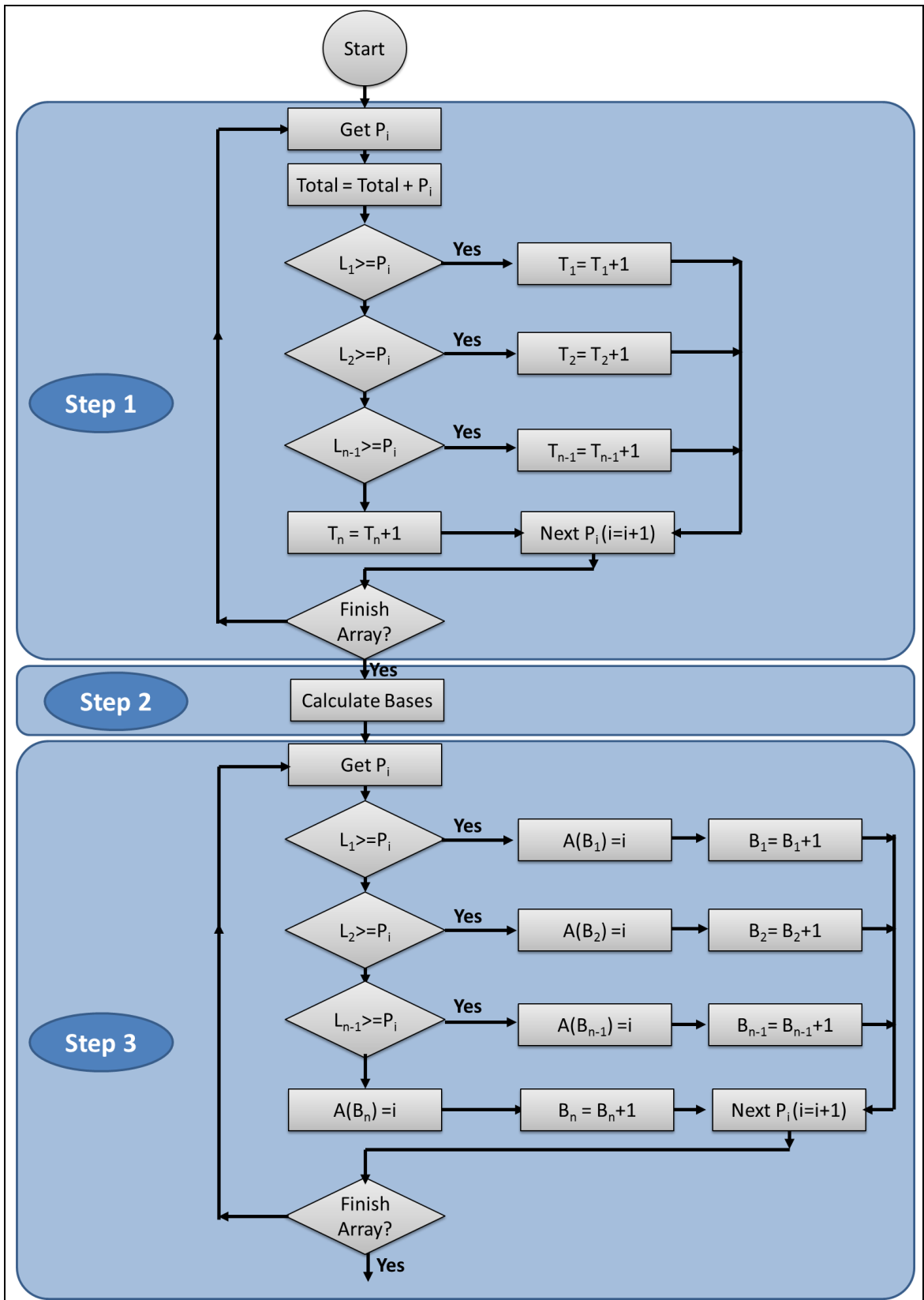


**Figure 3-9 The sorting stage.** This needs two main scans through the array to sort the indexes

The third step in the sorting algorithm requires one more scan for the pixels' values ( $P_i$ ), in order to fill the output array ( $A$ ) with an approximately sorted addresses of the pixels. This is accomplished by comparing the pixel value ( $P_i$ )

with the upper bound of each group ( $L_1, L_2, L_3... L_{n-1}$ ), then if less than this value the index of the pixel ( $i$ ) is stored at the output array ( $A$ ) in the selected base address ( $B_1, B_2, B_3, \dots, B_n$ ), then the selected base address is incremented by one to refer to the next pixel in the selected group.

The result of the example after executing the third step of the sorting stage is updated with the following approximately sorted addresses array:

<b>B</b>	<b>Index array (A)</b>	<b>Pixels value (P)*</b>
<b>B<sub>1</sub></b>	<b>1</b>	<b>2</b>
<b>B<sub>2</sub></b>	<b>2</b>	<b>4</b>
<b>B<sub>2</sub></b>	<b>3</b>	<b>5</b>
<b>B<sub>2</sub></b>	<b>7</b>	<b>7</b>
<b>B<sub>3</sub></b>	<b>5</b>	<b>10</b>
<b>B<sub>3</sub></b>	<b>6</b>	<b>8</b>
<b>B<sub>4</sub></b>	<b>4</b>	<b>12</b>
<b>B<sub>4</sub></b>	<b>8</b>	<b>15</b>
<b>B<sub>4</sub></b>	<b>9</b>	<b>13</b>
* (P) is added for demonstration only, the output is (A)		

The output of the third step in sorting is an array of approximately sorted addresses ( $A$ ), used to determine which array elements should be started in the next stage of the even power distributor algorithm.

### 3.5.2 Pulse Width Modulation (PWM)

The second stage of the even power distributor is performing the actual PWM for the number  $SubFrameONLEDs$  calculated using equation 3-11. In this stage the pixels 1-D array is converted into 2-D **binary** array ( $O$ ), where the first dimension is 1-D pixels number ( $i$ ), and the second dimension is the sub-frame number ( $j$ ). This stage consists of three steps, as shown in Figure 3-10, the first step is to access the index array ( $A_i$ ), to retrieve the approximately sorted address of the pixel, to start the PWM with the group that has largest values. The second step is to load the pixel at the address ( $A_i$ ), returned in the first step, ( $P(A_i)$ ). The third step is to determine whether to do the PWM process or not. If **Total\_ON** (the number of ON-State pixels) is greater than  $SubFrameONLEDs$  (calculated using



equation 3-11), the binary output ( $O_{ij}$ ) is reset to zero, where ( $i$ ) is the pixel number and ( $j$ ) is the sub-frame number, in this case, no need for using PWM . On the other hand, if **Total\_ON** is less than *SubFrameONLEDs* , the PWM process is performed, these three steps are repeated every sub-frame till they finish and a new frame is loaded.

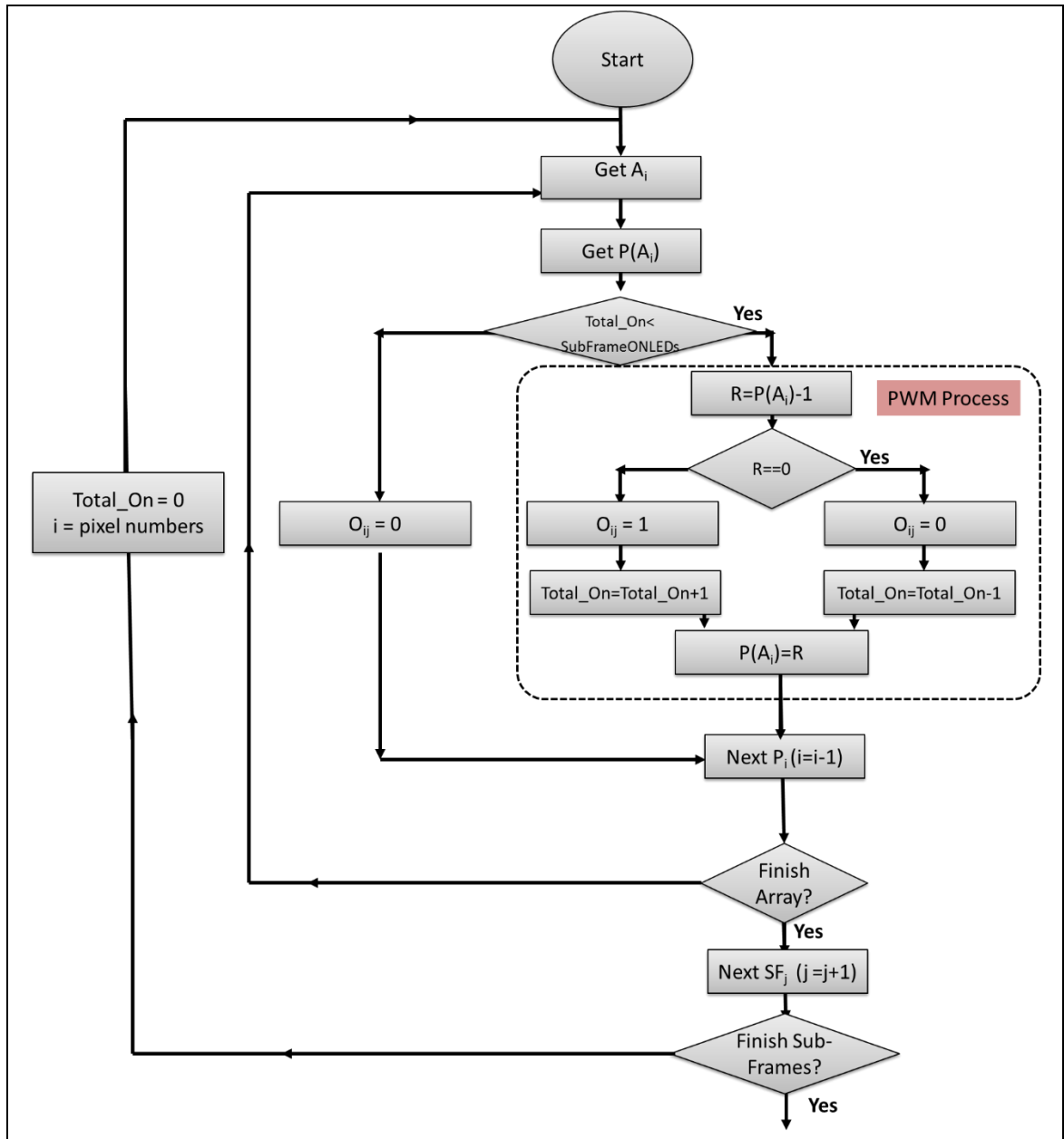


**Figure 3-10 The PWM stage.** Starting with setting the pulse level and then the pulse stays ON for a value equal to the intensity of that pixel

In the PWM process, the loaded pixel ( $P(A_i)$ ) is decremented by one, and stored in a temporary value ( $R$ ), as long as the value  $R$  is not zero, the output value ( $O_{ij}$ ) for pixel ( $i$ ) at that sub-frame ( $j$ ) is set to one and the (**Total\_ON**) variable is incremented. if ( $R$ ) equals zero, this means that this pixel has finished its ON-

State period, and the output value ( $O_{ij}$ ) for pixel ( $i$ ) at that sub-frame ( $j$ ) is reset to zero and the variable (**Total\_ON**) is decremented.

The output of this stage according to the example is:

	SF	SF	SF	SF	SF	SF	SF	SF	SF	SF	SF	SF	SF	SF	SF	SF
	1	2	3	4	5	6	7	8	9	10	11	12	13	14	15	16
P <sub>1</sub>	0	0	0	0	0	0	0	0	0	0	0	0	0	1	1	0
P <sub>2</sub>	0	0	0	0	0	0	0	0	0	0	0	0	1	1	1	1
P <sub>3</sub>	0	0	0	0	0	0	0	0	0	0	1	1	1	1	1	0
P <sub>4</sub>	1	1	1	1	1	1	1	1	1	1	1	1	0	0	0	0
P <sub>5</sub>	1	1	1	1	1	1	1	1	1	1	0	0	0	0	0	0
P <sub>6</sub>	1	1	1	1	1	1	1	1	0	0	0	0	0	0	0	0
P <sub>7</sub>	0	0	0	0	0	0	0	0	1	1	1	1	1	1	1	0
P <sub>8</sub>	1	1	1	1	1	1	1	1	1	1	1	1	1	1	1	0
P <sub>9</sub>	1	1	1	1	1	1	1	1	1	1	1	1	1	0	0	0

### 3.5.3 Control Signal Generation

The third stage of the even power distributor is control signal generation, in this stage, the values have been calculated in the previous stage for the output ( $O_{ij}$ ) for pixel ( $i$ ) at that sub-frame ( $j$ ) are not necessarily the data that are sent to the opto-electronic array. This depends on the array pixels type; for a 90x90 array, each pixel's internal memory uses a DFF to hold the pixel value, so there is no meaning for this stage. However, this is an important stage in the 16x16 array, where each pixel's internal memory uses a TFF, and so it is important to send only one in the case of change; this is done at the start and end point of the pulse, as shown in Figure 3-11, where an XOR gate is used to generate the control pulses ( $C_{ij}$ ) for pixel ( $i$ ) at that sub-frame ( $j$ ).

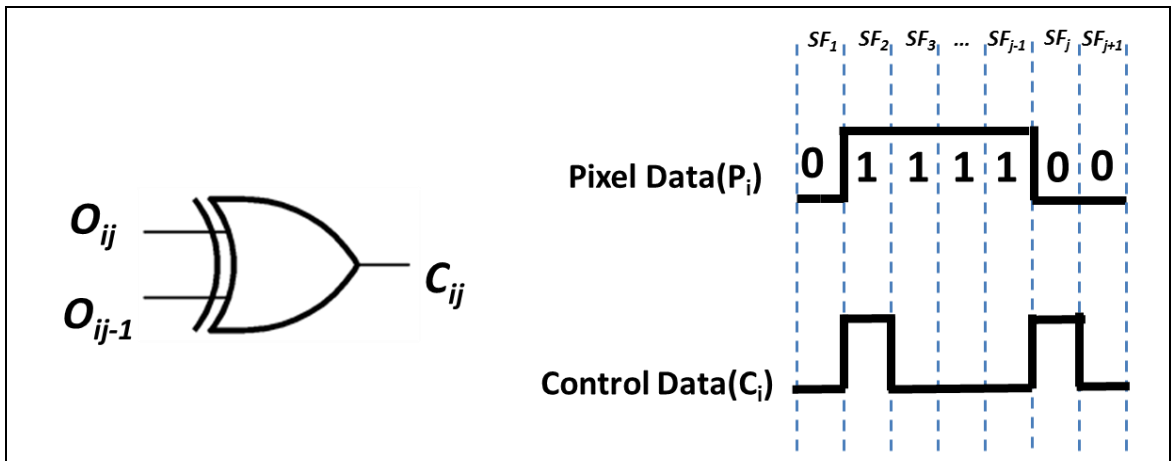


Figure 3-11 The control signal generator. It uses an XOR gate to generate control signals

The final output of this stage according to the example is:

	SF 1	SF 2	SF 3	SF 4	SF 5	SF 6	SF 7	SF 8	SF 9	SF 10	SF 11	SF 12	SF 13	SF 14	SF 15	SF 16
P <sub>1</sub>	0	0	0	0	0	0	0	0	0	0	0	0	0	1	0	1
P <sub>2</sub>	0	0	0	0	0	0	0	0	0	0	0	0	1	0	0	1
P <sub>3</sub>	0	0	0	0	0	0	0	0	0	0	1	0	0	0	0	1
P <sub>4</sub>	1	0	0	0	0	0	0	0	0	0	0	0	1	0	0	0
P <sub>5</sub>	1	0	0	0	0	0	0	0	0	0	1	0	0	0	0	0
P <sub>6</sub>	1	0	0	0	0	0	0	0	1	0	0	0	0	0	0	0
P <sub>7</sub>	0	0	0	0	0	0	0	0	1	0	0	0	0	0	0	1
P <sub>8</sub>	1	0	0	0	0	0	0	0	0	0	0	0	0	0	0	1
P <sub>9</sub>	1	0	0	0	0	0	0	0	0	0	0	0	0	1	0	0

These three stages are used to generate an evenly distributed signal through the whole frame time, and the importance behind using this even power distributor is that large array sizes can avoid a large current drawn for a short period.

Finally, the design is synthesized using the following FPGA device: Spartan-6 XC6SLX150t-3, and in Table 3-4 the utilization of the resources used in the design are presented.

**Table 3-4** The FPGA used resources with maximum frequency and power consumption.

Logic and Memory Resources	Used	Available	Utilization
<b>SPARTAN-6 xc6slx150t</b>			
<b>Number of Slice Registers</b>	319	184,304	1%
<b>Number of Slice LUTs</b>	582	92,152	1%
<b>Number of Occupied Slices</b>	255	23,038	1%
<b>Maximum Internal Frequency</b>	205.119MHz		
<b>Est. Power Consumption</b>	215 m W		

The even power distributor was implemented for a 16x16 stimulator size, since it was the only one available, as a step to be integrated with the existing CMOS based micro-LED array. The even power distributor utilized less than 1% of the available resources on the FPGA. The 215 mW is acceptable for optogenetic retinal prosthesis technology, taking into consideration that it will be wearable technology and higher resolutions are desirable.

### 3.6 Pulse Encoder

The pulse encoder is used to effectively control the opto-electronic micro-LED array. It utilizes the sparse nature of the retinal code, so it is possible to adapt the system using this block to minimize information transfer to the opto-electronic micro-LED array. Since the pulse encoder is used to control the micro-LED array, the internal architecture of the encoder depends on the way that this micro-LED array works. Two encoders are designed one for the 16x16 micro-LED, while the other is used to control the 90x90. The main architecture is the same but there are some additions to the latter that do not exist in the former. The opto-electronic array can be operated either by pixel mode, where only one pixel can change state at a time, or in row mode, where a whole row can change value at a time. The introduced pulse encoder was built to adapt a novel mixed mode. Instead of using one mode (pixel, row) at each frame time, the encoder selects them automatically, to achieve the best timing result.

### **3.6.1 The 16x16 Array Pulse Encoder**

Two versions of the 16x16 array were employed during this work: the first version was described in Section 2.5, and the second is a simplified version of the first with only two modes of operation, either pixel serial or row serial, with an external switch to select the mode. This pulse encoder is designed to control the second version of the 16x16 micro-LEDs.

The 16x16 array pulse encoder internal architecture is presented in Figure 3-12. It consists of Binary Image Memory that is used to hold the binary information generated from the even power distributor in each sub-frame. The 16 bit buffer register is used to hold the row value sent from the memory. To loop through all the memory rows and generate the column address, a 4 bit counter is used. The adder is used to add all ones in the row to determine the number of ones in that register, and this is used by the control unit to determine between row update or pixel update mode. The 16x4 priority encoder is used to send the address of the highest weight so it can be used in pixel mode. The four bit register is used to hold the result of the encoder, and then it is sent to MUX, which is a 2x1 MUX which selects between row mode and bit serial mode or pixel mode. Finally, the control unit controls all the elements in the pulse encoder as described below.

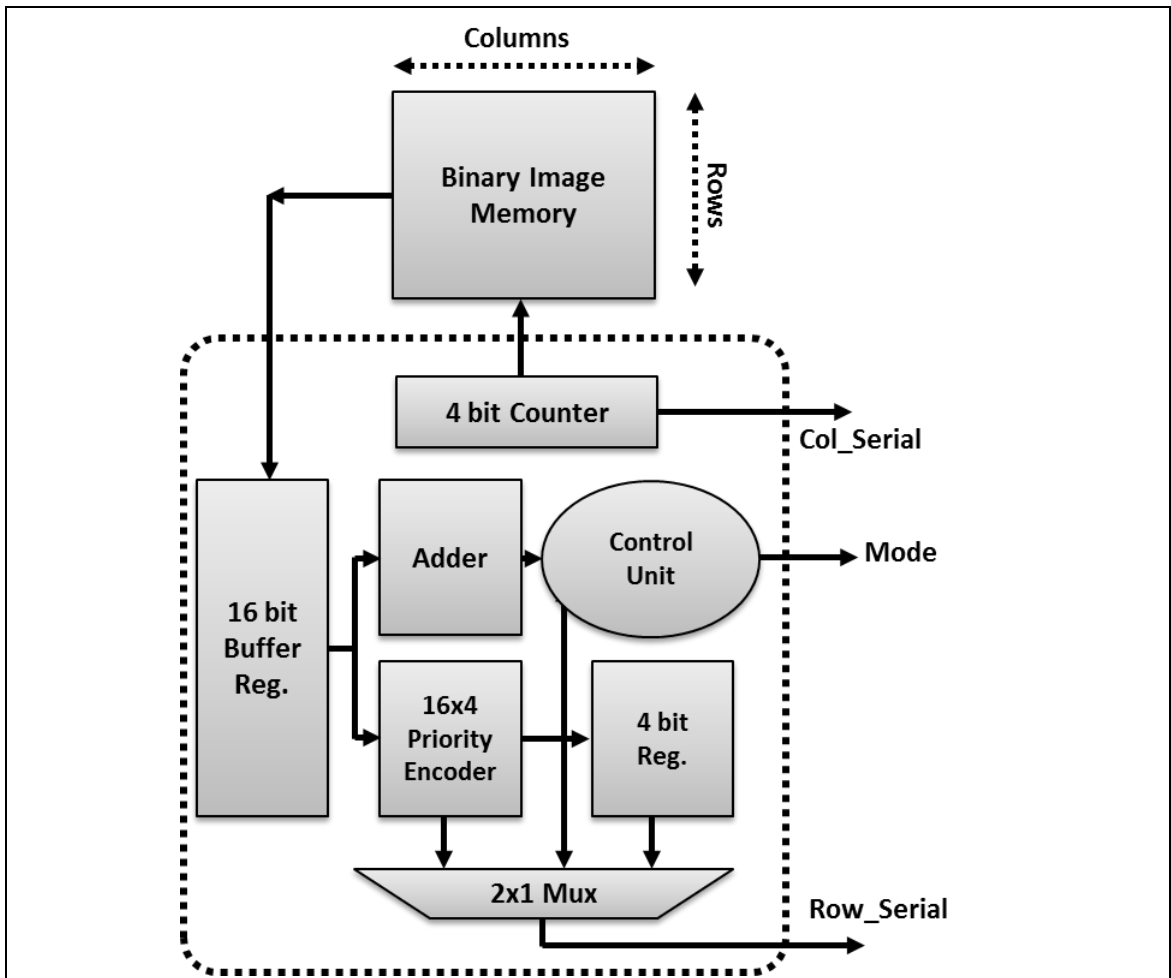


**Figure 3-12** The 16x16 array pulse encoder internal architecture, with an image memory connected to the controller input/output signals names and connections also shown

The control unit design uses an Algorithmic State Machine flow chart as shown in Figure 3-13. The flow chart shows the state transitions of the controller and the data path operations associated with those transitions. The system remains in the <idle> state until the start signal is asserted, and then this start signal is one when a new binary image is loaded. When this happens, the state moves to <load> state where all of the register values and parameters are loaded. At the next clock edge, depending on the value of the adder summation ( $\Sigma$ ), the state returns to load state, and this happens when the whole row is zero, or goes to <serial> state. From serial state, it moves either to <bit> (pixel) state or <row> state, according to threshold (t) value.

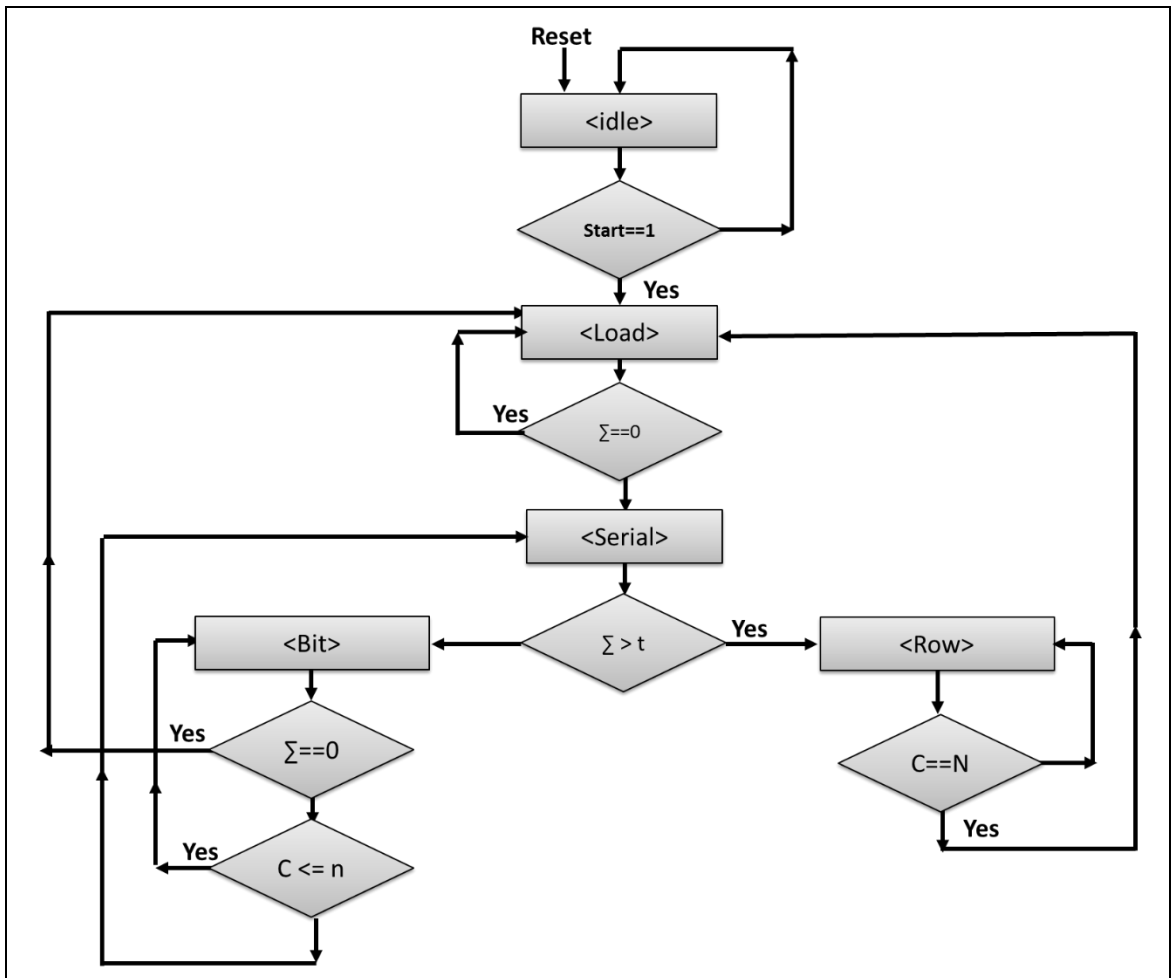


**Figure 3-13** The 16x16 pulse encoder ASM diagram which consists of five states to determine the flow of operations correctly

The threshold (t) is determined by the following equation:

$$\sum_{p=1}^N \leq \frac{N}{\log_2 N} \quad (3-12)$$

Where N is the number of rows i.e. for a 16 row array. If there are more than four pixels requiring a change in any given row, then it is more efficient to update it with a row update.

If the summation ( $\Sigma$ ) is greater than the threshold (t), next state is <row> state, and the control flow remains there N times (where N is the number of columns in the image) then returns to <load> state, to load the next row. On the other hand, if the summation ( $\Sigma$ ) is less than the threshold (t), the system will need for each one in the loaded register to wait n times (where n is determined by the  $(\log_2 N)$ ). Here, N is the number of columns due to the encoder (In this work N is used interchangeably for both the number of columns and row because the matrix is

square). Then, after n times the one will be cleared from the loaded register (for example if there are two ones in the loaded register, then we need to wait 2n time). After finishing, it clears the one in the register, and then this step will be repeated till all the ones are finished (i.e. the summation ( $\Sigma$ ) is zero) and it returns to the <load> state.

Finally, the design is synthesized using the following FPGA device: Spartan-6 XC6SLX150t-3, and in Table 3-5 the utilization of resources used in the design is presented.

**Table 3-5 The FPGA used resources with maximum frequency and power consumption**

<b>Logic and Memory Resources</b> <b>SPARTAN-6 xc6slx150t</b>	<b>Used</b>	<b>Available</b>	<b>Utilization</b>
<b>Number of Slice Registers</b>	202	184,304	1%
<b>Number of Slice LUTs</b>	451	92,152	1%
<b>Number of Occupied Slices</b>	195	23,038	1%
<b>Maximum Internal Frequency</b>	273.125MHz		
<b>Est. Power Consumption</b>	113 m W		

The pulse encoder for the 16x16 array size is implemented in FPGA towards integration with the existing CMOS controller. Table 3-5 shows the utilization of resources used in the design of controller. It is shown that it utilized about 1% of the available resources, and the rest of the logic could be used to implement image processing algorithms. I have used simulation data to look at the effect on the control chip as only a 16x16 array was available at the time.

### **3.6.2 The 90x90 Array Pulse Encoder**

The pulse encoder is used to send addresses to the micro-LED to switch either the ON or OFF state in a most efficient way. The internal architecture of the controller is displayed in Figure 3-14, where data can be sent to the micro-LED serial or parallel according to external signal (Ser/Par'). To achieve the most efficient timing in serial mode, it is needed to select between two modes of operation: pixel update (short shift), or row/column update (long shift), whereby information is sent to either change the ON/OFF state of an individual pixel, or all



the pixels in a given row/column. An update can then be achieved by rastering through all the individual pixels or columns, or by simply changing the states of those pixels that require a state change.

Row mode is efficient if the majority of pixels require updating. Where there are empty rows, skipping these with a row update can be efficient, and for sparse arrays, pixel updating is most efficient. Thus, for an individual row (or column), the determination of when to use pixel or row update is given by equation 3-12. The 90 bit buffer register that holds the row value is sent from the image memory, and the 90x7 priority encoder is used to generate the address of each one bit in the register to be used as the pixel address, either in parallel or short shift mode.

In order to determine between modes, an adder block adds all ones in the row to determine the number of ones in that register. This is used by the control unit to select between the two serial modes, row update or pixel update, according to equation 3-12. The 7 bit counter is used to track addresses through image rows, then the value of the counter is decoded by the 7x90 decoder to be used in the long shift mode. A 2x1 MUX is used to select between short shift and long shift in both column and row serial output and the selected mode is inserted as a header bit in both row and column serial to achieve the various communication modes, as illustrated in Section 2.5.

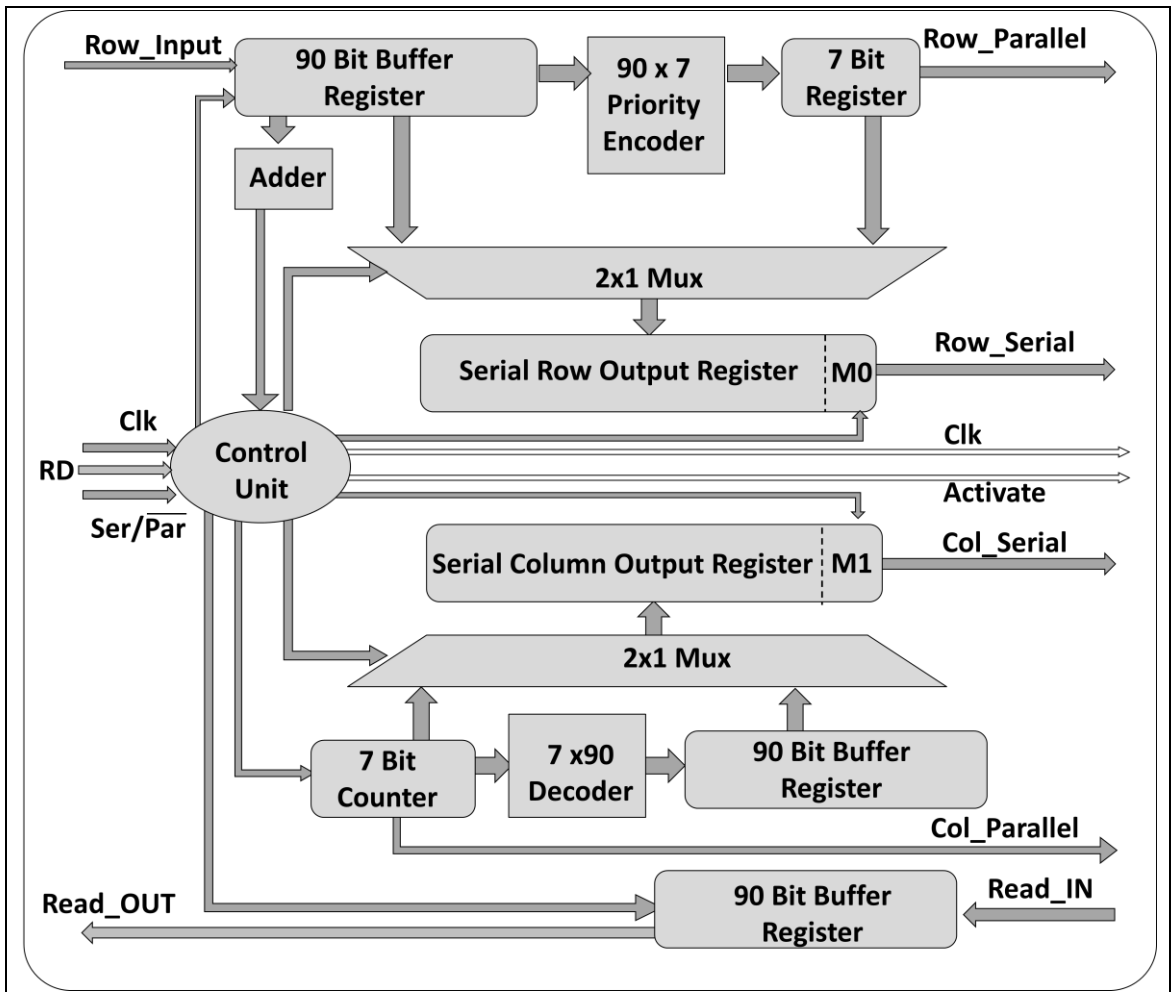


**Figure 3-14 Internal structure for the 90x90 micro-LED controller**

Finally, the (Read\_IN) input is used to store the data read from the micro-LED; this is done when the (RD) signal is asserted, and it is used to diagnose the purpose of the data stored in the 90 bit register. The control unit controls all the elements in the controller, including sending the activate signal.

The purpose here is to use the Register Transfer Language (RTL) to design the control unit to achieve the desired working speed. Figure 3-15 shows a simplified Algorithmic State Machine (ASM). The ASM diagram consists of seven states (idle, Load, Read, Serial, Parallel, Bit and Row) to determine the flow of encoder operations correctly.

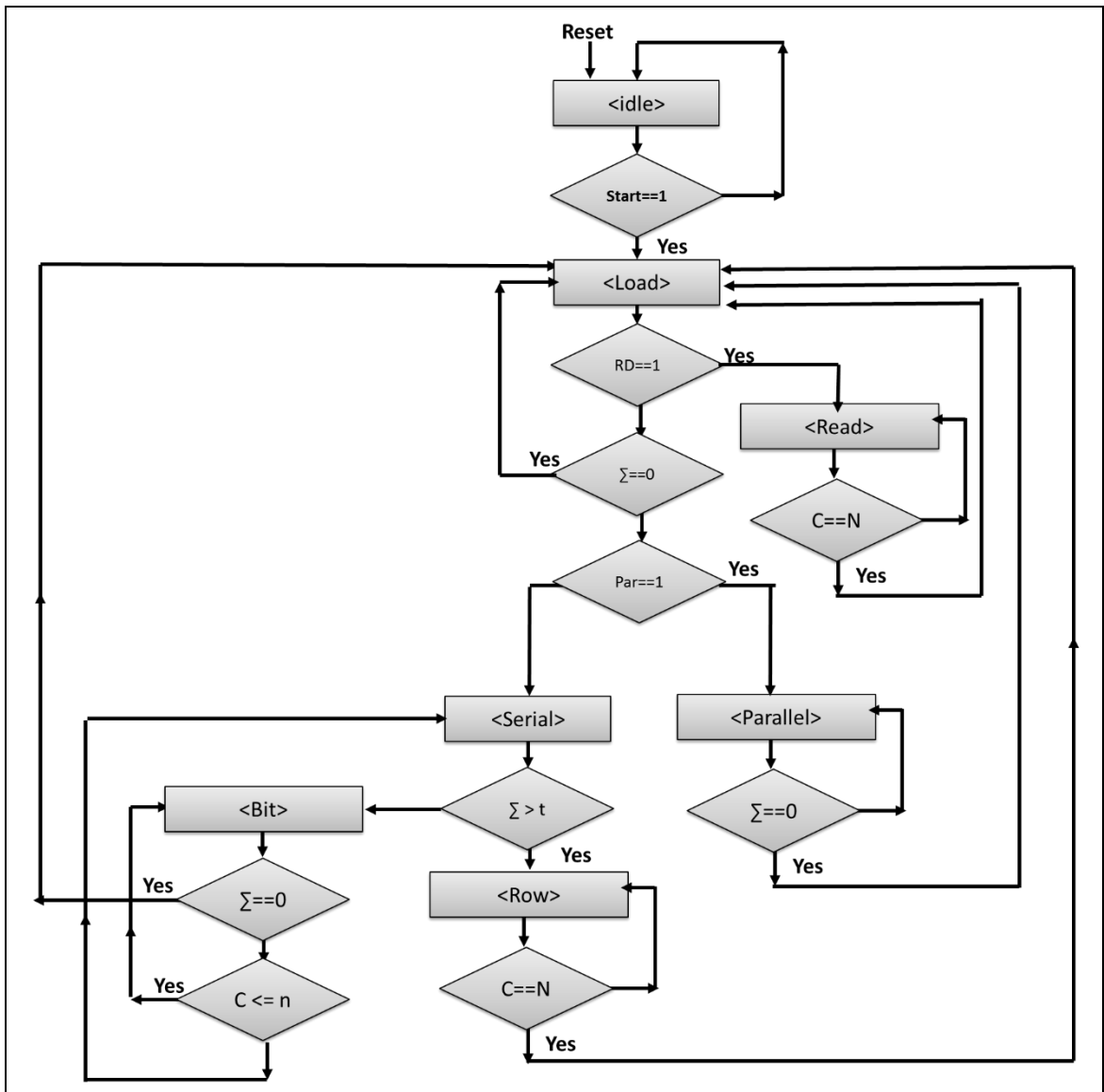


**Figure 3-15** The 90x90 pulse encoder ASM diagram, which consists of seven states to determine the flow of operations correctly

The controller starts in an **<idle>** state waiting for the start signal, in order to start the operation, and after receiving the signal the data will be loaded into the registers. The controller then transfers into **<Load>** state, and the (RD) signal is tested and if it is asserted then the next state is **<Read>**, where (N) cycles are needed to read the register into (READ\_OUT) output. If (RD) is zero, then the row buffer register is tested, if it is zero, there is no need to send an address to the LED array, so we return to **<Load>** state until a row that contains at least one is received and there is no (RD) signal. After this, a further external signal (Par) determines whether to use serial or parallel mode, in **<Parallel>** state, the data path sends the address of ones in the register till the row register is filled with zeros; then, it returns to **<Load>** state. If the selected mode is serial, then we go

to **<Serial>** state and count the number of ones in the register and determine between **<Bit>** state in serial mode, where the address of the column that contains the one is sent serially after being decoded into n bits, and **<Row>** state in serial mode, which sends the whole row using N cycles; the comparison threshold is given in equation 3-12. This 90x90 array pulse encoder shares the same basic functionality as a 16x16, with read data and parallel mode extra features.

### 3.7 Conclusion

In this chapter, I have explored different available implementation hardware platforms, and performed a comparison to find the most suitable one to implement the optogenetic retinal prosthesis framework. Then, the design and implementation of both high level and low level processing algorithms was introduced.

**Dual IR/Visible Simplification:** is a high level processing algorithm, which can be used with any visual prosthesis system. The implementation of this algorithm was explored in three steps: visible image preparation, IR image preparation, and the Visible-IR fusion.

**Frame Encoding and Even Power Distributor:** is a low level processing algorithm, which is designed and implemented for an optogenetic retinal prosthesis system. The frame encoding was introduced, and then a detailed design of the even power distributor was presented, as it is used to avoid large pulses for short duration (surge). It includes three steps: sorting, pulse width modulation, and control signal generation.

**Pulse Encoder:** is a low level processing algorithm, which is designed and implemented for an optogenetic retinal prosthesis system. The pulse encoder introduces a mixed mode pixel/row update for optimal timing. Two versions were introduced: a 16x16 version and a 90x90 version.

In the next chapter, the results will be introduced, including the image simplification and retinal processing, and the photonic stimulation controller.

### Relative contributions

Subject	Contribution
Mr Musa Al-Yaman	<ul style="list-style-type: none"><li>- Design and implementation of all different parts of the Photonic Stimulation Controller</li><li>- Implemented the Dual-spectrum Image preparation and validating the algorithm</li></ul>

# Chapter 4 Analysis and Results

## 4.1 Chapter Overview

Cochlear prosthesis has been a huge success, allowing people to understand conversations even over the telephone. Optogenetic Retinal prosthesis faces more challenges, and in this work a set of algorithms is presented to improve the displayed image. The findings of these algorithms are presented and analysed here.

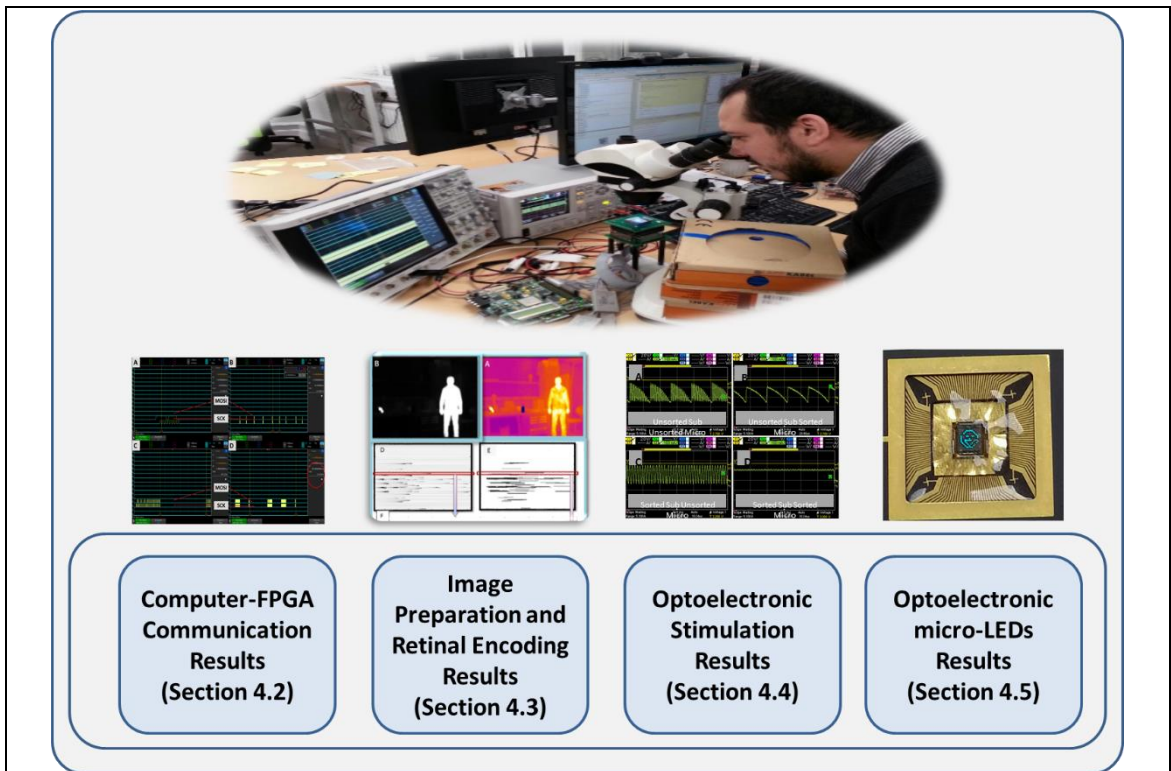


**Figure 4-1 Chapter Four overview.** The chapter presents computer-FPGA communication, the high-level image preparation and retinal encoding results, the low-level stimulation controller results, and the optoelectronic micro-LEDs results

In this chapter, I will discuss the results of my work, which focus on the optogenetic retinal prosthesis. This results are divided into four stages (computer-FPGA communication, image preparation and retinal image encoding, optoelectronic stimulation controller and the optoelectronic micro-LEDs), as shown in Figure 4-1. Firstly, in Section 4.2 the findings of computer-FPGA communication are presented. Secondly, in Section 4.3 the findings of the high level processing stage are presented, starting with the preparation of the image. This involves the dual spectrum image preparation, and then moves on to retinal encoding to present the obtained results. Thirdly, Section 4.4 introduces the

results of low level processing stage, represented by the optoelectronic stimulation controller, which consist of two main blocks, an even power distributor and a pulse encoder. Fourthly, Section 4.5 presents the results of optoelectronic micro-LEDs, with LED patterns and images. Finally, Section 4.6 will conclude the chapter and introduce the next.

## 4.2 Computer-FPGA Communication Results

The long term aim of this work is to develop a portable, wearable system which can be used in daily tasks, for optogenetic retinal prosthesis patients. To the best of my knowledge, early phase optogenetic retinal prosthesis systems are still under the animal testing phase, and no human trials are available. Thus, the practical experimental work was prepared for animal testing in vitro, as described in [152]. It is divided into three main stages as described in the block diagram in Figure 4-2.

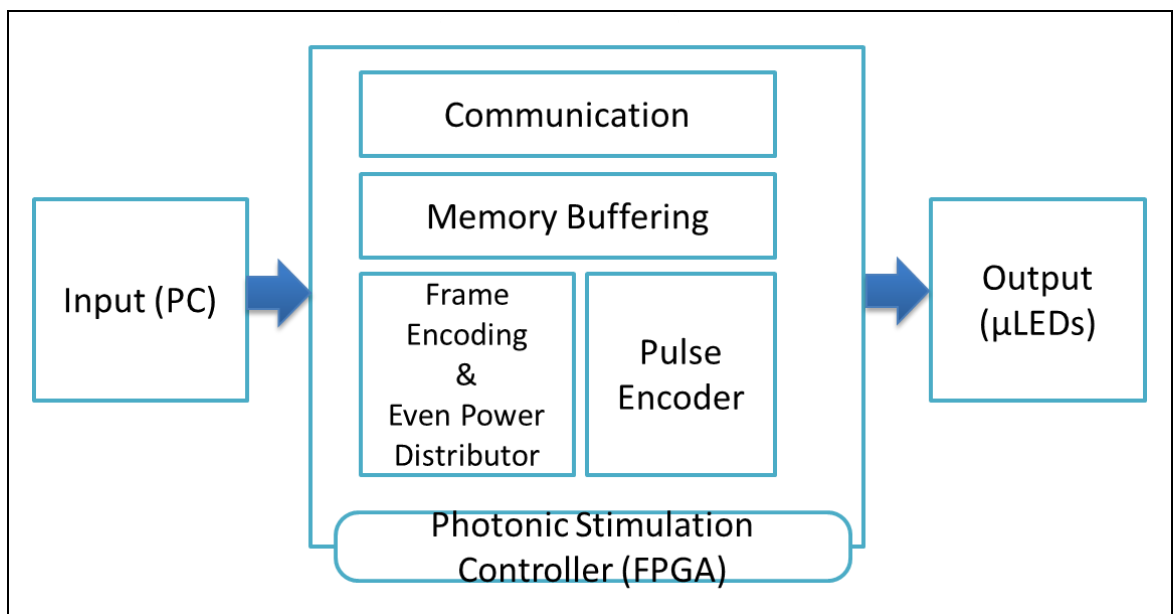


**Figure 4-2 Experimental setup for Optoelectronic Neural Stimulation.** The platform block diagram consists of three main stages: input, photonic stimulation controller, and output

- Input stage: PC-based software is used to input the pattern to be tested in the retinal cells
- Photonic stimulation controller stage: the main purpose of this stage is to receive a pattern from a previous stage, and then minimized methods (in terms of time and power) are used to control the next stage
- Output stage: this stage consists of the micro-LEDs used in biological experiments to shine light on the retinal cells.

**The input stage** is used to send test patterns, written by biologists, and the form of the data is that each pixel is sent as four bits (0-15) intensity. The number of sent pixels is 256, and they are packed in the form of two pixels per byte, since the input stage is not the main concern of this work. The following results will focus on the communication with the computer.

In the communication part, two standard protocols are used; Serial Peripheral Interface (SPI), RS232.

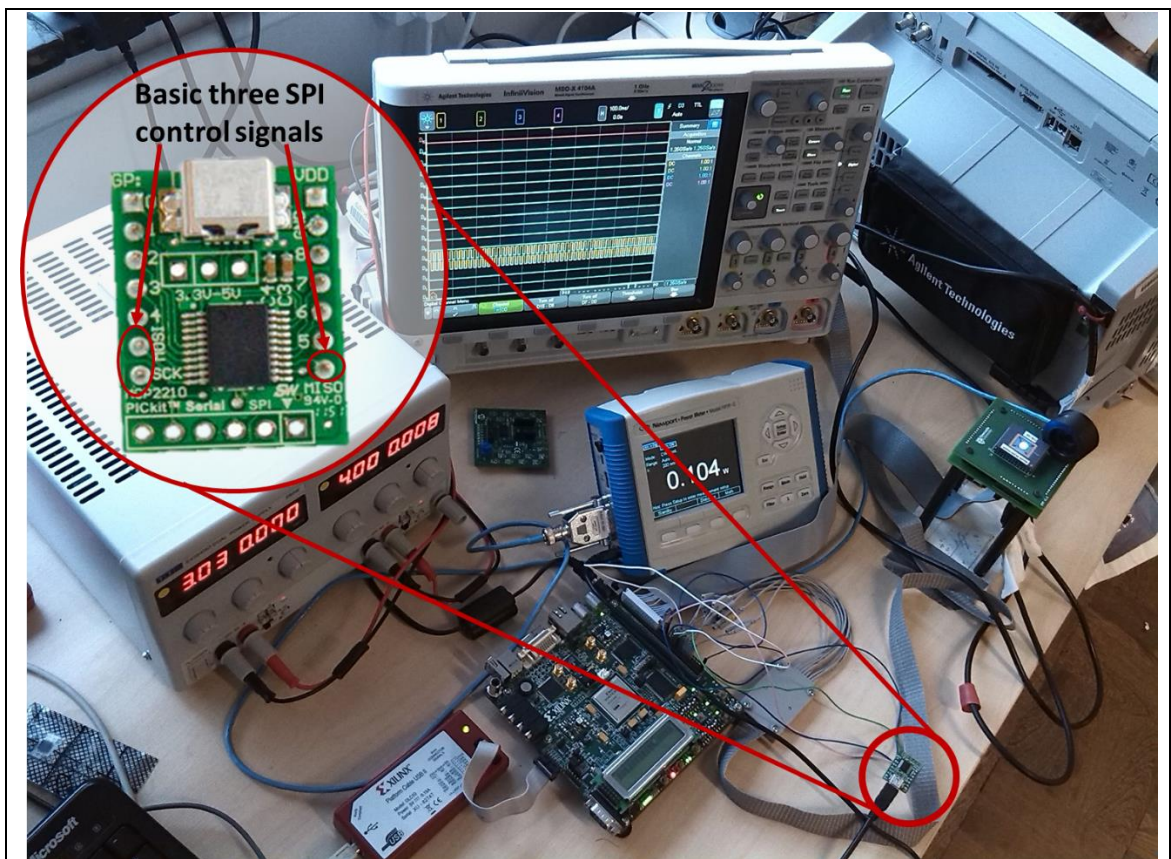


**Figure 4-3** The experimental setup with USB to SPI interface. The MCP2210 USB to SPI protocol converter zoomed, and the standard protocol uses three signals to be interfaced to the FPGA

- **The First Protocol SPI:** To interface the SPI with a computer, the USB to Serial Peripheral Interface (SPI) protocol converter MCP2210 from microchip was used. Figure 4-3 shows the experimental lab setup with zoomed USB to an SPI protocol converter (MCP2210), which uses the three standard SPI protocol signals: Serial Clock (SCK), Master Output Slave Input (MOSI) and Master Input Slave Output (MISO). The datasheet of MCP2210 states the following information about the specification of speed, buffer size: “Supports Full-Speed USB (12 Mb/s)”,



“128-Byte Buffer to Handle Data Throughput (64-byte transmit),” respectively. According to these numbers, the minimum frame transmission time ( $Min\_F\_Trans$ ) is calculated according to the following equation:

$$Min_{F_{Trans}} = \left( \frac{Number_{Trans\_bits}}{Max_{Trans_{Freq}}} \right) + Buffering\_Delay \quad (4-1)$$

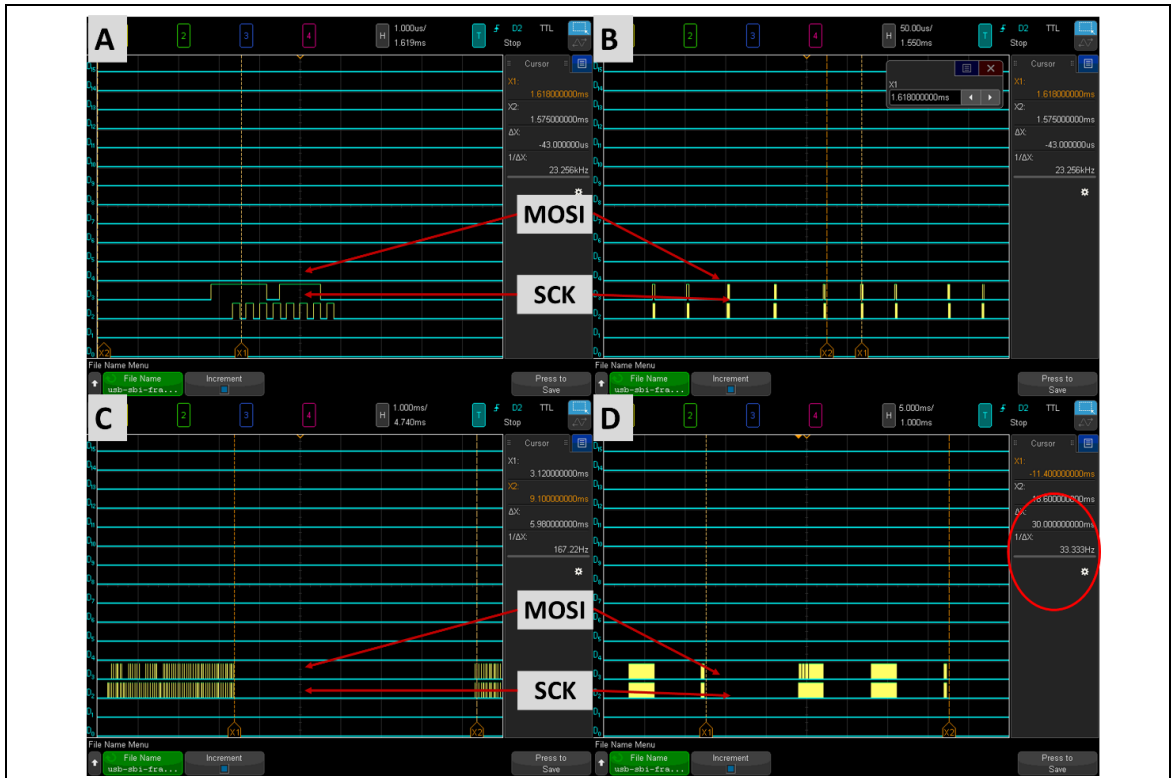


**Figure 4-4 The MCP2210 SPI timing.** (A) the full speed clock during MOSI byte transmission (B) the delay between each byte (C) the buffer delay and (D) the whole frame time.

There is no information about buffering delay. The actual data bits transmission time is calculated for 128 byte using maximum speed (86  $\mu$ s), so buffering delay was approximated to be (x10) actual transmission time, this due to the buffer size. This leads to  $Min\_F\_Trans$  equals around 1ms.

**Table 4-1 The  $Min\_F\_Trans$  calculated and actual measurements.**

	Calculation	Real Measurement
Buffering Delay	860 $\mu$ s	12000+6000x2+50x128 $\mu$ s
<b>Number<sub>Trans_bits</sub></b>	128x8	128x8
<b>Max<sub>Trans_Freq</sub></b>	12 MHz	8 MHz
<i>Min_F_Trans</i>	946 $\mu$ s	30 ms

The real calculation of the transmission time is achieved via oscilloscope measurements shown in Figure 4-4, and unfortunately this shows in (A) that the datasheet information is accurate only during byte transmission with maximum speed of 8 MHz. In (B), there was around (50  $\mu$ s) delay between each byte transmission that was not stated in the datasheet, and in (C) it was around (6ms) buffering delay, while in (D) there is an extra (12ms) at start of each frame, which leads that the actual frame transmission time was measured to be around (30 ms). The detailed calculations in shown in Table 4-1. This leads to have the frame transmission time that is greater than double frame processing time, thus to overcome this using standard serial RS232 protocol is suggested.

- **The Second Protocol RS232:** The standard serial RS232 is used with the maximum Baud Rate (115200 bps), although each byte contains two overhead bits (start, stop), and the baud rate is much slower than the USB to SPI code converter. The total transmission time according to equation 4-1 is calculated to be around 12 ms, due to the simple protocol implementation that avoids the buffering overheads. This delay approximately equals to frame processing time, thus, to utilize the processing time, pipelined double buffering is used. The input starts to fill Buffer 1, and when it is full it switches to Buffer 2. The reading process happens the opposite way, where while the data is filling Buffer 1, the reading is done from Buffer 2, and when the input starts to fill Buffer 2, the output switches to Buffer 1

### 4.3 Image Preparation and Retinal Encoding Results

All visual prosthesis systems need to prepare the image before displaying it to the patient; this preparation generally consists of two steps: the first step is to simplify the image. The second step is the processing that replaces the functionality of the damaged retinal layers, which called retinal encoding. These two steps are considered high-level processing.

### 4.3.1 Image Simplification Results

An infrared camera-based segmentation is used to segment key features in the visual scene based on the object temperature. This dual-spectral technique is used to simplify the processing.

The experimental setup of the system is comprised of two cameras, visible (mvBlueFOX-220AC) and infrared (Microbolometer: Optris PI 160), which were optically aligned via a visible/IR beam splitter to view the same visual scene. Figure 4-5(A) shows how the two cameras are optically aligned. Their imaging output and the resultant segmented image can be seen in Figure 4-5(B). The results are divided into IR preparation, visible preparation and image fusion.

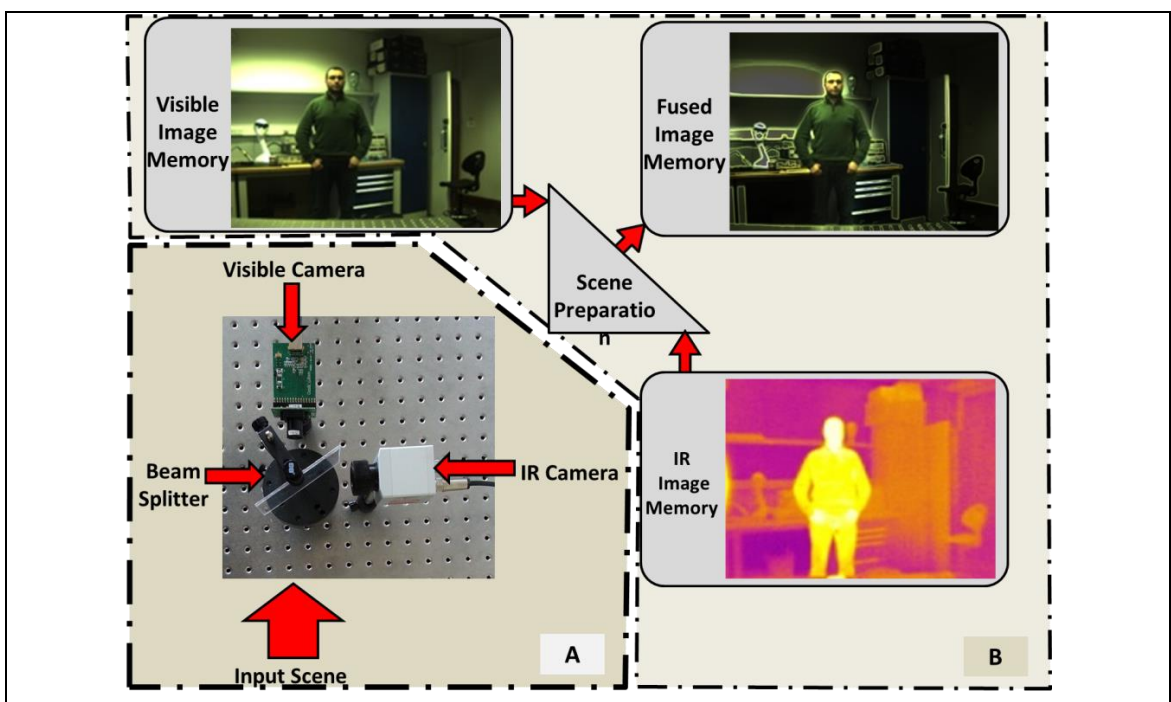


**Figure 4-5 Dual spectrum image simplification** (A) The optical system alignment of the infrared and visible cameras, according to input scene (B) General system flowchart illustrating the inputs and outputs of Scene Preparation block

**IR preparation**, the pathway is shown in Figure 4-6, the original IR image (A), which includes a person standing in a lab with his body temperature higher than the surrounding environment, a cold cup and a hot soldering iron on a table, this image is converted into a greyscale image (B), and then exponentially adjustment steps are taken as shown in (C). Finally, the image is convolved with a Gaussian filter as shown in (D).

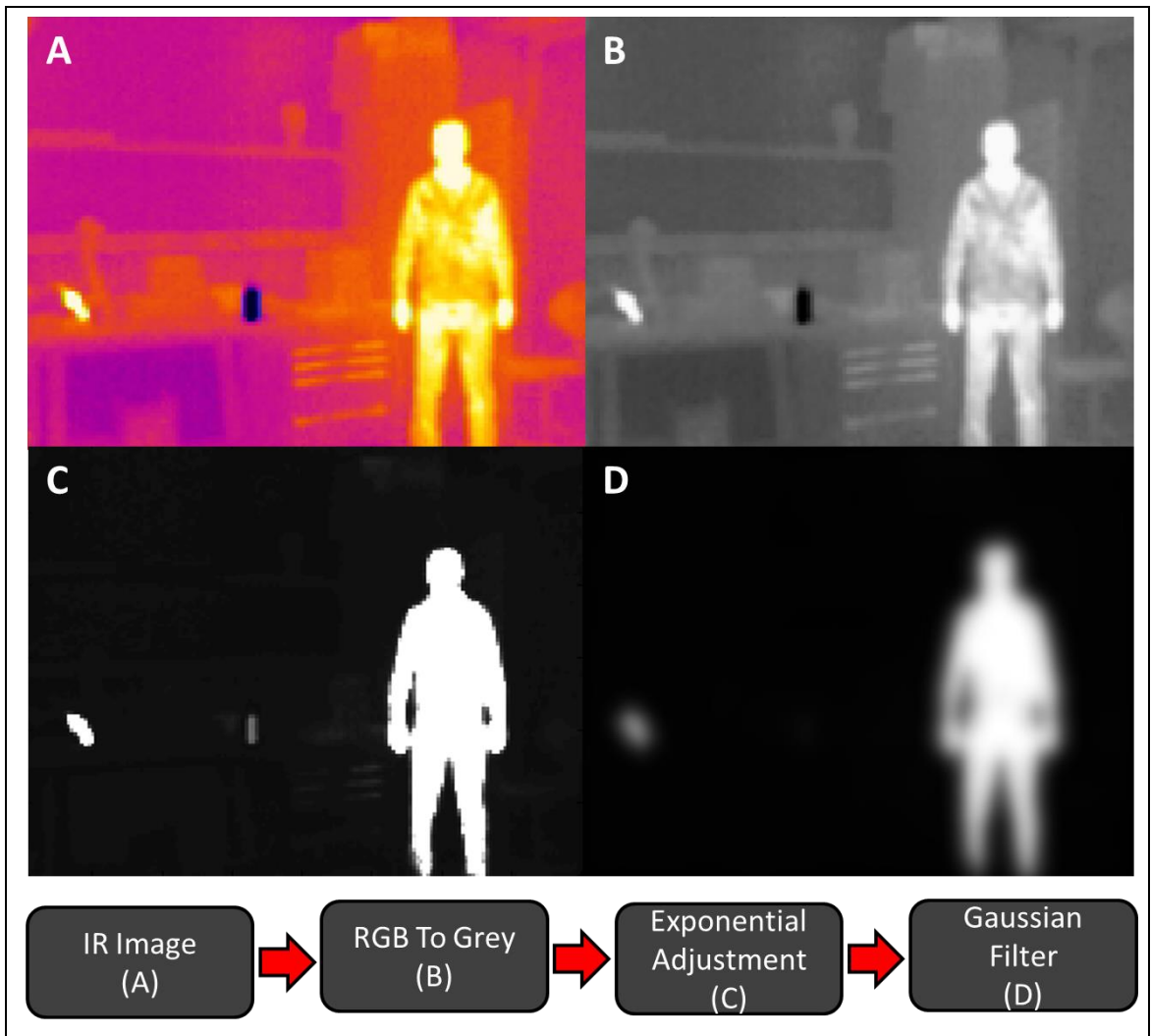


**Figure 4-6 The IR preparation pathway.** (A) Original IR image (B) Greyscale image (C) Exponentially adjusted image (D) Gaussian convolved image

The detailed IR image adjustment is presented in Figure 4-7, where (A) shows the IR image contains hot and cold objects, they are extracted by exponentially scaling the dynamic range of the original image and its negative image so that brighter objects are enhanced to higher intensity values while darker objects are suppressed. Adding the two scaled images together forms the segmented image, as shown in (D).

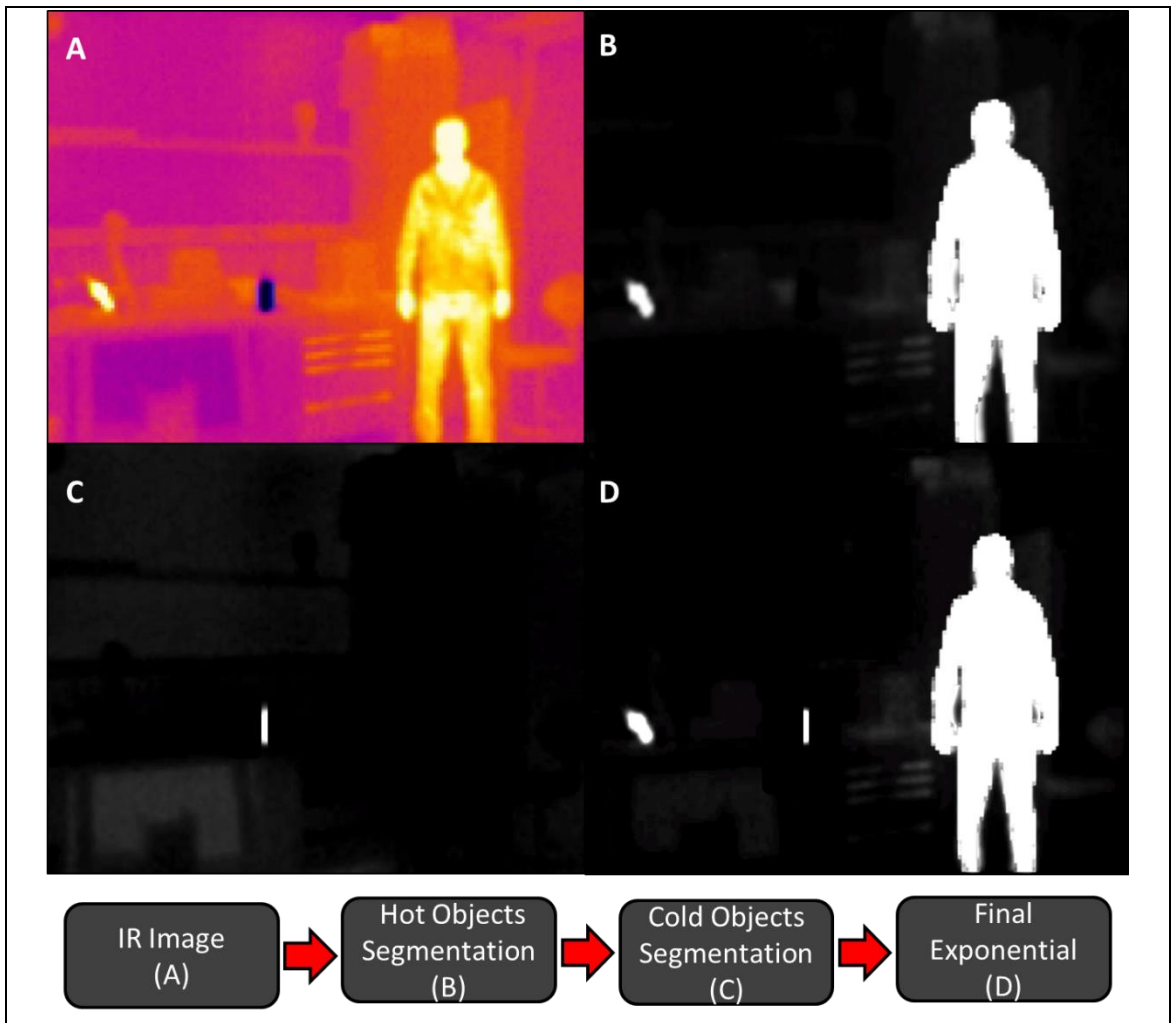


**Figure 4-7** The detailed IR scene exponentially adjusted. (A) an IR image showing objects with temperatures different than the room temperature. The image is segmented into hot and cold objects in (B) and (C) respectively. (D) is the combined hot and cold segmented image

The visual preparation and final fused image preparation pathway is shown in Figure 4-8. The original visible image (A), is converted to the Luma (Y') component of the image that shown in (B), then the anisotropic diffusion filter is applied (C), and finally the result of image fusion after thresholding is shown in (D).

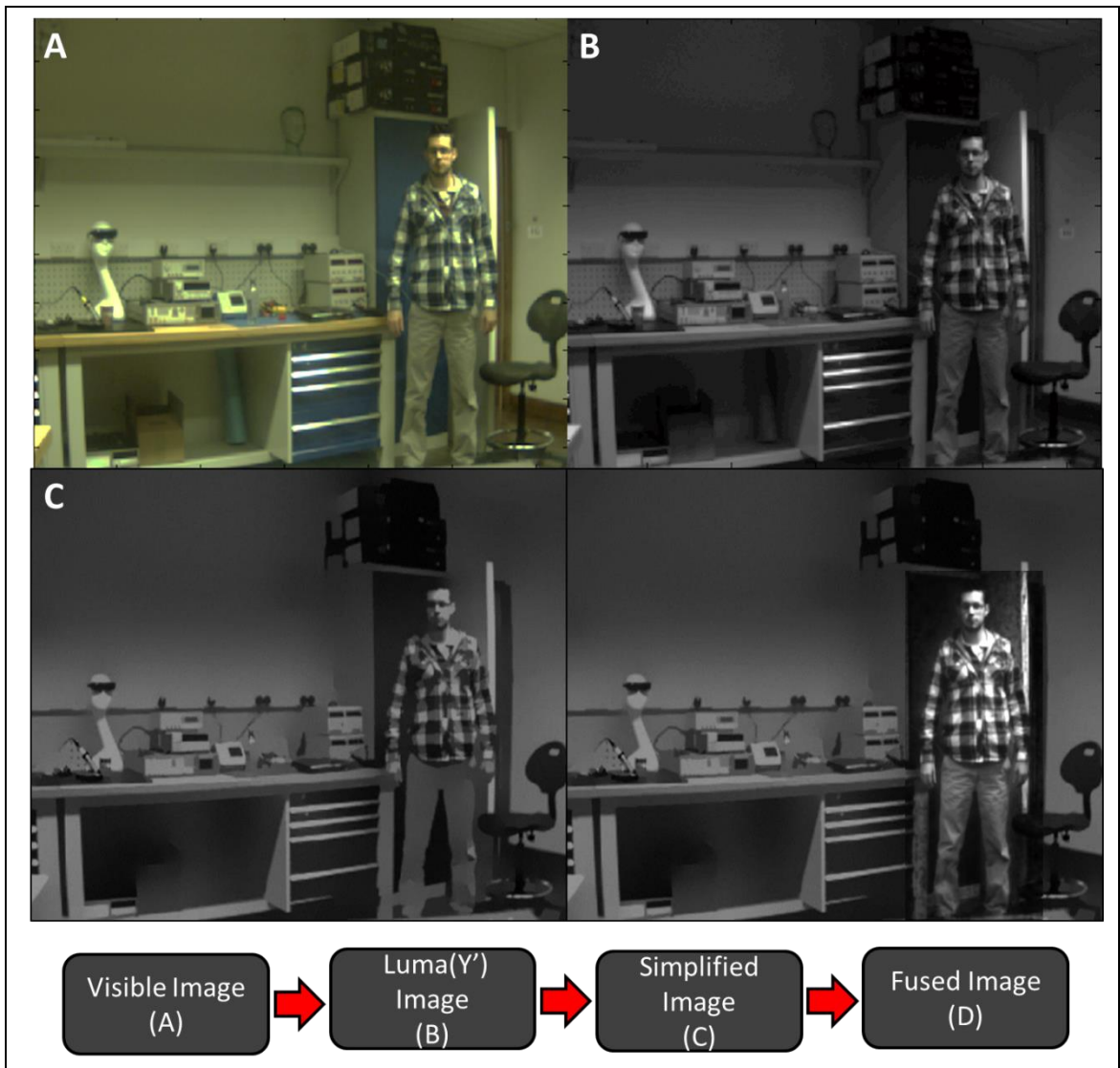


**Figure 4-8 The visible preparation pathway.** (A) Original visible image (B) Luma ( $Y'$ ) image (C) Anisotropic diffusion image (D) Fused image

The visual image contains great details and textures, so simplification is a crucial step in removing irrelevant background texture. By simplifying the scene, the key features of the person are enhanced. Figure 4-9 shows the simulated vision for different sizes of retinal prosthesis stimulator arrays. It can be noticed that at low resolution levels (e.g. 16x16 and 32x32), the details of the foreground objects have been fused with the background of the image when using the original image.

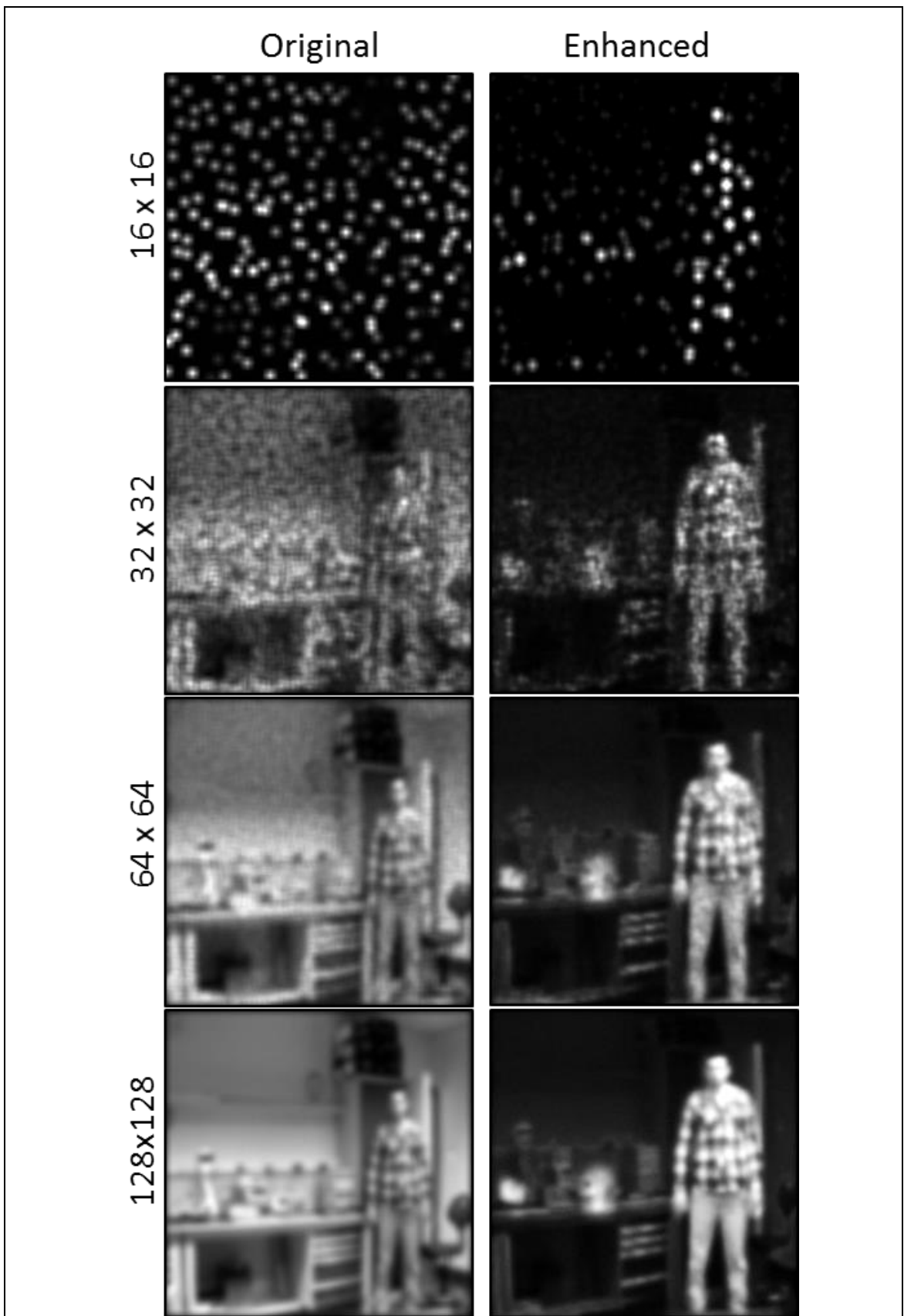


**Figure 4-9 The difference of stimulator output.** The left and right columns show how the original, enhanced respectively, may look to someone with a 16x16, 32x32, 64x64 and 128x128 stimulator retinal prosthesis, respectively. Images are non-linearly retargeted by 30% in both directions



### 4.3.2 Retinal Encoding Results

The stimulator for a visual system prosthesis can be variously placed in the visual pathway. For cortex and optical nerve prostheses, in addition to the image preparation stage, full retinal functionality must be added to the prosthesis system. However with retinal prostheses, only the bypassed layer(s) functionality needs to be replaced. For optogenetic retinal prostheses, photosensitization can be done for retinal ganglion cells or bipolar cells.

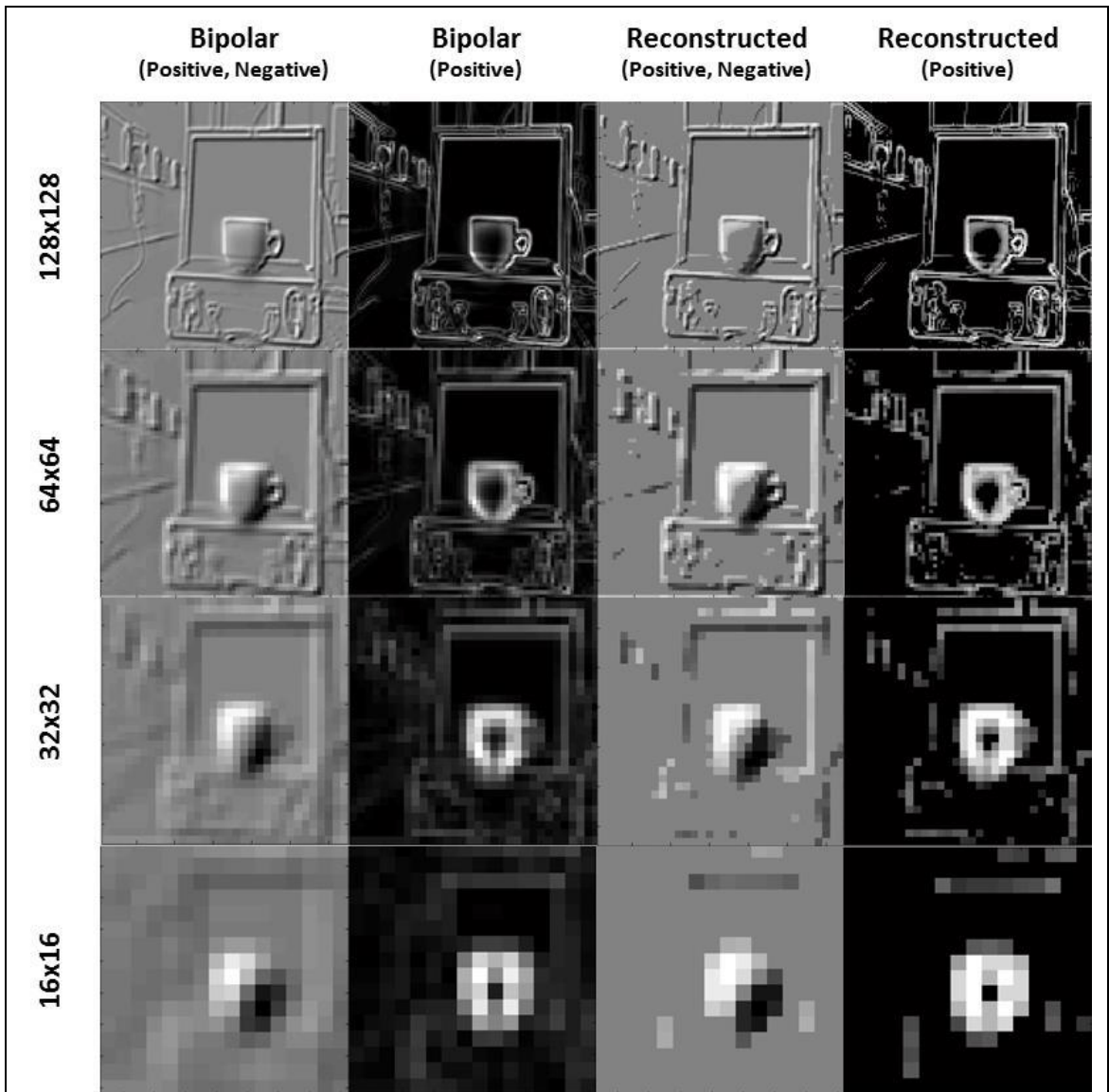


**Figure 4-10 The outputs of the bipolar cells and the reconstructed image.** The bipolar first and second columns show how full bipolar image and the approximate (using only positive values), respectively, may look to someone with a 16x16, 32x32, 64x64, 128x128 and 256x256 stimulator retinal prosthesis, respectively. The third and fourth columns show the reconstructed image for both full bipolar and approximate bipolar respectively for the above different stimulator sizes

In this work, ganglion cells were photosensitized, and therefore the first layer functionality is substituted by the imaging system as long as the simplification



process, and then bipolar cells layer functionality, is substituted using the difference of Gaussian function and finally the ganglion layer functionality is substituted by spike coding using time to first spike [153]. The simplified cup image with different sizes, is taken as input for bipolar cells, and then it is output presented as input to the ganglion cells having a spike code output.

In order to test the spike coding results, a reconstructed function is used to restore the digital result of the spike code into a bipolar image. The output of bipolar cells and the reconstructed images are presented in Figure 4-10, where each row shows a different simulator resolution starting with 256x256 down to 16x16. For each row, there are two representations for the bipolar cells output, and the first column is the exact bipolar cell output that includes the ON (positive) and OFF (negative) bipolar components in the same image. The second column presents the absolute of the gradients of the ON/OFF image in a single positive image for situations where only one pathway is to be stimulated. After conversion into spike frequencies, followed by pulse encoding, columns two and three show the ON/OFF and ON-only reconstructions based on time to first spike encoding. These are broadly in line with the originally processed images.

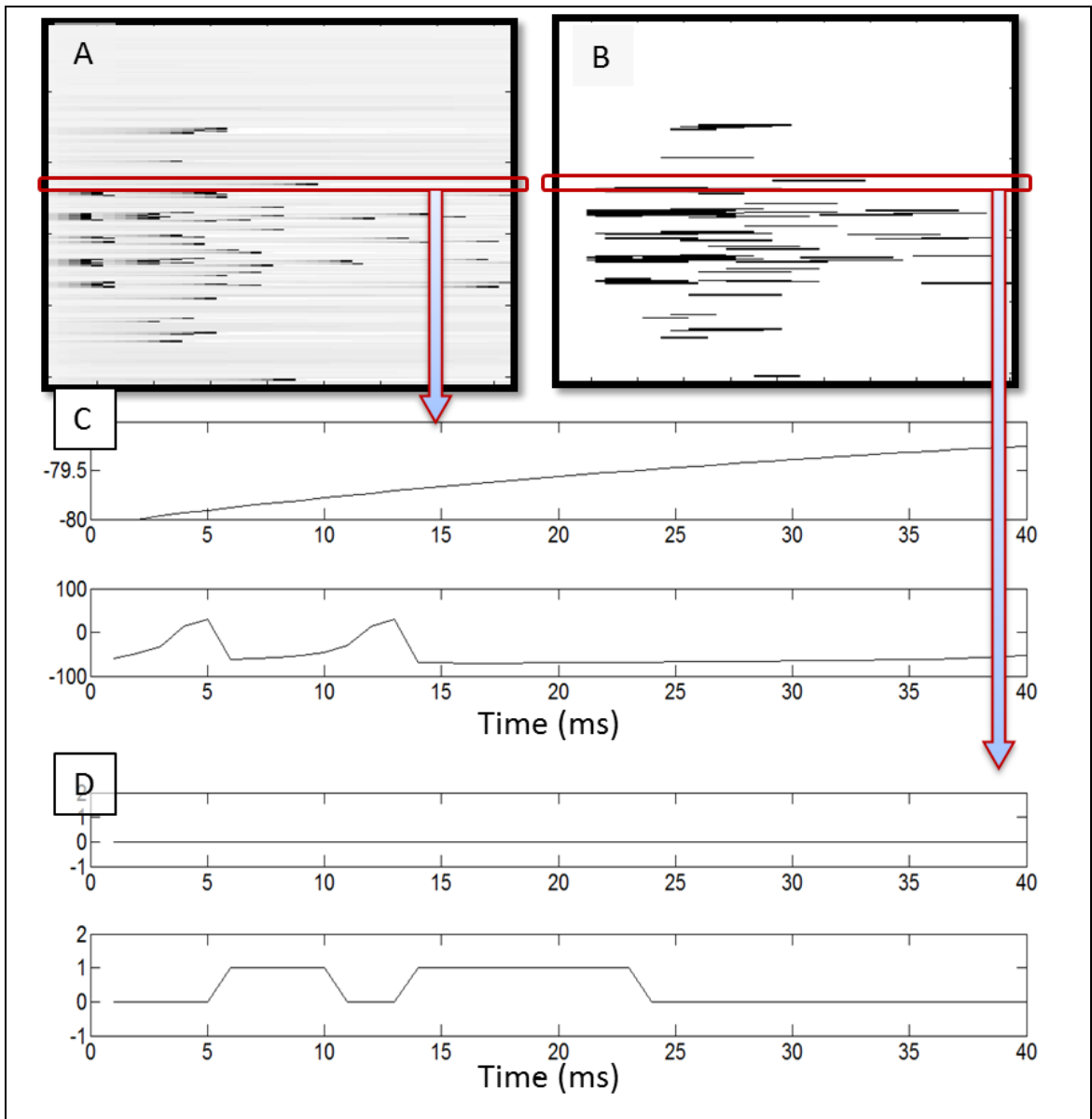


**Figure 4-11** *The analogue and digital spike coding, with zooming into two neuron outputs*

The output of retinal ganglion cell spike encoding is shown in Figure 4-11. The Izhikevich neuron model is used, and the analogue spikes for the 16x16 cup image are shown in (A). Meanwhile, the digital waveforms for the same image are shown in (B). A zoom up for two pixels in analogue and digital forms is shown in (C) and (D), respectively. The first pixel has an analogue voltage output less than the threshold (typically determined as 30mV), which is reflected in the first digital pixel by having zero over the frame time. The second pixel shows two spikes that are turned into digital form into two pulses, the first short and the second long as discussed in section 2.3.2.

## 4.4 Optoelectronic Stimulation Controller Results

Retinal prosthesis systems can be categorised into electronic and optogenetic retinal prostheses, and in the electronic approach electrodes are used to electrically stimulate retinal cells. In the optogenetic approach, photodiodes are used to stimulate retinal cells by light. The stimulator controller design is considered low-level processing because it differs according to the used approach. In this section, the results for photonic stimulation controller are shown, and these consist of two main components, the even power distributor and the pulse encoder. Both results are presented below.

### 4.4.1 Even Power Distributor Results

One important feature of the optoelectronic stimulator controller is the ability to scale-up to larger array sizes, due to the optogenetic retinal prosthesis stimulator dimensions growing. With larger stimulator sizes, the number of LEDs being in the ON-state for a short time lead to large current surges, and the suggested solution to this problem is to have an approximately equal number of ON-state LEDs all the time, achieved using the even power distributor.

To compare different ways for obtaining various intensities using PWM, two different ways are used. Starting with direct PWM conversion, all of the pixel pulses start at the same time, and then each pulse finishes in its turn. On the other hand, the even power distributor spreads these pulses over the whole sub-frame time. In Figure 4-12, different ways of implementing the PWM for the 64x64 Lena image are shown, dividing the frame time into 40 sub-frames to have one to one mapping, since the processed image has 40 intensity levels. The advantage with even distributed PWM over direct is that the number of LEDs in the ON-state is equal in all of the 40 sub-frames. However, the downside is that a highly accurate timing mechanism is required, which must scale to the required stimulator array size.

The control data shown in the same figure is the actual data that is sent to the next stage, which is the pulse encoder. This work is assumed using LEDs based on TFF, so the control data needs to be generated by comparing the previous sub-frame with the current sub-frame, and sending one if there is a difference, or zero if they have the same value.

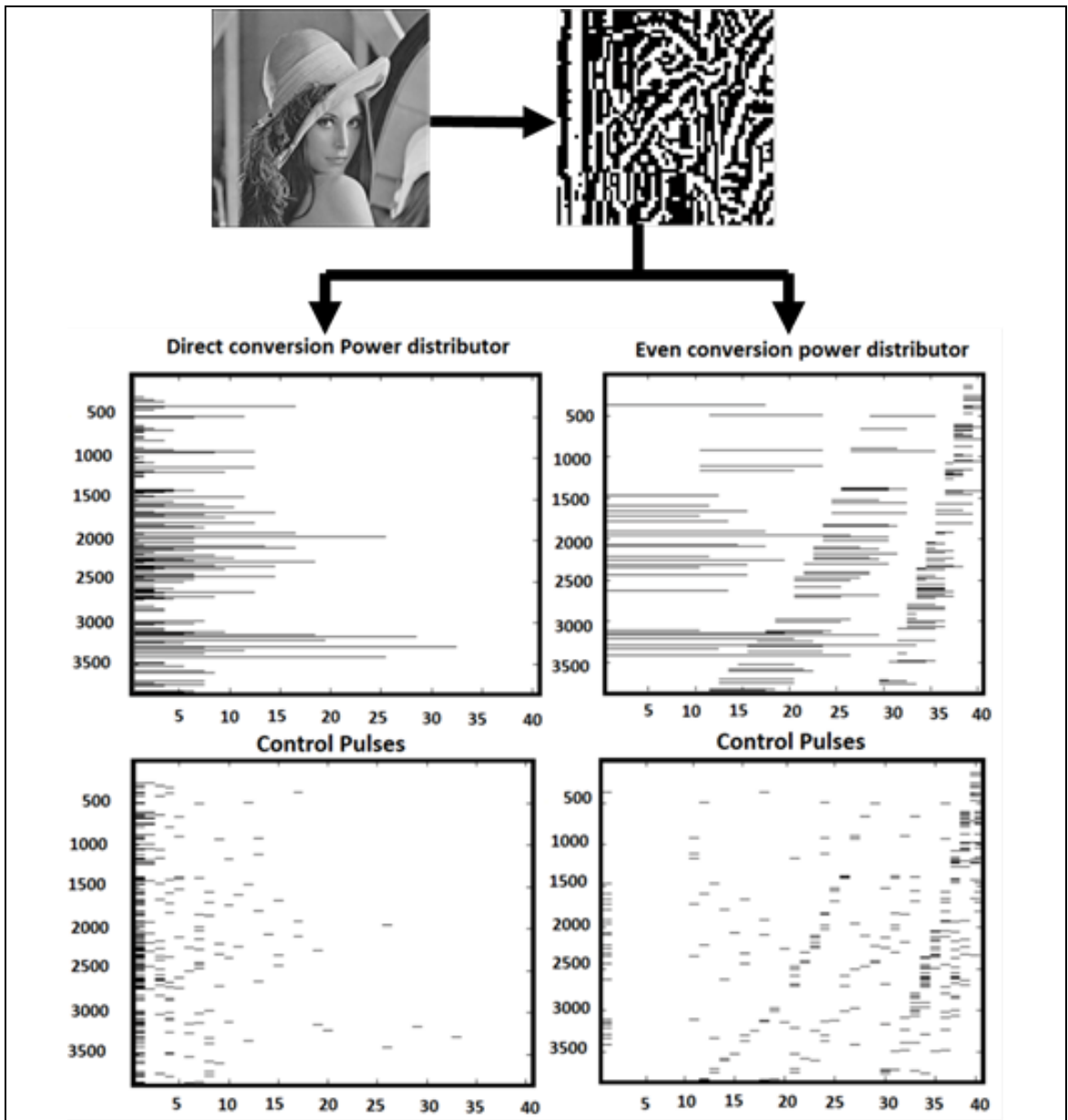


**Figure 4-12 Direct and even power distributions for the 64x64 Lena image.** After processing, each pixel has a value between (0-39) that will be converted into 40 sub-frames. PWM used to achieve the required intensity level. The first row shows the PWM: with the direct method (left) all pixels start at the same time, then continue until they finish; in the new approach (right), PWM starts at different times, under the condition that the number of LEDs in the ON-state is even each time.. The final row shows the control signals sent to have this pattern in both ways

For scaling-up testing, different stimulator array sizes are compared in Figure 4-13, where the Lena image size starts from 4x4 up to 256x256. The figure compares both the even power case with the worst case of the direct way, and the latter MAX power happens at the first sub-frame, when all ON-state LEDs are lighted at the same time. This result assumes that each LEDs consumes (1 mW) power at each sub-frame time.

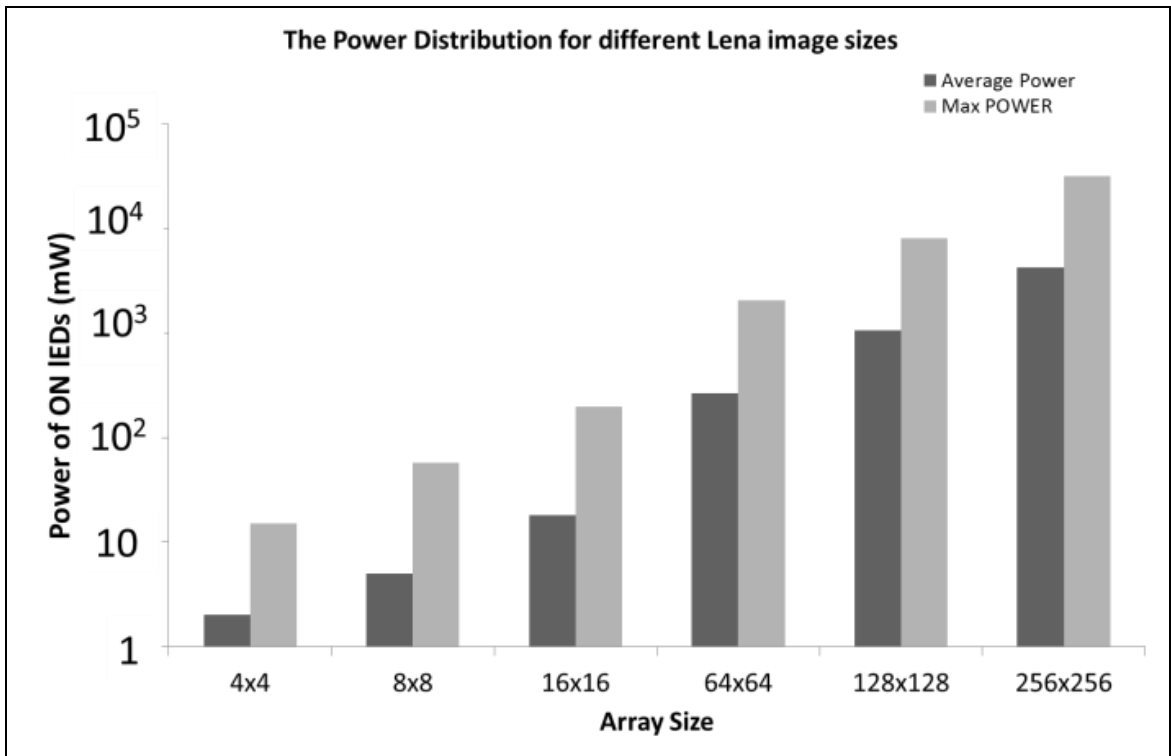


**Figure 4-13** The power versus different array sizes, for the Lena image

To test the power distribution through one frame time, Figure 4-14 shows the power distribution for the 64x64 Lena image, assuming 40 sub-frames. In the direct way, the first 25% has more power than the even method, and then the power goes to zero for 85% of the sub-frames. With the even power distributor, power remains constant through almost all the 40 sub-frames. The area under both curves (direct, even) is equal, where the power explained in the Y axis as logarithmic scale.

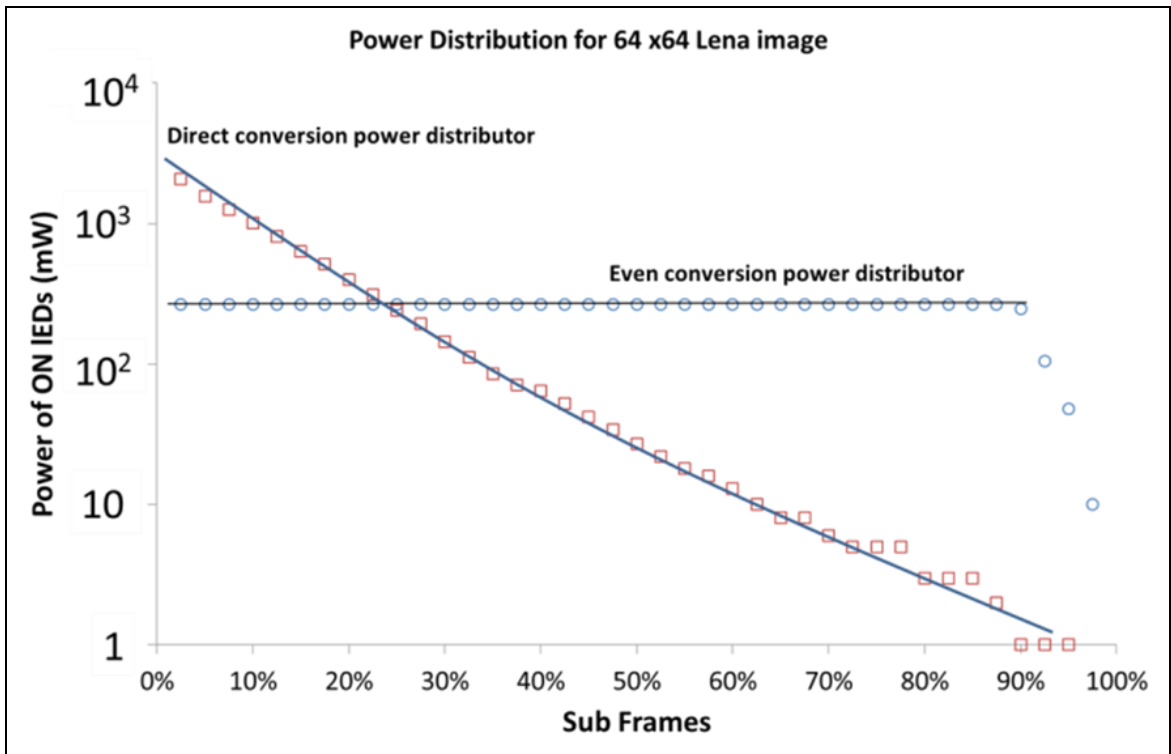


**Figure 4-14** The power distribution for the 64 x64 Lena image. The main image shows that using the even algorithm, power is stable over all the sub frames, while with the direct way the power at the beginning is high and then low

To achieve real time operation, 25 fps was targeted with different stimulator sizes, and this made the frame processing time 40ms. Thus, 40 levels of intensity were used in this work, giving 40 sub-frames and (1ms) sub-frame time. This time is considered small compared to FPGA operating frequencies, and thus dividing a sub-frame further into micro-frames (sub-sub-frames) is suggested, where the main functionality of micro-frame is to match the different illumination levels of LEDs, this is due to manufacturing issues. The micro-frame is used to compensate the different levels of illuminations for different LEDs within a sub-frame, and it is used also to reduce the effect of low frequency response of the ChR2. Scaling-up the number of micro-frames can vary, as larger array sizes use fewer micro-frames. The concept of even power distributor PWM can be applied again at the micro-frame level, and this gives four possible combinations, as presented in Table 4-2, for using even power or not with sub/micro-frames.

**Table 4-2** The four possible states for applying or not even PWM in micro/sub-frame level

<b>State</b>	<b>Does the sub-frame apply the even power distributor?</b>	<b>Does the micro-frame apply the even power distributor?</b>
A	No	No
B	No	Yes
C	Yes	No
D	Yes	Yes

To test the power distribution through one frame time, using the four possible combinations, Figure 4-15 shows the power distribution for the 64x64 Lena image, assuming 40 sub-frames, 100 micro-frames, one LED power consumption equals to (1mW) and there is a 50% mismatch for the LEDs. It can be noticed that the general asymptote of the graph can be determined by the sub-frame, while within each sub-frame the micro-frame determines the power distribution.

The most important task of the even power distributor is to avoid large spikes of current from the battery, and the micro-frames are fixed based on the LED illumination. All of this leads to the application of even power at the sub-frame level, and pre-calculation of the time of the micro-frame, which is then embedded in the next stage of the stimulation controller (i.e. the pulse encoder).

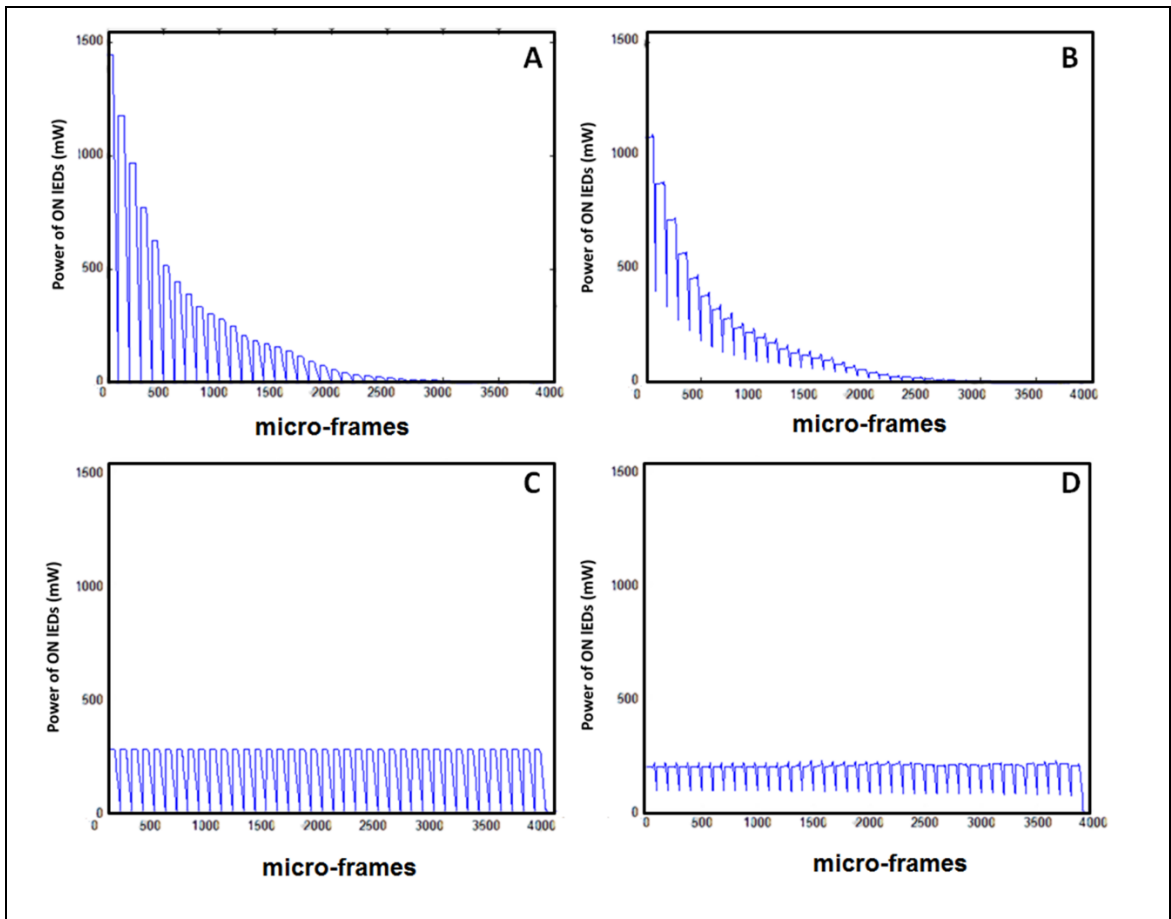


**Figure 4-15** The power distribution for the 64 x64 Lena image. four possible combinations. Where the Y-axis represents the power consumption in mW for: (A) even power applied for neither sub-frames nor micro-frames (B) even power applied for micro-frames but not sub-frames (C) even power applied for sub-frames but not micro-frames and (D) even power applied for both micro-frames and sub-frames

The even power distributor's effect on the retinal prosthesis system is analysed, by sending predefined frames, and then the results are tested using Agilent N6705B DC Power Analyzer. It is used to supply a fixed voltage, and then measure the drawn current. The even power distributor block was tested by sending a frame that contains all pixels with an intensity equal to 1, where each pixel can have a level up to 16 intensity, running at 6V. The diagrams in Figure 4-16 represent the same frame repeated five times, where the left diagram represents the current drawn using the direct PWM way, and all LEDs start the ON-state at the first sub-frame. For this frame, all the LEDs will be ON for only the first sub-frame, and this draws about 70mA for only 0.7ms (sub-frame time). The right diagram represents the current drawn for the same frame, using evenly distributed ON-state LEDs. This leads to the consistent consumption of a fixed current of approximately 10 mA. Extending this to larger array sizes with a shorter



sub-frame duration may lead to current spikes that will affect the battery operating the visual prosthesis system.



**Figure 4-16** The current drawn by the optoelectronic micro-LEDs, by continuously sending a frame containing all pixels with an intensity value equal to 1. (Left) data sent using direct PWM (Right) data sent using an even power distributor

The second frame is the same as the first except that all the pixels' intensity equals 7, and the diagrams in Figure 4-17 represent the same behaviour frame with seven sub-frames drawing about 70mA for 6ms. In the right diagram, the value of the drawn current is increased to around 30mA due to the increasing pixel intensities.

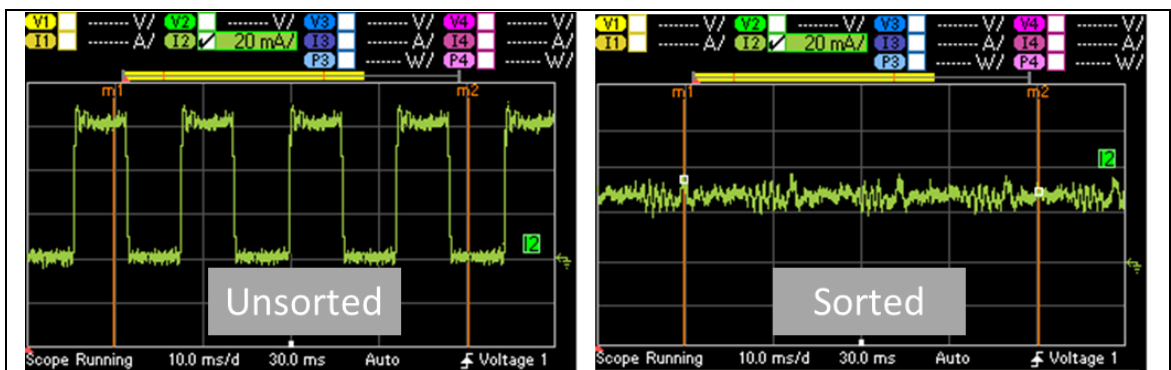


**Figure 4-17** The current drawn by the optoelectronic micro-LEDs, by continuously sending a frame containing all the pixels with an intensity value equal to 7 (Left) data sent using direct PWM (Right) data sent using the even power distributor

The third frame used to test the even power distributor block was the 16x16 Lena frame that contains pixels with different intensities ranging between (0-15), running at 6V. The diagrams in Figure 4-18 represent the same frame repeated five times; the left diagram represents the current drawn using the direct PWM, where all LEDs start in the ON state at the first sub-frame, and then start to switch to the OFF-state as they finish their intensity values. This oscillates the drawn current between (0-70) mA in 12ms period (frame time). The right diagram

represents the current drawn for the same frame, using evenly distributed ON-state LEDs. This leads to the consistent consumption of a fixed current of approximately 40mA. Extending this to larger array sizes with shorter sub-frame duration may lead to unstable current being drawn from the battery, which will affect the visual prosthesis system operation.

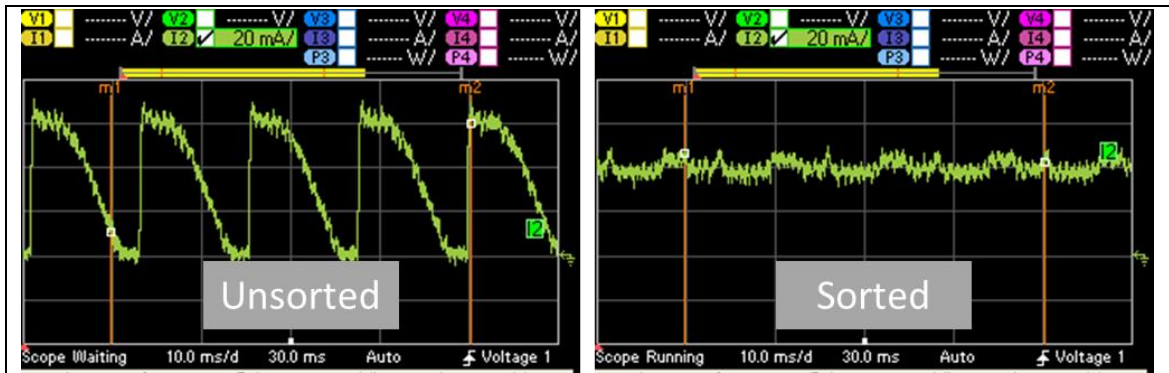


**Figure 4-18** The current drawn by the optoelectronic micro-LEDs, by continuously sending a frame containing the 16x16 Lena image, with different pixel intensities. (Left) data sent using direct PWM, (Right) data sent using even power distributor

A fourth pattern was used to test the even distribution, using the four possible combinations, of employing or not the even PWM at the sub\micro frame level. Figure 4-19 shows the power distribution for the 16x16 Lena image, assuming 16 sub-frames, 100 micro-frames, running at 8V. It can be noticed that the general asymptote of the graph can be determined by the sub-frame, while applying the even PWM at the micro-frame level smooths the drawn current, and also increases the current due to voltage increase.

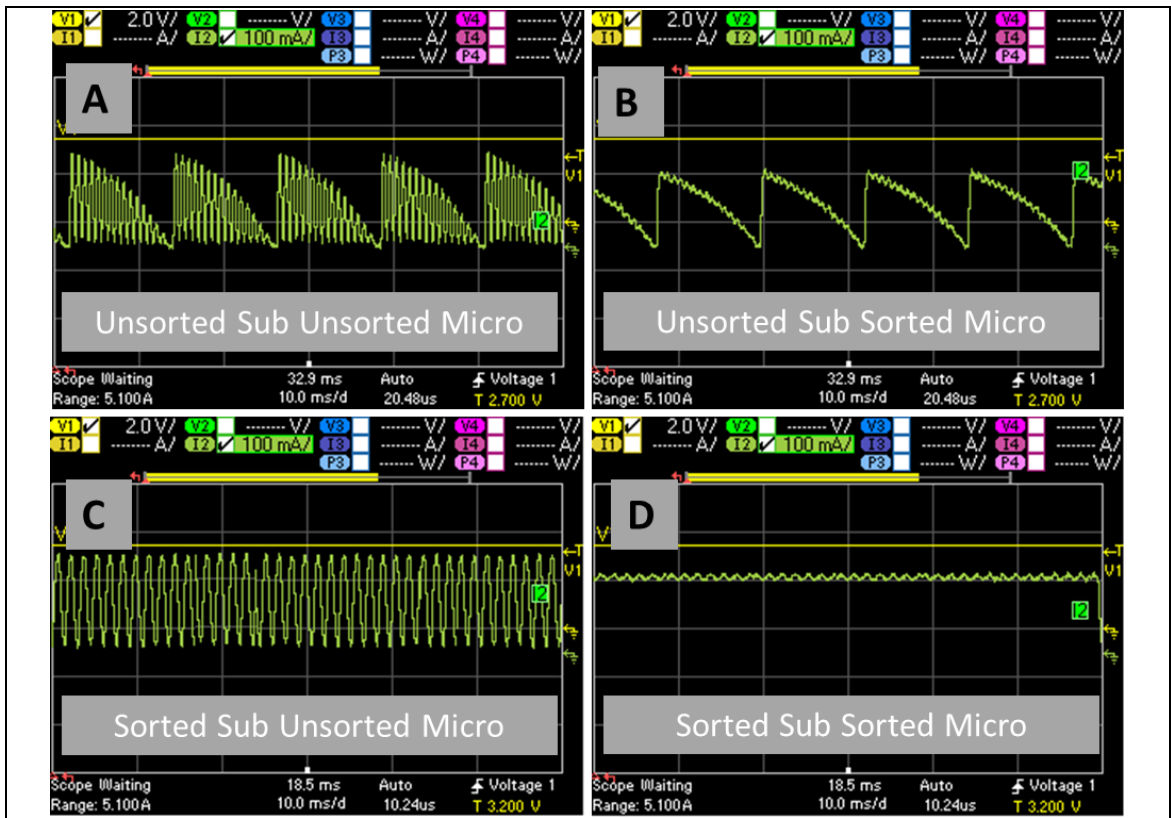


**Figure 4-19 Four possible even PWM states.** For frames containing the 16x16 Lena image, with different pixel intensities: (A) even power is not applied to the sub-frames, or the micro-frames (B) even power is applied to the micro-frames but not sub-frames (C) even power is applied to sub-frames but not micro-frames and (D) even power is applied to both micro-frames and sub-frames

#### 4.4.2 Pulse Encoder Results

The processed data can be sent to the opto-electronic micro-LED array used in this work via different modes of operation. Thus, the pulse encoder is designed to have the capability of utilizing these various methods to operate the array in an optimum way. The selection between these different modes should be done automatically depending on the data. The 16x16 array has two modes of operation: first, the pixel operation mode is used to update only one pixel using four clock cycles, due to using a 16 x16 array and internal 4x16 encoder. The second is the row operation mode that is used to update a whole row using 16 clock cycles, due to using an internal 16 bit shift register. In this design, the pulse encoder introduces a mixed operation mode where for each row it automatically selects between pixel or row mode, depending on the number of ones in a given row. If there are more than four it is better to use the row mode, but otherwise use the pixel mode.

The simulation results for the different operating modes using the 16x16 array size, in terms of time, are shown in Figure 4-20. The X-axis represents the array

percentage utilization, which means the number of pixels required to be changed divided by the total number of ones in the array (i.e. 256). The Y-axis represents the number of clock cycles needed to update that percentage of utilization. When the array is fully utilized, i.e. all the stimulating pixels are to have their state toggled, then row mode uses fewer clock cycles. For sparse utilization, the pixel update is most efficient. There was no difference between using either of the previous two, at around 20% utilization. On the other hand, using the mixed mode, which allows simultaneous the use of either, better results were achieved than using either mode independently.

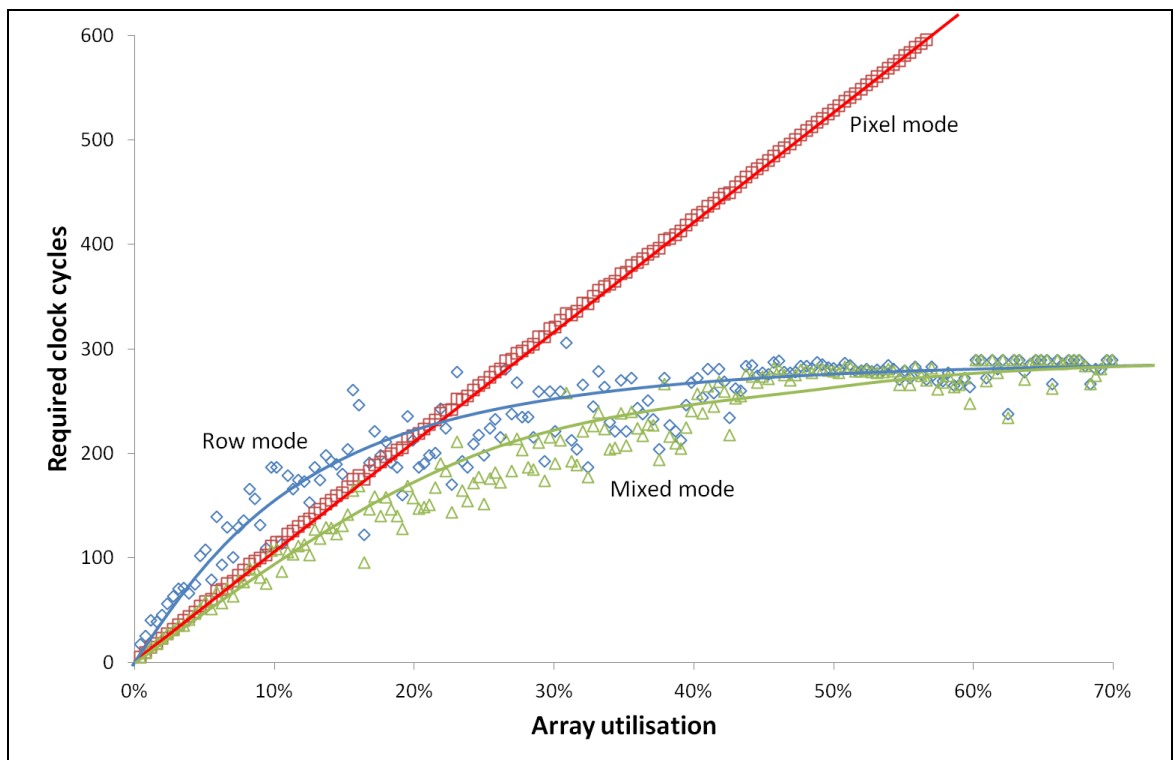


**Figure 4-20** The number of clock cycles versus array utilisation in the 16x16 array

In Figure 4-21, different stimulator array sizes are compared. The X-axis represents the array percentage utilization, which means the number of pixels required to be changed divided by the total number of ones in the array, where the Y-axis represents the percentage of improvement. This is calculated using the following equation:

$$\text{Percentage of Improvement} = \frac{\text{Max}_{\text{ClkCycles}(\text{Row,Pixel})} - \text{Min}_{\text{ClkCycles}(\text{Row,Pixel})}}{\text{Max}_{\text{ClkCycles}(\text{Row,Pixel})}} \quad (4-2)$$

A crossover point appears when the required time is equal to row/pixel mode. The crossover point varies but it is decreased for larger array sizes. Under a typical pulse width modulation operation, the first turn on the pulse will utilise a large percentage of the pixels, perhaps requiring predominantly row mode. Then to achieve the pulse width, the stimulating pixels which have been turned on will need to be turned off at various sub-frames. This will be a predominantly pixel operation depending on the array size, with some row updating. Using evenly distributed pulses, the mode used depends on the number of changes needed per sub-frame, and there is no predominant mode at a certain time. For each sub-frame, the time saved from the stimulation raster can be passed to the sensors, allowing information extraction from the chip.

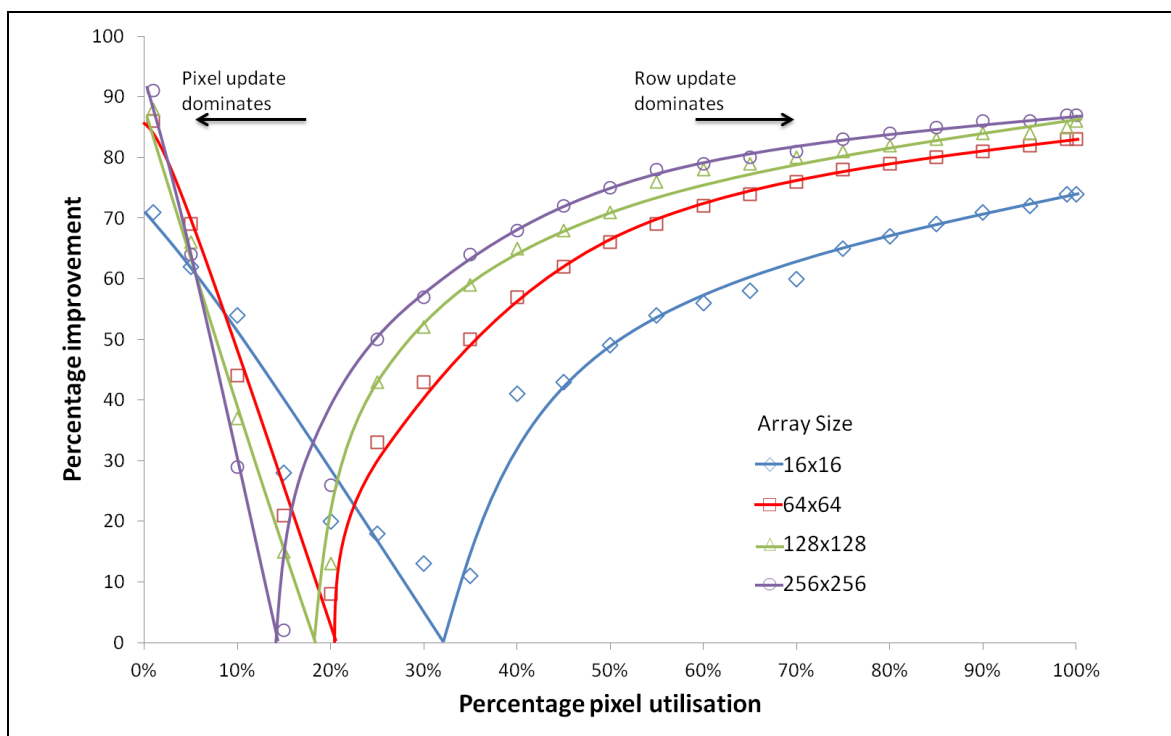


**Figure 4-21** The percentage of filling array versus the percentage, of improvement using different array sizes

The simulation results of the different operating modes in terms of energy are shown in Figure 4-22. The X-axis represents the array percentage utilization which means the number of pixels required to be changed divided by the total number of ones in the array (i.e. 256). The Y-axis represents the percentage of energy needed for switching the CMOS controlling circuit for the array. Two points are shown in the diagram: the first is called MaxE, which indicates the maximum energy consumed using the mixed mode. The second is called  $t$ , indicating the

minimum energy consumed using the mixed mode. The energy utilisation for pixel, row and mixed modes is presented. Although the pixel arbiter that allocates access to LEDs is pipelined and thus time efficient for individual pixel updates, the arbiter requires more switching states and thus energy than the shift register. Therefore, the mixed mode will consume a peak in energy for sparse arrays. The energies are small for smaller arrays for which the LED power will be dominant. For larger arrays, row updating would be more energy (even if not time) efficient.

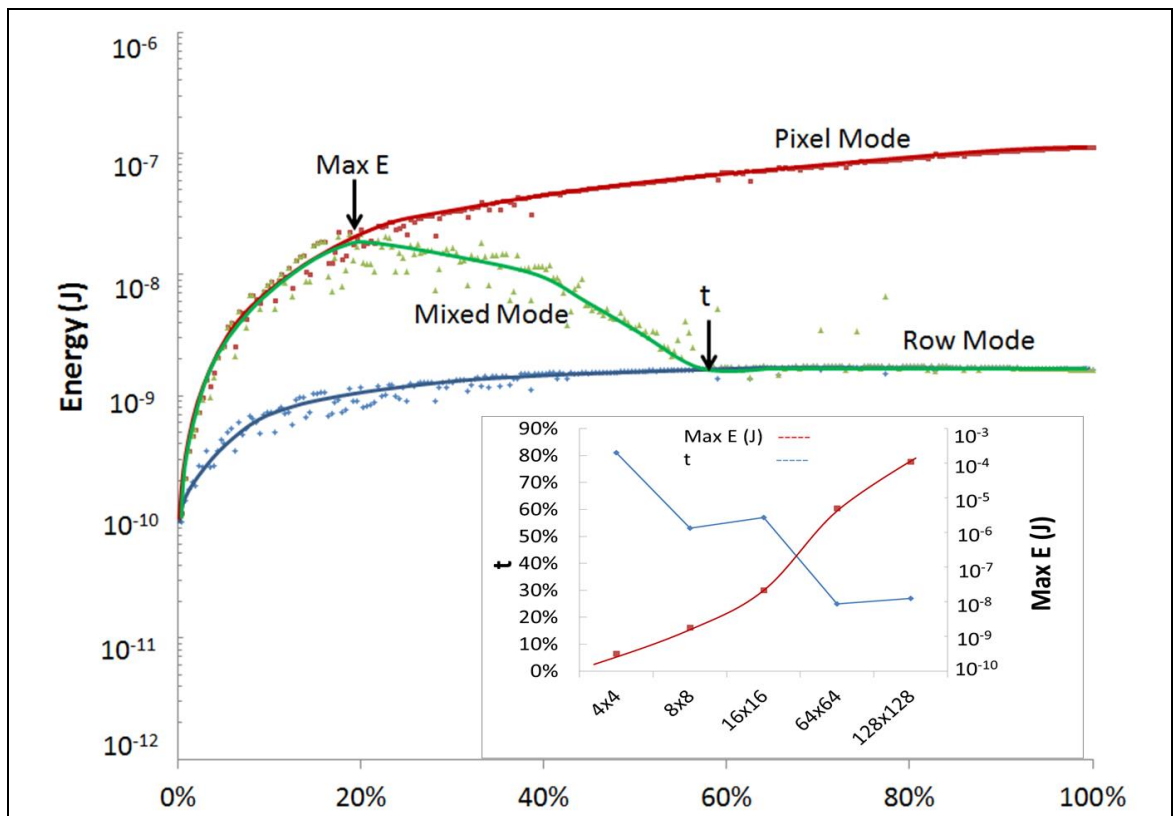


**Figure 4-22** The energy utilization of the neural stimulator, according to the control methodology. The main image shows the data for the 16x16 array. The MaxE point is the maximum energy utilization of the mixed mode, and the t point shows the value where the mixed mode and row mode have the same results. The insert shows how these points scale with array size

For the growing array sizes used in optogenetic retinal prostheses, the effect of using a mixed mode is further analysed in Figure 4-23, where the simulation results for 16x16 and 64x64 are shown. The X-axis represents the array percentage utilization, which means the number of pixels required to be changed divided by the total number of ones in the array, where the Y-axis represents the number of clock cycles needed to update that percentage of utilization. It is noticeable that the area of advantage that can be achieved using the mixed mode becomes less when the array size becomes large. Given that this coincides with

the increased energy consumption for using pixel arbiters in large arrays, it is recommended to utilize mixed pixel/row to update only those arrays smaller than 128x128. Beyond that, a simple row update is efficient.

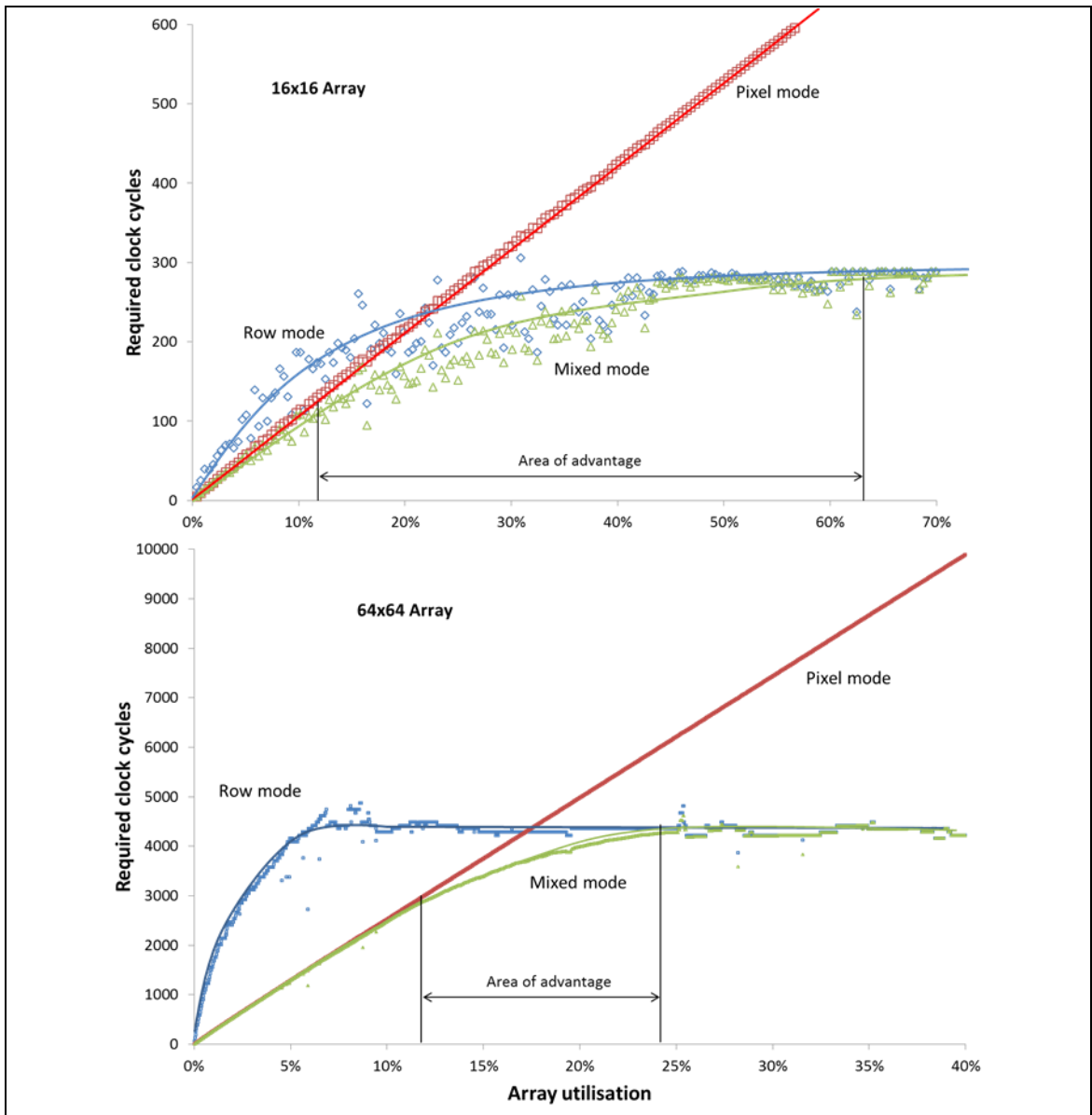


**Figure 4-23** The number of clock cycles versus the array utilisation, in 16x16 and 64x64 arrays, for different control modes. The area of advantage describes the region where mixed mode is advantageous over pixel/row modes. In other regions it becomes same to either row or pixel mode

The practical results for the pulse encoder design for the optoelectronic micro-LEDs, which based on selecting between two serial addressing modes (short or long), using a new mode of address called a mix mode. These modes are available in the 16x16 array used in this work; however, they do not work except the AER parallel mode (i.e. by updating a pixel each time) is working. A new design for the pulse encoder is used to operate the array. It scans the 256 pixels



one at a time every micro-frame, and needs three clock cycles for each pixel update. This work uses a FPGA run at 100MHz clock frequency, 100 micro-frames and 16 sub-frames, and this leads to a total frame time equal to  $(3 \times 256 \times 100 \times 16 \times 10\text{ns})$  12.228ms. To scale this to larger array sizes, the number of micro-frames can be reduced.

In this section, the results of both blocks of the optoelectronic stimulation controller, the even power distributor and pulse encoder, are presented. It shows the importance of the even power distributor, to spread the ON-state LEDs through the whole frame time, which helps to avoid large current spikes so it is recommended for larger stimulator sizes. However, larger array sizes are preferable for updating using a simple row scan mode rather than pixel or even mixed mode, due to the higher energy used by the LED CMOS control circuit. Therefore, it is not recommended to use the pulse encoder for array sizes greater than 128x128.

Finally, the full photonic stimulation module, including the serial communication and buffering, is synthesized using the following FPGA device: Virtex-5 5v1x50ff676-1, and in Table 4-3 the utilization of resources used in the design is presented.

**Table 4-3** *The FPGA used resources with maximum frequency and power consumption*

<b>Logic and Memory Resources</b>	<b>Used</b>	<b>Available</b>	<b>Utilization</b>
<b>VIRTEX-5 5v1x50ff676</b>			
<b>Number of Slice Registers</b>	4167	28,800	14%
<b>Number of Slice LUTs</b>	2106	28,800	7%
<b>Number of Occupied Slices</b>	1338	7200	18%
<b>Maximum Internal Frequency</b>	146.757MHz		
<b>Est. Power Consumption</b>	545 m W		

The full controller unit for a 16x16 stimulator size array was implemented in Virtex5 development kit for use in the biological experiments. It utilized less than 20% of the available resources on the FPGA. One counter argument to what is presented in this work is that the photonic stimulation controller will increase the



power budget. Where the overall power budget for the prosthesis is estimated to be similar to that of tablets or smartphones, i.e.  $\sim 2\text{W}$ . This could feasibly be recharged on a daily basis utilizing a 30WHr battery. The FPGA has a power consumption of about 0.5W that around the quarter of total estimated power, this to be reduced further when final system implemented into an ASIC circuit. In the next section, the optoelectronic LEDs measurement results are presented and discussed.

#### **4.5 Optoelectronic Micro-LED Results**

The opto-electronic stimulation LED array has different illuminations per pixel, due to the manufacturing process. This mismatch needs to be measured in order to correct it with micro-frames PWM. The measurement of illumination is done using a Newport power meter 1918-c. An FPGA code is used to light each LED individually and then the power is measured by a photodiode, which indicates the illumination of each LED. Then, all the LEDs are given an individual percentage by dividing the lowest measured value by the LED value. The obtained percentage results are used in micro-frame PWM. Figure 4-24 shows: (A) the power meter used in measurements, (B) the result of calibration for the array at 6V, (C) the histogram of the calibration results and (D) the calibration results shown as a 16x16 intensity map.

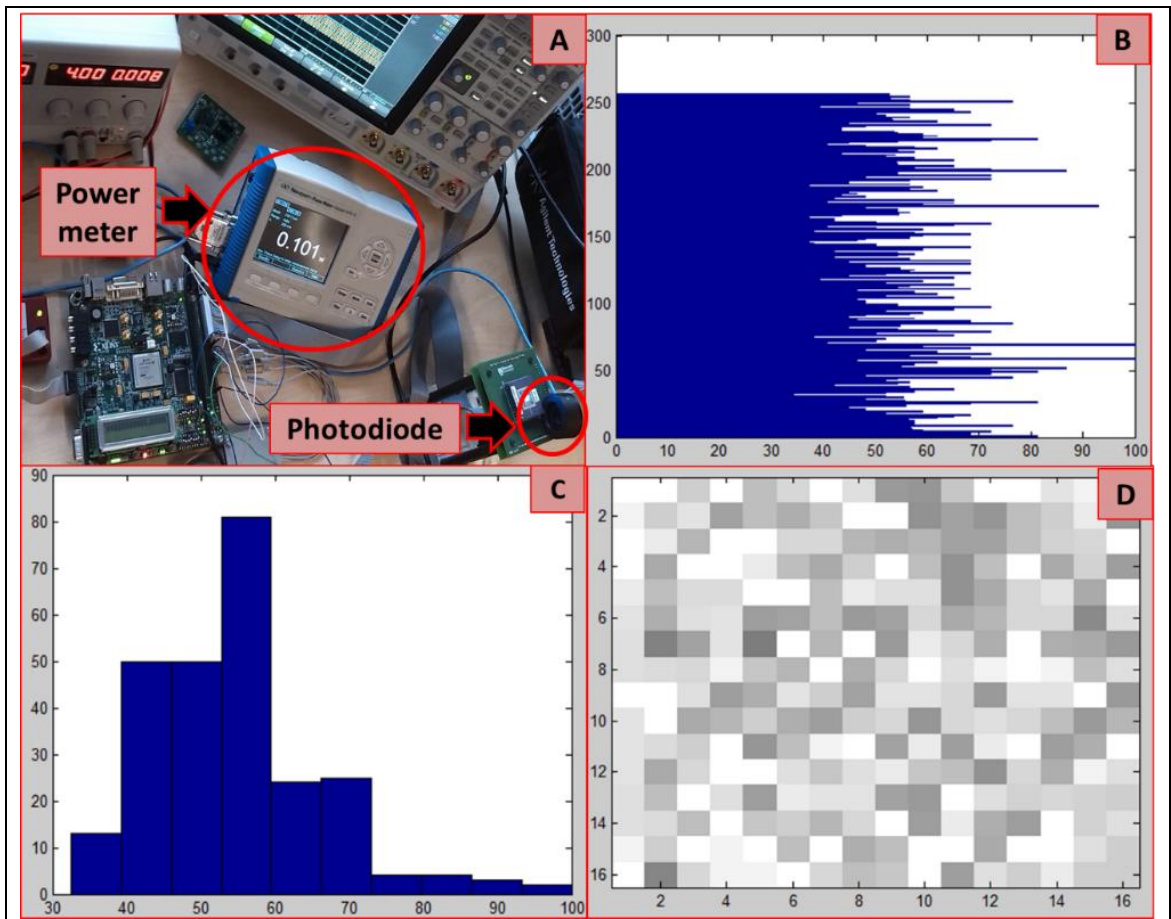


**Figure 4-24** The power meter with different mismatch measurements. (A) The power meter with photodiode, (B) the 256 LEDs' mismatch percentages, (C) the histogram for LEDs' mismatch and (D) the 16x16 intensity map

The mismatch of the LEDs varies with different operation voltages, and the calibration process is repeated for different operation voltages. The summary of measured illuminations is shown in Figure 4-25, where LEDs from 1-256 are presented in the X-axis. The measured power in mW is presented in the Y-axis, where it can be noticed that as the operating voltage increases the mismatch between LEDs increases. Thus, when operating in higher voltages, it important to take into consideration the mismatch calibration for retinal prosthesis opto-electronic stimulator arrays.

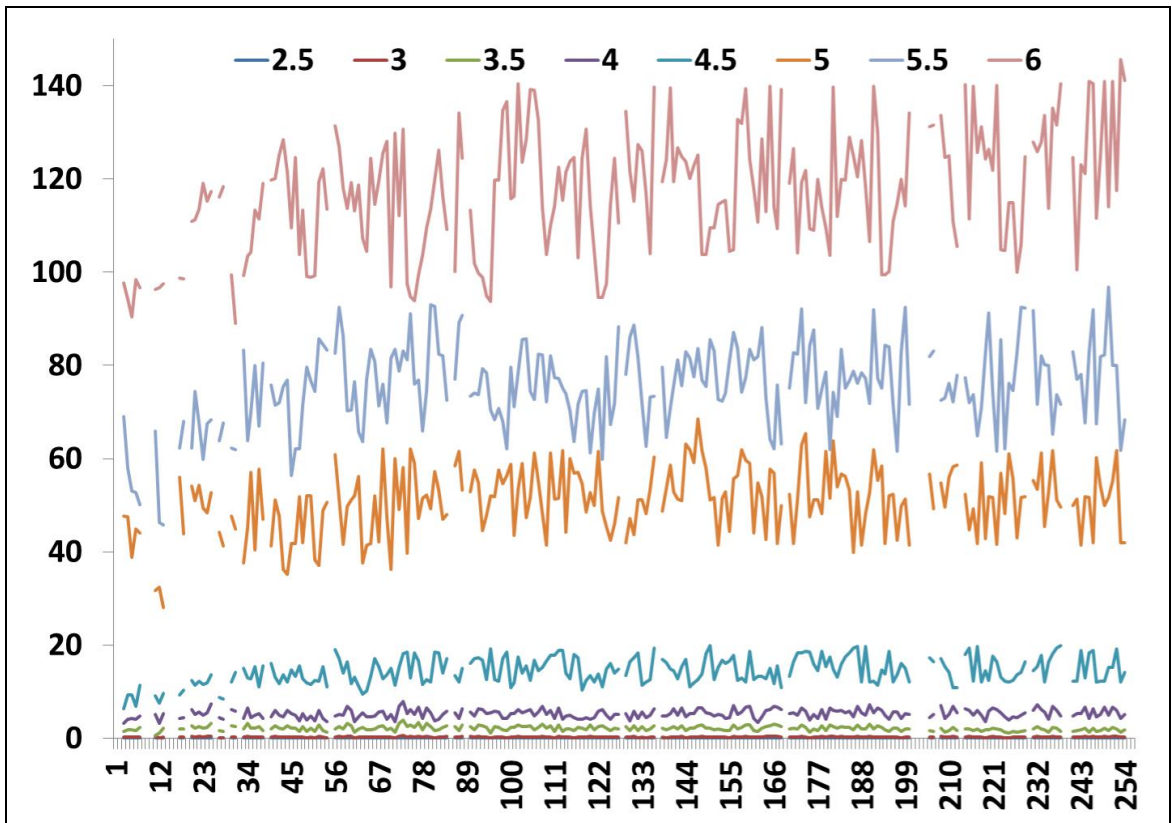


**Figure 4-25** The measured illumination for different operating voltages

Finally, the following figures display some of test patterns sent to the optoelectronic stimulator array. In Figure 4-26, all the array is lighted ON with and without mismatch calibration; the black LEDs are faulty ones and are excluded from the calibration process.

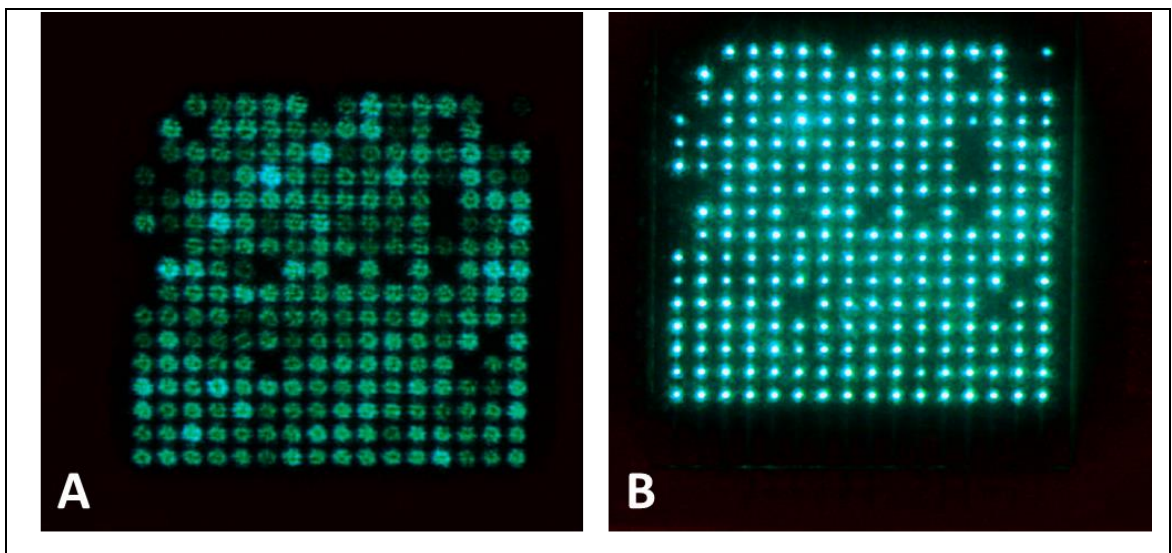


**Figure 4-26** Optoelectronic LEDs mismatch. The difference between (A) without mismatch correction, (B) with mismatch correction

In Figure 4-27, all the array is lighted ON (A) with different 16 level intensities, and (B) two intensity levels are used (15,1).

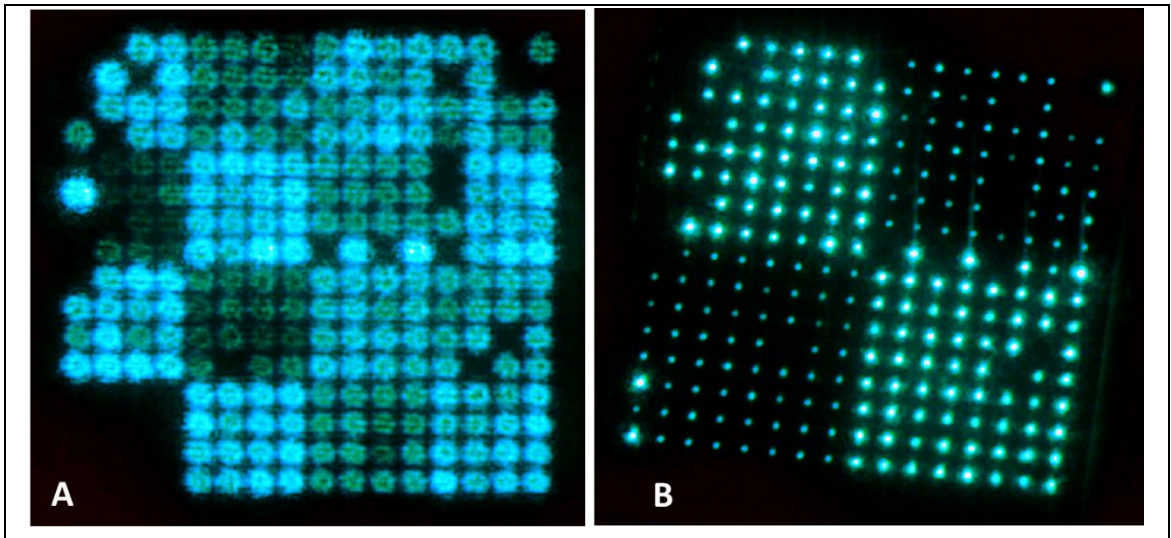


**Figure 4-27 Optoelectronic LEDs intensities.** All LEDs ON with different intensities (A) 15 levels of intensity, (B) 2 levels of intensity

In Figure 4-28, two final images of (A) a smiling face and (B) a star are shown.

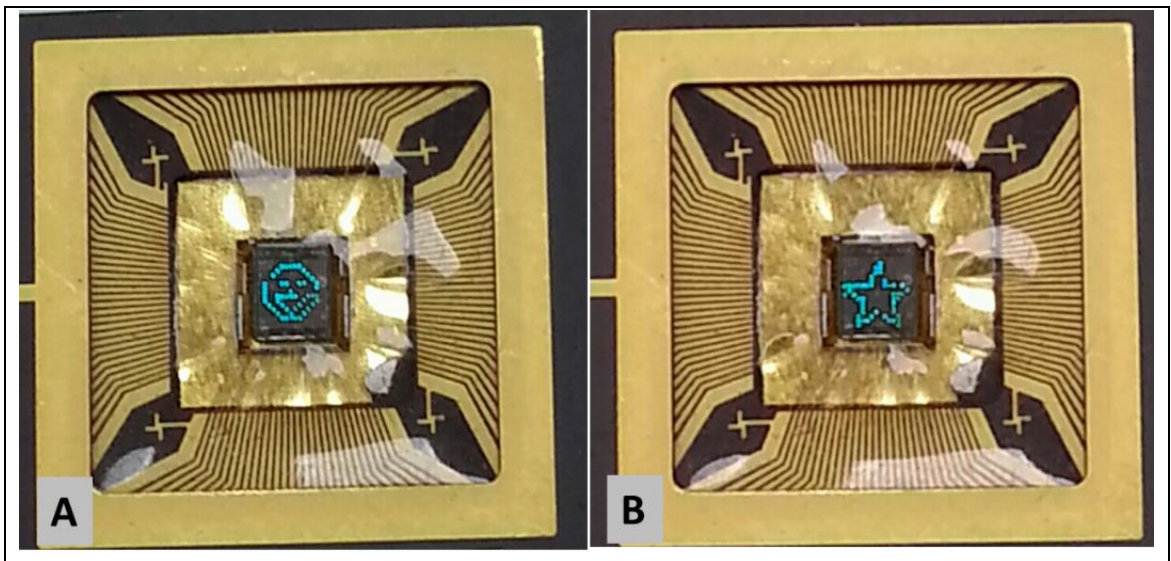


**Figure 4-28 Two patterns: (A) Smiling face (B) Star**

## 4.6 Conclusion

In this chapter, I have displayed and discussed the results of the software/hardware implementation for the work, which includes the following: input stage results, high level processing results, low level processing results, and output results.

**Input Stage Results:** in this work the input stage starts with the test patterns written by biologists, and then these patterns needed to be transferred from the computer to FPGA. Thus, the results are about the used computer-FPGA communication.

**High Level Processing Results:** I presented the dual spectrum image simplification based on both IR and Visible images to segment the important features in the image. This segmentation helps with the image retargeting, which recently is a requirement for most visual prosthesis systems. Then, the retinal image processing results were presented for both bipolar and ganglion layers in the retina.

**Low Level Processing Results:** the optoelectronic stimulation controller results were presented, starting with the even power distributor, then moving to the pulse encoder results.

**Output Stage Results:** these discussed the calibration of the 16x16 optoelectronic micro LED array and some images displayed on it.

In the next chapter, the conclusions of the thesis and future work are presented.

### Relative contributions

Subject	Contribution
Mr Musa Al-Yaman	<ul style="list-style-type: none"><li>- Results of computer-FPGA communication</li><li>- Results of the Dual-spectrum Image preparation</li><li>- Results of the Izhikevich neuron model and bipolar cell reconstruction</li><li>- Results of all parts of the Photonic Stimulation Controller</li><li>- Results of 16x16 calibration and images</li></ul>
Dr. Walid Al Atabany	<ul style="list-style-type: none"><li>- Result of <i>image Retargeting</i> algorithm</li></ul>



## Chapter 5 Conclusions and Future Work

This chapter summarises the contribution to the field of the optogenetic retinal prosthesis developed in this work. After that, the work in this thesis is evaluated, and suggestions for improvements are presented. This is achieved by reviewing the work performed for each retinal prosthesis stage, and then concluding and setting out the challenges and recommendations for future enhancements.

The human visual system is one of the most sophisticated systems in the human body. The first stage of perception starts with the eyes, where the retina photoreceptors (rod and cones) sense the light, and next the retinal processing layers perform spatial/temporal processing. After this, the communication layer transmits information to the optic nerve, and finally the image reaches the visual cortex so that it can be understood.

The main issue for the retinal disorders caused by aging is that it is hard to find a solution for such disorders that leads to a cure. However, although in future gene therapy may prevent eye diseases such as RP, it cannot recreate lost vision. With RP patients, although they start to lose rod photoreceptors, the other communication circuitry of the retina is largely undamaged, since this is mainly comprised of the ganglion cells. This has led to the development of a retinal prosthesis to enable RP patients to regain their sight.

The retinal prosthesis is considered a possible solution for some eye aging disorders such as Retinitis Pigmentosa (RP). The retinal prosthesis can be based on either electrical or optical stimulation for intact retinal cells. For optical stimulation, the targeted retinal cells need to be genetically modified to become light sensitive, which is done by injecting a virus into it. The optogenetic retinal prosthesis is still in its early stages, but rapid progress in the field may be made with human trials due to take place in the next few years.

The main contribution of this work can be presented by the following two points:

**The first point:** the work has introduced a new stack for the retinal prosthesis field, and this stack divides the retinal prosthesis into four main stages instead of three, this accomplished by splitting the processing stage into high and low processing as illustrated in Figure 5-1.

In the new stack, high level processing can be utilized by any visual prosthesis approach. In my opinion, this separation can help researchers using different approaches to concentrate on the functionality of this layer, rather than implementation details. Then, low level processing, it is specific for each approach, this will focus more on the stimulator interface and implementation details.

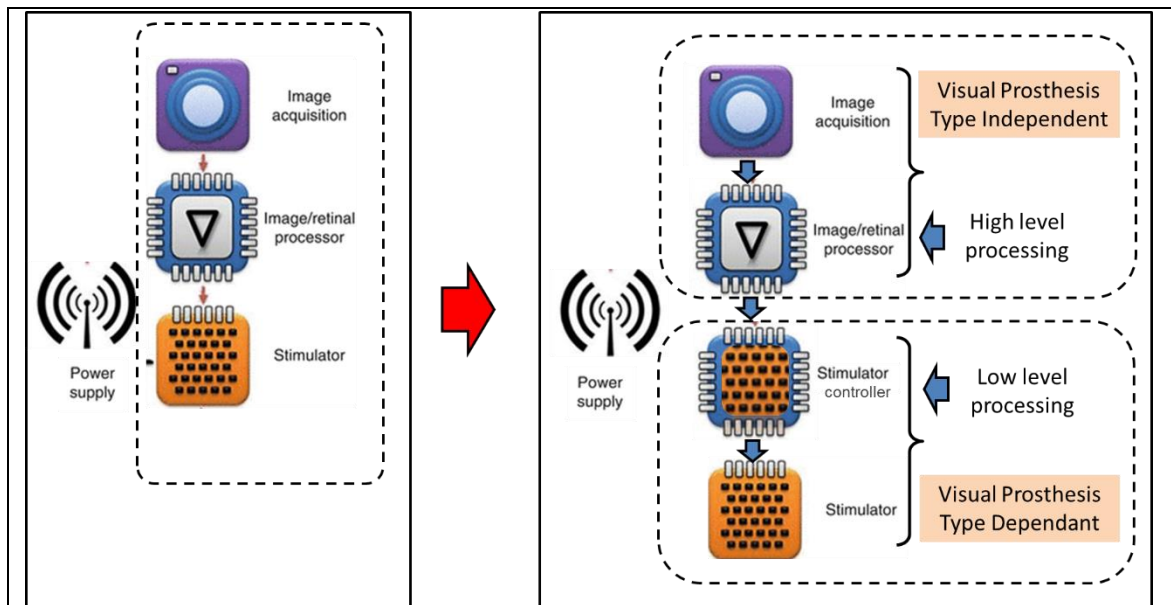


**Figure 5-1** The visual prosthesis processing stack. Left: old stack consists of three stages: input, processing and output. Right: the processing stage is split into high and low level processing, which helps in focusing on the functionality during the high level processing, and interface and implementation details in the low level processing

**The second point:** The design and implementation for the optogenetic retinal prosthesis approach in the low level processing stage includes two main blocks: the first novel block is the frame encoding and the even power distributor, which is used to spread the ON-State LEDs through the frame time, to avoid a power surge. The second block is the pulse encoder, which is used to control the micro-LED array in an optimum timing.

As stated earlier, the main interest of this work is the optogenetic retinal prosthesis, which is based on optical stimulation rather than electrical. However, some parts of this work can be utilized in any visual prosthesis system. Thus, the evaluation and recommendation of this work is presented based on the suggested visual prosthesis processing stack; starting with the input stage, and then the high level processing stage. This is followed by the low level processing



stage, and finally the output stage. These stages are shown in Figure 5-2, which represents the work achieved in each stage.

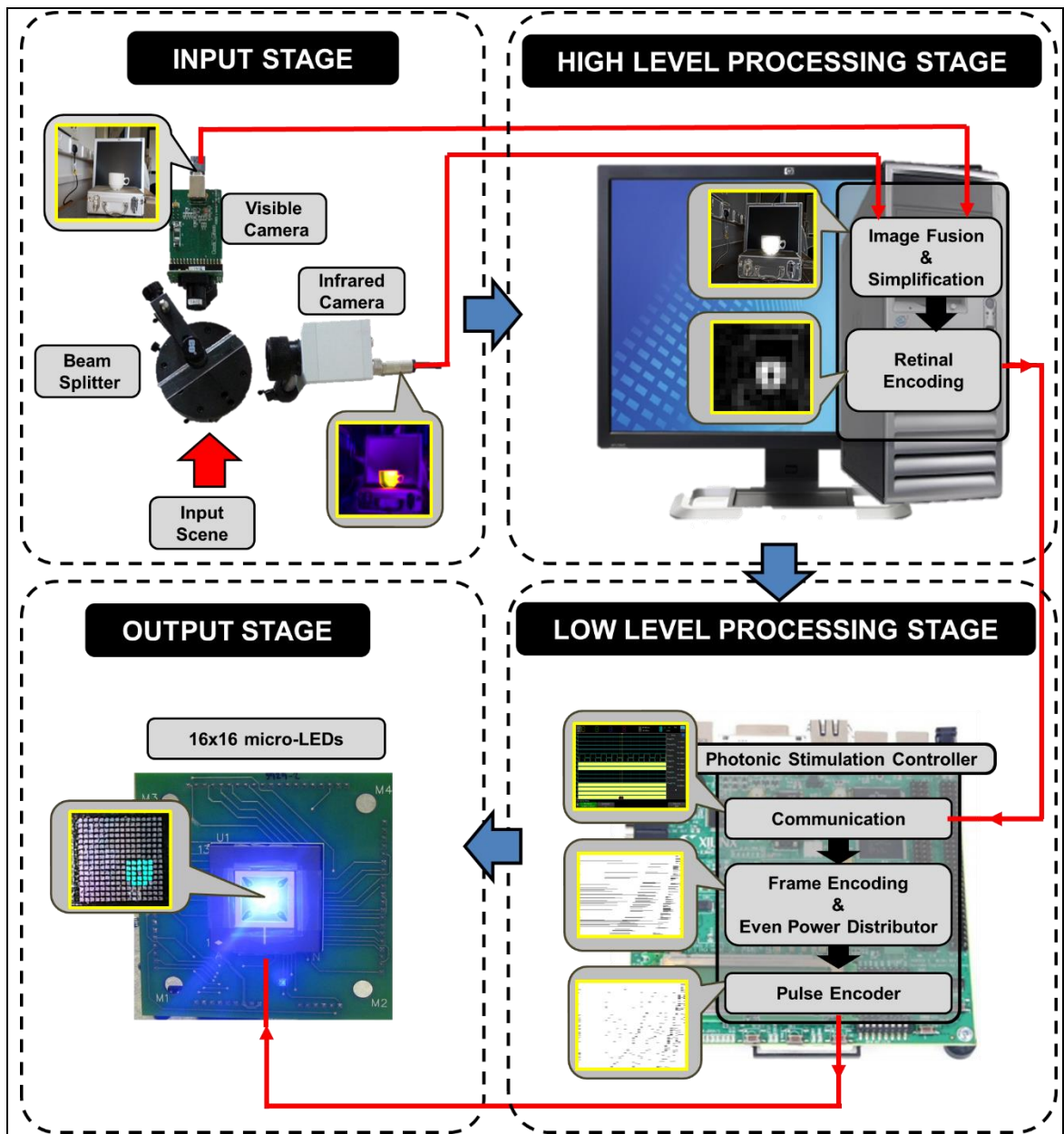


**Figure 5-2** The completed parts of the optogenetic retinal prosthesis framework. The input stage: the dual IR/Visible image sensors acquisition. The high level processing stage: the image fusion and simplification, followed by retinal encoding. The low level processing stage: the communication with computer, then frame encoding and even power distributor, and then the pulse encoder. The output stage: the 16x16 micro-LED array is presented

- Input Stage:** In this work, the image acquisition was performed using dual spectrum IR/Visible image sensors. One counter argument to the use of dual IR/Visible images sensors is that adding an additional camera will increase the power budget. An Optris camera was used which had a power consumption of between 0.5 and 1W. It is too bulky to be used in a head

mounted display especially with the beam splitter arrangements. However, there has recently been rapid improvement in the compactness, power consumption and cost of these systems. It is now possible to obtain more compact systems with power consumption as low as 150mW [154]. The power consumption for these devices is expected to improve further in the coming years. Recently, a new product from FLIR called FLIR ONE has become commercially available on the market. This is a thermal camera that can be attached to an iPhone, and then an application can be downloaded that overlays the IR image to a visible image. The power consumption of this device is around 350 mW [155]. On this basis, mixed IR/visible imaging for a retinal prosthesis may become feasible when power consumption is reduced to around 50-100mW (similar to a visible camera).

A recommendation for future work is using an eye tracking system, where tracking the eye's position is an essential part of designing an effective augmented vision system. Such a system can enable the capturing of scenes with a large field of view, and it only applies the enhancement algorithms locally to the Region of Interest (ROI) at which the patient is looking. This makes the movement of the patient's head and eye more natural, rather than moving their whole head. Moreover, an eye tracking device that will track the movement of the eye could be used to implement a new artificial image processing algorithm that uses this device to concentrate on the scene that the patient is looking at, by zooming only to the object that is under consideration[156].

- **High Level Processing Stage:** the aim of this stage is to enhance and maximize the useful visual information included in the image before stimulating the retina. In this work, an improvement of the image simplification processing time has been achieved, using a dual spectral IR-visible approach. The current low spatial stimulator arrays require an additional image non-linear retargeting step [125], which is computationally expensive. Thus, it can utilize the IR-visible segmentation map to speed-up the retargeting step. In this work, the Izhikevich neuron model was implemented, and recently this model has become increasingly employed due to its power and simplicity. This makes the work more

similar to the actual retinal ganglion cell (RGC) operation. Therefore, in the high level processing, both simplification and retinal encoding algorithms were developed; these can act as a visual prosthesis front end processing interface, which is used to prepare the information for the next low level processing.

Another recommendation for future work is using special purpose image vision chips, which integrates high level processing with the image acquisition system. A further recommendation is to use classification to identify the objects in an image. Image segmentation is a critical step in image analysis since good results from the segmentation step are vital for feature extraction. After segmentation comes classification, and then recognition, which derives a description or some other interpretation of the scene, which can be done using cloud computing. Adding other more interactive features could be considered to mimic the actual human machine interaction.

- **Low Level Processing Stage:** this part of the work is specific to optogenetic retinal prosthesis systems. The first stage is the stimulator controller, which is a novel part that was introduced for the first time (previously, the stimulator was simply controlled by the integrated CMOS chip). The controller consists of two main parts: first, the frame encoding and even power distributor and, second, the pulse encoder. The frame encoding and even power distributor, for large array sizes, can avoid large pulses which may affect the stimulator array for a short duration (surge). The pulse encoder was used as an optimum control methodology for the opto-electronic stimulator arrays. For larger stimulator arrays, it was found that a simple shift register-based row update methodology is optimal, from the perspective of both time and energy. For the smaller arrays which may be used in implantable prostheses, mixed mode pixel/row update is optimal.

An FPGA-based hardware implementation platform was used to implement this low level stimulator controller; its ability to process data in real time is very important, and moreover it must be scalable and able to operate within the power budget of portable processing devices. The previous specifications were taken into consideration in the

implementation as the following: for processing speed, the implementation achieved 80 fps, 28 fps frame rate for the 16x16 and 90x90 respectively, which is greater than the real time frame rate which is 25 fps. For estimated power consumption, the system was estimated to consume around 0.5W, and is within the whole system power budget (~2W). Finally, the system is scalable since the number of micro-frame levels is flexible and can be reduced for larger array sizes. For the stimulator array, the current running array is 16x16 CMOS controlled by Gallium Nitride opto-electronic micro-LEDs. The next chip will be a 90x90 and is still under testing.

A recommendation for future work, after intensive tests of the controller on the FPGA platform, the ASIC implementation for final stimulator controller mass production needs to be considered. Further research is required on the central pulse controller algorithms that can be used to control the four tiled 90x90 optoelectronic stimulator arrays (the four tiled 90x90 is explained in the next stage).

- **Output Stage:** the optogenetic retinal prosthesis approach uses an optical stimulation. In this work, an array of 16x16 is used, and the calibration and operation of this microLED array is completed in this work. At the time of writing, the Newcastle group was testing a 90x90 stimulator array, to be used in the next set of experiments. A recommendation for future work, is to have four of these 90x90 microLEDs tiled together to achieve a 180x180 stimulator size.

Finally, this work has proposed a framework for an optogenetic retinal prosthesis system, for Retinitis Pigmentosa (RP) patient trials. A combination of software/hardware approaches were used to achieve this goal. The selection of these two approaches was based on the problems and the requirements of the biological visual human system, which transformed into an engineering problem to be solved. The application of the selected approaches was demonstrated by simulation, and then the hardware implementation which based on the FPGA platform is used.

## References

- [1] A. Bharath and M. Petrou, *Next Generation Artificial Vision Systems Reverse Engineering the Human Visual System*: ARTECH HOUSE, INC., 2008.
- [2] B. A. Wandell, *Foundations of vision*. Sunderland, Mass.: Sinauer Associates, 1995.
- [3] <http://cvseventh.com/12395/human-eye-anatomy/>.
- [4] R. Snowden, P. Thompson, and T. Troscianko, *Basic Vision, An Introduction to Visual Perception*, 2012.
- [5] C. A. Morillas, S. F. Romero, A. Martínez, F. J. Pelayo, E. Ros, and E. Fernández, "A design framework to model retinas," *Biosystems*, vol. 87, pp. 156-163, 2// 2007.
- [6] J. E. Dowling, *The Retina: An Approachable Part of the Brain*: Harvard University Press, 1990.
- [7] R. Gonzalez and R. Woods, *Digital Image Processing*. Upper Saddle River, New Jersey 07458: Prentice Hall, 2002.
- [8] M. D. Davis, R. E. Gangnon, L. Y. Lee, L. D. Hubbard, B. E. Klein, R. Klein, *et al.*, "The Age-Related Eye Disease Study severity scale for age-related macular degeneration: AREDS Report No. 17," *Arch Ophthalmol*, vol. 123, pp. 1484-98, Nov 2005.
- [9] A. K. O. Denniston and P. I. Murray, *Oxford handbook of ophthalmology*, 2nd ed. Oxford ; New York: Oxford University Press, 2009.
- [10] S. Merin, *Inherited eye diseases : diagnosis and clinical management*. New York, N.Y.: Dekker, 1991.
- [11] E. L. Berson, "Retinitis pigmentosa. The Friedenwald Lecture," *Invest Ophthalmol Vis Sci*, vol. 34, pp. 1659-76, Apr 1993.
- [12] R. K. Sharma and B. Ehinger, "Management of hereditary retinal degenerations: present status and future directions," *Surv Ophthalmol*, vol. 43, pp. 427-44, Mar-Apr 1999.
- [13] W. Al-Atabany and P. Degenaar, "Scene optimization for optogenetic retinal prosthesis," in *Biomedical Circuits and Systems Conference (BioCAS), 2011 IEEE*, 2011, pp. 432-435.
- [14] E. Peli and T. Peli, "Image-Enhancement for the Visually Impaired," *Optical Engineering*, vol. 23, pp. 47-51, 1984.
- [15] H. Segond and D. Weiss, "Human spatial navigation via a visuo-tactile sensory substitution system," *Perception*, vol. 34, pp. 1231-1249, 2005.
- [16] P. Bach-y-Rita, "Tactile sensory substitution studies," *Ann N Y Acad Sci*, vol. 1013, pp. 83-91, May 2004.
- [17] R. Kupers and M. Ptito, ""Seeing" through the tongue: cross-modal plasticity in the congenitally blind," *Frontiers in Human Brain Topography*, vol. 1270, pp. 79-84, 2004.
- [18] A. Amedi, W. M. Stern, J. A. Camprodon, F. Bermpohl, L. Merabet, S. Rotman, *et al.*, "Shape conveyed by visual-to-auditory sensory substitution activates the lateral occipital complex," *Nat Neurosci*, vol. 10, pp. 687-9, Jun 2007.
- [19] B. Saha, B. Bhowmick, and A. Sinha, "An embedded solution for visually impaired," in *Consumer Electronics, 2009. ISCE '09. IEEE 13th International Symposium on*, 2009, pp. 467-471.
- [20] S. E. Boye, S. L. Boye, A. S. Lewin, and W. W. Hauswirth, "A Comprehensive Review of Retinal Gene Therapy," *Mol Ther*, vol. 21, pp. 509-519, 03//print 2013.
- [21] I. R. Schwab and R. R. Isseroff, "Bioengineered corneas - The promise and the challenge.," *New England Journal of Medicine*, vol. 343, pp. 136-138, Jul 13 2000.
- [22] T. V. Johnson, N. D. Bull, and K. R. Martin, "Transplantation prospects for the inner retina," *Eye*, vol. 23, pp. 1980-1984, Oct 2009.
- [23] M. Eiraku and Y. Sasai, "Mouse embryonic stem cell culture for generation of three-dimensional retinal and cortical tissues," *Nat. Protocols*, vol. 7, pp. 69-79, 01//print 2012.

- [24] N. D. Radtke, M. J. Seiler, R. B. Aramant, H. M. Petry, and D. J. Pidwell, "Transplantation of intact sheets of fetal neural retina with its retinal pigment epithelium in retinitis pigmentosa patients," *Am J Ophthalmol*, vol. 133, pp. 544-50, Apr 2002.
- [25] J. R. Boyle, A. J. Maeder, and W. W. Boles, "Region-of-interest processing for electronic visual prostheses," *Electron Imaging*, vol. 17, February 15, 2008.
- [26] P. Degenaar, "Retinal Prosthesis," in *Encyclopedia of Biophysics*, G. K. Roberts, Ed., ed: Springer Berlin Heidelberg, 2013, pp. 2227-2231.
- [27] L. B. Merabet, J. F. Rizzo, A. Amedi, D. C. Somers, and A. Pascual-Leone, "What blindness can tell us about seeing again: merging neuroplasticity and neuroprostheses," *Nat Rev Neurosci*, vol. 6, pp. 71-77, 01//print 2005.
- [28] A. Y. Chow, M. T. Pardue, V. Y. Chow, G. A. Peyman, C. P. Liang, J. I. Perlman, *et al.*, "Implantation of silicon chip microphotodiode arrays into the cat subretinal space," *IEEE Transactions on Neural Systems and Rehabilitation Engineering*, vol. 9, pp. 86-95, Mar 2001.
- [29] A. Y. Chow, V. Y. Chow, K. H. Packo, J. S. Pollack, G. A. Peyman, and R. Schuchard, "The artificial silicon retina microchip for the treatment of vision loss from retinitis pigmentosa," *Archives of Ophthalmology*, vol. 122, pp. 460-469, Apr 2004.
- [30] H. N. Schwahn, F. Gekeler, K. Kohler, K. Kobuch, H. G. Sachs, F. Schulmeyer, *et al.*, "Studies on the feasibility of a subretinal visual prosthesis: data from Yucatan micropig and rabbit," *Graefes Archive for Clinical and Experimental Ophthalmology*, vol. 239, pp. 961-967, Dec 2001.
- [31] E. Zrenner, K. D. Miliczek, V. P. Gabel, H. G. Graf, E. Guenther, H. Haemmerle, *et al.*, "The development of subretinal microphotodiodes for replacement of degenerated photoreceptors," *Ophthalmic Research*, vol. 29, pp. 269-280, Sep-Oct 1997.
- [32] M. S. Humayun, J. D. Weiland, G. Chader, E. Greenbaum, R. Wilke, M. Bach, *et al.*, "Testing Visual Functions in Patients with Visual Prostheses," in *Artificial Sight*, E. Greenbaum, Ed., ed: Springer New York, 2008, pp. 91-110.
- [33] E. Zrenner, D. Besch, K. Bartz-Schmidt, F. Gekeler, and V. ..., *Subretinal chronic multi-electrode arrays implanted in blind patients*, 2006.
- [34] E. Zrenner, K. U. Bartz-Schmidt, H. Benav, D. Besch, A. Bruckmann, V.-P. Gabel, *et al.*, *Subretinal electronic chips allow blind patients to read letters and combine them to words* vol. 278, 2011.
- [35] J. D. Loudin, D. M. Simanovskii, K. Vijayraghavan, C. K. Sramek, A. F. Butterwick, P. Huie, *et al.*, "Optoelectronic retinal prosthesis: system design and performance," *NEURAL ENGINEERING*, vol. 4, pp. 72-84, 2007.
- [36] D. Boinagrov, X. Lei, G. Goetz, T. I. K. Kamins, K. Mathieson, L. Galambos, *et al.*, "Photovoltaic Pixels for Neural Stimulation: Circuit Models and Performance," *Biomedical Circuits and Systems, IEEE Transactions on*, vol. PP, pp. 1-1, 2015.
- [37] R. Eckmiller, "Learning retina implants with epiretinal contacts," *Ophthalmic Research*, vol. 29, pp. 281-289, Sep-Oct 1997.
- [38] M. S. Humayun, E. deJuan, G. Dagnelie, R. J. Greenberg, R. H. Prost, and D. H. Phillips, "Visual perception elicited by electrical stimulation of retina in blind humans," *Archives of Ophthalmology*, vol. 114, pp. 40-46, Jan 1996.
- [39] J. F. Rizzo, J. Wyatt, J. Loewenstein, S. Kelly, and D. Shire, "Methods and perceptual thresholds for short-term electrical stimulation of human retina with microelectrode arrays," *Investigative Ophthalmology & Visual Science*, vol. 44, pp. 5355-5361, Dec 2003.
- [40] R. Eckmiller, D. Neumann, and O. Baruth, "Tunable retina encoders for retina implants: why and how," *J Neural Eng*, vol. 2, pp. S91-S104, Mar 2005.
- [41] M. Javaheri, D. S. Hahn, R. R. Lakhnani, J. D. Weiland, and M. S. Humayun, "Retinal prostheses for the blind," *Ann Acad Med Singapore*, vol. 35, pp. 137-44, Mar 2006.
- [42] <http://www.doheny.org/research/retina.html>.

- [43] J. D. Weiland, A. K. Cho, and M. S. Humayun, "Retinal Prostheses: Current Clinical Results and Future Needs," *Ophthalmology*, vol. 118, pp. 2227-2237.
- [44] G. Lazzi, S. C. DeMarco, L. Wentai, J. D. Weiland, and M. S. Humayun, "Computed SAR and thermal elevation in a 0.25-mm 2-D model of the human eye and head in response to an implanted retinal stimulator - part II: results," *Antennas and Propagation, IEEE Transactions on*, vol. 51, pp. 2286-2295, 2003.
- [45] A. Asher, W. A. Segal, S. A. Baccus, L. P. Yaroslavsky, and D. V. Palanker, "Image Processing for a High-Resolution Optoelectronic Retinal Prosthesis," *Biomedical Engineering, IEEE Transactions on*, vol. 54, pp. 993-1004, 2007.
- [46] J. Dowling, "Current and future prospects for optoelectronic retinal prostheses," *Eye*, vol. 23, pp. 1999-2005, Oct 2009.
- [47] G. J. Chader, J. Weiland, M. S. Humayun, E. M. H. I. H. J. W. A. B. B. G. J. B. Joost Verhaagen, and F. S. Dick, "Artificial vision: needs, functioning, and testing of a retinal electronic prosthesis," in *Progress in Brain Research*. vol. Volume 175, ed: Elsevier, 2009, pp. 317-332.
- [48] G. Nagel, T. Szellas, W. Huhn, S. Kateriya, N. Adeishvili, P. Berthold, *et al.*, "Channelrhodopsin-2, a directly light-gated cation-selective membrane channel," *Proceedings of the National Academy of Sciences*, vol. 100, pp. 13940-13945, November 25, 2003 2003.
- [49] P. Degenaar, N. Grossman, M. A. Memon, J. Burrone, M. Dawson, E. Drakakis, *et al.*, "Optobionic vision-a new genetically enhanced light on retinal prosthesis," *Journal of Neural Engineering*, vol. 6, pp. -, Jun 2009.
- [50] A. Soltan, H. Zhao, L. Chaudet, M. Neil, P. Maaskant, and P. Degenaar, "An 8100 Pixel Optoelectronic Array for Optogenetic Retinal Prosthesis," presented at the Biomedical Circuits and Systems Conference,(BIOCAS), 2014.
- [51] M. E. Brelen, F. Duret, B. Gerard, J. Delbeke, and C. Veraart, "Creating a meaningful visual perception in blind volunteers by optic nerve stimulation," *J Neural Eng*, vol. 2, pp. S22-8, Mar 2005.
- [52] J. Delbeke, M. Oozeer, and C. Veraart, "Position, size and luminosity of phosphenes generated by direct optic nerve stimulation," *Vision Res*, vol. 43, pp. 1091-102, Apr 2003.
- [53] C. Veraart, M.-C. Wanet-Defalque, B. Gérard, A. Vanlierde, and J. Delbeke, "Pattern Recognition with the Optic Nerve Visual Prosthesis," *Artificial Organs*, vol. 27, pp. 996-1004, 2003.
- [54] V. Cazenave-Loustalet, Q.-L. Qiao, L.-M. Li, and Q.-S. Ren, "Evoked membrane potential change in rat optic nerve fiber: Computer simulation," *Neuroscience Bulletin* vol. 23, pp. 348-356, 2007.
- [55] A. Banarji, V. S. Gurunadh, S. Patyal, T. S. Ahluwalia, D. P. Vats, and M. Bhadauria, "Visual prosthesis : Artificial vision," *Medical Journal Armed Forces India*, vol. 65, pp. 348-352, 10// 2009.
- [56] G. S. Brindley and W. S. Lewin, "The sensations produced by electrical stimulation of the visual cortex," *Physiol*, vol. 196, pp. 479-493, 1968.
- [57] K. Cha , K. Horch, and R. A. Normann, "Simulation of a phosphene-based visual field: Visual acuity in a pixelized vision system," *Annals of Biomedical Engineering* vol. 20, pp. 439-449, 1992.
- [58] J. M. Ferrandez and E. Fernandez, "Development of a Cortical Visual Neuroprostheses for the Blind," *Life Science Systems and Applications Workshop*, vol. 0, pp. 1-2, 2006.
- [59] <http://cortivis.umh.es/>.
- [60] E. Fernandez, B. Greger, P. A. House, I. Aranda, C. Botella, J. Albisua, *et al.*, "Acute human brain responses to intracortical microelectrode arrays: challenges and future prospects," *Front Neuroeng*, vol. 7, p. 24, 2014.



- [61] S. K. Kelly, D. B. Shire, J. Chen, P. Doyle, M. D. Gingerich, S. F. Cogan, *et al.*, "A Hermetic Wireless Subretinal Neurostimulator for Vision Prostheses," *Biomedical Engineering, IEEE Transactions on*, vol. 58, pp. 3197-3205, 2011.
- [62] J. F. Rizzo, D. B. Shire, S. K. Kelly, P. Troyk, M. Gingerich, B. McKee, *et al.*, "Overview of the boston retinal prosthesis: Challenges and opportunities to restore useful vision to the blind," in *Engineering in Medicine and Biology Society, EMBC, 2011 Annual International Conference of the IEEE*, 2011, pp. 7492-7495.
- [63] J. D. Weiland, M. S. Humayun, and A. R. Tanguay, Jr., "Out of Darkness: Helping the Blind See with Artificial Vision," *Solid-State Circuits Magazine, IEEE*, vol. 4, pp. 43-45, 2012.
- [64] J. G. Light, J. W. Fransen, A. N. Adekunle, A. Adkins, G. Pangen, J. Loudin, *et al.*, "Inner retinal preservation in rat models of retinal degeneration implanted with subretinal photovoltaic arrays," *Experimental Eye Research*, vol. 128, pp. 34-42, 11// 2014.
- [65] N. Barnes, "An overview of vision processing in implantable prosthetic vision," in *Image Processing (ICIP), 2013 20th IEEE International Conference on*, 2013, pp. 1532-1535.
- [66] E. Zrenner, K. U. Bartz-Schmidt, H. Benav, D. Besch, A. Bruckmann, V.-P. Gabel, *et al.*, "Subretinal electronic chips allow blind patients to read letters and combine them to words," *Proceedings of the Royal Society B: Biological Sciences*, p. rspb20101747, 2010.
- [67] R. Eckmiller, R. Schatten, and O. Baruth, "Portable Biomimetic Retina for Learning, Perception-based Image Acquisition," in *Neural Networks, 2007. IJCNN 2007. International Joint Conference on*, 2007, pp. 2436-2441.
- [68] R. Eckmiller, O. Baruth, and D. Neumann, "On Human Factors for Interactive Man-Machine Vision: Requirements of the Neural Visual System to transform Objects into Percepts," in *Neural Networks, 2006. IJCNN '06. International Joint Conference on*, 2006, pp. 307-311.
- [69] A. B. Musa Al Yaman, Patrick Degenaar, and Pleun Maaskant., "FPGA design of a pulse encoder for optoelectronic neural stimulation and recording arrays," presented at the IEEE Biomedical Circuits and Systems Conference (BioCAS), Rotterdam, the Netherlands, 2013.
- [70] M. Al Yaman and P. Degenaar, "FPGA design of an even power distributor for optoelectronic neural stimulation," in *Applied Electrical Engineering and Computing Technologies (AEECT), 2013 IEEE Jordan Conference on*, 2013, pp. 1-4.
- [71] T. Yagi, Y. Ito, H. Kanda, S. Tanaka, M. Watanabe, and Y. Uchikawa, "Hybrid retinal implant: fusion of engineering and neuroscience," in *Systems, Man, and Cybernetics, 1999. IEEE SMC '99 Conference Proceedings. 1999 IEEE International Conference on*, 1999, pp. 382-385 vol.4.
- [72] T. Yagi, "Biohybrid Visual Prosthesis for Restoring Blindness," *INTERNATIONAL JOURNAL OF APPLIED BIOMEDICAL ENGINEERING*, vol. 2, 2009.
- [73] G. Khalili Moghaddam, N. H. Lovell, R. G. Wilke, G. J. Suaning, and S. Dokos, "Performance optimization of current focusing and virtual electrode strategies in retinal implants," *Comput Methods Programs Biomed*, vol. 117, pp. 334-42, Nov 2014.
- [74] G. K. Moghaddam, R. G. H. Wilke, S. Dokos, G. J. Suaning, and N. H. Lovell, "Electrode design to optimize ganglion cell activation in a retinal neuroprosthesis: A modeling study," in *Neural Engineering (NER), 2011 5th International IEEE/EMBS Conference on*, 2011, pp. 542-545.
- [75] C. Veraart, F. Duret, M. Brelen, and J. Delbeke, "Vision rehabilitation with the optic nerve visual prosthesis," in *Engineering in Medicine and Biology Society, 2004. IEMBS '04. 26th Annual International Conference of the IEEE*, 2004, pp. 4163-4164.
- [76] T. D. D. Thil Marie-Anne, Colin Ides M., Delbeke Jean, "Time course of tissue remodelling and electrophysiology in the rat sciatic nerve after spiral cuff electrode implantation," *Journal of Neuroimmunology*, vol. 185, pp. 103-114, 2007.
- [77] K. S. Mathews, H. A. C. Wark, and R. A. Normann, "Assessment of rat sciatic nerve function following acute implantation of high density utah slanted electrode array (25



- electrodes/mm<sup>2</sup>) based on neural recordings and evoked muscle activity," *Muscle & Nerve*, vol. 50, pp. 417-424, 2014.
- [78] E. Fernandez, F. Pelayo, S. Romero, M. Bongard, C. Marin, A. Alfaro, *et al.*, "Development of a cortical visual neuroprosthesis for the blind: the relevance of neuroplasticity," *J Neural Eng*, vol. 2, pp. R1-12, Dec 2005.
- [79] J. M. Ferrandez, E. Liano, P. Bonomini, J. J. Martinez, J. Toledo, and E. Fernandez, "A Customizable Multi-channel Stimulator for Cortical Neuroprosthesis," in *Engineering in Medicine and Biology Society, 2007. EMBS 2007. 29th Annual International Conference of the IEEE*, 2007, pp. 4707-4710.
- [80] D. C. Bradley, P. R. Troyk, J. A. Berg, M. Bak, S. Cogan, R. Erickson, *et al.*, *Visuotopic Mapping Through a Multichannel Stimulating Implant in Primate V1* vol. 93, 2005.
- [81] G. P. Kaskhedikar, H. Zhe, G. Dagnelie, and P. R. Troyk, "Proposed Intracortical vision prosthesis system for phosphene mapping and psychophysical studies," in *Neural Engineering (NER), 2013 6th International IEEE/EMBS Conference on*, 2013, pp. 880-882.
- [82] A. Downton and D. Crookes, "Parallel architectures for image processing," *Electronics & Communication Engineering Journal*, vol. 10, pp. 139-151, 1998.
- [83] N. R. Pal and S. K. Pal, "A review on image segmentation techniques," *Pattern Recognition*, vol. 26, pp. 1277-1294, 1993.
- [84] Y. J. Zhang, *An Overview of Image and Video Segmentation in the Last 40 Years*: IRM Press, 2006.
- [85] P. K. Sahoo, S. Soltani, A. K. Wong, and Y. C. Chen, "A survey of thresholding techniques," *Computer Vision, Graphics, and Image Processing*, vol. 41, pp. 233-260, 1988.
- [86] Y. Xiao, Z. Cao, and S. Zhong, "New entropic thresholding approach using gray-level spatial correlation histogram," *Optical Engineering*, vol. 49, pp. 127007-127007-13, 2010.
- [87] N. Otsu, "A threshold selection method from gray-level histograms," *IEEE Transactions on Systems, Man and Cybernetics*, vol. 9, pp. 62-66, 1979.
- [88] <http://edge.rit.edu/edge/P06441/public/Results%20Recorded%20from%20Histogram%20Stretching>.
- [89] J. Canny, "A computational approach to edge detection," *IEEE Transactions on Pattern Analysis and Machine Intelligence*, vol. 8, pp. 679-698, November 1986.
- [90] R. Sedgewick and K. D. Wayne, *Introduction to Programming in Java: An Interdisciplinary Approach*: Pearson Addison-Wesley, 2008.
- [91] T. B. Lawton, "Improved Word Recognition for Observers with Age-Related Maculopathies Using Compensation Filters," *Clinical Vision Sciences*, vol. 3, 1988.
- [92] E. Peli, R. B. Goldstein, G. M. Young, Clement L. Trempe, and S. M. Buzney, "Image-Enhancement for the Visually-Impaired - Simulations and Experimental Results," *Investigative Ophthalmology & Visual Science*, vol. 32, pp. 2337-2350, Jul, 1991.
- [93] J. S. Wolffsohn, D. Mukhopadhyay, and M. Rubinstein, "Image enhancement of real-time television to benefit the visually impaired," *Am J Ophthalmol*, vol. 144, pp. 436-440, Sep, 2007.
- [94] E. Peli, G. Luo, A. Bowers, and N. Rensing, "Applications of augmented-vision head-mounted systems in vision rehabilitation," *Journal of the Society for Information Display*, vol. 15, pp. 1037-1045, Dec 2007.
- [95] P. E., "Evaluation of a prototype Minified Augmented-View device for patients with impaired night vision," *Ophthalmic and Physiological Optics*, vol. 24, pp. 296-312, 2004.
- [96] F. Vargas-Martín, M. D. Peláez-Coca, E. Ros, J. Diaz, and S. Mota, "A generic real-time video processing unit for low vision," *International Congress Series*, vol. 1282, pp. 1075-1079, 9// 2005.
- [97] F. J. Toledo, J. J. Mart, F. J. Garrig, and J. M. Ferr, "An augmented reality visual prosthesis for people affected by tunneling vision," presented at the Proceedings of the First

- international conference on Mechanisms, Symbols, and Models Underlying Cognition: interplay between natural and artificial computation - Volume Part I, Canary Islands, Spain, 2005.
- [98] W. Atabany and P. Degenaar, "A Robust Edge Enhancement Approach for Low Vision Patients Using Scene Simplification," in *Biomedical Engineering Conference, 2008. CIBEC 2008. Cairo International, 2008*, pp. 1-4.
- [99] W. Al-Atabany, B. McGovern, K. Mehran, R. Berlinguer-Palmini, and P. Degenaar, "A processing platform for optoelectronic/optogenetic retinal prosthesis," *Biomedical Engineering, IEEE Transactions on*, vol. PP, pp. 1-1, 2011.
- [100] W. Al-Atabany, M. Memon, S. Downes, and P. Degenaar, "Designing and testing scene enhancement algorithms for patients with retina degenerative disorders," *BioMedical Engineering OnLine*, vol. 9, p. 27, 2010.
- [101] D. R. Hochbaum, Y. Zhao, S. L. Farhi, N. Klapoetke, C. A. Werley, V. Kapoor, *et al.*, "All-optical electrophysiology in mammalian neurons using engineered microbial rhodopsins," *Nat Meth*, vol. 11, pp. 825-833, 08//print 2014.
- [102] W. M. Haynes, *CRC Handbook of Chemistry and Physics*, 92nd Edition ed., 2011
- [103] D. Litwiller, "CMOS vs CCD: Maturing Technologies, Maturing Markets," *Photonics Spectra*, vol. 39, Aug 2005.
- [104] P. Magnan, "Detection of visible photons in CCD and CMOS: A comparative view," *Nuclear Instruments & Methods in Physics Research Section a-Accelerators Spectrometers Detectors and Associated Equipment*, vol. 504, pp. 199-212, May 21 2003.
- [105] O. Yadid-Pecht and R. Etienne-Cummings, *CMOS imagers : from phototransduction to image processing*. Boston ; London: Kluwer Academic, 2004.
- [106] B. E. Bayer, "Color imaging array," ed: Google Patents, 1976.
- [107] M. H. Ettenberg, M. J. Cohen, R. M. Brubaker, M. J. Lange, M. T. O'Grady, and G. H. Olsen, "Indium Gallium Arsenide imaging with smaller cameras, higher resolution arrays, and greater material sensitivity," *Infrared Detectors and Focal Plane Arrays Vii*, vol. 4721, pp. 26-36, 2002.
- [108] G. H. Olsen, P. E. Dixon, M. J. Lange, J. J. Sudol, M. J. Cohen, A. R. Sugg, *et al.*, "Photodetector arrays from 100 mm diameter InGaAs/InP epitaxial wafers," *Journal of Crystal Growth*, vol. 222, pp. 693-696, 2001.
- [109] W. D. Al-Atabany, P., "Efficient scene preparation and downscaling prior to stimulation in retinal prosthesis," *Biomedical Circuits and Systems Conference (BioCAS)*, pp. pp.182-185, Oct. 31-Nov. 2 2013.
- [110] C. Pohl and J. L. Van Genderen, "Review article Multisensor image fusion in remote sensing: concepts, methods and applications," *International Journal of Remote Sensing*, vol. 19, pp. 823 - 854, 1998.
- [111] J. Nunez, X. Otazu, O. Fors, A. Prades, V. Pala, and R. Arbiol, "Multiresolution-based image fusion with additive wavelet decomposition," *IEEE Transactions on Geoscience and Remote Sensing*, vol. 37, pp. 1204-1211, May 1999.
- [112] G. Simone, A. Farina, F. C. Morabito, S. B. Serpico, and L. Bruzzone, "Image fusion techniques for remote sensing applications," *Information Fusion*, vol. 3, pp. 3-15, 2002.
- [113] R. R. Murphy, "Sensor and information fusion for improved vision-based vehicle guidance," *IEEE Intelligent Systems & Their Applications*, vol. 13, pp. 49-56, Nov-Dec 1998.
- [114] C. E. Reese and E. J. Bender, "Multi-spectral/image fused head tracked vision system (HTVS) for driving applications," *Helmet- and Head-Mounted Displays Vi*, vol. 4361, pp. 1-11, 2001.
- [115] Y. H. Cai, K. Q. Huang, T. N. Tan, and Y. H. Wang, "Context enhancement of nighttime surveillance by image fusion," *18th International Conference on Pattern Recognition, Vol 1, Proceedings*, pp. 980-983, 2006.

- [116] J. Li, T. Yang, Q. Pan, and Y. Cheng, "Combining scene model and fusion for night video enhancement," *Journal of Electronics (China)*, vol. 26, pp. 88-93, 2009.
- [117] F. Laliberte and L. Gagnon, "Registration and fusion of retinal images - An evaluation study," *IEEE Transactions on Medical Imaging*, vol. 22, pp. 661-673, May 2003.
- [118] Z. F. Zhang, J. Yao, S. Bajwa, and T. Gudas, ""Automatic" multimodal medical image fusion," *Smcia/03: Proceedings of the 2003 IEEE International Workshop on Soft Computing in Industrial Applications*, pp. 161-166, 2003.
- [119] G. H. Qu, D. Zhang, and P. F. Yan, "Medical image fusion using two dimensional discrete wavelet transform," *Data Mining and Applications*, vol. 4556, pp. 86-95, 2001.
- [120] Y. M. Kim, C. Theobalt, J. Diebel, J. Kosecka, B. Micusik, and T. S, "Multi-view Image and ToF Sensor Fusion for Dense 3D Reconstruction," in *IEEE Workshop on 3-D Digital Imaging and Modeling (3DIM)*, 2009.
- [121] H. A. Eltoukhy and S. Kavusi, "A computationally efficient algorithm for multi-focus image reconstruction," *Sensors and Camera Systems for Scientific, Industrial, and Digital Photography Applications Iv*, vol. 5017, pp. 332-341, 2003.
- [122] T. Wan, G. Tzagkarakis, P. Tsakalides, N. Canagarajah, and A. Achim, "Context enhancement through image fusion: A multiresolution approach based on convolution of Cauchy distributions," *2008 IEEE International Conference on Acoustics, Speech and Signal Processing, Vols 1-12*, pp. 1309-1312, 2008.
- [123] B. N. Kayani, A. M. Mirza, A. Bangash, and H. Iftikhar, "Pixel & feature level multiresolution image fusion based on fuzzy logic," *Innovations and Advanced Techniques in Computer and Information Sciences and Engineering*, pp. 129-132, 2007.
- [124] A. Castorina, A. Capra, S. Curti, E. Ardizzone, and V. Lo Verde, "Improved multi-resolution image fusion," *ICCE: 2005 International Conference on Consumer Electronics, Digest of Technical Papers*, pp. 131-132, 2005.
- [125] W. Al-Atabany, T. Tong, and P. Degenaar, "Improved content aware scene retargeting for retinitis pigmentosa patients," *BioMedical Engineering OnLine*, vol. 9, p. 52, 2010.
- [126] A. C. Bovik, *Handbook of Image and Video Processing*. Orlando, FL, USA: Academic Press, Inc., 2005.
- [127] P. Perona and J. Malik, "Scale-Space and Edge-Detection Using Anisotropic Diffusion," *IEEE Transactions on Pattern Analysis and Machine Intelligence*, vol. 12, pp. 629-639, Jul 1990.
- [128] S. Avidan and A. Shamir, "Seam carving for content-aware image resizing," *Acm Transactions on Graphics*, vol. 26, pp. -, Jul 2007.
- [129] Y. F. Zhang, S. M. Hu, and R. R. Martin, "Shrinkability Maps for Content-Aware Video Resizing," *Computer Graphics Forum*, vol. 27, pp. 1797-1804, Oct 2008.
- [130] L. F. Abbott, "Lapicque's introduction of the integrate-and-fire model neuron (1907)," *Brain Research Bulletin*, vol. 50, pp. 303-304, 11// 1999.
- [131] A. L. Hodgkin and A. F. Huxley, "A quantitative description of membrane current and its application to conduction and excitation in nerve," *J Physiol*, vol. 117, pp. 500-44, Aug 1952.
- [132] E. M. Izhikevich, "Simple model of spiking neurons," *Neural Networks, IEEE Transactions on*, vol. 14, pp. 1569-1572, 2003.
- [133] N. Grossman, K. Nikolic, C. Toumazou, and P. Degenaar, "Modeling Study of the Light Stimulation of a Neuron Cell With Channelrhodopsin-2 Mutants," *Biomedical Engineering, IEEE Transactions on*, vol. 58, pp. 1742-1751.
- [134] C.-k. Lee and M. Hamdi, "Parallel image processing applications on a network of workstations," *Parallel Computing*, vol. 21, pp. 137-160, 1995.
- [135] A. Krikelis and R. M. Lea, "A modular massively parallel computing approach to image-related processing," *Proceedings of the IEEE*, vol. 84, pp. 988-1004, 1996.

- [136] S. J. Carey, D. R. W. Barr, and P. Dudek, "Low power high-performance smart camera system based on SCAMP vision sensor," *Journal of Systems Architecture*, vol. 59, pp. 889-899, 11// 2013.
- [137] S. J. Carey and P. Dudek, "Vision chip with high accuracy analog S2I cells," in *Cellular Nanoscale Networks and their Applications (CNNA), 2014 14th International Workshop on*, 2014, pp. 1-2.
- [138] J. D. Owens, M. Houston, D. Luebke, S. Green, J. E. Stone, and J. C. Phillips, "GPU Computing," *Proceedings of the IEEE*, vol. 96, pp. 879-899, 2008.
- [139] J. Cohen and M. Garland, "Novel Architectures: Solving Computational Problems with GPU Computing," *Computing in Science & Engineering*, vol. 11, pp. 58-63, 2009.
- [140] R. Dubey, *Introduction to embedded system design using field programmable gate arrays*, 1st ed. New York: Springer, 2008.
- [141] J. Villasenor and B. Hutchings, "The flexibility of configurable computing," *IEEE Signal Processing Magazine*, vol. 15, pp. 67-84, Sep 1998.
- [142] W. Atabany and P. Degenaar, "Parallelism to reduce power consumption on FPGA spatiotemporal image processing," *Proceedings of 2008 IEEE International Symposium on Circuits and Systems, Vols 1-10*, pp. 1476-1479, 2008.
- [143] W. Atabany and P. Degenaar, "A Spatiotemporal Parallel Image Processing on FPGA for Augmented Vision System," *Advances in Computer and Information Sciences and Engineering*, pp. 558-561, 2008.
- [144] S. Asano, T. Maruyama, and Y. Yamaguchi, "Performance Comparison of Fpga, Gpu and Cpu in Image Processing," *Fpl: 2009 International Conference on Field Programmable Logic and Applications*, pp. 126-131, 2009.
- [145] S. A. Che, J. Li, J. W. Sheaffer, K. Skadron, and J. Lach, "Accelerating compute-intensive applications with GPUs and FPGAs," *2008 Symposium on Application Specific Processors*, pp. 101-107, 2008.
- [146] B. Cope, P. Y. K. Cheung, W. Luk, and S. Witt, "Have GPUs made FPGAs redundant in the field of video processing?," *FPT 05: 2005 IEEE International Conference on Field Programmable Technology, Proceedings*, pp. 111-118, 2005.
- [147] R. Kalarot and J. Morris, "Comparison of FPGA and GPU implementations of Real-time Stereo Vision," in *ECVW2010*, May 2010.
- [148] S. Kestur, J. D. Davis, and O. Williams, "BLAS Comparison on FPGA, CPU and GPU," in *IEEE Computer Society Symposium on VLSI*, July 2010.
- [149] D. B. Thomas, L. Howes, and W. Luk, "A comparison of CPUs, GPUs, FPGAs, and massively parallel processor arrays for random number generation," presented at the Proceeding of the ACM/SIGDA international symposium on Field programmable gate arrays, Monterey, California, USA, 2009.
- [150] <http://www.xilinx.com/products/boards-and-kits/AES-S6IVK-LX150T-G.htm>.
- [151] <http://flir.com/flirone/>.
- [152] B. McGovern, R. Berlinguer Palmimi, N. Grossman, E. Drakakis, V. Poher, M. A. A. Neil, et al., "A New Individually Addressable Micro-LED Array for Photogenetic Neural Stimulation," *Biomedical Circuits and Systems, IEEE Transactions on*, vol. 4, pp. 469-476, 2010.
- [153] T. Gollisch and M. Meister, "Rapid Neural Coding in the Retina with Relative Spike Latencies," *Science*, vol. 319, pp. 1108-1111, February 22, 2008 2008.
- [154] B. J. Hecht, "Photonic Frontiers: Room-temperature IR imaging," *Laser Focus World*, 2012.
- [155] [http://www.cs.uu.nl/docs/vakken/gr/2011/gr\\_lectures.html](http://www.cs.uu.nl/docs/vakken/gr/2011/gr_lectures.html).
- [156] A. C. Scherlen and V. Gautier, "Eye movements : sensory input to command and control adaptive visual aids," in *Neural Engineering, 2007. CNE '07. 3rd International IEEE/EMBS Conference on*, 2007, pp. 294-297.